Characterizing molecular-scale interactions between antimicrobial peptides and model cell membranes

A Dissertation

Submitted to the Faculty of

WORCESTER POLYTECHNIC INSTITUTE

In Partial Fulfillment of the Requirements for the

Degree of

DOCTOR OF PHILOSOPHY in

Biomolecular Engineering

April 2014

by

Kathleen F. Wang

Terri A Camesano, Ph.D.
Professor, Research Advisor
Department of Chemical Engineering
Worcester Polytechnic Institute

Ramanathan Nagarajan, Ph.D.
Research Chemical Engineer
Natick Soldier Research, Development & Engineering Center (NSRDEC)

Marsha Rolle, Ph.D.
Associate Professor of Biomedical Engineering
Worcester Polytechnic Institute

Amy M. Peterson, Ph.D.
Assistant Professor of Chemical Engineering
Worcester Polytechnic Institute

Table of Contents

Abstract

Due to the escalating challenge of antibiotic resistance in bacteria over the past several decades, interest in the identification and development of antibiotic alternatives has intensified. Antimicrobial peptides (AMPs), which serve as part of the innate immune systems of most eukaryotic organisms, are being researched extensively as potential alternatives. However, the mechanism behind their bactericidal capabilities is not well understood. Previous studies have suggested that AMPs may first attach to the cell membranes, leading to pore formation caused by peptide insertion, lipid removal in the form of peptide-lipid aggregates, or a combination of both mechanisms. In addition to the lack of mechanistic knowledge, a significant hurdle in AMP-based drug development is their potential cytotoxicity to mammalian cells. Understanding AMP interactions with eukaryotic model membranes would allow therapeutics to be tailored for preferential action toward specific classes of bacterial membranes. In this study, we developed novel methods of quartz crystal microbalance with dissipation monitoring (QCM-D) data analysis to determine the fundamental mechanism of action between eukaryotic and bacterial membrane mimics and select membrane-active AMPs. A new technique for creating supported membranes composed entirely of anionic lipids was developed to model Gram-positive bacterial membranes. Atomic force microscopy (AFM) imaging was also used to capture the progression of AMP-induced changes in supported lipid membranes over time and to validate our method of QCM-D analysis.

QCM-D and AFM were used to investigate the molecular-scale interactions of four peptides, alamethicin, chrysophsin-3, sheep myeloid antimicrobial peptide (SMAP-29) and indolicidin, with a supported zwitterionic membrane, which served as a model for eukaryotic cell membranes. Since established methods of QCM-D analysis were not sufficient to provide

information about these interaction mechanisms, we developed a novel method of using QCM-D overtones to probe molecular events occurring within supported lipid membranes. Also, most previous studies that have used AFM imaging to investigate AMP-membrane interactions have been inconclusive due to AFM limitations and poor image quality. We were able to capture high-resolution AFM images that clearly show the progression of AMP-induced defects in the membrane.

Each AMP produced a unique QCM-D signature that clearly distinguished their mechanism of action and provided information on peptide addition to and lipid removal from the membrane. Alamethicin, an α-helical peptide, predominantly demonstrated a pore formation mechanism. Chrysophsin-3 and SMAP-29, which are also α-helical peptides of varied lengths, inserted into the membrane and adsorbed to the membrane surface. Indolicidin, a shorter peptide that forms a folded, boat-shaped structure, was shown to adsorb and partially insert into the membrane. An investigation of rates at which the peptide actions were initiated revealed that the highest initial interaction rate was demonstrated by SMAP-29, the most cationic peptide in this study. The mechanistic variations in peptide action were related to their fundamental structural properties including length, net charge, hydrophobicity, hydrophobic moment, accessible surface area and the probability of α-helical secondary structures.

Due to the charges associated with anionic lipids, previous studies have not been successful in forming consistent anionic supported lipid membranes, which were required to mimic Gram-positive bacterial membranes. We developed a new protocol for forming anionic supported lipid membranes and supported vesicle films using a vesicle fusion process. Chrysophsin-3 was shown to favor insertion into the anionic lipid bilayer and did not adsorb to

the surface as it did with zwitterionic membranes. When introduced to supported anionic vesicle films, chrysophsin-3 caused some vesicles to rupture, likely through lipid membrane disruption.

This study demonstrated that molecular-level interactions between antimicrobial peptides and model cell membranes are largely determined by peptide structure, peptide concentration, and membrane lipid composition. Novel techniques for analyzing QCM-D overtone data were also developed, which could enable the extraction of more molecular orientation and interaction dynamics information from other QCM-D studies. A new method of forming supported anionic membranes was also designed, which may be used to further investigate the behavior of bacterial membranes in future studies. Insight into AMP-membrane interactions and development of AMP structure-activity relationships will facilitate the selection and design of more efficient AMPs for use in therapeutics that could impact the lives of millions of people per year who are threatened by antibiotic-resistant organisms.

Acknowledgements

There is no way I could have finished this dissertation without the vast array of intellectual, emotional, and financial support that I have received throughout the years. Thanks to the help of so many during my time at WPI, I believe I have matured as an individual and developed many of the skills necessary to continue to grow and learn as a researcher.

I would like to express my deepest appreciation and thanks to my research advisor, Dr. Terri A. Camesano. She has been a patient and supportive mentor and I am grateful to have had the opportunity to learn from her. Her help in guiding my research and teaching me how to share our work by composing papers and presenting at conferences was invaluable. I am so fortunate to have found such a patient, encouraging, and kind advisor during this stage of my career.

I would also like to acknowledge Dr. Ramanathan Nagarajan, without whom this project would not have progressed as much as it did. Despite his packed schedule, he amazingly managed to find time to meet with me for 4+ hours at a time. His enthusiasm for his work is infectious and he taught me to think and analyze data on a higher level.

I wish thank my committee members, Dr. Amy Peterson and Dr. Marsha Rolle for their guidance in completing this thesis. They have generously given their time and expertise in reading my dissertation and offering insightful feedback to better my work. It has been an honor to work with them.

This work would not have been possible without the help of Dr. Tanja Dominko, Dr. Sabyasachi Sarkar and Dr. Arne Gericke, who generously allowed me to use equipment in their labs. Dr. Sarkar kindly took time out of his busy schedule to help me with ellipsometry

experiments and Dr. Gericke's lab was very helpful in teaching me lipid vesicle formation procedures for this study.

I am also grateful for the funding that I received to pursue this research from the Natick Soldier Research, Development & Engineering Center (NSRDEC), the Oak Ridge Institute for Science and Education (ORISE) and the Koerner Family Graduate Fellowship.

I wish to thank my lab mates and friends at WPI over the years: Paola, Prachi, Charu, Harita, Yatao, Josh, Angela, Sena, Laila, Mary, Christina, Ellie, Lindsay, Todd, Felicia, and Tiffany, who have made the past several years at WPI fun and rewarding. Paola taught me the importance and joy of having fun while you work and created a lab environment that made me excited to come to lab each day. Prachi was pretty much my thesis buddy and I am so glad that we were both able to focus and finish our degrees.

I am indebted to my parents, Lucy and Dan Wang, who went to great lengths to ensure that I received the best education possible. No matter the obstacle, they firmly believed that education was a priority and instilled that belief in me, as well.

Last, but certainly not least, I wish to acknowledge my boyfriend Jeff for his never-ending patience and support. He is a saint for putting up with me over the last few months of this thesis and I am grateful to have him by my side.

Authorship

The contents of this thesis are a representation of the work done by the main author. Contributions to this project were made by Dr. Ramanathan Nagarajan, a research chemical engineer at the US Army Natick Soldier Research, Development and Engineering Center (NSRDEC). Dr. Nagarajan was instrumental in developing the QCM-D overtone analysis process, in performing AMP structural analysis and modeling of the expected overtone outcomes.

Dr. Charlene M. Mello is an adjunct professor at University of Massachusetts Dartmouth and a research chemist at NSRDEC. Dr. Mello contributed to helpful discussions when preparing the manuscript presented in Chapter 3.

Publications

This thesis is a compilation of the following manuscripts:

Chapter 3: Wang, K. F., Nagarajan, R., Camesano, T. A. Comparison of peptide structure-lipid bilayer interactions for alamethicin, chrysophsin-3, indolicidin and SMAP-29: Differentiation through QCM-D signatures. (submitted)

Chapter 4: Wang, K. F., Nagarajan, R., Mello, C. M., Camesano, T. A. Characterization of supported lipid bilayer disruption by chrysophsin-3 using QCM-D. *J. Phys. Chem. B* **115** (2011), 15228–35.

Chapter 5: Wang, K. F., Nagarajan, R., Camesano, T. A. Antimicrobial peptide alamethicin insertion into lipid bilayer: A QCM-D exploration. *Colloids Surfaces B Biointerfaces* **116** (2014), 472–481.

Chapter 6: Wang, K. F., Nagarajan, R., Camesano, T. A. AFM Imaging of AMP-induced membrane defects. (in preparation)

Chapter 7: Wang, K. F., Nagarajan, R., Camesano, T. A. A novel technique for forming supported anionic lipid membranes through vesicle fusion and an investigation of its interactions with chrysophsin-3. (in preparation)

Conference Abstracts

Wang KF, Nagarajan R, Camesano TA. (Apr 2013) Using QCM-D to compare the actions of antimicrobial peptides alamethicin, chrysophsin-3, indolicidin, and SMAP-29 on a supported lipid membrane. *ACS Spring 2013 National Meeting & Exposition*, New Orleans, LA. (Oral presentation)

Wang KF, Nagarajan R, Mello CM, Camesano TA. (Mar 2012) Using QCM-D to deduce the mechanism of SMAP-29 action on a model membrane. *ACS Spring 2012 National Meeting & Exposition*, San Diego, CA. (Oral presentation)

Wang KF, Nagarajan R, Mello CM, Camesano TA. (Nov 2011) Deducing the mechanism of indolicidin's action on a model membrane using QCM-D. *QCM-D Scientific World Tour*, Boston, MA. (Oral presentation)

Wang KF, Nagarajan R, Mello CM, Camesano TA. (Mar 2011) Quartz crystal microbalance with dissipation monitoring (QCM-D) studies and comparison of alamethicin and chrysophsin-3 action on cell membranes. *ACS Spring 2011 National Meeting & Exposition*, Anaheim, CA. (Oral presentation)

Wang KF, Nagarajan R, Mello CM, Camesano TA. (Aug 2010) Using QCM-D to predict antimicrobial peptide action on membranes. *ACS Fall 2010 National Meeting & Exposition*, Boston, MA. (Oral presentation)

Wang KF, Nagarajan R, Mello CM, Camesano TA. (Nov 2009) Using quartz crystal microbalance with dissipation monitoring (QCM-D) to predict antimicrobial peptide action on membranes. *QCM-D Scientific Meeting*, New York, NY. (Oral presentation)

Wang KF, Nagarajan R, Mello CM, Camesano TA. (Oct 2009) Using quartz crystal microbalance with dissipation monitoring (QCM-D) to predict antimicrobial peptide action on membranes. *ACS Northeast Regional Meeting (NERM)*, Hartford, CT. (Oral presentation)

Glossary of Abbreviations

β	Fraction of the affected membrane area where peptide clusters form
βME	β-mercaptoethanol
ΔD	Change in energy dissipation
Δf	Change in frequency
ΔG_{HA}	Change in Gibbs free energy of hydrophobic association
Δm	Change in mass
δ	Penetration depth of acoustic wave
δ_a	Angle of amino acid side chain
δ_L	Decay length of the acoustic wave in liquid
η_f	Viscosity of the film
η_L	Viscosity of the liquid
λ	Fraction of the bilayer area affected by peptide interactions
μ_q	Shear modulus of the crystal (2.947×10^{11} g/cm·s^2)
ρ_f	Density of the film
ρ_q	Density of quartz (2.648 g/cm^3)
Φ	Hydrophobicity of the peptide
Φ_n	Hydrophobicity for peptide residue n
A	Piezoelectrically active crystal area
A_H	Area per pore
A_p	Area per peptide (horizontal)
a_p	Area per peptide (vertical)

Aib	α-aminoisobutyric acid
AFM	Atomic force microscopy
AMP	Antimicrobial peptide
APTMS	(3-aminopropyl)trimethoxysilane
ASA	Accessible surface area
C	Sauerbrey constant
CD	Circular dichroism
D	Dissipation
D_H	outer diameter of a pore
d_P	Diameter of the peptide
DLPC	1,2-dilauroyl-*sn*-glycero-3-phosphatidylcholine
DLS	Dynamic Light Scattering
DMSO	Dimethyl sulfoxide
DMPC	Dimyristoyl-Phosphatidylcholine
DMPG	1,2-dimyristoyl-*sn*-glycero-3-phospho-*rac*-(1-glycerol)
DOPC	1,2-dioleoyl-*sn*-glycero-3-phosphocholine
DOPS	1,2-dioleoyl-*sn*-glycero-3-phospho-L-serine
DPPA	L-α-dipalmitoylphosphatidic acid
DPPC	Dipalmitoyl phosphatidylcholine
DSPC	1,2-distearoyl-*sn*-glycerol-3-phosphocholine
EC_{50}	Half maximal effective concentration
EDTA	ethylenediaminetetraacetic acid
f	Frequency

f_0	Resonant frequency of the quartz crystal (5 MHz)
G'	Storage modulus
G''	Loss modulus
LPG	1-palmitoyl-2-hydroxy-***sn***-glycero-3-phospho-(1'-***rac***-glycerol)
LPS	Lipopolysaccharide
MAD	Multiwavelength anomalous diffraction
MIC	Minimum inhibitory concentration
m_f	Mass per unit area
M_L	Molecular mass of lipid
M_P	Molecular mass of peptide
m_q	Areal mass of the quartz crystal
MRSA	Methicillin-resistant *Staphylococcus aureus*
N	Total number of amino acid residues
n	Overtone number
N_{LO}	Total number of lipid molecules initially present in the bilayer
NMR	Nuclear magnetic resonance
N_p	Total number of points measured with AFM
OCD	Oriented circular dichroism
P/L	Peptide-to-lipid raio
PC	Phosphatidylcholine
PEI	Polyethylenimine
PG	Egg L-α-phosphatidylglycerol
Phl	L-phenylalaninol

POPG	1-palmitoyl-2-oleoyl-*sn*-glycero-3-phosphoglycerol
QCM-D	Quartz crystal microbalance with dissipation monitoring
RMS	Root-mean-square
R_q	Roughness (AFM topography)
SDS	Sodium dodecyl sulfate
SFG	Sum frequency generation
SLB	Supported lipid bilayer
SUV	Small unilamellar vesicle
SVL	Supported vesicle layer
SMAP-29	Sheep myeloid antimicrobial peptide containing 29 amino acids
SMAPc	Sheep myeloid antimicrobial peptide containing terminal cysteine residue
Tris-NaCl	100 mM sodium chloride and 10 mM tris(hydroxymethyl)aminomethane buffer
Z_i	specific height (Z) value measured using AFM

Chapter 1

Overview

1.1 Research motivation

Antibiotics have served as a valuable tool in the fight against infections for the last 70 years, but their wide usage has allowed pathogens to adapt against them, making the drugs less effective. The CDC estimates that every year, more than 2 million people are sickened by antibiotic resistant infections and at least 23,000 die as a result.[1] Patients can become infected with antibiotic resistant pathogens through contact with multiple sources, including hospital environments and meat products derived from animals that are given antibiotics to treat disease and improve growth. These illnesses typically require prolonged or more expensive treatments and have a greater risk of disability and death than infections that respond to antibiotic therapy. The resulting healthcare costs have been estimated to be as high as $20 billion/year with an additional cost to society of $35 billion/year due to lost productivity.[1] Clearly, antibiotics must be replaced with alternatives that are equally as effective at killing pathogens but do not cause the same level of resistance.

Antimicrobial peptides (AMPs) are being actively researched for their potential as an alternative to antibiotics. AMPs are naturally derived molecules that form part of the innate immune system in most eukaryotic organisms. Approximately 2,000 AMPs have been isolated from natural sources such as frogs, moths, or fungi.[2] Many of these peptides are membrane-active, meaning that they kill bacteria by destabilizing their membranes and causing the cells to lyse. Due to their unique bactericidal mechanism, they do not cause the same level of resistance as antibiotics. To resist the action of AMPs, bacteria must significantly alter the compositions of their membranes, develop a mechanism to degrade the peptides through proteolysis, or extrude the peptides from the cell.[3] Using similar mechanisms, AMPs are also able to kill cancer cells

and microbes that are resistant to antibiotics.[4-6] Oncolytic AMPs, for instance, are thought to disrupt plasma membranes of target tumor cells or destabilize mitochondrial membranes.[2]

Although AMPs are thought to kill pathogens by disrupting their membranes, the exact mechanism behind the membrane destabilization is not fully understood. Theoretical models of AMP-membrane interactions suggest that some AMPs may insert into cell membranes and form pores, allowing large molecules to enter and exit the cell.[7] The formation of large pores may also disturb ion gradients, thereby killing the cell. Other theories postulate that AMPs may adsorb to the membrane surface and rearrange the lipid molecules to form micelles or peptide-lipid aggregates that can leave the membrane, causing it to disintegrate.[8] Variations of these two primary models postulate that the mechanism of action depends on the peptide concentration and structure.[9]

Understanding AMP-membrane interactions and the role of AMP structural characteristics in determining their action is crucial for the selection and design of AMPs for use in therapeutics. Before these peptides can be approved as drugs, their effects on both pathogens and patients must be fully understood. Therefore, investigations of AMP interactions must be conducted on at least two types of membranes: eukaryotic and bacterial.

Studying AMP-membrane interactions could also provide valuable information about how bacteria are unable to develop resistance to AMPs and give clues about other peptide-lipid interactions in biological systems. The membrane destabilization mechanism used by AMPs is believed to hinder the development of bacterial resistance, but understanding the factors behind this phenomenon will enable us to design novel peptides that have the same robust properties. Peptides in general (not necessarily antimicrobial) also play a large role in biological systems as

signaling molecules (e.g. neuropeptides) and fundamental knowledge about how they interact with lipid membranes can be valuable in designing other types of therapeutics or understanding biological systems in general.

Our research is driven by increasing interest in selecting and designing AMPs to target and kill specific pathogens. To accomplish this, we must first develop a fundamental understanding of AMP interactions with eukaryotic and bacterial membranes on a molecular level. Our aims in this study were to:

1. **Develop a method for analysis of quartz crystal microbalance with dissipation monitoring (QCM-D) data** that will enable the **characterization of interactions** between 4 AMPs (chrysophsin-3, indolicidin, alamethicin, SMAP-29) and a zwitterionic membrane that models an eukaryotic membrane. At the start of this study, a method of QCM-D interpretation that could give detailed information about molecular-scale membrane interactions did not exist. We therefore developed an analysis method that helped us derive mechanistic models and infer details about the dynamics of AMP-membrane interactions.
2. **Use atomic force microscopy (AFM) to image AMP-induced changes in a supported lipid membrane** and relate the observed interactions to our mechanistic models derived from QCM-D results. By using AFM to capture visible AMP-induced changes to a lipid membrane, we could validate the QCM-D analysis method developed in Aim 1.
3. **Develop a novel procedure for forming a fully anionic supported lipid bilayer,** which models a Gram-positive bacterial membrane, and **determine the mechanism of action of AMPs** on this membrane. Previous studies have had limited success with forming bilayers composed entirely of lipids with anionic headgroups, which is an invaluable

system for studying Gram-positive bacterial membrane behavior. We developed a simple method for forming these membranes and examined the action of various AMP concentrations on 3 different anionic lipid membrane systems.

The following sections of this document focus on the completion and results of these aims. The implications of this study with respect to understanding AMP-membrane interactions for future applications are also discussed.

1.2 Research summary

Chapter 2 contains a literature review of AMPs and QCM-D. Structural characteristics unique to AMPs are discussed, as well as potential applications and limitations as therapeutics. QCM-D is one of the main techniques used in this study to examine AMP-membrane interactions and the theory behind QCM-D is presented in this chapter. More in-depth data presentation and analysis methods that were developed during this study are introduced in the following chapters.

Chapter 3 represents the culmination of our investigation of AMP action on eukaryotic membrane mimics. The membrane interactions of four peptides: alamethicin, chrysophsin-3, indolicidin, and sheep myeloid antimicrobial peptide (SMAP-29) were examined and related to their unique structural properties. Since previous methods of QCM-D overtone interpretation did not give sufficient information about the structural organization of surface supported membranes that was necessary for our work, we developed a novel method of QCM-D overtone interpretation. This QCM-D analysis technique enabled us to infer detailed information about molecular processes occurring within lipid bilayers during interactions with AMPs.

Chapter 4 describes an in-depth study on chrysophsin-3 action on zwitterionic membranes that laid the groundwork for the work presented in Chapter 3 and is provided for the reader's reference. This chapter discusses the theory behind QCM-D overtone analysis and documents our early work with examining AMP-membrane interactions. The QCM-D results for chrysophsin-3 in this study are included as one of the AMPs presented in Chapter 3.

Chapter 5 documents an in-depth examination of alamethicin action on zwitterionic membranes that built upon the QCM-D analysis process explored in Chapter 4 and is also provided for the reader's reference. In this study, we calculated bilayer and peptide-induced pore properties from QCM-D results, allowing us to further develop our QCM-D interpretation methods. The QCM-D results shown in this study for alamethicin action on zwiitterionic membranes are also presented in Chapter 3 as one of the 4 experimental AMPs.

Chapter 6 presents an AFM study on AMP action on zwitterionic membranes and expands on the work presented in Chapters 3, 4 and 5. AFM imaging of morphological changes in lipid bilayers resulting from exposure to alamethicin and indolicidin was used to validate the suggested models derived from the QCM-D experiments. Visual evidence of pore formation and mass loss from the membrane at concentrations were compared to processes identified in our mechanistic models.

Chapter 7 documents our attempts at developing a technique to create supported lipid membranes composed purely of anionic lipids. We performed a preliminary screening study to examine the bilayer-forming capabilities of various lipid compositions, buffers, vesicle sizes, and surface treatments. Membrane formation was monitored using QCM-D and three successful anionic lipid membrane systems were chosen (based on similarity of the QCM-D responses to those of the zwitterionic lipid membrane formation that was detailed in Chapters 3 and 4) for

further examination and verification of bilayer formation. Chrysophsin-3 action on these anionic lipid films was monitored using QCM-D to demonstrate the capability of these films as bacterial membrane mimics. Interactions between chrysophsin-3 on anionic and zwitterionic membranes were also compared.

Chapter 8 presents the overall conclusions from this project and identifies how the techniques developed in this study can benefit future research. Recommendations are made for future studies on AMP-membrane interactions and the potential for AMP use in therapeutics is discussed.

1.3 References

(1) CDC. (2013) Antibiotic Resistance Threats in the United States, http://www.cdc.gov/drugresistance/threat-report-2013/pdf/ar-threats-2013-2508.pdf.
(2) Phoenix, D. A., Dennison, S. R. and Harris, F., *Antimicrobial Peptides*. 2013, Weinheim: Wiley-VCH.
(3) Peschel, A. and Sahl, H. G. (2006) The co-evolution of host cationic antimicrobial peptides and microbial resistance, *Nat Rev Microbiol 4*, 529-536.
(4) Hoskin, D. W. and Ramamoorthy, A. (2008) Studies on anticancer activities of antimicrobial peptides, *Biochim Biophys Acta 1778*, 357-375.
(5) Harris, F., Dennison, S. R., Singh, J. and Phoenix, D. A. (2011) On the selectivity and efficacy of defense peptides with respect to cancer cells, *Med Res Rev 33*, 190-234.
(6) Afacan, N. J., Yeung, A. T., Pena, O. M. and Hancock, R. E. (2012) Therapeutic potential of host defense peptides in antibiotic-resistant infections, *Curr Pharm Des 18*, 807-819.
(7) Shai, Y. (2002) Mode of action of membrane active antimicrobial peptides, *Biopolymers 66*, 236-248.
(8) Shai, Y. and Oren, Z. (2001) From "carpet" mechanism to de-novo designed diastereomeric cell-selective antimicrobial peptides, *Peptides 22*, 1629-1641.
(9) Huang, H. W. (2000) Action of antimicrobial peptides: two-state model, *Biochemistry 39*, 8347-8352.

Chapter 2

Antimicrobial Peptides and QCM-D

2.1 Antimicrobial peptides

AMPs are naturally occurring molecules that can be chemically synthesized or derived from various organisms, including frogs and moths.[1, 2] Australian tree frogs, for instance, secrete a wealth of AMPs, such as maculatin 1.1, from their skin when exposed to surface electrical shocks or pharmacological stimulation (e.g. adrenaline).[3, 4] Over 2,000 naturally occurring AMPs have been identified and shown to kill a broad spectrum of pathogenic bacteria, fungi, and viruses.[5] Many of these peptides protect their hosts against bacterial infection primarily by disturbing the membrane and causing the cells to lyse. AMPs are thought to be able to target bacteria over mammalian cells due to different membrane characteristics. Detailed knowledge of the mechanism behind AMP action on both bacterial and mammalian cells is essential for developing effective AMPs for use in therapeutics.

AMPs can exhibit a wide range of different structural characteristics that are thought to influence their interactions with cell membranes. Each AMP's unique amino acid sequence may lend charges to the molecule, enabling cationic AMPs to target anionic cell membranes, for example. Techniques such as circular dichroism (CD) and nuclear magnetic resonance (NMR) spectroscopy have been used to determine the secondary structures of antimicrobial peptides.[6-8] Many membrane-active AMPs exhibit random structural conformations in solution and form α-helical structures when in contact with biological membranes.[9] Some cationic AMPs that are rich in cysteine residues, such as protegrins, can adopt β-sheet structures by stabilizing the structure with disulfide bond formation.[5] Other peptides do not exhibit a specific motif due to intramolecular interactions and high concentrations of specific residues that may limit their structure. Indolicidin, for instance, contains a large number of tryptophan residues and assumes a folded, boat-shaped structure due to intramolecular cation-π electron interactions.[8, 10, 11]

Calculating the solvent accessible surface area (ASA) of component amino acid residues using the web-based tool NetsurfP also gives clues about the conformation of AMPs.[12] ASA gives information about the level of exposure or accessibility each amino acid will have with surrounding molecules and is related to the hydrophobicity of the amino acids.

AMPs can also exhibit variations in hydrophobicity, which is derived from the relative hydrophobicities of its component amino acid residues. Various hydrophobicity scales have been developed to describe the relative hydrophobicity of each amino acid. Urry et al., for instance, based their scale on the hydrophobic association between peptides and determined the contribution of each amino acid to the hydrophobic association free energy of a model protein.[13, 14] White et al. developed hydrophobicity scales based on experimentally determined transfer free energies for each amino acid.[15-17] A comparison of prominent hydrophobicity scales showed that the varied methods used to derive these scales resulted in variations in the assignment of relative hydrophobicity values to each amino acid.[18] Some of the values can be correlated across different scales, however, and provide a sense of the relative hydrophobicities of each peptide.

Peptides can differ in hydrophobic moment, which is a measure of amphiphilicity. For an amino acid sequence consisting of N residues, with residue n having the hydrophobicity Φ_n, the hydrophobic moment can be calculated using

$$\mu_H = \lfloor \{\Phi_n \cos(\delta_a n)\}^2 + \{\Phi_n \sin(\delta_a n)\}^2 \rfloor^{1/2} \quad (2.1)$$

where δ_a is the angle (in radians) of the amino acid side chains. The amphiphilic nature of many peptides is believed to enable their interactions with both hydrophilic lipid headgroups and hydrophobic lipid bilayer interiors.[19]

2.2 AMP-membrane interactions

Plasma membranes of bacterial cells differ from those in eukaryotic membranes. The lipid composition of Gram-positive bacterial membranes (e.g. *Staphylococcus aureus*) is predominantly composed of anionic lipids, while that of eukaryotic membranes primarily consists of zwitterionic lipids.[20] Gram-negative bacterial membranes, like those of *Escherichia coli*, contain a mixture of anionic and zwitterionic lipids (Table 2.1). Bacterial membranes are encased by a peptidoglycan layer, which allow particles that are approximately 2 nm in size to pass.[21] Many α-helical peptides such as alamethicin can be modeled as cylinders that are 1.1 nm in diameter and are therefore able to pass through this layer.[22, 23]

Table 2.1. Examples of membrane lipid compositions[a]

	Zwitterionic			**Negatively Charged**			
	PE	PC	SM	PS	PG	DPG	LPG
Erythrocyte membrane		50%	50%				
E. coli (Gram-negative)	82%				6%	12%	
S. aureus (Gram-positive)					57%	5%	38%
PE - phosphatidylethanolamine, PC - phosphatidylcholine, SM - sphingomyelin, PS - phosphatidylserine, PG - phosphatidylglycerol, DPG - diphosphatidylglycerol, LPG – lysophosphatidylglycerol							

[a] Adapted from Blondelle et al.[20]

Gram-negative bacteria also contain an outer membrane that includes lipopolysaccharides (LPS) and proteins. Cationic peptides are able pass through the LPS and outer membrane by interacting with negatively charged divalent-cation-binding sites on the LPS. Once attached, the

bulky AMPs disrupt the barrier properties of the outer membrane, resulting in "cracks" that enable peptides and other molecules to enter.[24]

Two main theories have been proposed to explain how AMPs destabilize bacterial cell membranes. In each case, the peptides first attach to bacterial membranes through electrostatic interactions.[25] In the barrel-stave model, the AMPs insert themselves into the bacterial cell membrane perpendicularly and form a pore (Figure 2.1B).[9, 26] The pores enable large molecules to enter or exit the cell and disrupt ion gradients, causing the cell to die. The carpet model postulates that AMPs align themselves parallel to the membrane surface (Figure 2.1A), which is facilitated by their amphipathicity. AMPs surround the lipids, forming micelles that detach from the lipid membrane (Figure 2.1C). The mechanism is thought to differ among AMPs and is related to the structure and charge of the peptide, as well as the lipid composition of the cell membrane.[27, 28] In some cases, both micelle formation and pore insertion may occur, depending on the peptide-to-lipid concentration ratio.[29] Further studies are required to understand the factors that enable AMP targeting and interactions with bacterial membranes.

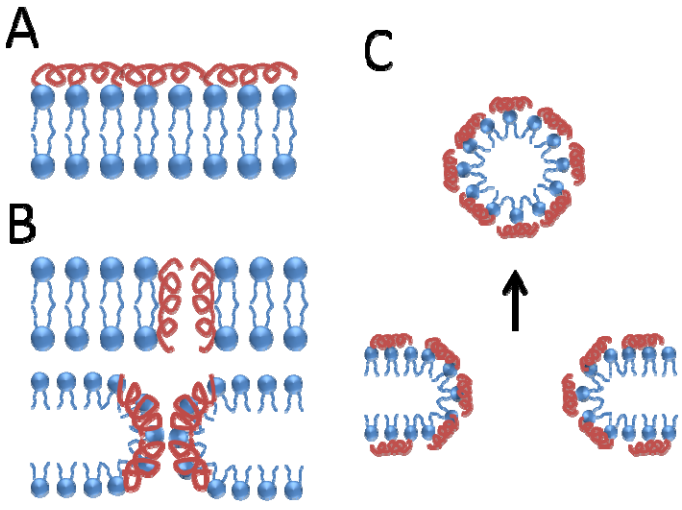

Figure 2.1 Possible mechanisms of AMP action on cell membranes. (A) Surface adsorption, (B) membrane insertion, (C) mass loss from the membrane.

Some AMPs may target intracellular components, such as DNA or ribosomes, once they have passed across the plasma membrane. Indolicidin, for instance, has been found to inhibit protein and nucleic acid synthesis, leading to cell death.[25, 30] Anionic peptides have also been shown to induce flocculation or aggregation of intracellular components.[31] Other peptides may also impede cytoplasmic membrane septum formation during cell division,[30, 32, 33] inhibit cell wall synthesis,[34] or inhibit enzymatic activity.[35, 36]

2.3 Potential applications of AMPs

Infections involving antibiotic-resistant microbes have increased dramatically in recent decades, posing a significant health threat to patients. The short doubling time exhibited in bacteria enables them to evolve quickly, thereby increasing their likelihood of developing drug resistance. In the United States, hospitalizations related to methicillin-resistant *Staphylococcus aureus* (MRSA) more than doubled from 127,036 in 1999 to 278,203 in 2005.[37] AMPs are being studied as an alternative to antibiotics, therapeutically and in self-decontaminating surfaces.[38] Due to the nature of the mechanism of interaction, membrane-active AMPs are less prone to the development of pathogen resistance than antibiotics. Bacterial resistance to antibiotics typically occurs when bacteria (a) are able to alter cellular components to that certain antibiotics cannot reach or interact with its intracellular target or (b) induce chemical modification and subsequent inactivation of the antibiotic.[39] By targeting bacterial cell membranes (based on membrane charge, which is difficult for cells to change) and relying on membrane destabilization to kill cells, membrane-active AMPs do not easily induce bacterial resistance.

Potential uses for AMPs also include wound healing applications. The human cathelicidin antimicrobial peptide LL37, for example, has been found to promote wound healing through re-epithelialization and vascularization. Wounds in mice that were treated with LL37 formed a higher number of new blood vessels.[40]

Interest in AMP-coated surfaces has also increased recently due to public health concerns related to pathogenic bacteria. Self-decontaminating materials may be incorporated into children's toys, medical devices, and instruments used in the food-industry to kill hazardous pathogens.[38] Previous studies in our lab have shown that certain orientations of the AMP, cecropin P1, attached to a surface may facilitate binding and killing of bacteria.[41] Another study

from our lab has also shown that peptides that are chemically linked to a surface are more effective in killing bacteria than adsorbed AMPs.[42]

Regardless of the application, one of the primary gaps in knowledge that limits AMP use is its exact mechanism of interaction. *Understanding this mechanism and how it is affected by AMP structure will facilitate the selection and design of more effective AMPs for targeting specific pathogens.* Detailed information about how specific amino acid combinations can affect AMP action may also allow them to be combined with other drugs to create therapeutics with multiple types of antimicrobial activity. These multi-faceted, or "dirty" drugs would further decrease the risk of developing resistance and are being considered for the treatment of complex diseases such as cancer.[43, 44]

2.4 Limitations as therapeutics

Despite showing promise as antimicrobial agents, AMPs have not been approved for use in therapeutics. Indolicidin- and magainin-based topical drugs have demonstrated efficacy in treating infections, but failed during Phase III clinical trials due to safety concerns or failing clinical endpoints due to low numbers of enrolled patients.[45, 46] Problems with commercialization primarily stem from issues such as peptide stability *in vivo*, high cost, and toxicity to eukaryotic cells at bactericidal concentrations.[47, 48] Peptides can be susceptible to proteolysis by enzymes present in bodily fluids and if taken orally, may be broken down in the digestive tract if not protected. Synthetic peptides are also expensive to produce and are 100-500 times more expensive than conventional antibiotics.[45] Therefore, identifying structural characteristics of AMPs that allow them to be effective at lower concentrations will be crucial for making AMP therapeutics more affordable.

Although AMP activity is largely targeted towards bacteria, the effects of these same AMPs on mammalian cells are not well known. Studies have shown promising results that indicate that some AMPs are more destructive to bacteria than eukaryotic cells at low concentrations. The AMP chrysophsin-1 which is lethal to *E. coli* at a peptide concentration of 0.25 μM, for example, is only toxic to cultured human lung fibroblasts at the higher concentration of EC_{50} = 4.6 μM (half maximal effective concentration).[6, 49] NMR experiments revealed that chrysophsin-1 attached to the cell membranes, aligning parallel to the membrane surface and disrupting the lipid bilayer structure.[49] Melittin, however, is toxic to mouse fibroblast and human erythrocyte cells at a minimum inhibitory concentration (MIC) of 1 μM, but requires higher concentrations (3-6 μM) to kill Gram-positive and Gram-negative bacteria (also hypothesized to occur through membrane destabilization).[50] Jacob et al. have synthesized sheep myeloid antimicrobial peptide (SMAP) analogs that retained the original peptide's antimicrobial effectiveness and reduced hemolytic activity.[51] More research is needed to examine the effects of more AMPs on eukaryotic cells to determine if they can be altered to be less toxic to mammalian cells while retaining their antimicrobial activity.

2.5 Quartz crystal microbalance with dissipation monitoring (QCM-D)

Using quartz crystal microbalance with dissipation monitoring (QCM-D), we can monitor real-time mass and viscoelasticity changes during AMP exposure to a supported lipid membrane with a sensitivity of ~1.8 ng/cm^2 in liquid. Inside the QCM-D chamber, mass (e.g. lipids) is added to the surface of an oscillating quartz sensor crystal (Figure 2.2) while measuring changes in frequency (Δf) and energy dissipation (ΔD) of the crystal due to alterations in the film.

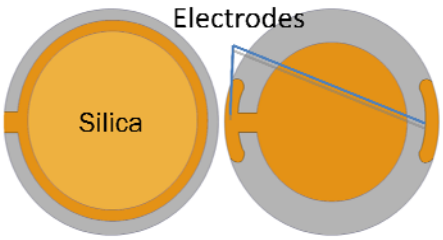

Figure 2.2. Diagram showing both faces of a QCM-D sensor crystal. Mass is deposited on the silica surface and the electrodes enable voltage to be applied to the crystal to induce oscillation.

The Sauerbrey equation describes the relationship between Δf and change in mass (Δm) in a rigid film:

$$\Delta f = \frac{-2f_0^2}{A\sqrt{\rho_q \mu_q}} \Delta m \tag{2.2}$$

where f_0 is the resonant frequency of the quartz crystal (5 MHz), A is the piezoelectrically active crystal area, ρ_q is the density of quartz (2.648 g/cm^3), and μ_q is the shear modulus of the crystal (2.947 x 10^{11} g/cm·s^2). Therefore, the change in frequency is inversely related to the change in mass attached to the sensor. In the case of a less rigid film, such as the films used in this study, the frequency is still inversely related to mass, but the Sauerbrey equation must be adjusted to reflect the effects of a viscoelastic film and the bulk solution.[52, 53] Also, since QCM-D measurements are taken at consistent time intervals (0.7 s), the rate of frequency change (related to mass change) can be derived from these measurements.

Changes in dissipation are related to the rigidity of the film and can be described by

$$D = \frac{G''}{2\pi G'} \tag{2.3}$$

where G" is the loss modulus and G' is the storage modulus. A softer film will result in a larger *D*.

Several different frequency overtones, or harmonics, are measured and can be related to processes throughout the film. Overtone analysis has been used by Mechler et al. to infer details about the fundamental mechanisms behind AMP action on supported bilayers.[54] The penetration depth, δ, of an acoustic wave can be found:

$$\delta = \left(\frac{\eta_f}{n\pi f_0 \rho_f}\right)^{1/2} \tag{2.4}$$

where η_f is the viscosity of the film, n is the overtone number, and ρ_f is the density of the film.[55] As a result, higher overtones can be related to processes closer to the sensor surface. Larger frequency decreases at the 3rd overtone, for instance, indicate that mass has been added to the surface of the mass, farthest from the sensor surface. Similar Δf and ΔD values at all overtones indicate a homogeneous change in mass and viscoelasticity of the membrane on the crystal's surface.

In this study, QCM-D measurements were taken in liquid after the instrument was allowed to equilibrate in buffer to establish stable f and D baselines. Lipid vesicle solutions were then flowed over the QCM-D sensors until stable lipid bilayers were formed, as detailed in Chapters 3-5 (representative QCM-D traces shown in Figure 2.3). Buffer was injected to remove weakly attached particles from the bilayers, which was followed by the addition of an AMP solution of the desired concentration. The AMP solution was allowed to flow for 10 minutes to insure that the QCM-D chamber was filled with the correct concentration and the flow was paused for 1 h for the AMP action occur and equilibrate. Finally, the chamber was rinsed with

buffer and the changes in frequency (Δf) and dissipation (ΔD) resulting from AMP exposure were determined (Δf = (final f) – (f at time point 4)).

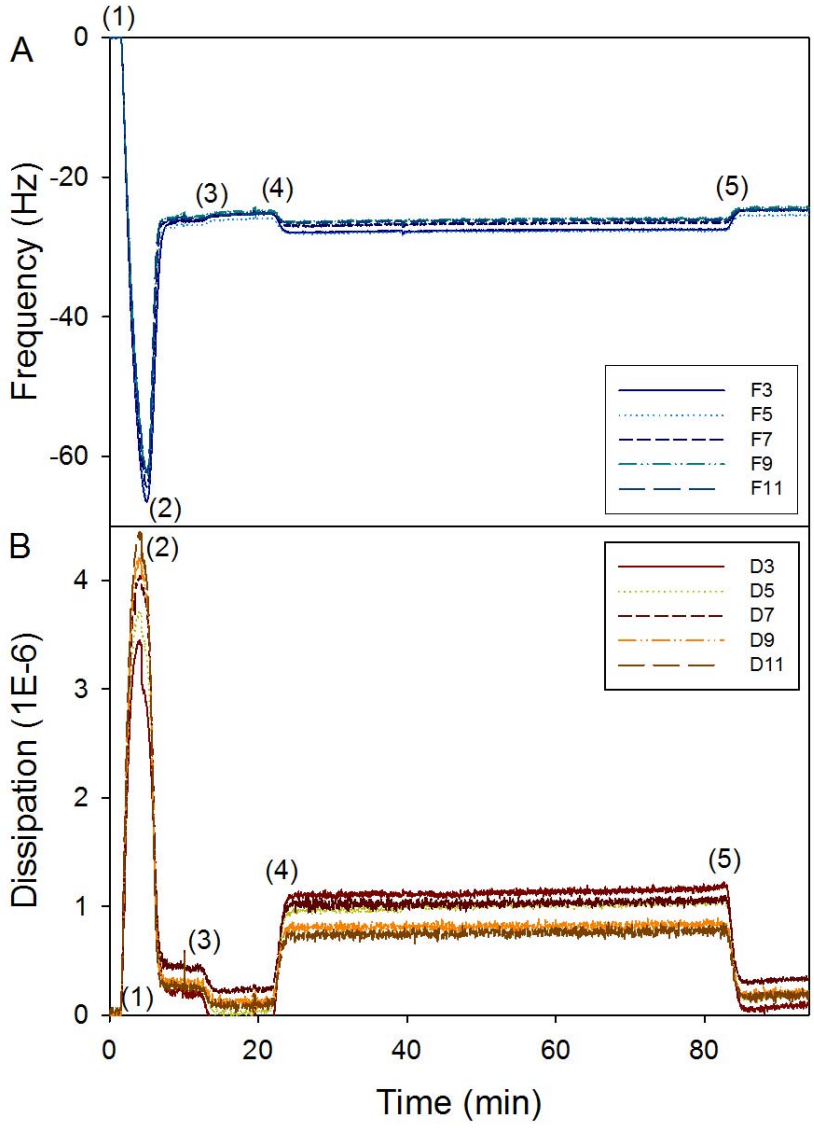

Figure 2.3. Typical frequency and dissipation measurements taken during an experiment examining AMP interactions with membranes. (1) Injection of lipid vesicle solution, (2) vesicle ruptures into a supported lipid bilayer on the QCM-D sensor surface, (3) buffer rinse, (4) injection of AMP solution, and (5) final buffer rinse.

Monitoring overtone similarity can provide information about the mechanism of action of AMPs on a lipid bilayer surface. Initial adsorption of AMPs onto the membrane surface will result in non-homogeneous negative Δf values at lower overtones (e.g. 3rd) if no other action occurs (Figure 2.4A). The barrel-stave model for peptide-membrane interactions should therefore result in uniformly negative Δ*f* values at all overtones, which would represent cylindrical pore formation (Figure 2.4B). In the case of toroidal pore formation, however, more lipids would be lost at the top and bottom of the bilayer and replaced by pore-forming peptides, resulting in heterogeneous frequency changes at different overtones. Combinations of membrane surface adsorption and pore formation will result in non-uniform Δ*f* results across overtones. Given that a full phosphatidylcholine (PC) lipid bilayer (~5 nm thick) assembled on a clean QCM-D crystal corresponds with a Δ*f* of ~-26 Hz, we can calculate the approximate Δ*f* due to adsorption of a monolayer of α-helical peptides (~1.2 nm thick) to be ~2-4 Hz.[56, 57] Therefore, if the carpet model is operative, membrane lysis will be demonstrated through uniform positive Δ*f* values up to 26 Hz at all overtones (Figure 2.4C).

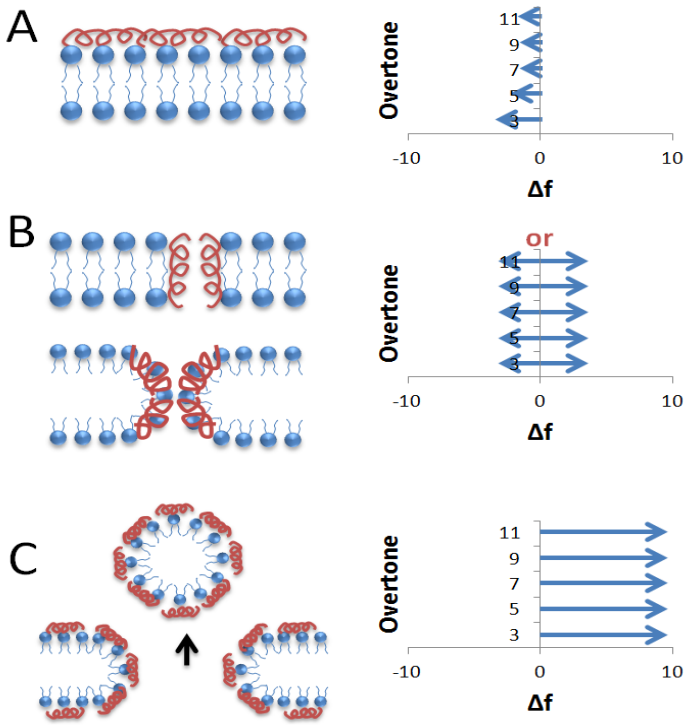

Figure 2.4. Expected frequency responses corresponding with various models of AMP-membrane interactions. (A) Peptide (shown in red) adsorption on the lipid bilayer (blue) surface, (B) cylindrical and toroidal pore formation through peptide insertion into the membrane, (C) mass loss from the membrane through removal of lipid-peptide aggregates.

The equations presented in this chapter represent the fundamental theory behind QCM-D measurements and overtone analysis. A more detailed discussion of QCM-D data interpretation that was developed in the following studies is presented in Chapters 3, 4, and 5.

2.6 References

(1) Skarnes, R. C. and Watson, D. W. (1957) Antimicrobial factors of normal tissues and fluids, *Bacteriol Rev 21*, 273-294.
(2) Gazit, E., Miller, I. R., Biggin, P. C., Sansom, M. S. and Shai, Y. (1996) Structure and orientation of the mammalian antibacterial peptide cecropin P1 within phospholipid membranes, *J Mol Biol 258*, 860-870.
(3) Bevins, C. L. and Zasloff, M. (1990) Peptides from frog skin, *Annu Rev Biochem 59*, 395-414.
(4) Simmaco, M., Mignogna, G. and Barra, D. (1998) Antimicrobial peptides from amphibian skin: what do they tell us?, *Biopolymers 47*, 435-450.

(5) Phoenix, D. A., Dennison, S. R. and Harris, F., *Antimicrobial Peptides*. 2013, Weinheim: Wiley-VCH.
(6) Iijima, N., Tanimoto, N., Emoto, Y., Morita, Y., Uematsu, K., Murakami, T. and Nakai, T. (2003) Purification and characterization of three isoforms of chrysophsin, a novel antimicrobial peptide in the gills of the red sea bream, Chrysophrys major, *Eur J Biochem 270*, 675-686.
(7) McManus, A. M., Otvos, L., Jr., Hoffmann, R. and Craik, D. J. (1999) Conformational studies by NMR of the antimicrobial peptide, drosocin, and its non-glycosylated derivative: effects of glycosylation on solution conformation, *Biochemistry 38*, 705-714.
(8) Rozek, A., Friedrich, C. L. and Hancock, R. E. (2000) Structure of the bovine antimicrobial peptide indolicidin bound to dodecylphosphocholine and sodium dodecyl sulfate micelles, *Biochemistry 39*, 15765-15774.
(9) Shai, Y. (2002) Mode of action of membrane active antimicrobial peptides, *Biopolymers 66*, 236-248.
(10) Hsu, C. H., Chen, C., Jou, M. L., Lee, A. Y., Lin, Y. C., Yu, Y. P., Huang, W. T. and Wu, S. H. (2005) Structural and DNA-binding studies on the bovine antimicrobial peptide, indolicidin: evidence for multiple conformations involved in binding to membranes and DNA, *Nucleic Acids Res 33*, 4053-4064.
(11) Khandelia, H. and Kaznessis, Y. N. (2007) Cation-pi interactions stabilize the structure of the antimicrobial peptide indolicidin near membranes: molecular dynamics simulations, *J Phys Chem B 111*, 242-250.
(12) Petersen, B., Petersen, T. N., Andersen, P., Nielsen, M. and Lundegaard, C. (2009) A generic method for assignment of reliability scores applied to solvent accessibility predictions, *BMC Struct Biol 9*, 51.
(13) Urry, D. W. (1997) Physical chemistry of biological free energy trasduction as demonstrated by elastic protein-based polymers, *J. Phys. Chem. B 101*, 11007-11028.
(14) Urry, D. W. (2004) The change in Gibbs free energy for hydrophobic association: Derivation and evaluation by means of inverse temperature transitions, *Chemical Physics Letters 399*, 177-183.
(15) Wimley, W. C. and White, S. H. (1996) Experimentally determined hydrophobicity scale for proteins at membrane interfaces, *Nat Struct Biol 3*, 842-848.
(16) Wimley, W. C., Creamer, T. P. and White, S. H. (1996) Solvation energies of amino acid side chains and backbone in a family of host-guest pentapeptides, *Biochemistry 35*, 5109-5124.
(17) White, S. H. and Wimley, W. C. (1999) Membrane protein folding and stability: physical principles, *Annu Rev Biophys Biomol Struct 28*, 319-365.
(18) Wang, K. F., Nagarajan, R. and Camesano, T. A. (submitted) Comparison of peptide structure-lipid bilayer interactions for alamethicin, chrysophsin-3, indolicidin and SMAP-29: Differentiation through QCM-D signatures,
(19) Kaiser, E. T. and Kezdy, F. J. (1987) Peptides with affinity for membranes, *Annu Rev Biophys Biophys Chem 16*, 561-581.
(20) Blondelle, S. E., Lohner, K. and Aguilar, M. (1999) Lipid-induced conformation and lipid-binding properties of cytolytic and antimicrobial peptides: determination and biological specificity, *Biochim Biophys Acta 1462*, 89-108.
(21) Demchick, P. and Koch, A. L. (1996) The permeability of the wall fabric of Escherichia coli and Bacillus subtilis, *J Bacteriol 178*, 768-773.

(22) Qian, S., Wang, W., Yang, L. and Huang, H. W. (2008) Structure of the alamethicin pore reconstructed by x-ray diffraction analysis, *Biophys J 94*, 3512-3522.
(23) Wang, K. F., Nagarajan, R. and Camesano, T. A. (2014) Antimicrobial peptide alamethicin insertion into lipid bilayer: A QCM-D exploration, *Colloids Surf B Biointerfaces 116*, 472-481.
(24) Hancock, R. E. and Chapple, D. S. (1999) Peptide antibiotics, *Antimicrob Agents Chemother 43*, 1317-1323.
(25) Brogden, K. A. (2005) Antimicrobial peptides: pore formers or metabolic inhibitors in bacteria?, *Nat Rev Microbiol 3*, 238-250.
(26) Pouny, Y., Rapaport, D., Mor, A., Nicolas, P. and Shai, Y. (1992) Interaction of antimicrobial dermaseptin and its fluorescently labeled analogues with phospholipid membranes, *Biochemistry 31*, 12416-12423.
(27) Shai, Y. and Oren, Z. (2001) From "carpet" mechanism to de-novo designed diastereomeric cell-selective antimicrobial peptides, *Peptides 22*, 1629-1641.
(28) Shai, Y. (1999) Mechanism of the binding, insertion and destabilization of phospholipid bilayer membranes by alpha-helical antimicrobial and cell non-selective membrane-lytic peptides, *Biochim Biophys Acta 1462*, 55-70.
(29) Huang, H. W. (2000) Action of antimicrobial peptides: two-state model, *Biochemistry 39*, 8347-8352.
(30) Subbalakshmi, C. and Sitaram, N. (1998) Mechanism of antimicrobial action of indolicidin, *FEMS Microbiol Lett 160*, 91-96.
(31) Brogden, K. A., De Lucca, A. J., Bland, J. and Elliott, S. (1996) Isolation of an ovine pulmonary surfactant-associated anionic peptide bactericidal for Pasteurella haemolytica, *Proc Natl Acad Sci U S A 93*, 412-416.
(32) Shi, J., Ross, C. R., Chengappa, M. M., Sylte, M. J., McVey, D. S. and Blecha, F. (1996) Antibacterial activity of a synthetic peptide (PR-26) derived from PR-39, a proline-arginine-rich neutrophil antimicrobial peptide, *Antimicrob Agents Chemother 40*, 115-121.
(33) Salomon, R. A. and Farias, R. N. (1992) Microcin 25, a novel antimicrobial peptide produced by Escherichia coli, *J Bacteriol 174*, 7428-7435.
(34) Brotz, H., Bierbaum, G., Leopold, K., Reynolds, P. E. and Sahl, H. G. (1998) The lantibiotic mersacidin inhibits peptidoglycan synthesis by targeting lipid II, *Antimicrob Agents Chemother 42*, 154-160.
(35) Andreu, D. and Rivas, L. (1998) Animal antimicrobial peptides: an overview, *Biopolymers 47*, 415-433.
(36) Otvos, L., Jr., O, I., Rogers, M. E., Consolvo, P. J., Condie, B. A., Lovas, S., Bulet, P. and Blaszczyk-Thurin, M. (2000) Interaction between heat shock proteins and antimicrobial peptides, *Biochemistry 39*, 14150-14159.
(37) Klein, E., Smith, D. L. and Laxminarayan, R. (2007) Hospitalizations and deaths caused by methicillin-resistant Staphylococcus aureus, United States, 1999-2005, *Emerg Infect Dis 13*, 1840-1846.
(38) Fulmer, P. A., Lundin, J. G. and Wynne, J. H. (2010) Development of antimicrobial peptides (AMPs) for use in self-decontaminating coatings, *ACS Appl Mater Interfaces 2*, 1266-1270.
(39) Benveniste, R. and Davies, J. (1973) Mechanisms of antibiotic resistance in bacteria, *Annu Rev Biochem 42*, 471-506.

(40) Ramos, R., Silva, J. P., Rodrigues, A. C., Costa, R., Guardao, L., Schmitt, F., Soares, R., Vilanova, M., Domingues, L. and Gama, M. (2011) Wound healing activity of the human antimicrobial peptide LL37, *Peptides 32*, 1469-1476.
(41) Strauss, J., Kadilak, A., Cronin, C., Mello, C. M. and Camesano, T. A. (2010) Binding, inactivation, and adhesion forces between antimicrobial peptide cecropin P1 and pathogenic E. coli, *Colloids Surf B Biointerfaces 75*, 156-164.
(42) Ivanov, I. E., Morrison, A. E., Cobb, J. E., Fahey, C. A. and Camesano, T. A. (2012) Creating antibacterial surfaces with the peptide chrysophsin-1, *ACS Appl Mater Interfaces 4*, 5891-5897.
(43) Peschel, A. and Sahl, H. G. (2006) The co-evolution of host cationic antimicrobial peptides and microbial resistance, *Nat Rev Microbiol 4*, 529-536.
(44) Frantz, S. (2005) Drug discovery: playing dirty, *Nature 437*, 942-943.
(45) Eckert, R. (2011) Road to clinical efficacy: challenges and novel strategies for antimicrobial peptide development, *Future Microbiol 6*, 635-651.
(46) Fox, J. L. (2013) Antimicrobial peptides stage a comeback, *Nat Biotechnol 31*, 379-382.
(47) Hancock, R. E. and Sahl, H. G. (2006) Antimicrobial and host-defense peptides as new anti-infective therapeutic strategies, *Nat Biotechnol 24*, 1551-1557.
(48) Tew, G. N., Scott, R. W., Klein, M. L. and Degrado, W. F. (2010) De novo design of antimicrobial polymers, foldamers, and small molecules: from discovery to practical applications, *Acc Chem Res 43*, 30-39.
(49) Mason, A. J., Bertani, P., Moulay, G., Marquette, A., Perrone, B., Drake, A. F., Kichler, A. and Bechinger, B. (2007) Membrane interaction of chrysophsin-1, a histidine-rich antimicrobial peptide from red sea bream, *Biochemistry 46*, 15175-15187.
(50) Javadpour, M. M., Juban, M. M., Lo, W. C., Bishop, S. M., Alberty, J. B., Cowell, S. M., Becker, C. L. and McLaughlin, M. L. (1996) De novo antimicrobial peptides with low mammalian cell toxicity, *J Med Chem 39*, 3107-3113.
(51) Jacob, B., Kim, Y., Hyun, J. K., Park, I. S., Bang, J. K. and Shin, S. Y. Bacterial killing mechanism of sheep myeloid antimicrobial peptide-18 (SMAP-18) and its Trp-substituted analog with improved cell selectivity and reduced mammalian cell toxicity, *Amino Acids 46*, 187-198.
(52) Kanazawa, K. K., Gordon II, J.G. (1985) The oscillation frequency of a quartz resonator in contact with liquid., *Analytica Chimica Acta 175*, 99-105.
(53) Voinova, M. V., Jonson, M. and Kasemo, B. (2002) Missing mass effect in biosensor's QCM applications, *Biosens Bioelectron 17*, 835-841.
(54) Mechler, A., Praporski, S., Atmuri, K., Boland, M., Separovic, F. and Martin, L. L. (2007) Specific and selective peptide-membrane interactions revealed using quartz crystal microbalance, *Biophys J 93*, 3907-3916.
(55) Voinova, M. V., Rodahl, M., Jonson, M., Kasemo, B. (1999) Viscoelastic acoustic response of layered polymer films at fluid-solid interfaces: continuum mechanics approach, *Physica Scripta 59*, 391-396.
(56) Keller, C. A. and Kasemo, B. (1998) Surface specific kinetics of lipid vesicle adsorption measured with a quartz crystal microbalance, *Biophys J 75*, 1397-1402.
(57) Cremer, P. S. a. B., Steven, G. (1999) Formation and spreading of lipid bilayers on planar glass supports, *J. Phys. Chem. 103*, 2554-2559.

Chapter 3

Comparison of peptide structure-lipid bilayer interactions for alamethicin, chrysophsin-3, indolicidin and SMAP-29: Differentiation through QCM-D signatures

3.1 Abstract

Many antimicrobial peptides (AMPs) are thought to kill bacteria by attaching to cell membranes and disrupting the lipid bilayer structure. They act either by creating stable pores through which ions and molecules may travel or by destroying the membrane through lipid removal. Although many studies have confirmed the pore formation and membrane lysis caused by the AMPs, the direct relationship between AMP structural characteristics and its mechanism of membrane interaction are not yet well understood. In this study, we have used quartz crystal microbalance with dissipation monitoring (QCM-D) to probe the interactions between a phosphatidylcholine (PC) supported bilayer membrane and the four peptides: alamethicin, chrysophsin-3, indolicidin, and sheep myeloid antimicrobial peptide (SMAP-29), with the goal of identifying QCM-D signatures that clearly differentiate the mechanism of action of these peptides. Multiple signatures from the QCM-D measurements were extracted that provided information on peptide addition to and lipid removal from the membrane, the dynamics of their interactions and the rates at which the peptide actions are initiated. The QCM-D signatures were interpreted in terms of molecular processes including pore formation, surface adsorption of peptide, and the insertion of the peptide or peptide aggregate into the bilayer. We found that the membrane interactions of each peptide involved a different sequence of molecular processes. These mechanistic variations in peptide action were related to the fundamental structural properties of the peptides including the number of amino acids, net charge, hydrophobicity, hydrophobic moment, accessible surface area and the probability of α-helical secondary structures. The study demonstrates that QCM-D provides a rich collection of unique signatures capable of differentiating the detailed mechanism of action of antimicrobial peptides.

3.2 Introduction

Antimicrobial peptides (AMPs) are pathogen-killing molecules that were originally derived from various organisms, including frogs and moths.[1, 2] They are known to kill a broad spectrum of pathogenic bacteria, fungi, and viruses. AMPs are believed to kill bacteria by destabilizing bacterial membranes or translocating through the membranes to interact with intracellular targets. Because of the nature of these interactions, pathogenic bacteria are less able to develop resistance against the membrane-active AMPs, in contrast to the ease of developing antibiotic resistance. A bacterium must substantially change the characteristics of its membrane if it has to succeed in developing resistance to AMPs, but because the lipids are highly conserved in microorganisms, this possibility appears remote.[3-5] This unusual property of low or no susceptibility to development of AMP resistance by the microorganisms has stimulated major research efforts to chemically synthesize AMPs replicating some of the structural features of the naturally occurring AMPs, with the expectation of reproducing their mechanism of action in killing bacteria for practical applications.

The membrane-destabilizing mechanisms exhibited by AMPs are thought to fall into one of several categories. Many membrane-active peptides have been shown to insert into lipid bilayers and create pores using a mechanism described by the barrel-stave model.[6] These pores have been detected by studying voltage-dependent conductance that occurs via transmembrane channels that are created as a result of peptide insertion.[7, 8] The AMPs may also disrupt cell membranes by first attaching to the surface and forming lipid-peptide aggregates, which then leave the membrane causing lysis, in a mechanism described by the carpet model. Variations of these models have also been developed. For instance, the barrel-stave cylindrical pores, in which the edges are lined by perpendicularly-oriented peptides, may be distinguished from toroidal

pores, in which the pore edges consist of peptides and lipid head groups that bend continuously from the top bilayer leaflet to the bottom bilayer.[9] The mechanism of interaction between a peptide and a cell membrane may follow any one or a combination of these molecular events, depending on the type of peptide and lipid present in the system.

Peptide characteristics of secondary structure, charge, and hydrophobicity are usually thought to play substantial roles in determining AMPs' mechanisms of action on a cell membrane.[10] Studies have shown that increased helicity in AMPs can be correlated with increased antibacterial activity.[11, 12] The cationic nature of AMPs is also thought to play a large role in their ability to target negatively charged bacterial cell membranes. Electrostatic interactions are largely responsible for drawing cationic AMPs to anionic bacterial cell membranes. If the membrane is primarily made up of zwitterionic lipids, then the strong ionic attractions that exist between the anionic lipid membranes and the AMP are replaced by relatively weaker attractive interactions between the dipoles of the neutral membrane and the charges on the AMP. In this case, the hydrophobicity of the peptide may become a more significant factor in determining antimicrobial activity. Hydrophobicity has been shown to affect the antibacterial and hemolytic activity of AMPs, but the correlation with antibacterial activity may not be strong.[10, 13-17] Although numerous studies in the literature have examined the relationship between AMP structure and antibacterial or hemolytic activity (represented by experimentally determined minimum inhibitory concentrations), less is known about how the structure of the AMP and its resulting physicochemical properties determine the specific mechanism of interaction with cell membranes.

Table 3.1 Characteristics and Natural Sources of Various Antimicrobial Peptides

Peptide	Number of Amino Acids	Predominant Secondary Structure[a]	Nominal Charge at pH 7	Comments
Alamethicin	20	α-helix[18]	0 [19]	Contains unnatural amino acids aminoisobutyric acid and phenylalaninol
Chrysophsin-3	20	α-helix[20]	+4 [21]	
Indolicidin	13	Folded, boat-shaped conformation[22]	+4 [23]	Smallest peptide with dominant presence of tryptophan and proline
SMAP-29	29	α-helix[24]	+10 [25]	Cysteine was attached at the c-terminus to support other research

[a]The secondary structures mentioned in the literature for the peptides.

To discover the mechanistic variations between different AMPs, four molecules, alamethicin, chrysophsin-3, indolicidin, and sheep myeloid antimicrobial peptide (SMAP-29), with varying secondary structure, charge, and hydrophobicity were chosen for this study (Table 3.1). The helical wheel diagrams for these four peptides are shown in Figure 3.1. This diagram provides a projection of amino acids perpendicular to the helix long axis assuming that the peptide exists in an α-helical secondary structure. Since the α-helix contains 3.6 residues per turn, adjacent residues on the peptide are separated by 100^{o} on the helical wheel. The extent of separation of the hydrophobic and hydrophilic residues on the wheel either confirms or rejects the possible existence of the peptide in the α-helical secondary structure. The helical wheel representation of α-helical alamethicin, for example, reveals that its non-polar (shown in blue) amino acid side chains are positioned on one side of the wheel, enabling the α-helical conformation to create a non-polar section in the peptide. Indolicidin does not show clustering of

non-polar side chains and, in fact, exhibits a folded conformation, rather than an α-helical structure.

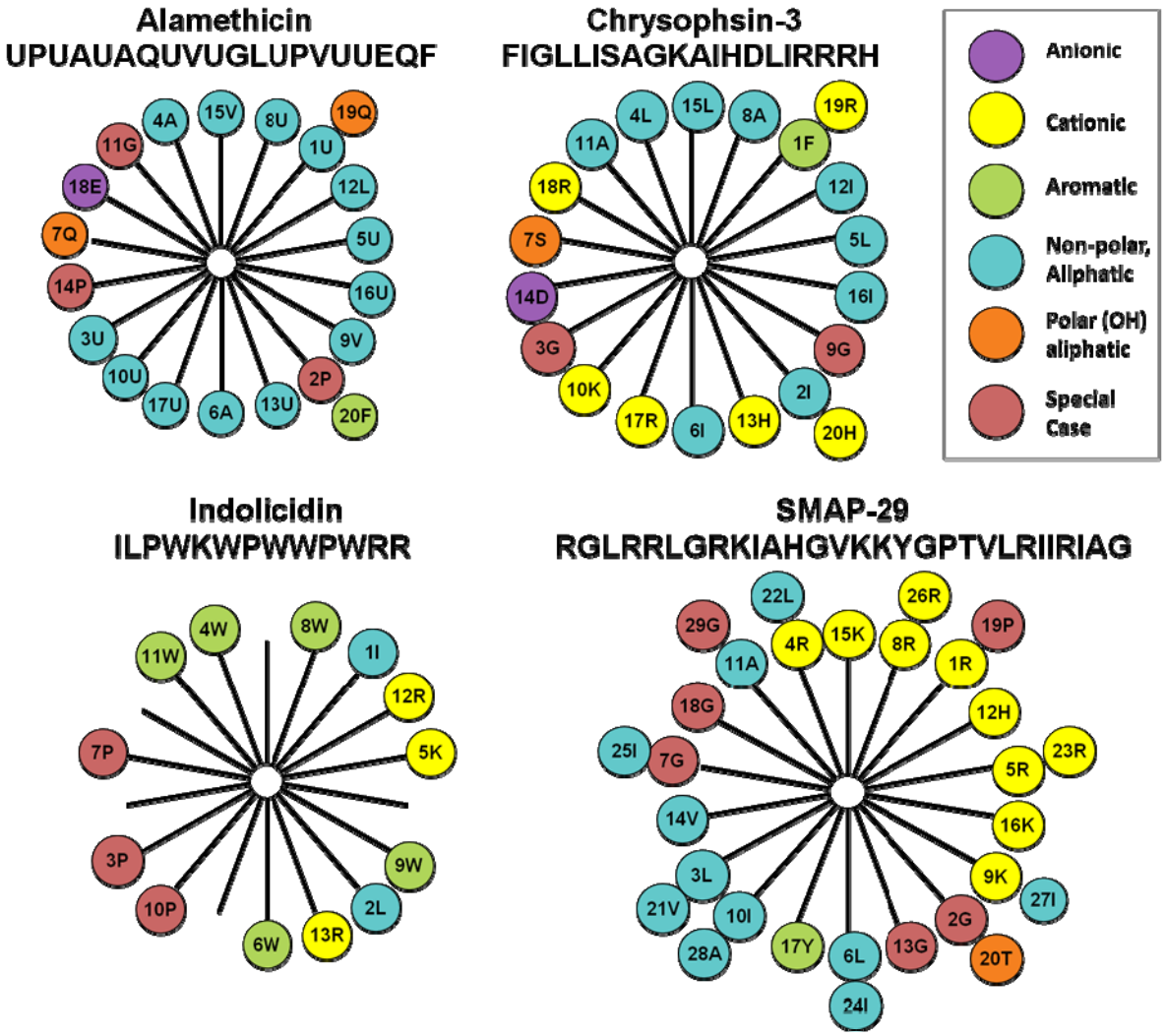

Figure 3.1. Helical wheel diagrams for alamethicin, chrysophsin-3, indolicidin, and SMAP-29. α-Aminoisobutyric acid and L-phenylalaninol are represented by "U" and "F," respectively. These diagrams reveal differences in the placement of charged amino acid residues, as well as hydrophobic and polar side chains. "Special Case" amino acids exhibit unique properties, such as being able to form disulfide bonds (cysteine) or being more flexible than other amino acids (glycine).

The first AMP, alamethicin, is a 20-amino-acid, α-helical peptide that is derived from the fungus *Trichoderma viride* and is known to insert into membranes at higher concentrations, forming well-defined cylindrical pores.[26-28] The structure of alamethicin is unique because it

includes two amino acids that are rarely found in nature, aminoisobutyric acid and L-phenylalaninol. Alamethicin contains a negative charge associated with the glutamic acid residue near the C-terminus. However, this side chain is typically protonated when the peptide is oriented in a transmembrane state, making alamethicin's net charge effectively zero in a peptide-lipid membrane system.[19] The helical wheel diagram shows a clear separation between the dominant hydrophobic face and a smaller polar face in the alpha-helical structure for this peptide.

Chrysophsin-3, another 20-amino-acid AMP, is derived from the gills of the red sea bream, *Chyrsophrys major*.[20] It also assumes an α-helical structure when in contact with a biological membrane and is amphipathic. Chrysophsin-3 exhibits a positive net charge of +4, which differentiates it from alamethicin.[21] Again in this case, the helical wheel diagram shows a clear separation between the dominant hydrophobic face and a polar charged face in the alpha-helical structure for this peptide.

Indolicidin, a 13-residue AMP derived from bovine neutrophils, is one of the smallest of the known naturally occurring linear peptides.[29] Indolicidin's amino acid content is quite remarkable because of its five tryptophan and three proline residues. Indolicidin carries a net charge of +4 at pH 7 and assumes a specific coiled and folded conformation when in contact with a cell membrane, unlike the α-helical or β-sheet conformations formed by most other AMPs.[23, 30] Intramolecular cation-π electron interactions allow it to assume a folded, boat-shaped conformation with positive charges at the peptide termini and a hydrophobic core.[22, 31, 32] Studies have shown that indolicidin does not cause hemolytic lysis at concentrations below 30 μM.[33] The helical wheel diagram shows a separation of hydrophobic and hydrophilic residues but the large

presence of prolines in this small peptide prevent it from assuming a α-helical secondary structure.

Sheep myeloid antimicrobial peptide (SMAP-29) is a cationic AMP composed of 29 amino acids that carries a +10 net charge at pH 7.[25] Its structure is predominantly α-helical, with the hydrophobic residues aligned along one side and the polar residues along the other[24, 34, 35] as can be seen from the helical wheel diagram. The SMAP-29 used in our study contains a terminal cysteine residue, which was introduced to support other research where the AMP was attached to fluorescent dyes or other surfaces through the sulfhydryl functionality of cysteine.[36, 37] The presence of the terminal cysteine could possibly give rise to the formation of SMAP dimers in solution through disulfide bonding. Bulky dimers could interact with lipid membranes differently than SMAP-29 monomers and would contribute more mass when attaching to the membranes. The presence of large peptide aggregates could be detected with dynamic light scattering experiments to determine the particle sizes in solution. β-mercaptoethanol could also be added to the AMP solution to reverse dimerization and QCM-D experiments could be conducted to determine if the interaction mechanisms changed as a result.

We used quartz-crystal microbalance with dissipation monitoring (QCM-D) to follow AMP interactions with lipid membranes in real-time and to search for QCM-D signatures specific to each peptide. Nanoscale changes in mass and viscoelasticity of a solid surface-supported lipid bilayer can be monitored by the changes in frequency (Δf) and energy dissipation (ΔD), respectively, of a sensor on which the bilayer is assembled.[37-43] Multiple frequency overtones, or harmonics, can also be measured and related to homogeneity of processes through the depth of the bilayer. Due to varying penetration depths of the different overtones, higher overtones are correlated with processes occurring closer to the sensor surface.[38] Similar Δf and

ΔD values at all overtones indicate a homogeneous change in mass and viscoelasticity of the membrane on the crystal's surface. Overtone analysis was pioneered by Mechler et al. to infer details about the fundamental mechanisms behind AMP action on supported bilayers.[39]

Since the formation of highly reproducible bilayers has been demonstrated for zwitterionic phospholipids,[41-43] we have used PC as the lipid in all the experiments reported and discussed here. Egg PC was chosen for the model membrane because we were able to form supported lipid bilayers (SLBs) consistently from PC vesicles using the method described previously.[40]

Further, monitoring the dynamic behavior of AMPs on lipid membranes has typically been difficult, due to the small scale of these interactions. However, QCM-D offers some information on the dynamics of the process because of the real time monitoring of very small mass and dissipation changes. Information about specific structural characteristics of each AMP, such as charge and hydrophobicity, were also gathered and compared with the QCM-D results to correlate peptide structural characteristics with their membrane interactions. Since we have already reported on the QCM-D studies on chrysophsin-3[40] and alamethicin,[41] only the information pertinent to making comparison between all four peptides is discussed in this paper.

3.3 Materials and methods

3.3.1 Materials

Indolicidin and cysteine-terminated SMAP-29 were purchased from New England Peptide (Gardner, MA). Alamethicin was purchased from Sigma-Aldrich (St. Louis, MO) and chrysophsin-3 was acquired from Bachem (Torrance, CA). Peptide and lipid vesicle solutions were prepared in Tris-NaCl buffer [100 mM sodium chloride and 10 mM

tris(hydroxymethyl)aminomethane at pH 7.8]. Lyophilized egg phosphatidylcholine (PC) was purchased from Avanti Polar Lipids (Alabaster, AL) and stored in ethanol at -20˚C.

3.3.2 Supported lipid bilayer preparation

The stored egg PC was dried with nitrogen gas to remove the ethanol and stored under vacuum in a desiccator overnight. The dried lipids were then resuspended in Tris-NaCl buffer and brought to a final concentration of 2.5 mg/mL. The mixture was subjected to 5 freeze-thaw cycles and small unilamellar vesicles (SUVs) were formed using an ultrasonic dismembrator (Model 150T, Fisher Scientific, Waltham, MA) in pulse mode for 30 min at 0˚C. The pulse was set to stay on for 3 sec at an amplitude of 60, followed by a 7 sec pause, resulting in a 30% duty cycle. The SUV solution was then centrifuged at 17,500 rpm (37,000 g) for 10 min at 4˚C (J2-MI Centrifuge, Beckman Coulter, Brea, CA). The supernatant containing homogeneous SUVs was collected and stored under nitrogen at 4˚C for up to 5 weeks. This stock solution was aliquoted and diluted to 0.1 mg/mL before each experiment. Experiments were performed with peptide concentrations between 0.5 μM and 10 μM. Lower concentrations between 0.01 μM (data presented in Appendix A1.1) and 0.5 μM were also tested with alamethicin, chrysophsin-3, and SMAP-29 to determine the critical concentration at which AMP action occurs.

3.3.3 Quartz crystal microbalance with dissipation monitoring (QCM-D)

The Q-SENSE E4 system (Biolin Scientific, Stockholm, Sweden) was used to monitor the formation of an SLB on a silica surface and changes to the membrane upon exposure to AMPs in real-time. This technique uses the piezoelectric qualities of a quartz sensor crystal to measure the relative change in mass on its surface. The instrument measures the change in frequency (Δf) and change in energy dissipation (ΔD) of the crystal and any associated mass.

All the experiments involved the following steps (see a typical trace of frequency and dissipation measurements over time in Appendix 2). First, at time t_0, a PC vesicle solution (0.1 mg/mL) was allowed to flow over the QCM-D silica sensor surface at 0.15 mL/min at 23˚C until the frequency and dissipation stabilized, indicating the formation of a stable bilayer.[42, 43] The vesicles initially attach to the silica surface and when a critical concentration of vesicles on the surface is reached, they rupture spontaneously forming a stable and uniform membrane. Then at time t_1, the buffer was injected into the QCM-D chamber to rinse away any unattached particles. When the system showed a stable response at time t_2, a solution of the AMP in the buffer at the desired peptide concentration was allowed to flow. After 10 minutes of AMP injection (enough time for the QCM-D chamber to completely fill with the AMP solution), at time t_3, the flow was stopped and the system was left to equilibrate for 1 hr. This incubation was performed to allow the AMPs time to act on the membrane. Following this equilibration step, at time t_4, a final buffer rinse was applied until the frequency and dissipation stabilized at time t_5. The change in frequency Δf and change in dissipation ΔD data reported everywhere in this paper are the difference in values between that at time point t_2 associated with a stable supported bilayer just before AMP injection and the time point t_5 at the end of the final buffer rinse. The differences thus reflect solely the consequences of AMP interaction with the bilayer and are unaffected by all other system variables.

The Δf and ΔD values were measured with the 3rd, 5th, 7th, 9th, and 11th harmonics, or overtones, of the QCM-D crystal's resonant frequency. Due to different penetration depths of the acoustic waves associated with different overtones, higher overtones (e.g. the 9th and 11th harmonics) are associated with activity near the crystal surface and lower overtones are more related to processes occurring near the external surface of the attached mass.[39, 40] Homogeneous

Δf and ΔD values at all overtones suggest that the processes occurring throughout the thickness of the bilayer are uniform.

3.3.4 QCM-D data analysis

Methods to relate the measured frequency and dissipation changes to changes in mass and in the viscoelastic properties of the membrane on the surface are briefly outlined here. For a rigid film on the crystal surface exposed to air, the areal mass m_f (mass per unit area) is related to the normalized (with respect to the overtone number) frequency change Δf by the Sauerbrey equation, while the dissipation change ΔD is zero.

$$\Delta f = -f_o \frac{m_f}{m_q} = -C\, m_f\,, \quad \Delta D = 0 \tag{3.1}$$

Here, f_o is the natural frequency of the oscillator, m_q is the areal mass of the quartz crystal and C is the Sauerbrey constant. Net mass addition is reflected by a negative Δf while net mass loss is indicated by a positive Δf. If the film is not rigid but viscoelastic and is submerged in a Newtonian liquid (water or buffer), then the frequency and dissipation changes are given by

$$\begin{aligned} \Delta f &= -\frac{\eta_L}{2\pi\delta_L m_q} - f_o \frac{m_f}{m_q}\left[1 - \frac{2}{\rho_f}\left(\frac{\eta_L}{\delta_L}\right)^2 \frac{G''}{G'^2 + G''^2}\right], \\ \Delta D &= \frac{\eta_L}{n\pi f_o \delta_L m_q} + \frac{m_f}{m_q}\left[\frac{4}{\rho_f}\left(\frac{\eta_L}{\delta_L}\right)^2 \frac{G'}{G'^2 + G''^2}\right] \end{aligned} \tag{3.2}$$

where ρ_f is the density of the film on the crystal, η_L is the viscosity of the liquid, δ_L is the decay length of the acoustic wave in the liquid, and G'' and G' are the loss modulus and the storage modulus connected to the dissipation, $D = G''/(2\pi G')$. The first term in the expressions for Δf and ΔD are due to the solvent effect and they vanish when we consider peptide-induced changes in the bilayer for our purposes. Since the bilayer is immersed in the liquid both before and after contact with the peptide, which is the time period that is considered when calculating Δf and ΔD,

the solvent is negligible in our calculations. The mass change is now given by the Sauerbrey term with a correction factor accounting for the viscoelastic properties of the film. The change in dissipation ΔD is related to the changes in the rigidity or viscoelasticity of the bilayer. Small ΔD implies bilayer rigidity similar to that of the unperturbed bilayer and in this case the mass change is given by the simple Sauerbrey term without the viscoelastic correction.

3.4 Results

3.4.1 Dependence of frequency changes on peptide interaction modes

In order to link the frequency changes measured in the QCM-D experiments to molecular events, we first established a connection between the frequency changes and the different modes of peptide interaction with the bilayer. Four different states of peptide interacting with the membrane are shown in Figure 3.2: (i) peptide is inserted into the bilayer as a single molecule, occupying an area a_p per peptide; (ii) peptide is adsorbed on the bilayer surface in the lipid head group region, occupying an area A_p; (iii) peptide is inserted into the bilayer as an aggregate without any water channel, occupying an area a_p per peptide and (iv) peptide is inserted into the bilayer as a n-size cluster forming the pore wall around a water channel, occupying an area A_H/n per peptide, A_H being the pore area. On the addition of peptide to the bilayer, lipid molecules are removed from the bilayer and replaced either by pores or inserted peptides or peptide aggregates. In contrast, if the peptide adsorbs on the bilayer surface, it will not require any lipid removal from the membrane to do so. If a fraction λ of the bilayer area is affected by these peptide interactions, then the resulting frequency changes can be calculated (see details in Appendix 3) as the areal mass change divided by the Sauerbrey constant C:

$$\Delta f = -\frac{\lambda}{C}\left[\frac{M_P}{a_P} - 2\frac{M_L}{a_L}\right] \quad \text{Insertion of peptide/peptide clusters}$$

$$\Delta f = -\frac{\lambda}{C}\left[\frac{M_P}{\frac{A_H}{n}} - 2\frac{M_L}{a_L}\right] \quad \text{Formation of pores} \qquad (3.3)$$

$$\Delta f = -\frac{\lambda}{C}\left[\frac{M_P}{A_p}\right] \quad \text{Adsorption of peptides}$$

In this equation, M_P and M_L are molecular masses of the peptide and lipid molecule, respectively, calculated from their molecular weights.

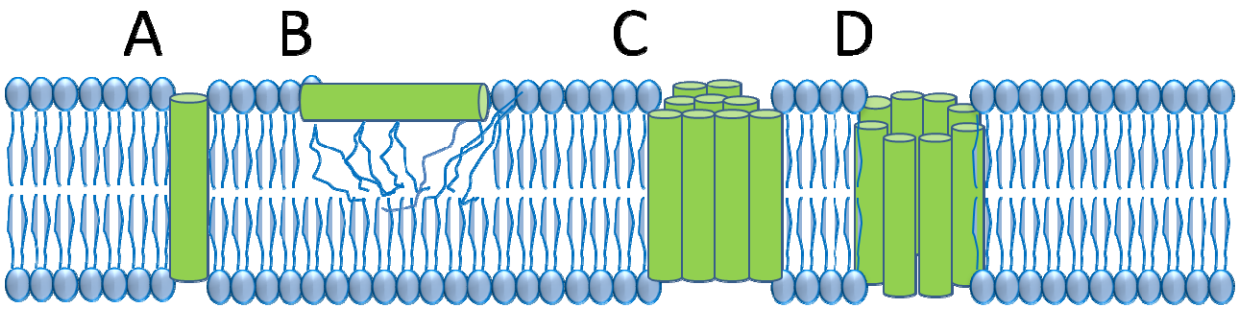

Figure 3.2. Four states of peptide-membrane interactions: (A) peptide insertion into the bilayer as a single molecule, (B) peptide adsorption to the membrane surface, (C) peptide insertion as an aggregate without a water channel and (D) peptide insertion as a cluster forming a pore around a water channel. For simplicity, lipid removal as a result of peptide insertion is not shown in this figure.

Setting the fractional area λ to be unity, we have calculated the theoretical maximum in the frequency change and the results are given in Table 3.2. From the calculated results, we observe that for alamethicin, pore formation will give rise to a positive Δf and will be measurable. In contrast, if alamethicin simply inserts into the bilayer either as a single molecule or as an aggregate, Δf is negative but will be too small to be observed. QCM-D can measure small changes in frequency (smaller than 0.01 Hz changes), but variations within experimental repetitions typically result in standard deviations larger than 0.01 Hz. If alamethicin adsorbs on

the bilayer surface with the helix being flat, Δf will be negative and large enough to be observable. For chrysophsin-3, pore formation will give rise to a positive Δf and will be measurable. If the peptide simply inserts into the bilayer or if it adsorbs on the bilayer, the frequency change will be negative and measurable. For indolicidin, pore formation will give rise to a positive Δf and will be measurable. If the peptide simply inserts into the bilayer, Δf will be positive but too small to be measurable. If indolicidin adsorbs flat on the bilayer surface, Δf will be negative and large enough to be observable. For SMAP-29, formation of a large pore will give rise to a positive Δf, while for a small pore Δf will be negative. If the peptide simply inserts into the bilayer, Δf is negative and large enough to be observed. Also, if the peptide is adsorbed flat on the bilayer surface, Δf will be negative and large enough to be observable. Also included are the results for the dimeric state of SMAP-29 since there is the possibility of dimerization due to the presence of a terminal cysteine added to SMAP-29 tested in our work. For the SMAP-dimer, all states of interaction give rise to negative Δf and the magnitude is significantly large compared to all other cases considered in Table 3.2. These calculated maximum Δf estimates allow us to look at specific peptide induced changes on the bilayer in molecular terms.

Table 3.2. Calculated estimates of maximum frequency changes resulting from various modes of peptide-bilayer interactions

Peptide	Molecular weight of peptide (Da)	Expected maximum change in Δf (Hz)			
		Insertion as monomer or as cluster	Pore formation with 8 peptides/pore	Pore formation with 20 peptides/pore	Surface adsorption Flat
Alamethicin	1965	- 0.10	6.92	12.08	- 4.85
Chrysophsin-3	2287	- 3.26	4.91	10.91	- 4.85
Indolicidin	1906	0.48	7.29	12.29	- 4.85
SMAP-29	3256	- 12.78	- 1.14	7.41	- 4.85
SMAP-29 Dimer	6512	- 44.74	- 21.47	- 4.37	- 4.85

3.4.2 Alamethicin prefers pore formation

The net changes in the frequency and the dissipation for the bilayer exposed to alamethicin are shown on Figure 3.3A for various concentrations of alamethicin in the aqueous phase. For all alamethicin concentrations, the experimental data show (i) that the frequency changes are positive suggesting a net mass loss occurs, (ii) all overtones show uniform responses, suggesting a process that is homogeneous along the depth of the bilayer and (iii) the dissipation changes are very small, indicating that the membrane retained the relatively rigid order similar to the unperturbed lipid bilayer. The mass loss and the uniform response at all overtones are consistent with alamethicin causing some amount of lipid molecules to be removed from the bilayer and creating cylindrical pores (Figure 3.3B). The very small dissipation change is consistent with alamethicin occupying the pore walls to make the bilayer as rigid as its original state.

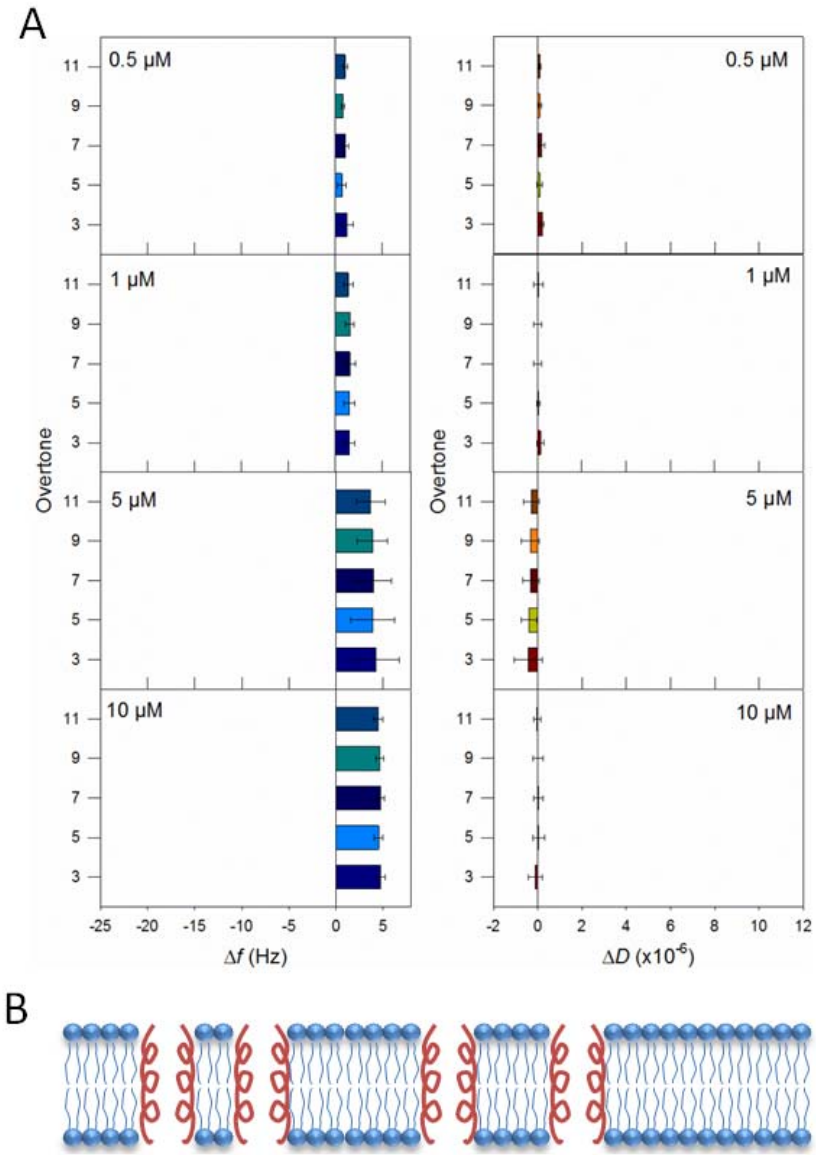

Figure 3.3. (A) Changes in frequency and dissipation corresponding to various concentrations of alamethicin interacting with a PC membrane (data previously published).[41] Error bars represent the standard deviation based on at least 3 replicate experiments. The uniform increases in frequency and dissipation at all overtones for each peptide concentration point to mass changes throughout the membrane thickness, which are indicative of peptide insertion (B). Peptides are represented in red and lipids are colored blue.

The dynamics of the interaction process are revealed by the ΔD vs. Δf plots in Figure 3.4. As discussed by McCubbin et al. and a previous paper from our lab,[41, 44] these plots reveal the time dependent changes that occurred in the membrane which are not captured by the plots of net

changes in ΔD and Δf shown on Figure 3.3. Net ΔD and Δf values capture changes that occurred over the entire time duration of AMP action, but do not reveal processes that may have occurred during this time. The direction of each line in the graphs in Figure 3.4 can be related to different molecular scale mechanisms occurring in the membrane. The x-axis is scaled such that the frequency changes to the "east" would correspond with mass increases. At bulk solution concentrations of 0.5 μM and 1 μM alamethicin, the membrane did not show significant changes. At 5 μM, simultaneous increases in mass and dissipation occurred initially, which corresponded with a line moving in the north-east direction (labeled *i*). The data then shifted to the north-west direction (labeled *ii*), indicating that the viscoelasticity of the membrane was still increasing, but mass had been lost. The bilayer then became more rigid with a small increase in mass and appreciable decrease in dissipation (labeled *iii*), followed again by mass loss (labeled *iv*). A similar phenomenon occurred at 10 μM alamethicin, but with larger changes in mass throughout the process and a faster initial rate of peptide adsorption to the membrane surface. These graphs showed that alamethicin first attached to the bilayer (mass addition) and caused the membrane to become more viscoelastic. The increasing "softness" of the bilayer could be due to decreasing organization of the membrane structure. The alamethicin then promotes pore formation in the bilayer, causing lipid removal and a more rigid bilayer structure as the peptides stabilized the edges of pores.

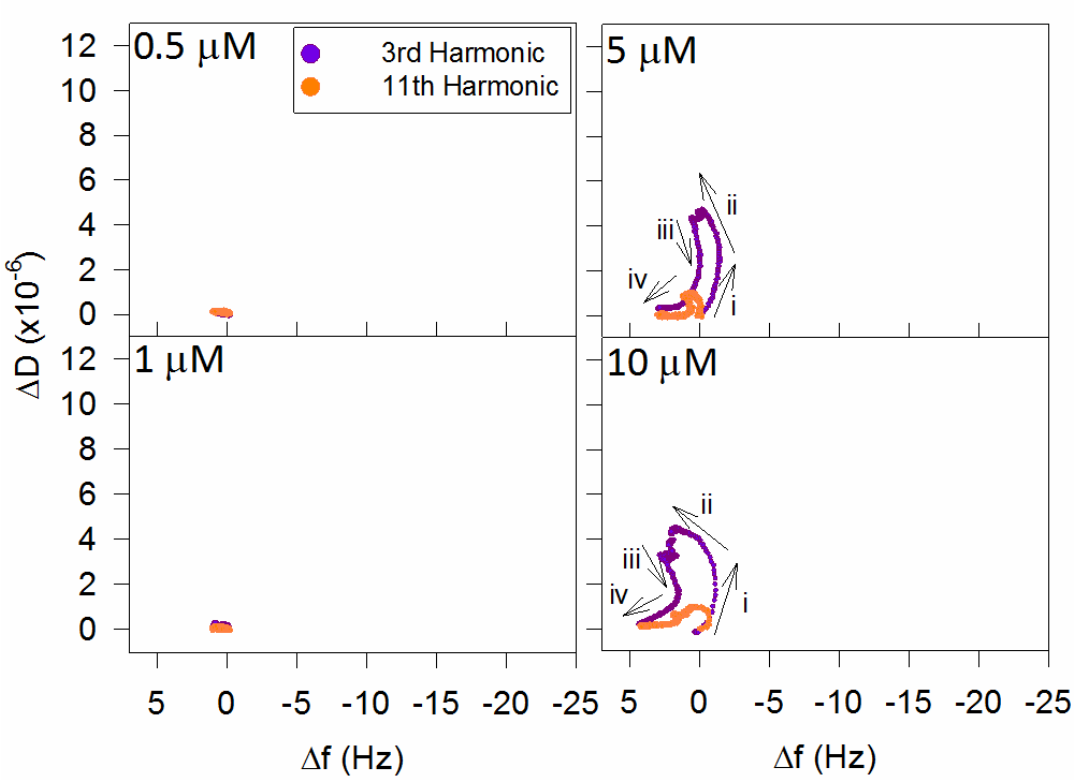

Figure 3.4. Representative *ΔD* vs. *Δf* plots showing the action of alamethicin at 0.5, 1, 5, and 10 µM concentrations on a supported PC membrane. The arrows indicate the progression of data points over time. The changing directions of the arrows (i-iv) can be related to several different processes occurring in the membrane. The frequency axis has been reversed so that increases in mass are represented by frequency shifts to the right. Representative data from each peptide concentration were chosen from sets of at least 3 replicate experiments.

3.4.3 Chrysophsin-3 displays insertion, surface adsorption and pore formation

Chrysophsin-3 exhibited a concentration-dependent interaction mechanism on the PC bilayer (Figure 3.5). At a concentration of 0.25 µM, *Δf* was negative and uniform at different overtones suggesting that a small amount of chrysophsin-3 was inserted into the membrane. Between 1 µM and 2 µM chrysophsin-3 (not shown), *Δf* was negative and the 3rd overtone showed a larger magnitude compared to the higher overtones suggesting that the peptide continued to insert into the membrane, but also was adsorbed on the bilayer surface. At 4 µM chrysophsin-3, the net *Δf* values and overtone responses were similar to that at 1 µM, indicating

peptide insertion and surface adsorption. The dissipation changes were larger, however, suggesting that the peptide induced actions were perturbing the organization of the bilayer. At the largest experimental chrysophsin-3 concentration of 10 μM, *Δf* became positive, overtone responses were more uniform, and the dissipation significantly decreased to small values, all suggesting that the net mass loss could be due to the formation of pores with the peptide stabilizing the pore walls and making the membrane reasonably rigid as in its unperturbed state.

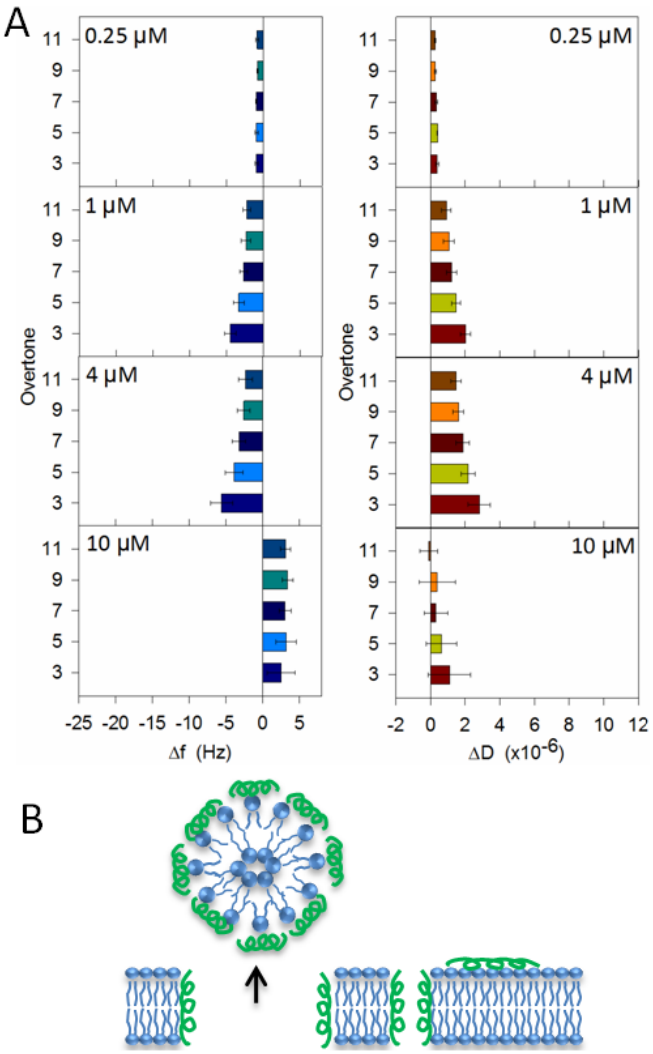

Figure 3.5. (A) Frequency and dissipation shifts for chrysophsin-3 (data previously published).[40] Frequency changes at all overtones suggest insertion of the peptide into the membrane and greater decreases in frequency at the 3rd overtone are indicative of peptide adsorption to the bilayer surface (B). Peptides are represented in green and lipids are colored blue.

The dynamics of the interactions between chrysophsin-3 and the PC bilayer displayed in the *ΔD* vs *Δf* plots in Figure 3.6 show that at the low concentration no significant change occurred on the bilayer. However, for 1 μM and 4 μM concentrations, an initial shift in the north-east direction (*i*) indicated simultaneous increases in mass and membrane viscoelasticity as peptide attached to the membrane. The 3rd overtone showed greater change than the 11th overtone, suggesting that most of the peptide-membrane dynamics was taking place near the surface of the membrane. The graph then shifted to a south-west direction (*ii*), indicating that mass had been lost from the membrane, leaving a more structurally organized and rigid film that still contained more mass than the original lipid membrane before peptide exposure. The results at 10 μM showed the same trends, but revealed a larger initial mass addition to the membrane, followed also by a larger mass loss (*ii)*, resulting in a more rigid film.

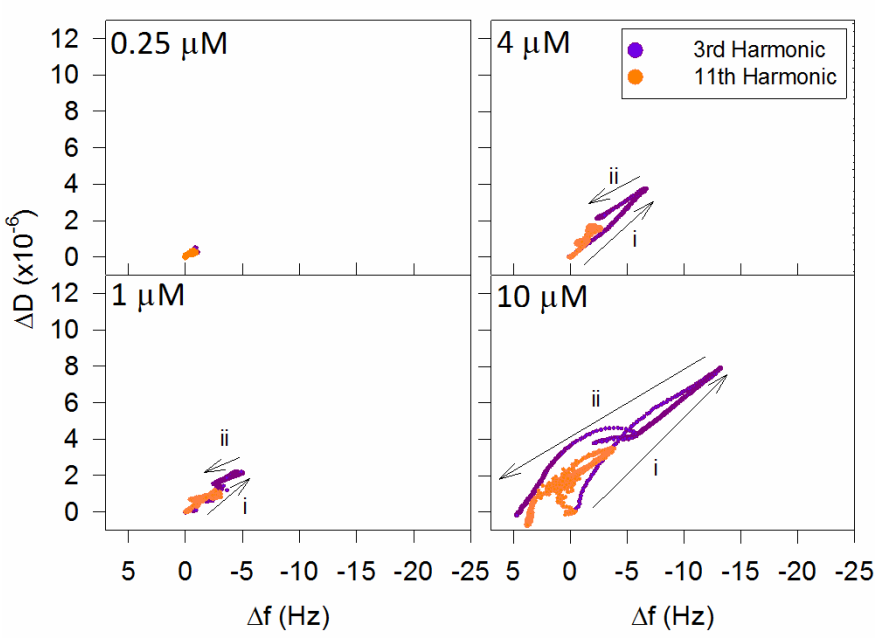

Figure 3.6. Representative *ΔD* vs. *Δf* plots for chrysophsin-3 at 0.25, 1, 4, and 10 μM concentrations. The arrows reveal two distinct processes occurring in the membrane as a result of exposure to chrysophsin-3: (i) increasing mass and dissipation, due to peptide incorporation into the bilayer and (ii) simultaneous decreasing mass and dissipation.

3.4.4 Indolicidin prefers surface adsorption

The QCM-D responses for indolicidin at different peptide concentrations are shown on Figure 3.7A. The QCM-D responses for 0.5 μM and 1 μM indolicidin were not strong, indicating some interactions but no significant changes to the membrane. At 5 μM indolicidin, frequency change was negative at the 3rd harmonic, but positive at higher overtones, suggesting that mass had been added to the bilayer surface, but removed from within the bilayer. These results showing both mass gain and loss may be explained by simultaneous peptide adsorption at the surface (corresponding to the negative frequency shift in the 3rd harmonic) and promoting some lipid loss from the bilayer (corresponding to the positive frequency shift at higher overtones). The dissipation changes also show significant positive values indicating that the membrane organization is somewhat disrupted because of the removal of lipids without accompanying space filling by the peptide. At the highest concentration of 10 μM indolicidin, the membrane experienced mass gain that was non-uniform at different overtones, the largest gain being in the 3rd overtone. This indicated significant surface adsorption of indolicidin with increasing concentration and partial peptide insertion into the membrane space where lipid molecules had been removed (Figure 3.7B). The 10 μM indolicidin concentration also resulted in larger ΔD values and, therefore, the "softest" film compared to other indolicidin concentrations. The creation of a "softer" film suggests that the lipid bilayer has been disrupted, allowing more water to enter the membrane space since the inserted amount of peptide was probably small compared to the adsorbed amount of peptide.

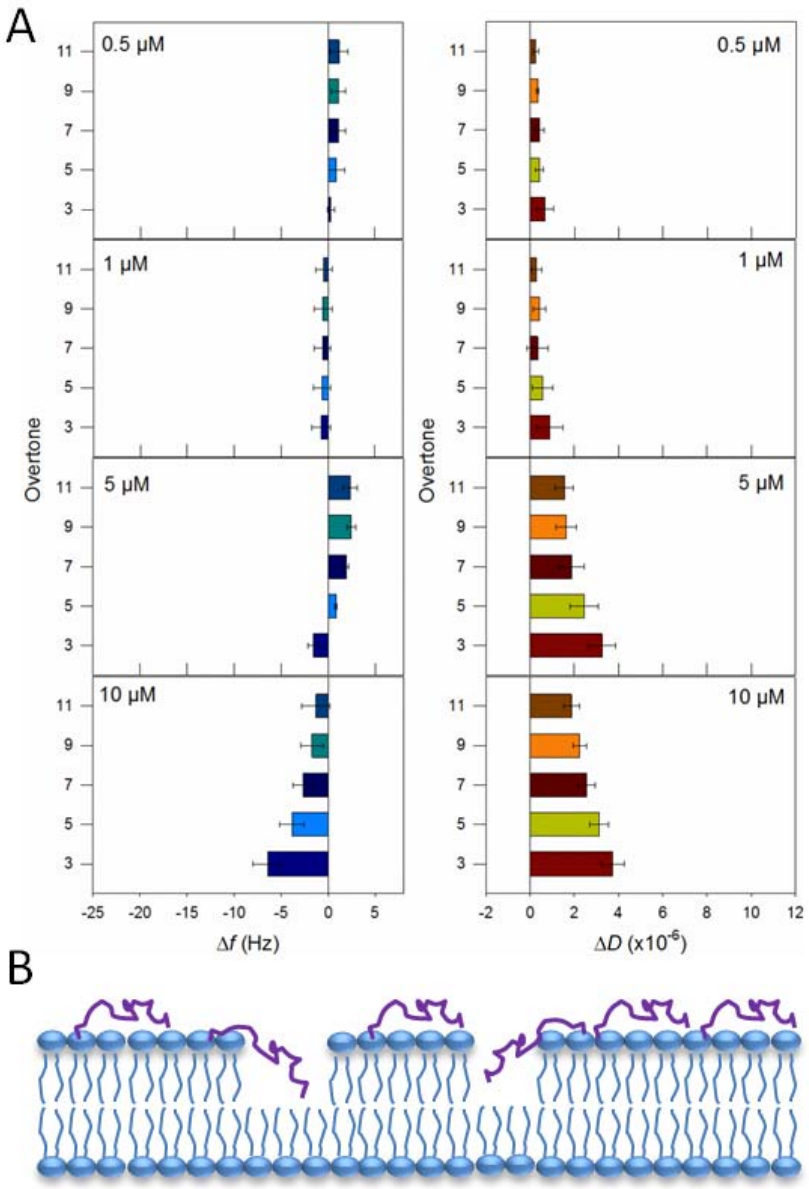

Figure 3.7. (A) Frequency and dissipation shifts resulting from indolicidin action on a supported PC bilayer at various peptide concentrations. The differences shown in each overtone indicate that the processes occurring throughout the membrane thickness are not uniform. The error bars represent the standard deviation based on at least 3 replicate experiments. (B) The hypothesized mechanism of interaction between indolicidin (violet) and PC membranes (blue): surface adsorption and partial insertion.

The dynamics of indolicidin action on PC membranes as seen from the ΔD vs. Δf plot (Figure 3.8) showed that the rate of peptide attachment to the bilayer at the beginning of the

process was higher than with alamethicin and chrysophsin-3 discussed earlier. This is revealed by the substantial separation of data points in the *ΔD* vs. *Δf* trace (since two adjacent frequency data points correspond to some fixed time interval, points separated by long distance indicate a rapid change of frequency compared to a situation where the points are very close to one another). The plot at 10 μM indolicidin indicated a higher rate of initial adsorption in the 3rd harmonic (*i*), followed by a slower loss of mass from the membrane (*ii*). Before the membrane stabilized during the 1-hr incubation period with the peptide, the bilayer regained a small amount of mass and continued to decrease in dissipation (*iii*), indicating that the molecules within the membrane were becoming more ordered. The subsequent increases in dissipation and mass (*iv*) resulted from the start of buffer flow after incubation with the peptide. The mechanism then shifted to a loss in mass and dissipation (*v*) as the membrane lost weakly attached particles and began to stabilize.

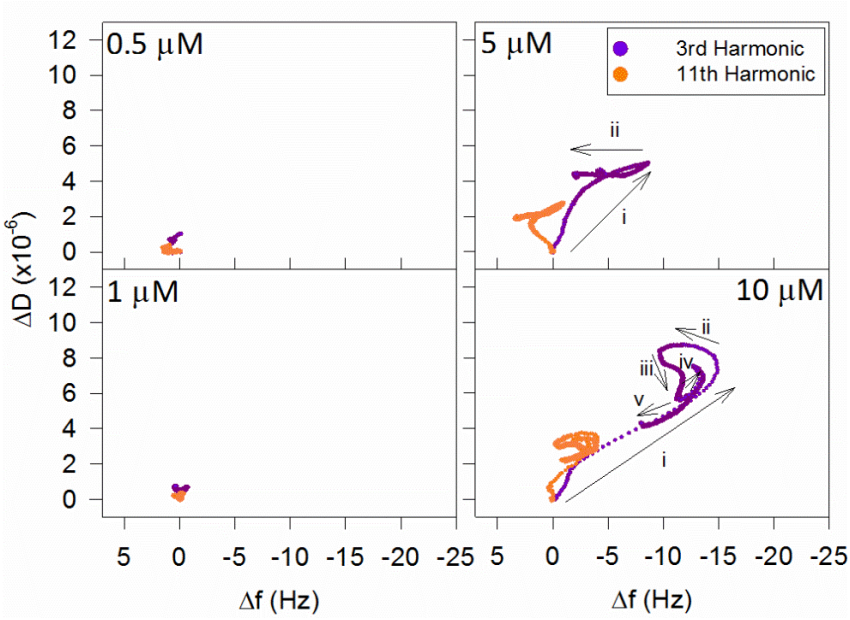

Figure 3.8. Representative *ΔD* vs. *Δf* plots for indolicidin at 0.5, 1, 5, and 10 μM concentrations. The arrows show that the addition of peptide into the membrane (i) is followed by a series of more complex interactions (ii-v) as time progresses.

3.4.5 SMAP-29 adsorption, insertion and presence of dimers

For SMAP-29, significant changes in frequency or dissipation were not observed at or below the 1.0 μM concentration (Figure 3.9A). Between 2 μM and 10 μM peptide concentrations, large frequency decrease and dissipation increase occurred, that were not homogeneous over the various overtones. The negative shifts in frequency were larger at lower overtones and the largest Δf values were observed for 10 μM SMAP-29. These results indicate that more mass was added to the membrane surface than throughout the membrane thickness, suggesting that peptides were adsorbing as well as inserting into the bilayer (Figure 3.9B). Pore formation is also possible but as the estimates in Table 3.2 show, the positive frequency change due to pore formation can be more than compensated by the negative frequency change associated with peptide insertion and surface adsorption.

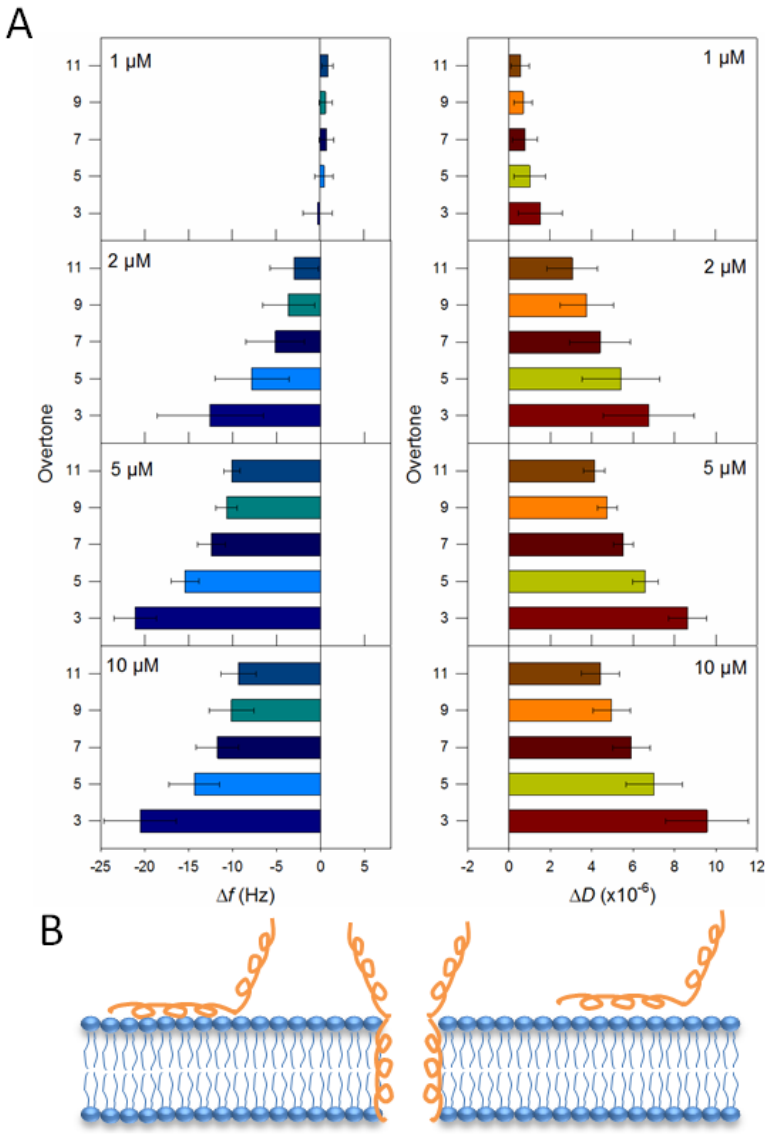

Figure 3.9. (A) Frequency and dissipation shifts resulting from SMAP-29's action on a supported PC bilayer at various peptide concentrations. Error bars represent the standard deviation based on at least 3 replicate experiments. The non-uniform changes at each overtone indicate that the interaction mechanism consists of a combination of peptide adsorption and insertion (B). Peptides are shown as orange coils and lipids are shown in blue (B).

The frequency change for concentrations of 5μM to 10 μM SMAP-29 was notably large, about -21 Hz at the 3rd overtone. The calculated maximum free energy changes in Table 3.2 for SMAP are well below this value for all states of the peptide considered. Therefore, the large

frequency shifts resulting from exposing the lipid bilayer to these concentrations of SMAP-29 require alternate molecular reasoning. The most likely explanation comes from the possible dimerization of SMAP because of the formation of disulfide bonds between the terminal cysteine residues attached to the peptide. This phenomenon was reported previously in a study by Uzarski et al., in which cysteine-terminated cecropin-P1 peptide formed disulfide bonds, resulting in peptide dimers.[36] The peptide dimer could still insert into the membrane or form a pore in the membrane but a significant portion of the dimer (almost 30 amino acid residues) would remain exposed to water on the bilayer surface.

Positive shifts in dissipation indicating a softer membrane were observed for all peptide concentrations with the largest ΔD values recorded for the third overtone. We noted that the SMAP dimers inserted into the bilayer or the dimers forming pores would have a significant part of them outside the bilayer membrane creating a water filled region crowded with the exposed parts of the dimers. Such a molecular system would make the effective membrane soft or viscoelastic and would give rise to the high dissipation changes observed.

The presence of dimerized SMAP-29 molecules could also explain the fast rate of initial mass attachment (*i*) to the lipid bilayer at 5-10 μM concentrations (Figure 3.10). The membrane became substantially more viscoelastic upon this mass addition, suggesting that it was becoming more structurally disorganized. The rate of change slowed as peptide attachment reached a saturation point around $\Delta f = 18$ Hz for both concentrations and the membrane began to lose mass, while increasing in viscoelasticity (*ii*). During the final buffer rinse, the dissipation then continued to increase along with the membrane mass (*iii*). This suggests that the mass gain may stem from trapping of some buffer by the exposed parts of peptide dimer on the bilayer surface

while the increase in dissipation or viscoelasticity may reflect a structural disorganization of a more hydrated, peptide containing region on the bilayer surface.

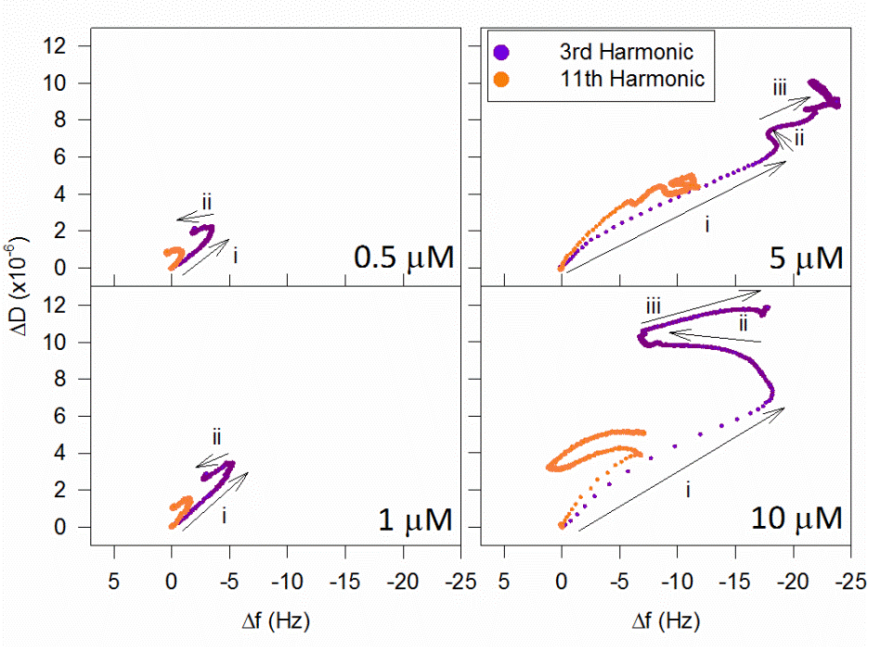

Figure 3.10. Representative *ΔD* vs. *Δf* plots for SMAP-29 at 0.5, 1, 5, and 10 µM concentrations. The spacing between the data points indicates that mass was added to the membrane at a faster rate than the other peptides, possibly due to the large mass of the dimerized SMAP-29 molecules.

3.4.6 Comparison of kinetics of peptide-membrane interactions

We have used the QCM-D data to estimate some kinetic information about how the peptides interact with bilayer. The frequency response of the QCM-D traces show that when the peptide comes into contact with the bilayer, a significant change in the frequency occurs in the initial period of contact following time point denoted as t_2 in the experiment (see QCM-D time trace in Appendix 2). The duration of this initial period as well as the rate of change of frequency during this initial period are found to be different for the four peptides (Figure 3.11). The duration of change for this initial period of contact is the smallest for alamethicin and largest for chrysophsin-3 and the other two peptides have comparable behaviors. The rate of mass or frequency change in this initial period is the largest for SMAP-29 and smallest for alamethicin

and chrysophsin-3. Indolicidin exhibits an intermediate rate of change. We observe that the initial interaction times (duration of initial change) of the four peptides are better differentiated at lower peptide concentrations whereas the initial interaction rates (frequency change over time) of the four peptides are better differentiated at the higher peptide concentrations.

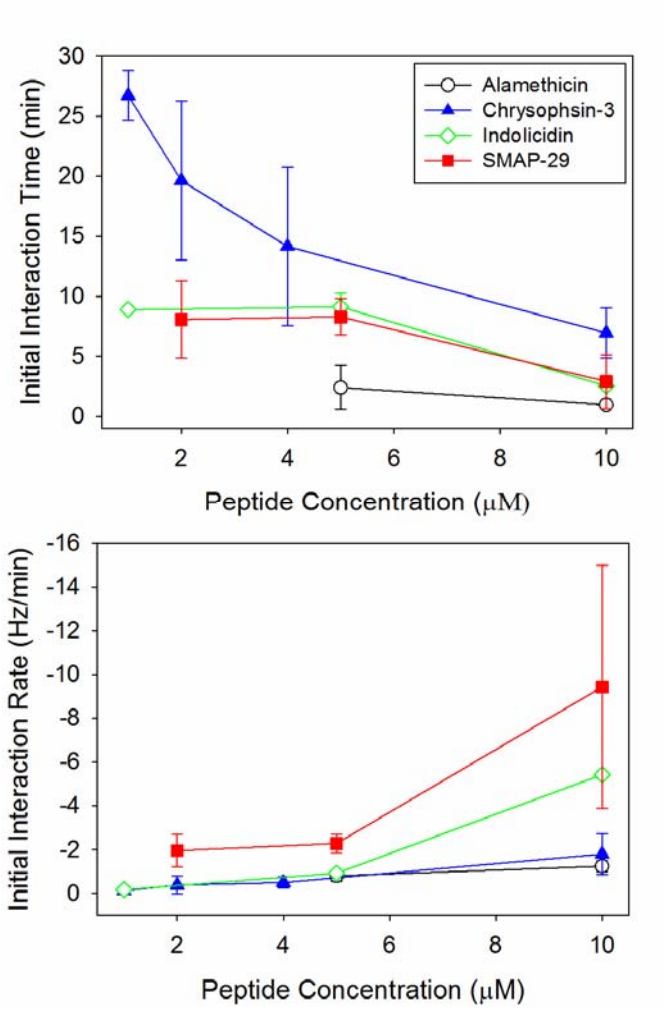

Figure 3.11. Initial interaction times and rates for various AMP concentrations. These values represent the rate of change during the initial stage of contact between the bilayer and the peptide.

3.4.7 Calculated peptide structural properties

Key peptide structural properties were calculated to establish a connection between the QCM-D results and the molecular processes they signify, with the molecular structural features of the peptides. The most common properties used to differentiate peptides in the literature are hydrophobicity, charge, and secondary structure. Many numerical scales of hydrophobicity Φ_n for each peptide residue n have been developed in the literature (see Appendix 4). Although they show some correlation with one another, the numerical measures can be very different. Therefore they are used more for the purposes of comparison. We have calculated the hydrophobicity of the four peptides using the normalized consensus scale of Eisenberg and the Urry scale based on phase inversion and the results are provided in Table 3.3.[45, 46] The hydrophobicity of the entire peptide Φ (= $\sum\Phi_n$ for all n=1 to N amino acids considered) and the hydrophobicity per residue (Φ/N) are both shown. For alamethicin containing two unnatural amino acids, the hydrophobicity of aminoisobutyric acid (U) was taken to be the average of the chemically similar amino acids, alanine and valine, and the hydrophobicity for phenylalaninol was taken to be the same as for phenylalanine.

Table 3.3. Hydrophobicity and hydrophobic moment of peptides

Peptide	Urry Hydrophobicity		Eisenberg Hydrophobicity		Eisenberg hydrophobic moment per residue
	For whole peptide	Per residue	For whole peptide	Per residue	
Alamethicin	-30.7	-1.54	6.22	0.3110	0.3084
Chrysophsin-3	-41.5	-2.08	1.52	0.0762	0.1537
Indolicidin	-44.45	-3.42	0.29	0.0223	0.0795
SMAP-29	-40.95	-1.41	-5.25	-0.1810	0.1957

In the Urry scale that is based on hydrophobic association, indolicidin was the most hydrophobic (both based on the entire peptide and also on a per residue basis) and alamethicin was the least hydrophobic, because of the large hydrophobicity estimates for tryptophan compared to the small estimates for alanine and valine. In the Eisenberg consensus scale based on various transfer free energies, alamethicin was the most hydrophobic while SMAP-29 was hydrophilic, reflecting the total absence of charge on alamethicin and the presence of 10 charged groups on SMAP-29.

A second characteristic used for analyzing amino acid sequences of membrane-related proteins is the hydrophobic moment, a measure of the amphiphilicity of the peptide. It is calculated for an amino acid sequence of *N* residues, with residue *n* having the hydrophobicity Φ_n from the definition,

$$\mu_H = \lfloor\{\Phi_n \cos(\delta_a n)\}^2 + \{\Phi_n \sin(\delta_a n)\}^2\rfloor^{1/2} \quad (3.4)$$

where δ_a is the angle (in radians) at which successive side chains emerge from the backbone when the peptide is viewed down its axis. For an α-helix, this angle is 100^o. The hydrophobic moment will be small for a helix where all residues are evenly distributed about the helix, and large for the case where most of the hydrophobic residues are on one side and most of the hydrophilic residues are on the other. Thus, the hydrophobic moment measures the extent of amphiphilicity of a helix. Any of the hydrophobicity scales could be used to provide the residue contributions Φ_n and we have used the Eisenberg consensus scale for this purpose. The calculated hydrophobicity moment per residue for all four peptides are also given in Table 3.3. The hydrophobic moment is the largest for alamethicin, indicating its preference for helical

secondary structure, and is the smallest for indolicidin, indicating the low probability of a α-helix. Both chrysophsin-3 and SMAP-29 have intermediate values of hydrophobic moment indicating a larger likelihood of α-helices.

In contrast to the hydrophobicity scales established for amino acids based on experimental measurements of free energy change of some relevant processes (discussed in Appendix 4), methods based on data mining have also been developed to predict the hydrophobicity and amphiphilicity of polypeptides.[46] Artificial neural networks were trained on a set of experimentally solved protein structures to predict properties including the relative surface accessibility of the amino acids and the probability of having a given secondary structure. In this approach, a given amino acid does not have a fixed value for a property but it depends on where the amino acid occurs in the peptide chain. The solvent accessible surface area (ASA) of amino acid residues within a native folded protein is calculated by rolling a sphere the size of a water molecule over the protein surface. For comparative purposes, the ASA is transformed into a relative surface area, which is calculated as the ASA of a given amino acid residue in the polypeptide chain, relative to the one where the amino acid is in maximal possible exposure, with the residue in the center of a tri-peptide between either glycine or alanine residues. The neural networks were also trained on the same protein data set to learn the probability of a secondary structure for each amino acid depending on where it may occur in a polypeptide.

Using the web-based tool NetSurfP where these neural network calculations can be implemented, we have calculated and plotted the relative solvent accessible surface area for the four peptides in Figure 3.12 and the probability of the residue being part of a α-helix in Figure 3.13. Since this neural network learning is based on a protein data set with experimentally solved protein structures, no information on the non-natural amino acids are available. For the

purposes of our calculations, we have used alanine and valine as replacements for aminoisobutyric acid and phenylalanine for phenylalaninol while calculating for alamethicin and have provided two sets of results corresponding to either alanine (A) or valine (V). The calculated results show a set of amino acids with larger surface accessibility and a set of amino acids with low surface accessibility for all peptides, suggesting the possibility of amphiphilic nature for their secondary structures. The fact that such facial segregation may not occur for indolicidin is likely due to the small number of amino acids present in it. The predicted probability of a residue having α-helical structure shown on Figure 3.13 clearly indicates that alamethicin, chrysophsin-3 and SMAP-29 can all have α-helical secondary structures while indolicidin has a random coil secondary structure (calculated data for random coils and beta structure are not plotted on the figure).

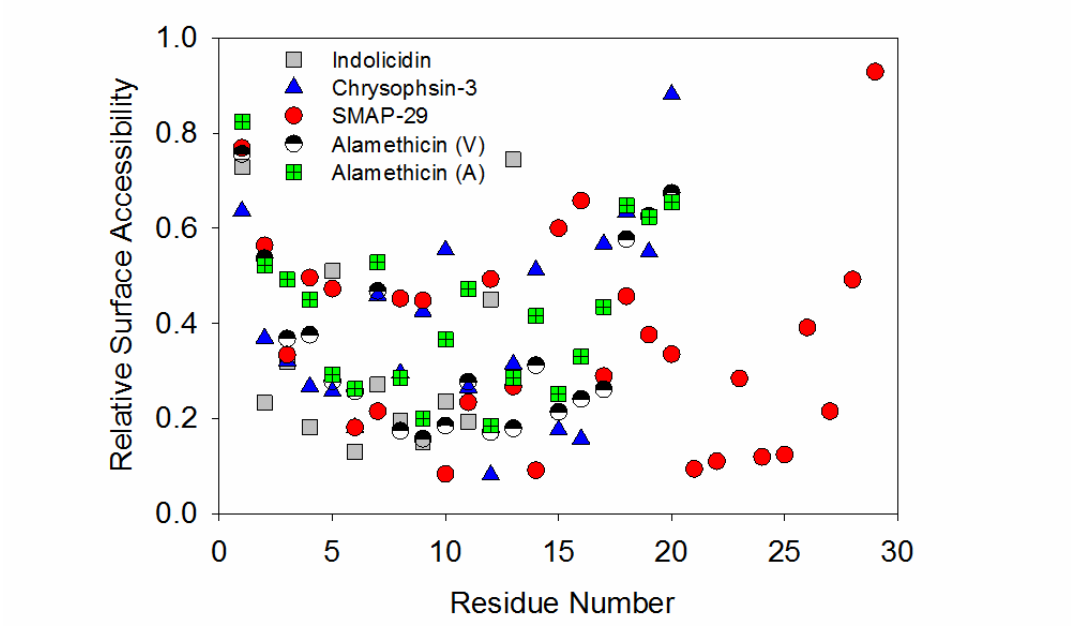

Figure 3.12. Relative solvent accessible surface area of the amino acid residues in each peptide. Alanine (A) and valine (V) were used as replacements for aminoisobutyric acid and phenylalanine was substituted for phenylalaninol. These values were calculated using NetSurfP.[46]

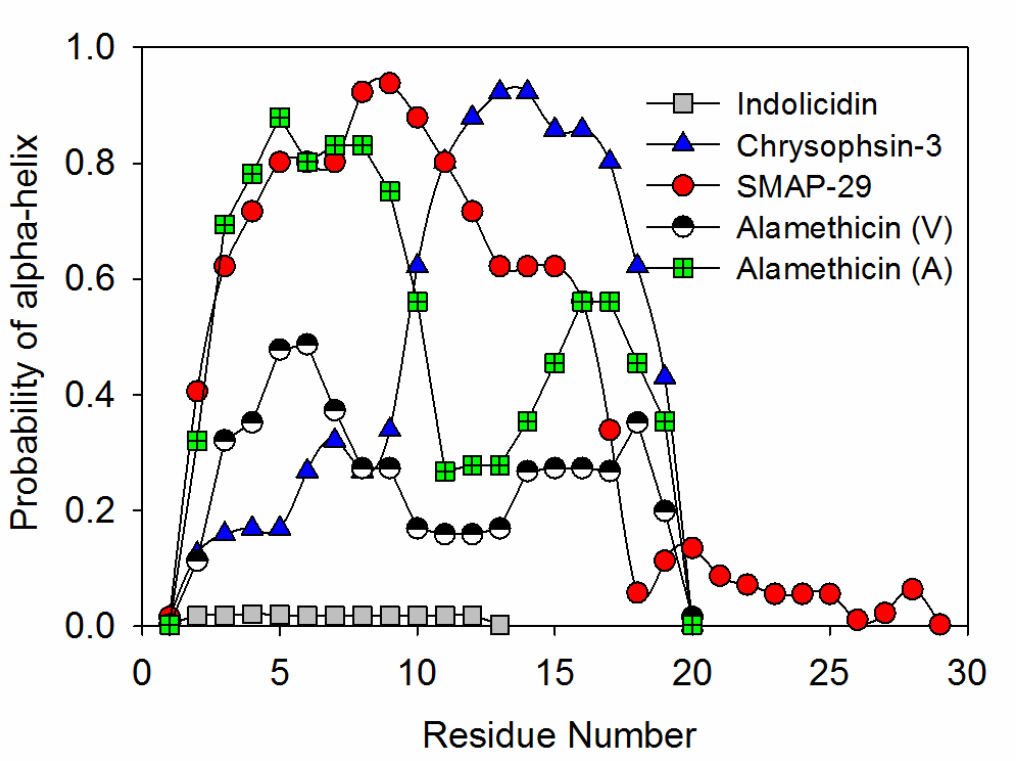

Figure 3.13. Probability of amino acid residues having an α-helical structure. These values were calculated using NetSurfP.[46]

3.5 Discussion

3.5.1 Linking peptide molecular structure to membrane interactions

The calculated structural properties of hydrophobicity, accessible surface area and probability of α-helical secondary structures as well as the net charge on the peptide can be related to the molecular scale descriptions of peptide-membrane interactions derived from QCM-D measurements. In Figure 3.14, we summarize the molecular scale models for peptide-bilayer interactions by combining the results obtained from the QCM-D experiments with the insights provided by the calculated peptide properties.

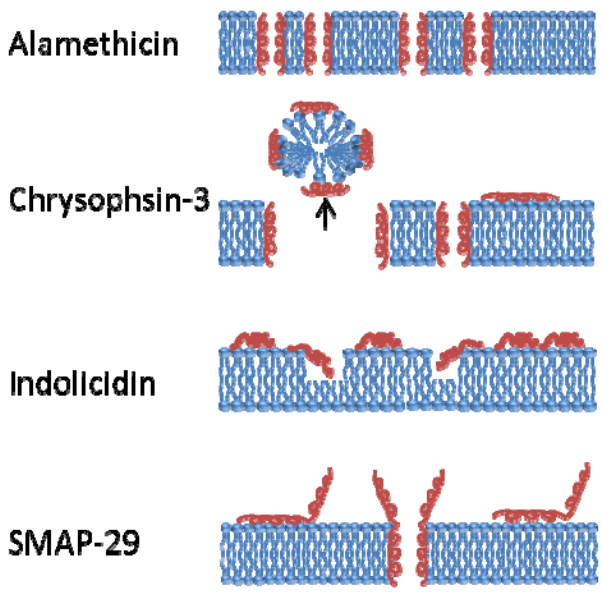

Figure 3.14. Representative mechanistic models for alamethicin, chrysophsin-3, indolicidin, and SMAP-29 action on a supported PC membrane. AMPs and lipids are shown in red and blue, respectively.

For alamethicin, the dominant molecular event suggested by QCM-D data is pore formation over the range of concentrations studied. Alamethicin is amphiphilic with α-helical structure as determined by the calculated hydrophobic moment, relative accessible surface area and the probability for α-helical secondary structure. It has zero charges on the surface. It has the largest hydrophobicity among the four peptides in the Eisenberg scale, which is based on the free energy of transfer water to a second bulk phase or to an interface. These molecular properties of alamethicin all promote its insertion into the bilayer creating pores, as part of the pore wall separating the lipid tails from water channels. Further, in the Urry scale which is based on hydrophobic association, the hydrophobicity of alamethicin is the smallest. That would suggest that it is less likely that alamethicin is inserted into the bilayer either as a single molecule or as an aggregate devoid of water channel, even though it cannot be ruled out.

For chrysophsin-3, the dominant molecular events suggested by the QCM-D data include membrane insertion and pore formation, as well as surface adsorption. Chrysophsin-3 is amphiphilic with α-helical structure as shown by the calculated hydrophobic moment, relative surface accessibility and the probability for α-helical secondary structure. Therefore it is reasonable to expect its presence in the bilayer as a part of pores, similar to alamethicin. The four charges on chrysophsin-3 can contribute to attractive charge-dipole interactions with the zwitterionic head groups on the PC bilayer, thereby allowing the peptide to also be in the adsorbed state on the bilayer. At the same time, the four charges are all concentrated near the C-terminus and the rest of the peptide is significantly hydrophobic as measured by both the Urry and Eisenberg scales. Consequently, chrysophsin-3 can also just insert as a single molecule or as an aggregate into the bilayer.

In the case of indolicidin, the dominant molecular events suggested by the QCM-D data include surface adsorption and partial insertion into the bilayer. The peptide is not amphiphilic, does not have the α-helical secondary structure and is really a random coil. Therefore, indolicidin does not promote pore formation in the bilayer (at least over the peptide concentration range studied). The low probability of indolicidin being part of a pore wall separating hydrophobic tails of the lipid from water channels is also supported by the small magnitude of hydrophobicity on the Eisenberg scale. Indolicidin has four charges and has the largest hydrophobicity, among the four peptides, in the Urry scale because of the presence of the tryptophan residues. As a result it can strongly adsorb at the bilayer surface both through the attractive charge-dipole interactions as well as through hydrophobic association with the bilayer surface uncovered by the lipid head groups. Further, because of the hydrophobicity and the coil-like conformation, it can also partially insert itself into the bilayer.

For SMAP-29, the QCM-D experiments suggest significant surface adsorption and also pore formation. Also, there was clear indication that the sample SMAP-29 used which contained a C-terminus cysteine had dimerized (this would not be relevant in the case of SMAP-29 without the cysteine modification). The calculated hydrophobic moment, accessible surface area and probability of α-helical secondary structure are all consistent with the possibility of pore formation with the peptide being at the pore walls. The large number of ten charges on the peptide supports the idea of strong surface adsorption through attractive charge-dipole interactions as well as hydrophobic association. The significantly large mass changes observed in the QCM-D required consideration of the peptide dimers and could not be explained if dimerization had not occurred.

3.5.2 QCM-D "fingerprinting" clearly differentiates antimicrobial peptides

The most interesting conclusion from this study, however, is the recognition that QCM-D provides many unique signatures or fingerprints to differentiate the action of antimicrobial peptides. The most obvious and easy to observe fingerprint was the static (actually difference between two steady-state conditions which we have termed static for simplicity) net frequency change and net dissipation change caused solely by the peptide, at different overtones and at different peptide concentrations as shown on Figures 3.3, 3.5, 3.7 and 3.9. Even if we had not been able to interpret these data in molecular mechanistic terms, there is no denying the obvious differences in the signatures shown by each of the four peptides. A second unique fingerprinting was provided by the dynamic Δf-ΔD plots, as shown on Figures 3.4, 3.6, 3.8 and 3.10. Although not as obvious as the static data, these dynamic data also showed significant variations in the multistep interactions of the peptides with the bilayer. A third fingerprint was the data quantifying the initial stage of contact of the peptide with the bilayer as shown on Figure 3.11.

Changes in the membrane occurred quickly in the first stage followed by a slower process. Both the time duration of this first stage as well as the rate or intensity of change in this first stage were peptide-specific. We believe that it may be possible to identify yet other unique signatures by performing additional data mining of the rich steady state and dynamic measurements derived from the QCM-D experiments,

3.6 Acknowledgements

We would like to thank Steve Arcidiacono (NSRDEC) for kindly providing the peptide SMAP-29 with cysteine termination, used in this study. This research was supported by funding from the Natick Soldier Research, Development & Engineering Center (NSRDEC), the Koerner Family Graduate Fellowship, and the Oak Ridge Institute for Science and Education (ORISE) Graduate Fellowship.

3.7 References

(1) Skarnes, R. C. and Watson, D. W. (1957) Antimicrobial factors of normal tissues and fluids, *Bacteriol Rev 21*, 273-294.
(2) Gazit, E., Miller, I. R., Biggin, P. C., Sansom, M. S. and Shai, Y. (1996) Structure and orientation of the mammalian antibacterial peptide cecropin P1 within phospholipid membranes, *J Mol Biol 258*, 860-870.
(3) Brogden, K. A. (2005) Antimicrobial peptides: pore formers or metabolic inhibitors in bacteria?, *Nat Rev Microbiol 3*, 238-250.
(4) Marr, A. K., Gooderham, W. J. and Hancock, R. E. (2006) Antibacterial peptides for therapeutic use: obstacles and realistic outlook, *Curr Opin Pharmacol 6*, 468-472.
(5) Powers, J. P. and Hancock, R. E. (2003) The relationship between peptide structure and antibacterial activity, *Peptides 24*, 1681-1691.
(6) Shai, Y. (2002) Mode of action of membrane active antimicrobial peptides, *Biopolymers 66*, 236-248.
(7) Harriss, L. M., Cronin, B., Thompson, J. R. and Wallace, M. I. (2011) Imaging multiple conductance states in an alamethicin pore, *J Am Chem Soc 133*, 14507-14509.
(8) Latorre, R., Miller, C. G. and Quay, S. (1981) Voltage-dependent conductance induced by alamethicin-phospholipid conjugates in lipid bilayers, *Biophys J 36*, 803-809.
(9) Huang, H. W. (2006) Molecular mechanism of antimicrobial peptides: the origin of cooperativity, *Biochim Biophys Acta 1758*, 1292-1302.

(10) Dathe, M. and Wieprecht, T. (1999) Structural features of helical antimicrobial peptides: their potential to modulate activity on model membranes and biological cells, *Biochim Biophys Acta 1462*, 71-87.
(11) Blondelle, S. E. and Houghten, R. A. (1991) Probing the relationships between the structure and hemolytic activity of melittin with a complete set of leucine substitution analogs, *Pept Res 4*, 12-18.
(12) Blondelle, S. E. and Houghten, R. A. (1991) Hemolytic and antimicrobial activities of the twenty-four individual omission analogues of melittin, *Biochemistry 30*, 4671-4678.
(13) Blondelle, S. E. and Houghten, R. A. (1992) Design of model amphipathic peptides having potent antimicrobial activities, *Biochemistry 31*, 12688-12694.
(14) Juvvadi, P., Vunnam, S., Merrifield, E. L., Boman, H. G. and Merrifield, R. B. (1996) Hydrophobic effects on antibacterial and channel-forming properties of cecropin A-melittin hybrids, *J Pept Sci 2*, 223-232.
(15) Mee, R. P., Auton, T. R. and Morgan, P. J. (1997) Design of active analogues of a 15-residue peptide using D-optimal design, QSAR and a combinatorial search algorithm, *J Pept Res 49*, 89-102.
(16) Bessalle, R., Gorea, A., Shalit, I., Metzger, J. W., Dass, C., Desiderio, D. M. and Fridkin, M. (1993) Structure-Function Studies of Amphiphilic Antibacterial Peptides, *J. Med. Chem. 36*, 1203-1209.
(17) Ohmori, N., Niidome, T., Hatakeyama, T., Mihara, H. and Aoyagi, H. (1998) Interaction of alpha-helical peptides with phospholipid membrane: effects of chain length and hydrophobicity of peptides, *J Pept Res 51*, 103-109.
(18) Fox, R. O., Jr. and Richards, F. M. (1982) A voltage-gated ion channel model inferred from the crystal structure of alamethicin at 1.5-A resolution, *Nature 300*, 325-330.
(19) Kessel, A., Cafiso, D. S. and Ben-Tal, N. (2000) Continuum solvent model calculations of alamethicin-membrane interactions: thermodynamic aspects, *Biophys J 78*, 571-583.
(20) Iijima, N., Tanimoto, N., Emoto, Y., Morita, Y., Uematsu, K., Murakami, T. and Nakai, T. (2003) Purification and characterization of three isoforms of chrysophsin, a novel antimicrobial peptide in the gills of the red sea bream, Chrysophrys major, *Eur J Biochem 270*, 675-686.
(21) Mason, A. J., Bertani, P., Moulay, G., Marquette, A., Perrone, B., Drake, A. F., Kichler, A. and Bechinger, B. (2007) Membrane interaction of chrysophsin-1, a histidine-rich antimicrobial peptide from red sea bream, *Biochemistry 46*, 15175-15187.
(22) Rozek, A., Friedrich, C. L. and Hancock, R. E. (2000) Structure of the bovine antimicrobial peptide indolicidin bound to dodecylphosphocholine and sodium dodecyl sulfate micelles, *Biochemistry 39*, 15765-15774.
(23) Subbalakshmi, C. and Sitaram, N. (1998) Mechanism of antimicrobial action of indolicidin, *FEMS Microbiol Lett 160*, 91-96.
(24) Shin, S. Y., Park, E. J., Yang, S. T., Jung, H. J., Eom, S. H., Song, W. K., Kim, Y., Hahm, K. S. and Kim, J. I. (2001) Structure-activity analysis of SMAP-29, a sheep leukocytes-derived antimicrobial peptide, *Biochem Biophys Res Commun 285*, 1046-1051.
(25) Neville, F., Ivankin, A., Konovalov, O. and Gidalevitz, D. (2010) A comparative study on the interactions of SMAP-29 with lipid monolayers, *Biochim Biophys Acta 1798*, 851-860.
(26) He, K., Ludtke, S. J., Heller, W. T. and Huang, H. W. (1996) Mechanism of alamethicin insertion into lipid bilayers, *Biophys J 71*, 2669-2679.

(27) Huang, H. W. and Wu, Y. (1991) Lipid-alamethicin interactions influence alamethicin orientation, *Biophys J 60*, 1079-1087.
(28) Meyer, C. E. and Reusser, F. (1967) A polypeptide antibacterial agent isolated from Trichoderma viride, *Experientia 23*, 85-86.
(29) Selsted, M. E., Novotny, M. J., Morris, W. L., Tang, Y. Q., Smith, W. and Cullor, J. S. (1992) Indolicidin, a novel bactericidal tridecapeptide amide from neutrophils, *J Biol Chem 267*, 4292-4295.
(30) Hsu, J. C. and Yip, C. M. (2007) Molecular dynamics simulations of indolicidin association with model lipid bilayers, *Biophys J 92*, L100-102.
(31) Hsu, C. H., Chen, C., Jou, M. L., Lee, A. Y., Lin, Y. C., Yu, Y. P., Huang, W. T. and Wu, S. H. (2005) Structural and DNA-binding studies on the bovine antimicrobial peptide, indolicidin: evidence for multiple conformations involved in binding to membranes and DNA, *Nucleic Acids Res 33*, 4053-4064.
(32) Khandelia, H. and Kaznessis, Y. N. (2007) Cation-pi interactions stabilize the structure of the antimicrobial peptide indolicidin near membranes: molecular dynamics simulations, *J Phys Chem B 111*, 242-250.
(33) Ahmad, I., Perkins, W. R., Lupan, D. M., Selsted, M. E. and Janoff, A. S. (1995) Liposomal entrapment of the neutrophil-derived peptide indolicidin endows it with in vivo antifungal activity, *Biochim Biophys Acta 1237*, 109-114.
(34) Raventos, D., Taboureau, O., Mygind, P. H., Nielsen, J. D., Sonksen, C. P. and Kristensen, H. H. (2005) Improving on nature's defenses: optimization & high throughput screening of antimicrobial peptides, *Comb Chem High Throughput Screen 8*, 219-233.
(35) Dawson, R. M. and Liu, C. Q. (2009) Cathelicidin peptide SMAP-29: comprehensive review of its properties and potential as a novel class of antibiotics., *Drug Development Research 70*, 481-498.
(36) Uzarski, J. R., Tannous, A., Morris, J. R. and Mello, C. M. (2008) The effects of solution structure on the surface conformation and orientation of a cysteine-terminated antimicrobial peptide cecropin P1, *Colloids Surf B Biointerfaces 67*, 157-165.
(37) Arcidiacono, S., Pivarnik, P., Mello, C. M. and Senecal, A. (2008) Cy5 labeled antimicrobial peptides for enhanced detection of Escherichia coli O157:H7, *Biosens Bioelectron 23*, 1721-1727.
(38) Voinova, M. V., Rodahl, M., Jonson, M., Kasemo, B. (1999) Viscoelastic acoustic response of layered polymer films at fluid-solid interfaces: continuum mechanics approach, *Physica Scripta 59*, 391-396.
(39) Mechler, A., Praporski, S., Atmuri, K., Boland, M., Separovic, F. and Martin, L. L. (2007) Specific and selective peptide-membrane interactions revealed using quartz crystal microbalance, *Biophys J 93*, 3907-3916.
(40) Wang, K. F., Nagarajan, R., Mello, C. M. and Camesano, T. A. (2011) Characterization of supported lipid bilayer disruption by chrysophsin-3 using QCM-D, *J Phys Chem B 115*, 15228-15235.
(41) Wang, K. F., Nagarajan, R. and Camesano, T. A. (2014) Antimicrobial peptide alamethicin insertion into lipid bilayer: A QCM-D exploration, *Colloids Surf B Biointerfaces 116*, 472-481.
(42) Keller, C. A. and Kasemo, B. (1998) Surface specific kinetics of lipid vesicle adsorption measured with a quartz crystal microbalance, *Biophys J 75*, 1397-1402.

(43) Keller, C. A., Glasmastar, K., Zhdanov, V. P. and Kasemo, B. (2000) Formation of supported membranes from vesicles, *Phys Rev Lett 84*, 5443-5446.
(44) McCubbin, G. A., Praporski, S., Piantavigna, S., Knappe, D., Hoffmann, R., Bowie, J. H., Separovic, F. and Martin, L. L. (2011) QCM-D fingerprinting of membrane-active peptides, *Eur Biophys J 40*, 437-446.
(45) Eisenberg, D. (1984) Three-dimensional structure of membrane and surface proteins, *Annu Rev Biochem 53*, 595-623.
(46) Urry, D. W. (2004) The change in Gibbs free energy for hydrophobic association: Derivation and evaluation by means of inverse temperature transitions, *Chemical Physics Letters 399*, 177-183.

Chapter 4

Characterization of supported lipid bilayer disruption by chrysophsin-3 using QCM-D

The Journal of Physical Chemistry B, 2011. **115** (51): 15228-35.

4.1 Abstract

Antimicrobial peptides (AMPs) are naturally occurring polymers that can kill bacteria by destabilizing their membranes. Quartz crystal microbalance with dissipation monitoring (QCM-D) was used to better understand the action of the AMP chrysophsin-3 on supported lipid bilayers (SLB) of phosphatidylcholine. Interaction of the SLB with chrysophsin-3 at 0.05 μM demonstrated changes in frequency (Δf) and energy dissipation (ΔD) that were near zero, indicating little change in the membrane. At higher concentrations of chyrsophsin-3 (0.25 - 4 μM), decreases in Δf of up to 7 Hz were measured. These negative frequency changes suggest that mass was being added to the SLB, possibly due to peptide insertion into the membrane. At a chrysophsin-3 concentration of 10 μM, there was a net mass loss, which was attributed to pore formation in the membrane. QCM-D can be used to describe a mechanistic relationship between AMP concentration and interaction with a model cell membrane.

4.2 Introduction

Antimicrobial peptides (AMPs) serve as a natural defense for living organisms against pathogenic bacteria. They can be derived from various organisms, including frogs, moths, and pigs, as well as synthesized.[1, 2] AMPs exhibit broad-spectrum activity against bacteria and are less prone to the development of pathogen resistance than antibiotics. Increasing concerns over antibiotic-resistant pathogens and public health issues have led to interest in using AMPs therapeutically and in self-decontaminating surfaces.[3, 4] For example, omiganan, a synthetic cationic peptide, has been shown to inhibit the growth of pathogens that cause catheter-associated infections, such as Gram-positive *Staphylococcus aureus* and Gram negative *Pseudomonas aeruginosa (P. aeruginosa*).[5]

The ability of AMPs to avoid pathogen resistance is largely due to the mechanism by which they kill bacteria. AMPs attach to bacterial cell membranes and, at a critical concentration, cause the cells to lyse by disrupting the membrane.[6] However, the mechanism of cell lysis is not well understood. The attachment of AMPs to cells, such as cecropin P1 to *E. coli*, has been studied, but questions remain on the exact nature of the cecropin P1-*E. coli* interaction.[7, 8] Detailed knowledge of the mechanism behind AMP action is essential for developing applications that make use of AMPs, such as biosensors or AMP-coated materials.

Two main theories have been proposed to explain how AMPs destabilize bacterial cell membranes. In each case, the AMPs first attach to components of bacterial surfaces through electrostatic interactions.[9] The carpet model supposes that AMPs align themselves parallel to the membrane surface, which is facilitated by their amphipathicity. AMPs surround the lipids and micelles break off from the lipid membrane. In the barrel-stave model, the AMPs insert themselves into the bacterial cell membrane perpendicularly and form a pore.[10, 11] The pores enable large molecules to enter or exit the cell and disrupt ion gradients, causing the cell to die. The disruption of the lipid membrane may also allow AMPs to enter the cell and destroy intracellular components.[8] The mechanism is thought to differ among AMPs and is related to the structure and charge of the peptide, as well as the lipid composition of the cell membrane.[12, 13] For some cases, both micelle formation and pore insertion may occur, depending on the peptide-to-lipid concentration ratio.[14]

The peptide investigated in this study is chrysophsin-3, a histidine-rich AMP that is found in red sea bream gills. The red sea bream, *Chrysophrys major*, secretes AMPs from exposed areas, such as gills, to defend itself against bacterial infection.[15] Chrysophsin-3 consists of 20 amino acids in an α-helical structure, which is highly cationic and amphipathic (Figure 4.1). It

exhibits antimicrobial activity against Gram-positive and Gram-negative pathogenic bacteria and exhibits hemolytic activity at approximately 1 μM.[16] AMPs have been shown to be effective against *P. aeruginosa in vivo* using rat models, suggesting that AMPs may still be used clinically, despite their hemolytic properties.[17] Peptide mimics may also play a role in therapeutic treatments, as chrysophsin-3 can be made less harmful to eukaryotic cells by removing the characteristic C-terminal RRRH amino acid sequence.[18]

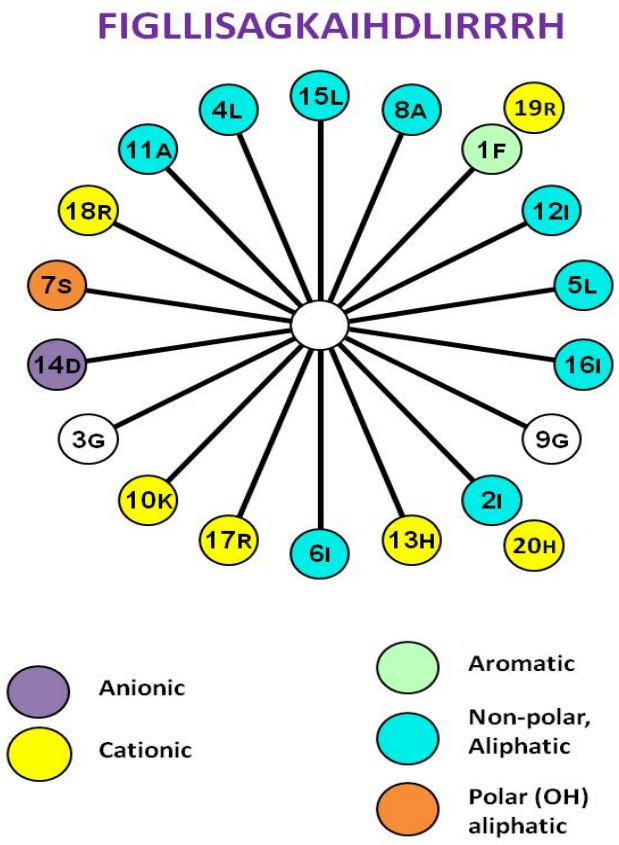

Figure 4.1. Helical wheel diagram of chrysophsin-3. The diagram represents the peptide viewed along the axis of the helix, in which the peptide backbone is shown by the inner circle and the spokes represent amino acids. The amino acids are numbered according to their sequence. The helical wheel diagram reveals the concentration of amino acids with positively charged side chains on one side of the helix and the clustering of non-polar, aliphatic side chains.

In this study, a supported phosphatidylcholine (PC) bilayer was used as a model zwitterionic membrane to observe the interaction between chrysophsin-3 and a cell. Phospholipid

vesicles have been studied extensively for their ability to self-assemble into planar bilayers on solid surfaces.[19, 20]

Quartz crystal microbalance with dissipation (QCM-D) monitoring was used to investigate the mechanism behind the peptide-lipid system of chrysophsin-3 and PC. QCM-D has become a valuable tool for monitoring real-time mass changes of various biological systems, including fatty acid attachment to supported lipid bilayers and cell adsorption to fibronectin.[21, 22] Frequency and dissipation measurements at various overtones can be used to determine the nature of mass attachment to a quartz sensor crystal.

Overtone analysis was used by Mechler et al. to infer details about the fundamental mechanisms behind AMP action on supported bilayers. Similar changes in frequency (Δf) and dissipation (ΔD) at all overtones indicate a homogeneous change in mass and viscoelasticity of the membrane on the crystal's surface. Studies exposing lipids 1,2-dimyristoyl-*sn*-glycero-3-phosphocholine (DMPC) and 1,2-dimyristoyl-*sn*-glycero-3-phospho-*rac*-(1-glycerol) (DMPG) to 1 to 20 μM concentrations of peptides aurein 1.2, maculatin 1.1, and caerin 1.1 resulted in qualitative and quantitative differences in the frequencies that were specific to each system.[23]

Monitoring overtone similarity can provide significant information about the mechanism of action of AMPs on a lipid bilayer surface. The barrel-stave model for peptide-membrane interactions should ultimately result in uniformly negative Δf and ΔD values at all overtones, which would represent cylindrical pore formation (Figure 4.2B, F). In the case of toroidal pore formation, however, more lipid would be lost at the top and bottom of the bilayer and replaced by pore-forming peptides, resulting in heterogeneous frequency changes at different overtones (Figure 4.2D). Initial adsorption of AMPs onto the membrane surface will theoretically result in non-homogeneous negative changes in frequency if no other action occurs (Figure 4.2A). Since

the changes occur primarily on the surface of the membrane, the adsorption process will not be homogeneous throughout the membrane, which would result in different response at various overtones. Combinations of membrane surface adsorption and pore formation will result in non-uniform Δf results across overtones (Figure 4.2C). Given that a full PC bilayer (~5 nm thick) assembled on a clean QCM-D crystal corresponds with a Δf of ~-26 Hz, we can calculate the approximate Δf due to adsorption of a monolayer of α-helical peptides (~1.2 nm thick) to be ~2-4 Hz.[20, 24] Therefore, if the carpet model is operative, membrane lysis will be demonstrated through uniform positive Δf values up to 26 Hz at all overtones (Figure 4.2E, G).

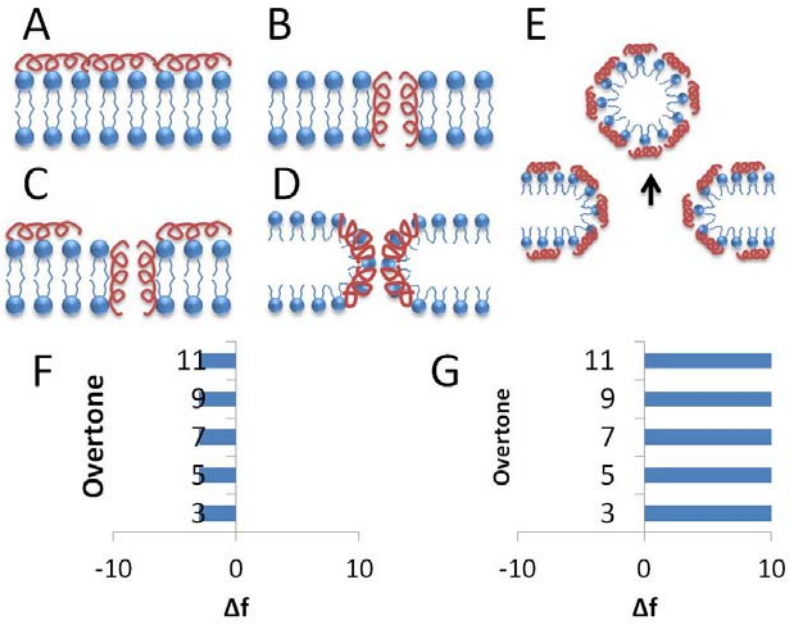

Figure 4.2. Possible mechanisms of peptide action on cell membranes (A-E) and corresponding estimated Δf values (F-G). A) Monolayer of peptide adsorbed on the lipid bilayer surface. B) Cylindrical pore formation. C) Pore formation with adsorption. D) Toroidal pore: lipids bend at the pore site to create a toroidal shape around peptides forming a pore. E) Large pore formation. Negative Δf values indicate mass addition (F), which may occur in A-D. Positive Δf values indicate mass removal (G), which corresponds to the large pore formation shown in E. The baseline at $\Delta f = 0$ would indicate the presence of a bilayer on the QCM-D crystal.

The action of chrysophsin-3 on a PC membrane supported on a QCM-D sensor crystal was monitored in real-time in this study. Changes and frequency and dissipation were monitored

when chrysophsin-3, at concentrations between 0.05 μM and 10 μM, interacted with the PC bilayer. Values of Δf and ΔD were also monitored after rinsing the system with buffer to remove any unattached particles and to reveal the irreversible effect of peptide on the lipid bilayer. QCM-D data is used to propose a mechanism for how chyrsophsin-3 interacts with cell membranes.

4.3 Experimental methods

4.3.1 Vesicle and peptide preparation

Lyophilized powder PC derived from chicken egg yolk was purchased from Sigma Aldrich (St. Louis, MO) and Avanti Polar Lipids (Alabaster, AL). PC was dissolved in ethanol to create 100 mg/mL stock solutions that were stored at -15˚C. A buffer of 100 mM sodium chloride and 10 mM tris(hydroxymethyl)aminomethane (Sigma-Aldrich, St. Louis, MO) at pH 7.9 was prepared in ultrapure water.[25]

The PC stock solution was measured and dried with nitrogen gas to remove the ethanol. Dried lipids were placed in a vacuum desiccator overnight and suspended in buffer at 2.5 mg/mL.[26] The lipid mixture was vortexed and homogenized through five freeze-thaw and subsequent vortexing cycles.[20]

Small unilamellar vesicles (SUVs) were formed by sonicating the mixture in a glass test tube with an ultrasonic dismembrator (Model 150T, Fisher Scientific, Waltham, MA) for 30 min in pulsed mode with a 30% duty cycle (3-second pulse at an amplitude of 60, followed by a 7-second pause) at 0˚C. Probe particles were removed from the solution through centrifugation (Sorvall Discovery 100SE, Kendro, Newtown, CT) at 15,000 rpm (38,500g) for 10 min at 4˚C. The supernatant containing the SUVs was collected and stored at 4°C under nitrogen for up to 5 weeks.[20] Dynamic light scattering experiments (Zetasizer Nano ZS, Malvern, Worcestershire,

UK) revealed the size of the vesicles to be approximately 37 nm in diameter. The stock solution was diluted to 0.1 mg/mL for each experiment.

Chrysophsin-3 (FIGLLISAGKAIHDLIRRRH) was purchased from Bachem (Torrance, CA) and stored at -15 ˚C. Samples were prepared at chyrsophsin-3 concentrations of 0.05, 0.25, 1, 2, 4, and 10 μM in tris buffer. Solutions were brought to 23°C before use in experiments.

4.3.2 Quartz crystal microbalance with dissipation monitoring (QCM-D)

QCM-D measurements were performed using the Q-SENSE E4 system (Biolin Scientific, Sweden). Quartz sensor crystals were placed into the QCM-D's four chambers and exposed to solutions of buffer, lipids, or peptides. We measured overtones, or harmonics, of the resonant frequency and the energy dissipation of the sensors as mass attached to the exposed silica-coated surfaces. The normal mass and dissipation sensitivities of QCM-D measurements in liquid are ~1.8 ng/cm^2 and ~0.1 x 10^{-6}, respectively.

The Sauerbrey equation describes the relationship between Δf and change in mass (Δm) in a rigid film:

$$\Delta f = \frac{-2f_0^2}{A\sqrt{\rho_q \mu_q}} \Delta m \qquad (4.1)$$

where f_0 is the resonant frequency of the quartz crystal (5 MHz), A is the peizoelectrically active crystal area, ρ_q is the density of quartz (2.648 g/cm^3), and μ_q is the shear modulus of the crystal (2.947 x 10^{11} g/cm·s^2). Therefore, the change in frequency is inversely related to the change in mass attached to the sensor. However, in the case of a less rigid film, the Sauerbrey equation must be adjusted to reflect the effects of a viscoelastic film and the bulk solution.[27, 28] Changes in dissipation are related to the rigidity of the film and can be described by

$$D = \frac{G''}{2\pi G'} \tag{4.2}$$

where *G*" is the loss modulus and *G'* is the storage modulus. A softer film will result in a larger ΔD.

Different harmonics of a sensor crystal can be correlated with changes in various depths of a film deposited on the crystal. The penetration depth, δ, of an acoustic wave can be found:

$$\delta = \left(\frac{\eta_f}{n\pi f_0 \rho_f}\right)^{1/2} \tag{4.3}$$

where η_f is the viscosity of the film, *n* is the overtone number, and ρ_f is the density of the film.[29] Penetration depths of various overtones are greater in the membrane than in water (Table 4.1).

Table 4.1. Penetration depths of different overtones in water and in a membrane.

overtone number	**penetration depth in water (ρ_f = 1 g·cm^{-3}, η_f = 0.01 g·cm^{-1}·s^{-1})[a]**	**penetration depth in membrane (ρ_f = 1 g·cm^{-3}, η_f = 1 g·cm^{-1}·s^{-1})[a]**
3	146 nm	1460 nm
5	113 nm	1130 nm
7	95 nm	950 nm
9	84 nm	840 nm
11	76 nm	760 nm

[a] ρ_f and η_f are the density and viscosity of the film, respectively.

QCM-D measurements can be sensitive to changes in viscosity and density of the bulk solution, which can complicate interpretation of the data. Bordes and Höök developed methods to quantify the bulk response and separate the bulk effect from the response of the adsorbed mass. The measured Δf is effectively a sum of the Δf of the adsorbed mass and Δf of the bulk solution (where the frequencies are normalized to each overtone).[30] The bulk solution effect in these experiments, which consists of the buffer, lipids, and/or AMPs, was determined to be negligible at the measured harmonics, which were the 3rd-11th harmonics of the sensor crystal's

natural frequency (5 MHz). Due to the low concentrations of AMPs and lipids used, the viscosity and density of the solutions would not change enough to produce a significant effect on the measured frequencies. The measured harmonics were normalized to each overtone (f/n, where f is frequency and n is the harmonic number) by the Q-SENSE software. The fundamental frequency was not analyzed due to a higher sensitivity to changes in the bulk solution during flow.[23]

4.3.3 Sensor preparation

Silica-coated sensor crystals were placed into the QCM-D flow chambers and cleaned by flowing ultrapure water, 2% sodium dodecyl sulfate solution (Sigma, St. Louis, MO), and ultrapure water through the system. The sensors and chambers were dried with nitrogen gas. A Plasma Prep II oxygen plasma cleaner (SPI Supplies, West Chester, PA) was used to etch the sensor surface before each experiment to remove the outer atomic layers of the crystal surface and make it more hydrophilic. This latter step facilitates vesicle rupture into a bilayer.

4.3.4 Bilayer formation and peptide exposure

Buffer was flowed over QCM-D sensors at 0.15 mL/min for ~15 min. until the frequency and dissipation responses were stable. The lipid SUV solution was flowed over the crystals for ~8 min. to form a stable supported lipid bilayer (SLB). The crystals were rinsed with buffer to remove any unattached lipids. After establishing a baseline, peptide solution was added for 10 min., at which time the pump was stopped. QCM-D crystals were exposed to a stagnant peptide solution for 1 hr, after which, the peptide solution was replaced with a final buffer rinse at 0.15 mL/min until the frequency stabilized. Each experiment was repeated at least 3 times for each concentration of chrysophsin-3.

4.4 Results

Bilayer formation was monitored by observing patterns in QCM-D frequency and dissipation responses. During bilayer formation, lipid vesicles first attach to the QCM-D sensor surface, adding mass. The vesicles then burst, releasing the fluid within the vesicle and creating a supported lipid bilayer.[31, 32] Typically, the frequency decreased by ~80 Hz when vesicles adsorbed, and showed an increase as soon as the vesicles ruptured to form the bilayer (Figure 4.3). The dissipation showed a characteristic increase to ~6 x 10^{-6} in response to the attachment of the water-filled vesicles. After bilayer formation, dissipation decreased because the bilayer is more rigid than vesicles. A complete bilayer could be characterized by a final Δf of ~26 Hz and change in dissipation (ΔD) of ~1 x 10^{-6} in the 3rd harmonic.

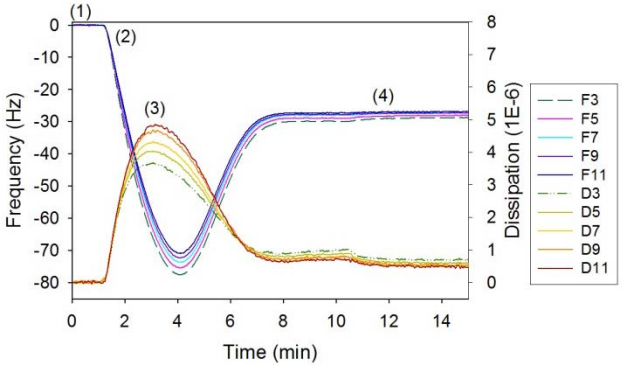

Figure 4.3. Typical QCM-D response for PC bilayer formation. (1) Initial buffer baseline, (2) vesicle deposition, (3) vesicle rupture and release of water, (4) stable bilayer. The lines represent different overtone responses for frequency and dissipation.

When peptide was added and allowed to remain in contact with the bilayer, changes in frequency and dissipation were monitored continuously for ~60 min (Figure 4.4). Typical frequency responses at all overtones showed an initial decrease in frequency, and therefore an increase in mass, on the crystal as peptides attached to the bilayer (Figure 4.5). The frequency

response produced using the 0.05 μM solution of chrysophsin-3 showed the smallest change of the concentrations tested (Figure 4.5A). Between chrysophsin-3 concentrations of 0.25 μM and 2 μM, the frequency decreased up to several Hz upon peptide exposure (Figure 4.5B-D). At higher chrysophsin-3 concentrations, dissipation values increased upon the sensor's contact with the peptide solution, suggesting that the film upon the sensor crystal became less rigid, or more saturated with fluid (Figure 4.4B). The subsequent buffer rinse resulted in a decrease in mass on the crystal and a more rigid film. Exposure to peptide at 4 μM and 10 μM concentrations also caused Δf to decrease rapidly, and this gradually stabilized to a value between -6 and -7 Hz, suggesting that the peptides approached a critical concentration on the supported lipid bilayer surface (Figures 4.5 E-F).

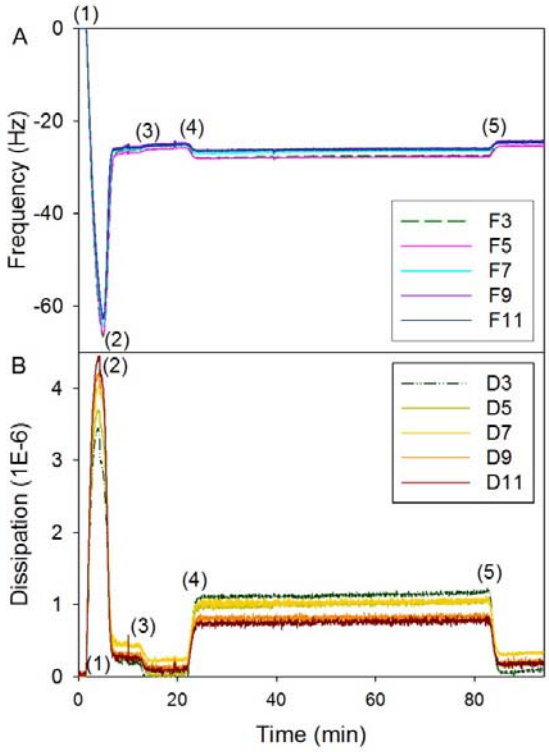

Figure 4.4. Typical frequency (A) and dissipation (B) responses for PC bilayer formation and subsequent chrysophsin-3 deposition. This experiment represents a chrysophsin-3 concentration of 4 μM. (1) Initial buffer baseline, (2) lipid vesicle deposition, (3 and 5) buffer rinse, (4) peptide addition.

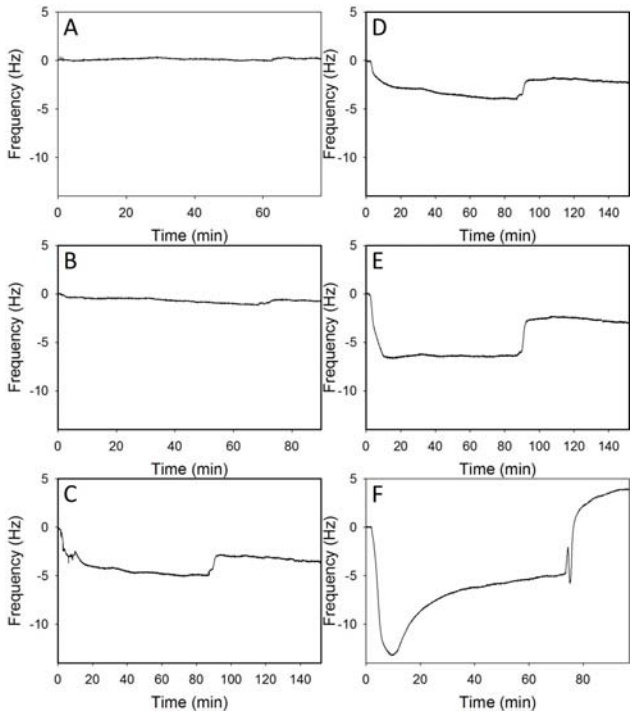

Figure 4.5. Typical concentration-dependent QCM-D responses in the 3rd harmonic for PC bilayers exposed to chrysophsin-3 at (A) 0.05 μM, (B) 0.25 μM, (C) 1 μM, (D) 2 μM, (E) 4 μM, (F) 10 μM chrysophsin-3 concentrations. The initial time of 0 min corresponds to time position (4) in Figure 4.4 and the final buffer rinse occurs at about 70 to 80 min, which corresponds to time position (5) in Figure 4.4.

Data were analyzed in terms of Δf and ΔD at all measured overtones before and after the final buffer rinse. The first measurement represents the stable state reached after 1 hr of peptide exposure, while the second measurement taken after the buffer rinse shows the irreversible change due to peptide-bilayer interactions. The Δf was calculated by taking the difference between frequencies at the beginning of peptide exposure and before (Figures 4.6, 4.7) or after the subsequent buffer rinse (Figures 4.8, 4.9):[23]

$$\Delta f = \left(\Delta f_{\text{bilayer and peptide}} - \Delta f_{\text{bilayer}}\right)\frac{1}{n} \tag{4.4}$$

At a very low concentration (0.05 μM chrysophsin-3), the peptide did not destabilize the bilayer, and Δf and ΔD were typically small, positive, and uniform across all overtones (Figures 4.6A, 4.7A, 4.8A, 4.9A). The average Δf for 0.25 μM chrysophsin-3 was between -0.7 Hz and -1.0 Hz

(Figures 4.6B, 4.8B) and the average Δ*D* was positive (Figures 4.7B, 4.9B). At intermediate chrysophsin-3 concentrations of 1, 2, and 4 μM, the greatest decreases in frequency and increases in dissipation occurred at the 3rd harmonic. The changes became less pronounced at higher overtones (Figures 4.6C-E, 4.7C-E, 4.8C-E, 4.9C-E). For the highest concentration tested (10 μM chrysophsin-3), non-homogeneous Δ*f* and Δ*D* values were produced at the stable stage before the buffer rinse (Figures 4.6F, 4.7F). However, positive Δ*f* values were observed at all overtones after the buffer rinse (Figure 4.8F), while the Δ*D* values were lower than those for 1, 2, and 4 μM and before the buffer rinse (Figure 4.9 F).

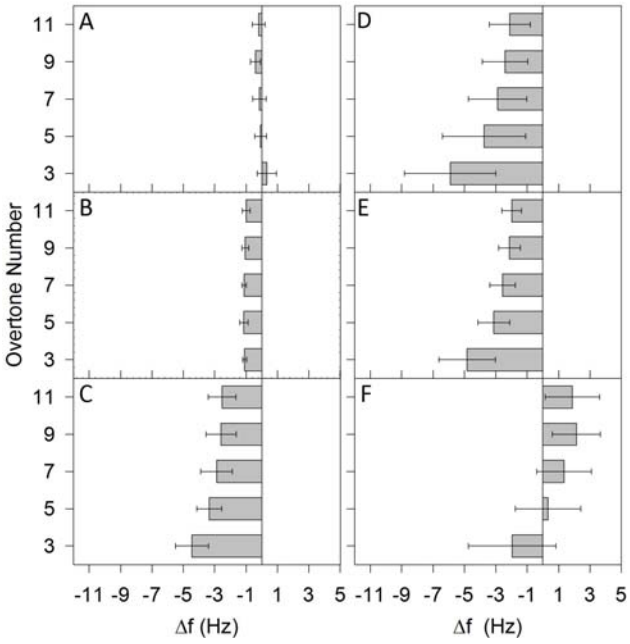

Figure 4.6. Average Δ*f* at different overtones for (A) 0.05 μM, (B) 0.25 μM, (C) 1 μM, (D) 2 μM, (E) 4 μM, (F) 10 μM chrysophsin-3 concentrations, before the buffer rinse. The graphs show the amount of mass that is attached to or removed from the bilayer after the SLB was exposed to chrysophsin-3 for 1 hr.

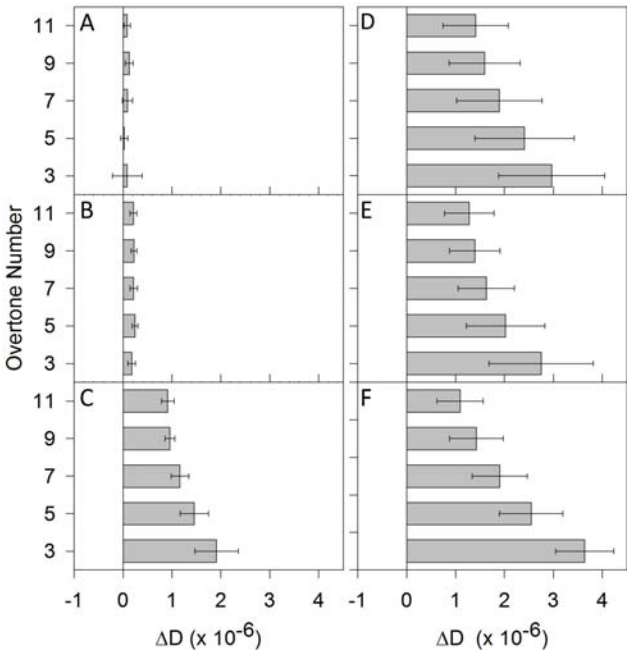

Figure 4.7. Average Δ*D* at different overtones for (A) 0.05 μM, (B) 0.25 μM, (C) 1 μM, (D) 2 μM, (E) 4 μM, (F) 10 μM chrysophsin-3 concentrations, before the buffer rinse. The changes reveal the homogeneous (at 0.05 and 0.25 μM concentrations) and heterogeneous (at larger concentrations) nature of the viscosity of the mass after exposure of the lipid bilayer to chrysophsin-3 for 1 hr.

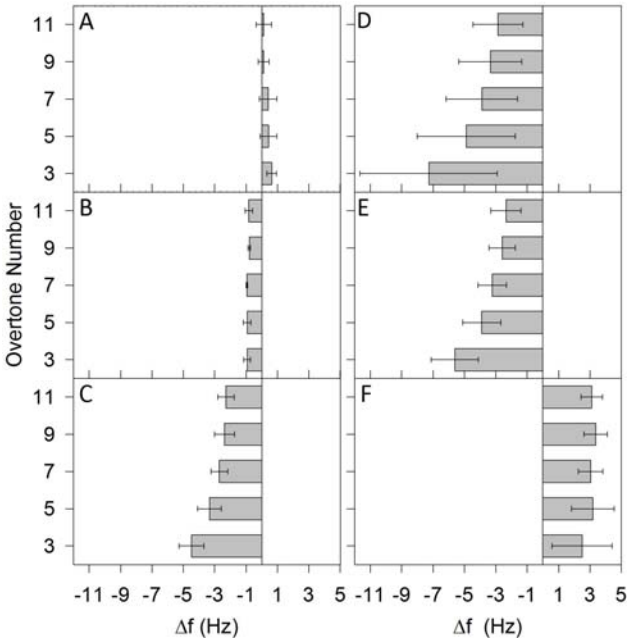

Figure 4.8. Average Δ*f* at different overtones for (A) 0.05 μM, (B) 0.25 μM, (C) 1 μM, (D) 2 μM, (E) 4 μM, (F) 10 μM chrysophsin-3 concentrations, after the buffer rinse. The changes show the amount of mass that is not removed by the final buffer rinse and is irreversibly attached to the crystal surface.

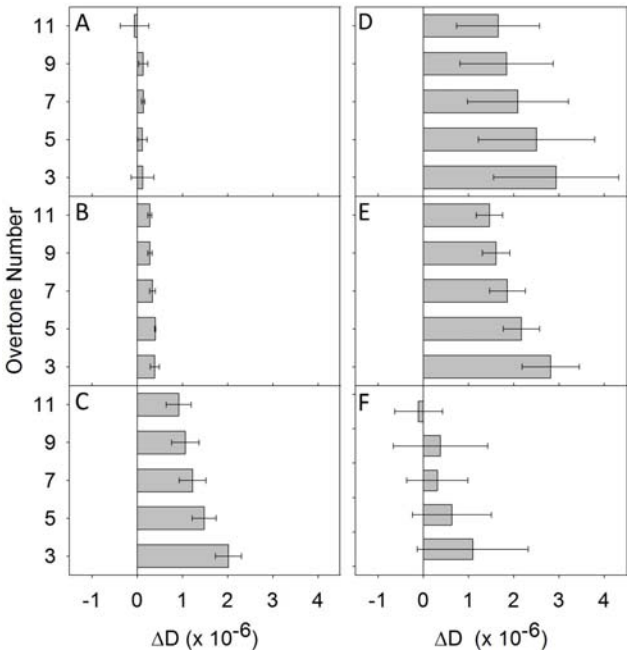

Figure 4.9. Average Δ*D* at different overtones for (A) 0.05 μM, (B) 0.25 μM, (C) 1 μM, (D) 2 μM, (E) 4 μM, (F) 10 μM chrysophsin-3 concentrations, after the buffer rinse.

4.5 Discussion

4.5.1 Formation of supported lipid bilayer

The Δ*f* values corresponding to PC bilayer formation were compared to published values.[20] According to prior researchers, a PC bilayer on silica corresponds to an initial Δ*f* of about -70 Hz, and a net change of -26 Hz, which are similar to what we observed. However, our initial Δ*f* was slightly higher at -80 Hz, which may be attributed to the use of Texas Red DHPE in this previous study, which we did not use.[20] Supported PC bilayers can be made reproducibly and easily on silica surfaces, which has led to them being used widely as model cell membranes.[24, 32, 33]

4.5.2 Mechanism of chrysophsin-3 action on PC bilayer

Once formation of the PC bilayer was validated through Δf and ΔD data, various concentrations of chrysophsin-3 were introduced to the membrane. At 0.05 μM chrysophsin-3, small Δf values (<1 Hz) were observed for each overtone (Figure 4.6A, 4.8A) and small, positive ΔD values were recorded before and after the final buffer rinse (Figure 4.7A, 4.9A). These results indicate that little or no mass change occurred in the bilayer. A small Δf (~0.4-0.7 Hz) was seen in the 3rd harmonic, which indicates a small amount of non-homogeneity in AMP action. The difference was not uniform at all overtones, and the positive Δf indicates that small amounts of mass are being removed after the final buffer rinse. Only a small fraction of lipid mass was removed, however, since the Δf values were much less than 26 Hz, which corresponds to removal of the full bilayer.

The frequency data for 0.25 μM chrysophsin-3 resulted in Δf values of ~-1 Hz (Figure 4.6B, 4.8B) and positive ΔD for all recorded overtones before and after the buffer rinse (Figure 4.7B, 4.9B), which indicates that the final buffer rinse did not significantly affect the mass and viscoelasticity of the membrane. Relatively uniform mass changes were observed at all measured overtones of the bilayer, which indicates that mass changes were homogeneous at all depths of the bilayer. The positive ΔD values observed at all overtones suggest that the membrane became less rigid with the addition of peptide. The Δf and ΔD data combined indicate cylindrical pore formation may have occurred, as peptides are positioned perpendicularly through the lipid bilayer and the mass changes at all depths are similar (Figure 4.10A). Also, the creation of pores would allow more water to enter the membrane space, making the film less rigid. At the 3rd harmonic, a mass change similar to that of the other overtones was observed. Therefore, the peptides that attached to the SLB likely formed pores and did not remain on the bilayer surface,

which would have resulted in heterogeneous changes and non-uniform responses. The difference in results at these low concentrations indicates that chrysophsin-3 will begin to form pores in the PC membrane at some critical concentration between 0.05 μM and 0.25 μM.

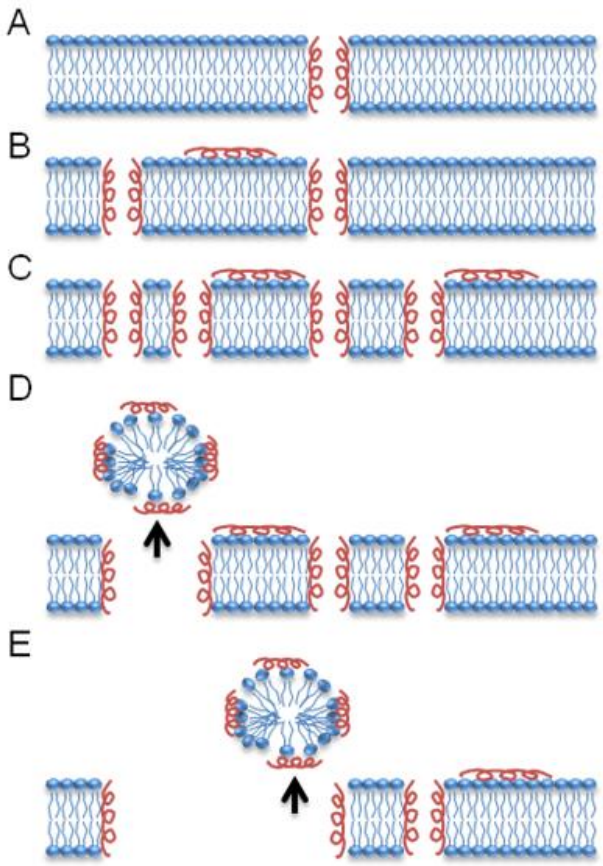

Figure 4.10. A proposed mechanism of chrysophsin-3 action on a supported PC bilayer as a function of peptide concentration. A) At low chrysophsin-3 concentrations (~0.25 μM), peptides prefer insertion into the membrane over adsorption onto the surface. B) As the concentration increases (~1 μM), peptides continue to form pores and begin to adsorb onto the bilayer surface. C) The amount of peptides adsorbed on the bilayer surface and inserted to form pores increases (~2 μM). D) At a certain critical concentration (~4 μM), peptide-lipid aggregates begin to be removed from the membrane. E) Large concentrations of chrysophsin-3 (~10 μM) result in the loss of large areas of the bilayer.

At 1, 2, and 4 μM concentrations, the 3rd harmonic exhibited the most mass addition (Δf) after peptide exposure and after the final buffer rinse. The other Δf values decreased in absolute magnitude with increasing overtones (Figures 4.6C-E, 4.8C-E). The 3rd harmonic also

demonstrated behavior of a less rigid film (ΔD) compared to the other harmonics, which also decreased as the overtones increased (Figures 4.7C-E, 4.9C-E). This indicates that the mass changes and viscoelasticity changes were heterogeneous throughout the membrane. One possible interpretation of these results is a large amount of peptide absorbed to the bilayer surface, resulting in non-uniform change in the bilayer. The ΔD results suggest that the film may be "softer" at the liquid-membrane interface due to the presence of water between the peptide molecules and the less rigid structure of the peptides adsorbed to the membranes. Since chrysophsin-3 formed cylindrical pores at 0.25 μM, the system likely consists of both pores and adsorbed AMPs at 1, 2, and 4 μM concentrations. In the proposed mechanism, the peptides adsorbed onto the surface of the SLB and formed pores in the membrane, as in the barrel-stave model (Figure 4.10B, C). The frequency response curve for 4 μM chrysophsin-3 shows the AMPs adsorbed on the lipid membrane rapidly reaching saturation, due to the Δf reaching steady state at -6.5 Hz (Figure 4.5E).

At a concentration of 10 μM, chrysophsin-3 addition to the PC bilayer resulted in negative Δf values at the 3rd harmonic and positive Δf values at higher overtones after 1 hour of peptide exposure (Figure 4.6F). However, the buffer rinse produced uniform positive Δf values at all overtones (Figure 4.8F). The raw frequency data showed an initial mass addition on the PC bilayer surface upon exposure to the AMP, followed by a decrease in mass that seemed to approach steady state (Figure 4.5F). These results suggest that at high concentrations, chrysophsin-3 initially adsorbs to the surface of the bilayer, forms pores in the membrane, and gradually causes mass removal, which may be in the form of peptide-lipid aggregates (Figure 4.10D, E). The mass loss was also increased by rinsing the system with buffer. The dissipation results suggest that the film became less rigid after 1 hour of peptide exposure (Figure 4.7F), but

more rigid after the buffer rinse (Figure 4.9F). The membrane also became more rigid with 10 μM chrysophsin-3 than it did at lower chrysophsin-3 concentrations. This could be due to the remaining large "islands," or areas, of lipids on the crystal surface surrounded by large regions of water created by mass lipid removal. The water may not be incorporated into the membrane as it is when there are fewer pores in the membrane, causing the measured film to be composed of the more rigid PC bilayer.

Mechler et al. followed a similar procedure to investigate the action of the peptides caerin 1.1, maculatin 1.1, and aurein 1.2 on DMPC and DMPC/DMPG (4:1) bilayers using QCM-D. The negative Δf resulting from chrysophsin-3 in this experiment correlated most closely with those of caerin 1.1, a 25-amino acid AMP isolated from the skin of the Australian tree frog[23]. Like chrysophsin-3, caerin 1.1 also exhibits an amphipathic α-helical conformation at the cell membrane surface.[34] On a DMPC bilayer, larger Δf values were measured for the 10 μM and 20 μM caerin 1.1 concentrations, which were significantly larger than those used in this study. The results for maculatin 1.1 revealed a critical concentration between 5 μM and 7 μM at which the system transitioned between overall mass removal and mass addition. Aurein 1.2 also appeared to exhibit different behavior at higher overtones between 7 μM and 10 μM solutions. The much smaller critical concentration of chrysophsin-3 may be attributed to the difference in peptide composition and structure, as well as the different lipids used in the membrane. Chrysophsin-3 has a higher molecular weight than aurein 1.2 and maculatin 1.1.[16, 23] Also, DMPC has a lower molecular weight than PC; the latter of which may be more conducive to pore formation.

4.5.3 Relating QCM-D results to chrysophsin-3 activity against bacteria

Pore formation can represent the start of the killing process in bacteria. Chrysophsin-3 has been tested for its antimicrobial activity against some Gram-negative and Gram-positive

bacteria, although the lethal concentration is different for each case. Iijima et al. found 0.25 μM to be the minimal lethal concentration of chrysophsin-3 required to kill 99% of *Bacillus subtilis* or *Escherichia coli*. Certain strains of Gram-positive and Gram-negative pathogenic bacteria, such as *Lactococcus garvieae* and *Vibrio anguillarum*, required 10 μM synthetic chrysophsin-3 to achieve the same level of killing, while other strains were resistant or required as low as 5 μM chrysophsin-3.[16] Research from our laboratory has shown that 0.22 mM chrysophsin-3, with added inosine and L-alanine, was needed to kill 99% of spores of *B. anthracis*, the cause of anthrax, and this killing occurred within one hour of exposure. Inosine and L-alanine are germination agents that promote the breakdown of the spore coat. Without any germinants, the same concentration of chrysophsin-3 killed about 80% of *B. anthracis* spores.[35]

In QCM-D experiments, we showed that at 0.25 μM chrysophsin-3, pore formation began to develop along the thickness of the membrane. At a much higher concentration of 10 μM, pore formation was greater and more mass was lost from the lipid bilayer membrane. These results seem consistent with the observed range of experimental lethal concentrations on bacterial cells. It is not yet known how specific differences in the lipid composition affect the ability to break down the membrane. The lipid PC, which we used in the present studies, has a zwitterionic headgroup. This is similar to the zwitterionic headgroup of *E. coli* and other Gram-negative bacterial membrane lipids.[36] Gram-positive bacteria, including *Bacillus spp*., have negatively charged headgroups in their lipid membranes.[36]

4.6 Conclusions

QCM-D frequency and dissipation data were used to elucidate the mechanism of AMP action on SLBs. Our results demonstrate that the nature of chrysophsin-3 interactions with a PC

bilayer is concentration-dependent. The AMP appears to destabilize the model membrane by forming pores and leaving the bilayer via peptide-lipid aggregates. QCM-D was shown to be an effective technique for studying AMP and SLB interactions. This method can be applied to other systems of peptides and lipid bilayers to provide a better understanding of AMP action on cell membranes.

4.7 Acknowledgements

We would like to thank Dr. Matthew C. Dixon (Biolin Scientific Inc.) for helpful discussions about QCM-D analysis. We thank Professor Alain Brisson (IECB) and Dr. Nam-Joon Cho (Stanford University) for useful discussions regarding preparing supported lipid bilayers. This work was supported by funding from the Natick Soldier Research, Development & Engineering Center (NSRDEC).

4.8 References

(1) Skarnes, R. C. and Watson, D. W. (1957) Antimicrobial factors of normal tissues and fluids, *Bacteriol Rev 21*, 273-294.

(2) Gazit, E., Miller, I. R., Biggin, P. C., Sansom, M. S. and Shai, Y. (1996) Structure and orientation of the mammalian antibacterial peptide cecropin P1 within phospholipid membranes, *J Mol Biol 258*, 860-870.

(3) Fulmer, P. A., Lundin, J. G. and Wynne, J. H. (2010) Development of antimicrobial peptides (AMPs) for use in self-decontaminating coatings, *ACS Appl Mater Interfaces 2*, 1266-1270.

(4) Decraene, V., Pratten, J. and Wilson, M. (2006) Cellulose acetate containing toluidine blue and rose bengal is an effective antimicrobial coating when exposed to white light, *Appl Environ Microbiol 72*, 4436-4439.

(5) Fritsche, T. R., Rhomberg, P. R., Sader, H. S. and Jones, R. N. (2008) Antimicrobial activity of omiganan pentahydrochloride tested against contemporary bacterial pathogens commonly responsible for catheter-associated infections, *J Antimicrob Chemother 61*, 1092-1098.

(6) Steiner, H., Andreu, D. and Merrifield, R. B. (1988) Binding and action of cecropin and cecropin analogues: antibacterial peptides from insects, *Biochim Biophys Acta 939*, 260-266.

(7) Gregory, K. and Mello, C. M. (2005) Immobilization of Escherichia coli cells by use of the antimicrobial peptide cecropin P1, *Appl Environ Microbiol 71*, 1130-1134.

(8) Boman, H. G., Agerberth, B. and Boman, A. (1993) Mechanisms of action on Escherichia coli of cecropin P1 and PR-39, two antibacterial peptides from pig intestine, *Infect Immun 61*, 2978-2984.

(9) Brogden, K. A. (2005) Antimicrobial peptides: pore formers or metabolic inhibitors in bacteria?, *Nat Rev Microbiol 3*, 238-250.

(10) Shai, Y. (2002) Mode of action of membrane active antimicrobial peptides, *Biopolymers 66*, 236-248.

(11) Pouny, Y., Rapaport, D., Mor, A., Nicolas, P. and Shai, Y. (1992) Interaction of antimicrobial dermaseptin and its fluorescently labeled analogues with phospholipid membranes, *Biochemistry 31*, 12416-12423.

(12) Shai, Y. and Oren, Z. (2001) From "carpet" mechanism to de-novo designed diastereomeric cell-selective antimicrobial peptides, *Peptides 22*, 1629-1641.

(13) Shai, Y. (1999) Mechanism of the binding, insertion and destabilization of phospholipid bilayer membranes by alpha-helical antimicrobial and cell non-selective membrane-lytic peptides, *Biochim Biophys Acta 1462*, 55-70.

(14) Huang, H. W. (2000) Action of antimicrobial peptides: two-state model, *Biochemistry 39*, 8347-8352.

(15) Cole, A. M., Darouiche, R. O., Legarda, D., Connell, N. and Diamond, G. (2000) Characterization of a fish antimicrobial peptide: gene expression, subcellular localization, and spectrum of activity, *Antimicrob Agents Chemother 44*, 2039-2045.

(16) Iijima, N., Tanimoto, N., Emoto, Y., Morita, Y., Uematsu, K., Murakami, T. and Nakai, T. (2003) Purification and characterization of three isoforms of chrysophsin, a novel antimicrobial peptide in the gills of the red sea bream, Chrysophrys major, *Eur J Biochem 270*, 675-686.

(17) Zhang, L., Parente, J., Harris, S. M., Woods, D. E., Hancock, R. E. and Falla, T. J. (2005) Antimicrobial peptide therapeutics for cystic fibrosis, *Antimicrob Agents Chemother 49*, 2921-2927.
(18) Mason, A. J., Bertani, P., Moulay, G., Marquette, A., Perrone, B., Drake, A. F., Kichler, A. and Bechinger, B. (2007) Membrane interaction of chrysophsin-1, a histidine-rich antimicrobial peptide from red sea bream, *Biochemistry 46*, 15175-15187.
(19) Tamm, L. K. and McConnell, H. M. (1985) Supported phospholipid bilayers, *Biophys J 47*, 105-113.
(20) Keller, C. A. and Kasemo, B. (1998) Surface specific kinetics of lipid vesicle adsorption measured with a quartz crystal microbalance, *Biophys J 75*, 1397-1402.
(21) Thid, D., Benkoski, J. J., Svedhem, S., Kasemo, B. and Gold, J. (2007) DHA-induced changes of supported lipid membrane morphology, *Langmuir 23*, 5878-5881.
(22) Wittmer, C. R., Phelps, J. A., Saltzman, W. M. and Van Tassel, P. R. (2007) Fibronectin terminated multilayer films: protein adsorption and cell attachment studies, *Biomaterials 28*, 851-860.
(23) Mechler, A., Praporski, S., Atmuri, K., Boland, M., Separovic, F. and Martin, L. L. (2007) Specific and selective peptide-membrane interactions revealed using quartz crystal microbalance, *Biophys J 93*, 3907-3916.
(24) Cremer, P. S. a. B., Steven, G. (1999) Formation and spreading of lipid bilayers on planar glass supports, *J. Phys. Chem. 103*, 2554-2559.
(25) Salafsky, J., Groves, J. T. and Boxer, S. G. (1996) Architecture and function of membrane proteins in planar supported bilayers: a study with photosynthetic reaction centers, *Biochemistry 35*, 14773-14781.
(26) Barenholz, Y., Gibbes, D., Litman, B. J., Goll, J., Thompson, T. E. and Carlson, R. D. (1977) A simple method for the preparation of homogeneous phospholipid vesicles, *Biochemistry 16*, 2806-2810.
(27) Kanazawa, K. K., Gordon II, J.G. (1985) The oscillation frequency of a quartz resonator in contact with liquid., *Analytica Chimica Acta 175*, 99-105.
(28) Voinova, M. V., Jonson, M. and Kasemo, B. (2002) Missing mass effect in biosensor's QCM applications, *Biosens Bioelectron 17*, 835-841.
(29) Voinova, M. V., Rodahl, M., Jonson, M., Kasemo, B. (1999) Viscoelastic acoustic response of layered polymer films at fluid-solid interfaces: continuum mechanics approach, *Physica Scripta 59*, 391-396.
(30) Bordes, R. and Hook, F. Separation of Bulk Effects and Bound Mass during Adsorption of Surfactants Probed by Quartz Crystal Microbalance with Dissipation: Insight into Data Interpretation, *Anal Chem*
(31) Richter, R., Mukhopadhyay, A. and Brisson, A. (2003) Pathways of lipid vesicle deposition on solid surfaces: a combined QCM-D and AFM study, *Biophys J 85*, 3035-3047.
(32) Keller, C. A., Glasmastar, K., Zhdanov, V. P. and Kasemo, B. (2000) Formation of supported membranes from vesicles, *Phys Rev Lett 84*, 5443-5446.
(33) Schonherr, H., Johnson, J. M., Lenz, P., Frank, C. W. and Boxer, S. G. (2004) Vesicle adsorption and lipid bilayer formation on glass studied by atomic force microscopy, *Langmuir 20*, 11600-11606.
(34) Stone, D. J. M., Waugh, R.J., Bowie, J.H., Wallace, J.C., Tyler, J.C. (1992) Peptides from Australian frogs. Structures of the caerins and caeridin 1 from *Litoria splendida*, *J. Chem. Soc. Perkin Trans. 1*, 3173-3178.

(35) Pinzon-Arango, P. A., Nagarajan, R. and Camesano, T. A. Interactions of antimicrobial peptide chrysophsin-3 with Bacillus anthracis in sporulated, germinated, and vegetative states, *J Phys Chem B 117*, 6364-6372.
(36) Blondelle, S. E., Lohner, K. and Aguilar, M. (1999) Lipid-induced conformation and lipid-binding properties of cytolytic and antimicrobial peptides: determination and biological specificity, *Biochim Biophys Acta 1462*, 89-108.

Chapter 5

Antimicrobial peptide alamethicin insertion into lipid bilayer: A QCM-D exploration

Colloids Surfaces B Biointerfaces, (2014). **116,** 472–481.

5.1 Abstract

Alamethicin is a 20-amino-acid, α-helical antimicrobial peptide that is believed to kill bacteria through pore formation in the inner membranes. We used quartz crystal microbalance with dissipation monitoring (QCM-D) to explore the interactions of alamethicin with a supported lipid bilayer. Changes in frequency (Δf) and dissipation (ΔD) measured at different overtones as a function of peptide concentration were used to infer peptide-induced changes in the mass and rigidity of the membrane as well as the orientation of the peptide in the bilayer. The measured Δf were positive, corresponding to a net mass loss from the bilayer, with substantial mass losses at 5 μM and 10 μM alamethicin. The measured Δf at various overtones were equal, indicating that the mass change in the membrane was homogeneous at all depths consistent with a vertical peptide insertion. Such an orientation coupled to the net mass loss was in agreement with cylindrical pore formation and the negligibly small ΔD suggested that the peptide walls of the pores stabilized the surrounding lipid organization. Dynamics of the interactions examined through Δf vs. ΔD plots suggested that the peptides initially inserted into the membrane and caused disordering of the lipids. Subsequently, lipids were removed from the bilayer to create pores and alamethicin caused the remaining lipids to reorder and stabilize within the membrane. Based on model calculations, we concluded that the QCM-D data cannot confirm or rule out whether peptide clusters coexist with pores in the bilayer. We have also proposed a way to calculate the peptide-to-lipid ratio (P/L) in the bilayer from QCM-D data and found the calculated P/L as a function of the peptide concentration to be similar to the literature data for vesicle membranes.

5.2 Introduction

Antimicrobial peptides (AMPs) are naturally occurring molecules that target and kill a broad spectrum of pathogenic bacteria, fungi, and viruses. All eukaryotic organisms that have

been analyzed for the production of AMPs, such as fish, frogs, and moths, have been found to express these molecules.[1, 2] AMPs, which are largely cationic and amphiphilic, are believed to kill bacteria by interacting with their negatively charged membranes. Once associated with the bacterial cell surface, AMPs can kill bacteria either by destabilizing the membrane or by translocating through the membrane to interact with intracellular targets. Because of this membrane destabilizing mechanism, the AMPs are less prone to the development of pathogen resistance than antibiotics.[3-6] Their broad spectrum of activity, lower levels of bacterial resistance, and the speed of their action on pathogens, hold promise for AMPs as alternatives to antibacterials, therapeutically and in self-decontaminating surfaces.[7, 8]

AMPs exist in solution with various secondary structures. When in contact with the membrane, many AMPs assume an α-helical secondary structure[3], with clearly differentiated hydrophilic and hydrophobic surfaces. They attach to and interact with lipid membranes through electrostatic interactions as well as through their hydrophobic and polar domain properties.[3] A fundamental model for AMP-membrane interactions has been advanced by Huang based on the proposition that the peptide exists in two distinct states in the membrane.[9-12] At very low peptide to lipid (*P/L*) ratios, the peptides are considered to be in adsorbed mode, referred to as the "surface" or "S" state, with the peptides embedded in the lipid head group region of the bilayer (Figure 5.1A). The resulting displacement of lipid head groups causes thinning of the lipid membrane.[9, 11] This perturbation of the lipids, at sufficiently high peptide to lipid ratios, drives a phase transition of the peptide to the "inserted" or "I" state wherein the peptides insert into the membrane, giving rise to the barrel-stave or cylindrical pores (Figure 5.1B). Some AMPs are presumed to form a different kind of pore structure in which the lipid head groups bend continuously from the outer membrane leaflet to the inner leaflet, giving rise to toroidal pores in

which the peptides are always in contact with the lipid headgroups. (Figure 5.1B).[13, 14] Once cylindrical or toroidal pores form, the cell is permeabilized, causing the cell to die.

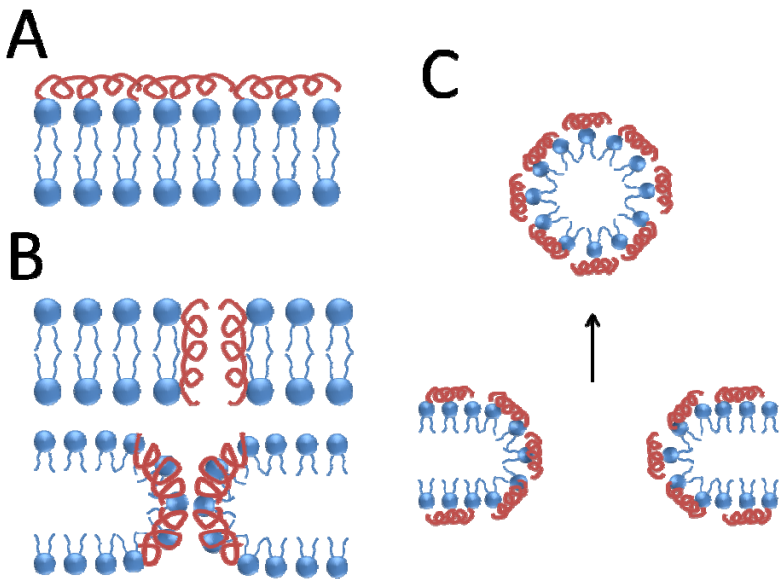

Figure 5.1. Mechanistic models of AMP action on lipid membranes with α-helical peptides represented as coils and lipids represented with headgroups and attached tails. (A) Peptide adsorption on the membrane surface or the "S" state, (B) peptide insertion into the bilayer resulting in cylindrical pore ("I" state) or toroidal pore formation, and (C) membrane disruption with the formation of lipid-peptide aggregates ("Carpet" model).

Another mode of interaction known as the carpet model [14] supposes that AMPs first align themselves parallel to the lipid membrane surface (Figure 5.1A) and at a large enough surface concentration of the peptide, directly cause membrane disintegration through the formation of peptide-lipid aggregates (micelles or bicelles) that detach from the membrane (Figure 5.1C). Some AMPs are also thought to translocate across the cell membrane and destroy intracellular components in addition to their membrane interactions.[15] The specific mechanism of action of the AMP is dependent on the structure and charge of the peptide, as well as the lipid composition of the cell membrane.[14]

Alamethicin is a 20-amino-acid, predominantly α-helical peptide that is derived from the fungus *Trichoderma viride*. It has been widely studied as a model for membrane proteins forming ion channels. Alamethicin is most effective against Gram-positive bacteria and fungi, with known minimum inhibitory concentrations (MICs) between ~1.5-25 μM against mollicutes, a class of bacteria that lack cell walls, and which are thought to have developed from Gram-positive bacteria. Alamethicin was also found to deform the helical cell structure of mollicute parasite *Spiroplasma melliferum* at a lower concentration of 0.1 μM.[16-19] Although alamethicin is less effective against Gram-negative bacteria, possibly due to the lipopolysaccharide barrier present in the bacterium's outer membrane, it can still inhibit growth at higher concentrations. Alamethicin at 25 μM was found to inhibit the growth of *Sinorhizobium meliloti*, a Gram-negative bacterium.[20]

Alamethicin (Ac-Aib-Pro-Aib-Ala-Aib-Ala-Gln-Aib-Val-Aib-Gly-Leu-Aib-Pro-Val-Aib-Aib-Glu-Gln-Phl) contains eight α-aminoisobutyric acid (Aib) residues and one L-phenylalaninol (Phl) residue, which are not commonly found in nature. The alamethicin sequence contains four residues having polar side chain groups: Gln^{7}, Glu^{18}, Gln^{19} and Phl^{20}. Alamethicin also contains a negative charge associated with the glutamic acid residue (Glu^{18}) located near the peptide's C-terminus. The helical wheel diagram for alamethicin is shown on Figure 5.2. A propensity for the α-helical secondary structure, a clear separation of hydrophobic and hydrophilic regions and significant hydrophobicity of this peptide are indicated by the helical wheel. The X-ray crystallographic structure of alamethicin[21] suggests that the amphipathic α-helical region is about 2.9 nm long. The crystal structure shows small deviations from a continuous α-helical conformation in the form of short (one to two residues) 3_{10} helical regions in the C-terminal domain, with a bend at the Pro^{14} residue. This conformation

allows for the formation of a polar region, consisting of the Gln[7] and Glu[18] residues and a nonpolar area that includes Val, Aib, Ala, and Leu residues. The Glu[18] side chain is typically protonated when the peptide is in a transmembrane state, making alamethicin's net charge effectively zero. The neutral nature of alamethicin is interesting in that AMPs are typically cationic, which plays a role in their ability to target negatively charged bacterial membranes. However, other factors, such as the hydrophobic side chains on many of alamethicin's amino acids, may increase alamethicin's affinity to bacterial membranes.

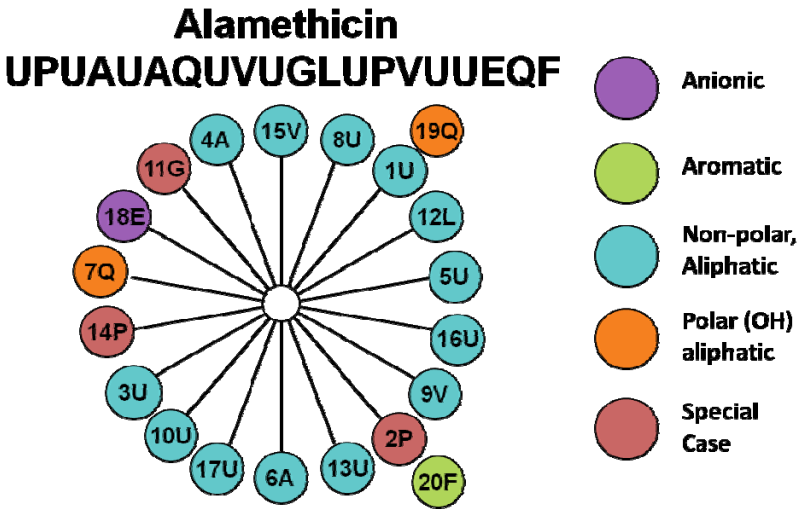

Figure 5.2. Helical wheel diagram of alamethicin. The diagram represents the peptide viewed along the axis of the helix, in which the peptide backbone is shown by the inner circle and the spokes represent amino acids. The amino acids are represented by their single letter codes and the number indicates their location in the primary structure starting from the amino end.
Since an α-helix contains 3.6 residues per turn, side-chains adjacent in the linear sequence are separated by 100° of arc on the wheel. Residues are color coded for their functionalities and the helical wheel shows a mostly hydrophobic peptide with a small region of hydrophilicity (see text for details).

Multiple techniques have been used to explore how alamethicin interacts with different model membrane systems and a brief survey of literature[22-37] is summarized in Table 5.1. It is reasonable to conclude that these studies offer evidence for membrane leakage due to pore formation,[23, 33] surface adsorbed state of the peptide,[24, 29, 30, 35, 36] membrane thinning,[25] and the

transition from the surface state of the peptide to the membrane inserted state.[24, 27, 29, 36] Different pore sizes have been proposed with 6 to 12 peptides per pore[22, 26, 28, 31, 32, 37] and the coexistence of peptide clusters along with water-filled pores has also been suggested.[31, 32] The most definitive experimental conclusions have come from studies using hydrated multilayers of stacked bilayers as membrane models rather than simple bilayers typical of cell membranes. In these studies, equilibrium structures generated at pre-determined peptide-to-lipid ratios were characterized and there was no possibility of discerning any information about the dynamics of the process when the peptide encounters the membrane.

Table 5.1. Brief survey of experimental methods and membrane models employed in the literature to explore alamethicin-membrane interactions[a]

Experimental Technique	Membrane System/ Lipids	Experimental observations	Ref.
Circular dichroism; phenylalaninol fluorescence	Vesicles in aqueous phase DMPC or DOPC	Alamethicin is not aggregated in the aqueous phase but aggregated in vesicle membrane; The *P/L* ratio in the vesicle was estimated as a function of peptide concentration in aqueous phase.	23
Oriented circular dichroism	Multilayers of oriented bilayers DPhPC	If *P/L* is below a critical value, most of the peptide molecules are on the membrane surface. If *P/L* is above the critical value, most of the peptide molecules are incorporated in the membrane.	24
X-ray lamellar diffraction	Multilayers of oriented bilayers DPhPC	Bilayer thickness decreases with increasing peptide concentration in proportion to the *P/L* ratio	25
Neutron in-plane scattering	Multilayers of oriented bilayers DLPC, DPhPC	In DLPC, the pores are made of 8-9 peptides, with a water pore 1.8 nm in diameter and an effective outside diameter of 4 nm. In DPhPC, the pores are made of 11 peptides, with a water pore of 2.6 nm in diameter and an effective outside diameter of 5 nm.	22, 26
Oriented circular dichroism	Multilayers of oriented bilayers DPhPC, DPhPE and mixtures	Observed sigmoidal insertion behavior indicating cooperative action in pore formation. Concluded that cooperativity is not associated with a micelle-like aggregation process, but instead, is driven by lipids through membrane-mediated interactions.	27
Multiwavelength anomalous diffraction (MAD)	Multilayers of oriented bilayers Brominated lipid (di 18:0 (9, 10 Br) PC)	Constructed electron density distribution profiles confirmed the formation of barrel-stave pores with eight alamethicin molecules per pore.	28
Calorimetry, sound velocity, atomic force microscopy	Unilamellar vesicles and (for AFM) fused vesicles on mica. DMPC, DPPC	Sound velocity data showed three distinct concentration dependent regions that can be associated with the "S" to "I" transition. AFM images in DPPC system showed peptide-induced defects ("holes").	29
Oriented ^{15}N solid-state NMR; Electron Paramagnetic Resonance-Electron Spin Echo Envelope Modulation	Multilayers of oriented bilayers DPPC	Alamethicin was in the surface-oriented "S" state at peptide concentrations of 1 mol % in gel-phase DPPC	30

X-ray scattering	Multilayers of oriented bilayers DOPC, di C22:1PC	Identified water containing pores with 6 peptides in DOPC and 9 peptides in diC22:1PC. Also proposed the presence of hexagonally packed alamethicin clusters (lacking water) in equilibrium with pores.	31, 32
Cryo-TEM and liposome leakage measurements.	Liposomes POPC or POPC/POPG	Leakage from liposomes clearly confirmed the formation of membrane pores, but the pore size was too small for direct detection by the TEM.	33
Small-angle neutron scattering with selective deuterium labeling	Vesicles DMPG and chain-perdeuterated DMPG and DMPC mixtures	Alamethicin enriched the outer leaflet of the vesicle with the negatively charged DMPG both in its "S" and "I" states.	34
Sum frequency generation (SFG) vibrational spectroscopy	Supported bilayer DMPC	Alamethicin was able to insert into fluid-phase membranes, but on the gel phase, it was on the surface either as single peptides or as aggregates and did not show significant insertion.	35
Sum frequency generation (SFG) vibrational spectroscopy	Supported bilayer POPC	Change in membrane orientation was consistent with "S" to "I" transition. Orientation of the α-helical component of alamethicin changed substantially while that of the 3_{10}-helical component remained unaffected.	36
Electrochemical scanning tunneling microscopy	Langmuir-Blodgett film DMPC + egg PG	Direct imaging showed the formation of cylindrical hexameric alamethicin pore incorporating a water channel.	37

[a] The lipid molecules are referred to in the Table and the text by abbreviations are as follows:
DLPC: 1,2-Dilauroyl-*sn*-Glycero-3-Phosphatidylcholine
DMPC: 1,2-Dimyristoyl-*sn*-Glycero-3-Phosphocholine
DMPG: 1,2-Dimyristoyl-*sn*-Glycero-3-Phosphocholine
DOPC: 1,2-Dioleoyl-*sn*-Glycero-Phosphatidylcholine
DPhPC: 1,2-Diphytanoyl-*sn*-Glycero-3-Phosphatidylcholine
DPhPE: 1,2-Diphytanoyl-*sn*-Glycero-3-Phosphoethanolamine
DPPC: 1,2-Dipalmitoyl-*sn*-Glycero-3-Phosphocholine
DPPG: 1,2-Dipalmitoyl-*sn*-Glycero-3-[Phospho-*rac*-(1-glycerol)]
DSPC: 1,2-Distearoyl-*sn*-Glycero-3-Phosphocholine
DSPG: 1,2-Distearoyl-*sn*-Glycero-3-[Phospho-*rac*-(1-glycerol)]
PC: Phosphatidylcholine
PG: Phosphatidylglycerol
POPC: 1-Palmitoyl-2-Oleoyl-*sn*-Glycero-3-Phosphocholine
POPG: 1-Palmitoyl-2-Oleoyl-*sn*-Glycero-3-[Phospho-*rac*-(1-glycerol)]

Indeed, monitoring the dynamic behavior of AMPs on lipid membranes has typically been difficult, due to the small scale of these interactions. We chose to examine the interactions of alamethicin with lipid membranes using quartz-crystal microbalance with dissipation monitoring (QCM-D), which can monitor these systems in real-time with a mass sensitivity of ~1.8 ng/cm^2 in liquid. Lipid bilayer supported on the quartz crystal was used as the model membrane. Changes in frequency (Δf) and energy dissipation (ΔD) of an oscillating sensor crystal were measured as mass attaches to and/or removed from the surface of the crystal, during the peptide-membrane interactions. A decrease in frequency can be related to an increase in

mass on the crystal surface and vice versa. Changes in dissipation can be related to changes in the viscoelasticity, or "softness," of the membrane on the sensor. Since disordering of lipids within a membrane can introduce spaces that would weaken the structure, dissipation measurements can reveal information about the level of disruption in a bilayer on the sensor surface. In this study, we examined the action of alamethicin on an egg phosphatidylcholine (PC) supported bilayer membrane at various peptide concentrations over a period of 1 h. From frequency and dissipation measurements at various overtones of the natural frequency of the crystal we have extracted qualitative and quantitative information on the equilibrium as well as dynamic nature of alamethicin-egg PC interactions.

5.3 Materials and methods

5.3.1 AMP and lipid vesicle preparation

Alamethicin was purchased from Sigma-Aldrich (St. Louis, MO). Peptide solutions were prepared in Tris-NaCl buffer [100 mM sodium chloride and 10 mM Tris(hydroxymethyl) amino methane (Sigma-Aldrich, St. Louis, MO) at pH 7.9]. Experiments were performed at 23˚C with peptide concentrations between 0.1 μM and 10 μM, which was within the range of MIC values found for alamethicin.[16-19] Lyophilized powder egg PC was purchased from Sigma Aldrich (St. Louis, MO) and Avanti Polar Lipids (Alabaster, AL). The PC was dissolved in ethanol and stored at -20˚C. To prepare small unilamellar vesicles (SUVs), the PC solution was dried with nitrogen gas and placed in a vacuum desiccator overnight. Tris-NaCl buffer was then added to the dried lipids, resulting in a final concentration of 2.5 mg/mL. The mixture was vortexed and homogenized through 5 freeze-thaw cycles. The solution was sonicated using an ultrasonic dismembrator (Model 150T, Thermo Fisher Scientific, Waltham, MA) in pulsed mode for 30 min at 0˚C. A 30% duty cycle was used for sonication (pulse on for 3 s, followed by a pause for

7 s) at an amplitude of 60. The vesicle solution was centrifuged at 17,500 rpm (37,000 g) for 10 min at 4˚C to remove probe particles from the ultrasonic dismembrator (J2-MI Centrifuge, Beckman Coulter, Brea, CA). The supernatant containing SUVs was collected and stored at 4˚C under nitrogen for up to 5 weeks.[38] Dynamic light scattering experiments (Zetasizer Nano ZS, Malvern, Worcestershire, UK) determined the diameter of the vesicles to be approximately 37 nm. The stock solution was diluted to 0.1 mg/mL in Tris-NaCl buffer before each QCM-D experiment.

5.3.2 Quartz crystal microbalance with dissipation monitoring (QCM-D)

The Q-Sense E4 system (Biolin Scientific, Sweden) was used to monitor the real-time mass and viscoelasticity changes to a supported lipid membrane deposited on the quartz crystal during AMP exposure. The supported lipid bilayer was formed using a vesicle deposition method at 23˚C, which was above the transition (gel-to-liquid) temperature of egg PC, allowing the lipids to remain in fluid phase during the experiment.[39, 40] The stock solution of PC vesicles injected into the QCM-D chamber at a flow rate of 0.15 mL/min. Changes in frequency and dissipation were monitored as the PC vesicles attached to the sensor's silica surface and ruptured to form a lipid bilayer. Since the mass and dissipation changes resulting from the attachment and rupturing of lipid vesicles on the crystal surface were consistent in each experiment, the QCM-D data served to confirm the consistent formation of a stable bilayer.[39, 40] This approach to supported bilayer formation was robust as we had confirmed in our previous QCM-D studies on chrysophsin-3.[41]

Following the formation of a stable supported lipid bilayer, the crystals were rinsed with buffer to remove any unattached lipids. After establishing a baseline, the solution of alamethicin was added for 10 min, at which time the pump was stopped. QCM-D crystals were exposed to a

stagnant peptide solution for 1 h, after which the peptide solution was replaced with a final buffer rinse at 0.15 mL/min to remove any unattached particles until the frequency stabilized. For each concentration of alamethicin, the Δf and ΔD values at different overtones were measured. The Δf was estimated by taking the difference between frequencies at the beginning of peptide exposure and after the subsequent buffer rinse. All the Δf and ΔD data presented in the results refer to the difference between two stages of the interaction process on the crystal surface: the lipid bilayer film after contact with the peptide and before contacting the peptide, thus accounting for only the peptide-induced effects on the bilayer. Effects due to liquid properties (such as density and viscosity) are cancelled out in this subtraction process. Experiments at each peptide concentration were repeated at least 3 times and the averages of the net changes in frequency and dissipation were reported as the final Δf and ΔD values taken after the buffer rinse. Error bars were determined from the standard deviation of the Δf and ΔD values.

5.3.3 Analysis of QCM-D data

Methods to relate the measured frequency and dissipation changes to changes in mass and in the viscoelastic properties of the membrane on the surface have been described in detail in the literature[42] and therefore only a brief summary is provided here. For a rigid film of areal mass m_f (mass per unit area) deposited on the crystal surface and exposed to air, the normalized frequency change Δf (with respect to the overtone number) and the areal mass of the film are related by the Sauerbrey equation, while the dissipation change ΔD is zero.

$$\Delta f = -f_o \frac{m_f}{m_q} \ , \ \Delta D = 0 \qquad (5.1)$$

Here, f_o is the natural frequency of the oscillator and m_q is the areal mass of the quartz crystal. The mass addition due to the film deposited on the crystal surface gives rise to a decrease in the frequency (negative Δf) while net mass loss is indicated by a positive Δf. The dissipation D is

related to the loss modulus G'' and the storage modulus G' in the form $D = G''/(2\pi\, G')$ and the change in dissipation ΔD can be related to the changes in the rigidity or viscoelasticity of the film attached to the crystal surface. Obviously, for the rigid film, the change is dissipation is zero.

If the rigid film is immersed in a Newtonian liquid like water, the frequency and dissipation changes are modified due to the presence of water and are now given by

$$\Delta f = -\frac{\eta_L}{2\pi\delta_L m_q} - f_o\frac{m_f}{m_q}\ ,\ \ \Delta D = \frac{\eta_L}{n\pi f_o \delta_L m_q} \tag{5.2}$$

where η_L is the viscosity of the liquid medium and δ_L is the decay length of the acoustic wave in the liquid medium. The first term in Δf and the term appearing in ΔD are due to the solvent effect due to the immersion of the crystal in the liquid and they vanish when we consider the changes in the crystal properties after and before the deposition of the rigid film. Effectively, the film mass changes are given just by the Sauerbrey term. If the film is not rigid but viscoelastic, then the frequency and dissipation changes are given by

$$\begin{aligned}\Delta f &= -\frac{\eta_L}{2\pi\delta_L m_q} - f_o\frac{m_f}{m_q}\left[1 - \frac{2}{\rho_f}\left(\frac{\eta_L}{\delta_L}\right)^2\frac{G''}{G'^2 + G''^2}\right],\\ \Delta D &= \frac{\eta_L}{n\pi f_o \delta_L m_q} + \frac{m_f}{m_q}\left[\frac{4}{\rho_f}\left(\frac{\eta_L}{\delta_L}\right)^2\frac{G'}{G'^2 + G''^2}\right]\end{aligned} \tag{5.3}$$

where ρ_f is the density of the film on the crystal surface. As in eq.(5.2), the first term in the expressions for Δf and ΔD are due to the solvent effect and they vanish when we consider changes in film properties when the film is immersed in the liquid both before and after the change. The film mass change is now given by the Sauerbrey term with a correction factor accounting for the viscoelastic properties of the film.

The contribution of viscoelasticity of the film to the measured frequency change (or equivalently, the measured mass) can be estimated from eq.(5.3). For a 5 MHz crystal, taking the density of water and of the bilayer to be 10^3 kg/m^3, the viscosity of water to be 10^{-3} N s/m^2, and the viscoelastic ratio G'/G'' = 0.1, the second term within the brackets, which provides the viscoelastic correction to unity, is approximately 0.03 for G''=1 MPa and 0.3 when G'' is 0.1 MPa. A viscoelastic ratio of 0.1 and G'' = 0.1 MPa were used by Voinova et al. for an adsorbed layer of vesicles[42], and for the supported bilayers, one may expect these values to be somewhat different.

There is also a non-vanishing ΔD accompanying the film mass change in eq.(5.3). An increase in ΔD indicates a less rigid, possibly more disordered film, and a decrease in ΔD indicates a more rigid film on the crystal surface. In experiments involving supported lipid bilayers (SLBs), ΔD can also provide information about changes in the structure and ordering of the lipids. Disruption of the membrane will cause the lipids to become less ordered and potentially allow more water to associate with the membrane, increasing the film's hydration and ΔD values.

As mentioned already, it is possible to measure not only the changes in the fundamental resonant frequency of the quartz crystal, but also changes in its harmonics. Available commercial instruments allow measurements of odd overtones up to the 13th (or even the 15th) multiple of the fundamental frequency. Since higher frequencies dissipate energy faster in a viscous medium, the higher overtones decay faster (the decay length is shorter) and are more confined to the surface region of the crystal. In this study, the 3rd through 11th overtones, or harmonics, were measured and related to processes throughout the film. Due to varying penetration depths of the acoustic waves associated with different overtones, higher overtones are qualitatively more

representative of processes occurring closer to the sensor surface while the lower overtones are representative of processes occurring near the water-film interface. Similar Δf and ΔD values at all overtones indicate a homogeneous change in mass and viscoelasticity over the depth of the film on the crystal's surface. On this basis, the overtone analysis has been used by Mechler et al.[43] to differentiate peptides inserted in bilayers with a vertical orientation (with respect to bilayer surface) compared to surface adsorbed peptides. Further, the molecular mass and viscoelasticity changes on the film can be monitored in real time by tracing the relation between Δf and ΔD over the entire course of the experiment.

5.4 Results and discussion

5.4.1 Changes in Δf and ΔD with peptide concentration and overtone number

The measured Δf and ΔD at 3rd to 11th overtones are presented in Figure 5.3 for aqueous phase peptide concentrations ranging from 0.25 μM to 10 μM. The dissipation changes ΔD were small at all peptide concentrations suggesting that the membrane with and without alamethicin was rigid and therefore, the measured frequency changes can be directly related to mass changes through the Sauerbrey equation. Exposure of the supported lipid membrane to alamethicin concentrations above 0.1 μM resulted in positive Δf values implying mass removal from the bilayer. The relative amount of mass lost from the bilayer increased with increasing alamethicin concentration. At 0.25 μM alamethicin, the Δf values were ~1 Hz, and they increased to ~5 Hz at 10 μM alamethicin. Since previous experiments showed that the formation of a complete bilayer corresponded to a Δf value of ~-25 Hz, frequency shifts between 1 and 5 Hz were indicative of 4-20% mass loss from the original lipid bilayer.[40, 41] Since the data show a net mass loss, any incorporation of alamethicin into the membrane must be overcompensated by depletion of lipid

molecules from the bilayer. This would be consistent with the creation of pore structures with water channels in the bilayer, since that would require removal of lipid molecules.

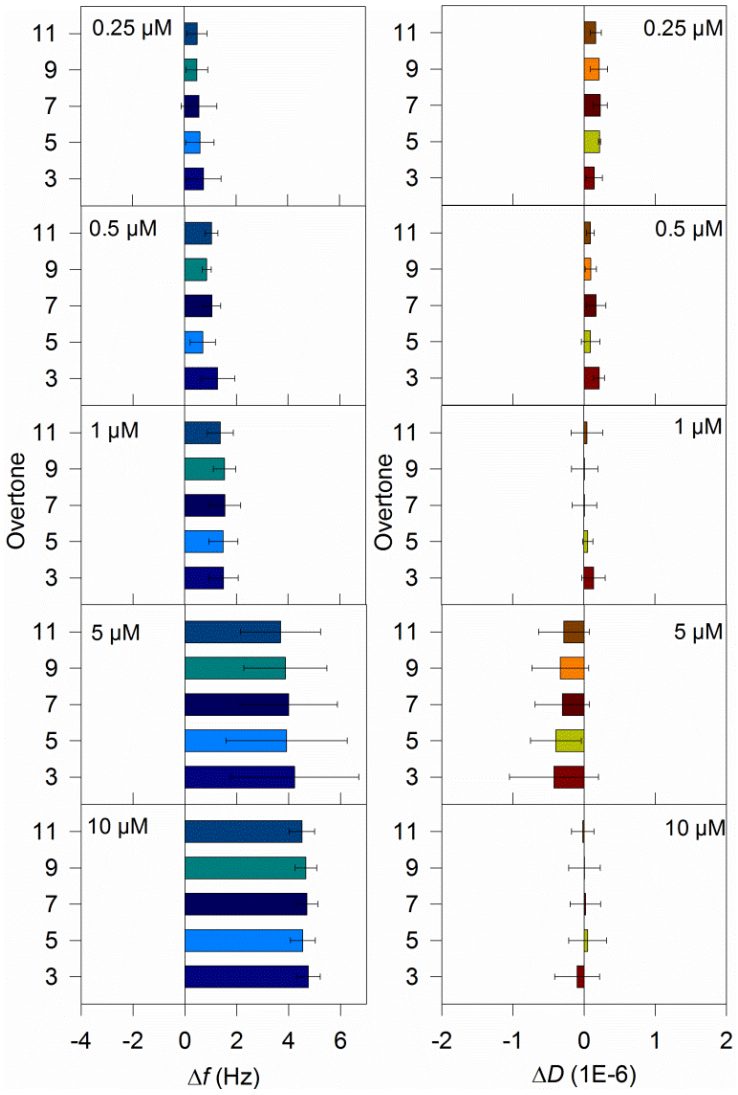

Figure 5.3. Changes in frequency and dissipation corresponding to various aqueous phase concentrations of alamethicin interacting with the PC membrane. Values for Δf and ΔD are shown for the 3rd through 11th overtones and represent the changes induced by alamethicin activity on a stable supported bilayer membrane. Initial measurements (t = 0 s) are taken after stable bilayer formation and final measurements are taken after the buffer rinse following 1 h of peptide incubation. Higher overtones are associated with changes closer to the sensor surface. Error bars represent the standard deviation based on at least 3 replicate experiments.

The measured Δf values were uniform across all overtones at each concentration of alamethicin (Figure 5.3). This would suggest that mass removal from the membrane was uniform along the depth of the membrane. This mass depletion likely occurred as a result of peptide insertion into the membrane, which was expected to create homogeneous overtone responses. This uniformity in the Δf values for all overtones is consistent with the formation of cylindrical pores since such a pore structure is characterized by uniform behavior along the depth of the bilayer.

The measured dissipation values ΔD were small at all peptide concentrations (Figure 5.3), suggesting that the ordering of molecules in the membrane before and after exposure to alamethicin resulted in the same membrane "stiffness," or viscosity. This would be consistent with a cylindrical pore structure where the lipids are allowed to remain unaffected thanks to the creation of peptide wall along the pore boundary. Even though water channels exist, they do not contribute to bilayer viscoelasticity because of the organization of the peptide walls that confine the lipids to a state similar to that in the original lipid bilayer.

One may note that lipid loss from the membrane was observed even at 0.05 μM alamethicin (data shown in Appendix 1.1). The Δf and ΔD data suggest that even at low peptide concentrations, alamethicin creates cylindrical pores and one may have to go to much lower alamethicin concentrations than what has been considered in this study, to observe a surface adsorbed "S" state.

The substantial membrane disruption that occurred at alamethicin concentrations above 1 μM in this study is consistent with results from a previous study that showed that alamethicin is effective against mollicutes at ~1.5-25 μM alamethicin.[18, 19] Alamethicin caused the removal of

at least ~20% of the lipid membrane mass at 10 μM peptide concentrations, which could lead to complete membrane destabilization. This estimate of the extent of lipid loss assumes that a stable lipid bilayer corresponds to a -25 Hz change in frequency, which was shown through consistent PC bilayer formation. Alamethicin has also been shown to inhibit Gram-negative bacterial growth at higher 25 μM concentrations. The discrepancy between the AMP concentrations needed to inhibit bacterial growth and to destabilize the PC membranes in these experiments may be due to the presence of a lipopolysaccharide barrier in the bacteria's outer membrane. Higher AMP concentrations may be necessary for AMPs to disrupt and pass through the barrier before disrupting the cell membranes. Also, bacterial cell membranes contain different lipids and membrane components (e.g. membrane proteins) than our model system in this study, which could lead to differences in AMP concentration-dependent behavior.

5.4.2 Time evolution of Δf vs ΔD and dynamics of alamethicin – bilayer interactions

Mechanistic information derived solely from overall Δf and ΔD values as in Figure 5.3 give no indication of the dynamic processes that would have occurred during the 1 h period in which the PC bilayer membrane was exposed to the peptide. Therefore, the QCM-D results were also analyzed using ΔD vs. Δf plots (Figures 5.4 and 5.5) to infer at least qualitatively the nature of dynamics controlling alamethicin–bilayer interactions. The points shown in these graphs represent Δf and ΔD values at evenly spaced time intervals (0.7 s between points). Larger spacing between points indicate that the mass or viscoelasticity changes in the membrane occur at a faster rate. Changes in slopes in these plots generally indicate a change in mechanism.[44]

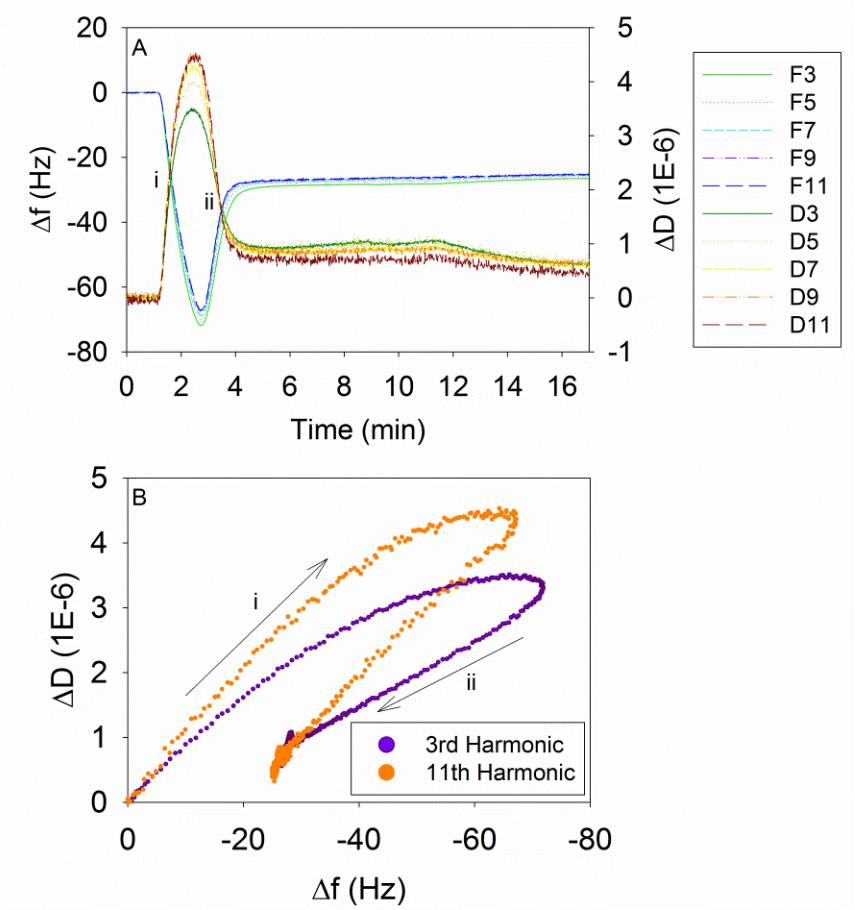

Figure 5.4. (A) ΔD and Δf measurements showing stable supported lipid bilayer (SLB) formation on silica, followed by a Tris-NaCl buffer rinse at t = 11.5 min to remove any unattached particles. (B) ΔD vs. Δf plot showing the dynamics of SLB formation. The frequency axis has been reversed to make interpretation more intuitive. As mass increases on the QCM-D sensor, frequency shifts to the right. The initial frequency decrease (*i*) shows the attachment of vesicles to the surface. The vesicles then rupture, releasing trapped water, and forming a bilayer (*ii*). The arrows (labeled *i* and *ii*) indicate the progression of data points with increasing time. Data points are taken at 0.7 s intervals. The silica surface of the sensor crystal is bare and submerged in Tris-NaCl buffer at t = 0 s.

Figure 5.4 describes how from the time evolution of ΔD and Δf (Figure 5.4A) the dynamic ΔD vs. Δf plots (Figure 5.4B) were constructed. As PC vesicles attached to the QCM-D sensor's silica surface, the mass on the sensor increased, causing the frequency to sharply decrease (Figure 5.4A). This process was shown in the corresponding ΔD vs. Δf as the points moved in the north-east direction (shown by the arrow labeled *i*), indicating an increase in mass

on the surface as well as the viscoelastic nature of adsorbed vesicle layer (Figure 5.4B). Arrows pointing east reveal increases in mass while those pointing north reveal an increase in softness or viscoelsticity. Once the vesicles broke up and organized into a planar bilayer, there was a mass loss due to release of water from vesicle interior as well as the loss of excess lipid from the vesicle. Simultaneously there was a decrease in dissipation change due to higher ordering of the planar bilayer compared to the soft water filled vesicles. Correspondingly, the ΔD vs. Δf trace changed in direction (labeled *ii*), resulting in a south-west trend that indicated a loss in mass and decrease in viscoelasticity. West pointing arrows indicate a decrease in mass while south-pointing arrows indicate an increase in membrane rigidity and therefore more organized molecules. In Figure 5.4B, data from the 3^{rd} and 11^{th} overtones showed similar behavior and extended over the same range of ΔD and Δf, both being large. This suggested that the bilayer formation process starting from adsorbed vesicles caused significant changes both near the crystal surface (11^{th} overtone) as well as at the interface with bulk water (3^{rd} overtone).

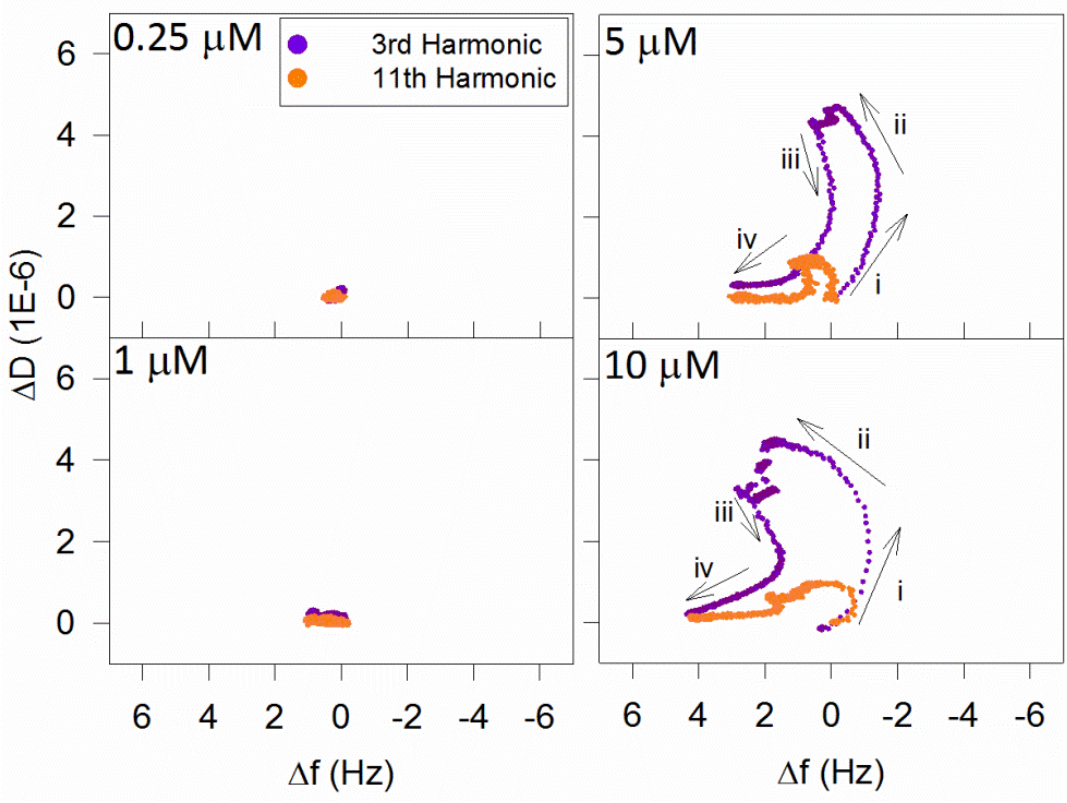

Figure 5.5. Δ*D* vs. Δ*f* plots of alamethicin-bilayer interactions at various concentrations of the peptide in aqueous phase. These plots show changes in viscoelasticity of the membrane in relation to the changes in mass during the time evolution of the interactions. At t = 0 s, a stable bilayer has been formed on the QCM-D crystal. The measurements include 1 h of incubation with the peptide and a subsequent buffer rinse. The 3rd and 11th harmonics are shown to represent the different processes occurring near the surface of the lipid membrane and near the surface of the QCM-D crystal. These graphs show representative data from one experiment based on at least 3 repeated measurements.

The dynamics of alamethicin-bilayer interactions were explored through the Δ*D* vs. Δ*f* traces during the time course of alamethicin contact with the bilayer in Figure 5.5. At 0.25 μM alamethicin, a very small change to membrane mass and virtually no change to viscoelasticity were observed at both the 3rd and 11th harmonics. At a concentration of 1 μM, the trace (labeled *i*) showed a similar small mass loss and no change in the lipid membrane ordering during exposure to alamethicin. Since mass was lost at both overtones, all depths of the membrane experienced a loss in lipid mass, possibly due to peptide insertion to create a small number of

cylindrical pores. At 5 μM, a much larger change in the membrane was observed. Both overtones revealed overall loss of lipid mass with simultaneous disordering of the membrane that was not captured by the static experimental data in Figure 5.3. Initially, the data points travelled in the north-east direction (labeled *i*), suggesting that alamethicin molecules were added on to the membrane and disrupted lipid ordering in the bilayer. Greater mass addition and molecular disordering was measured in the 3rd harmonic compared to the 11th harmonic, suggesting that the peptides had attached to the surface of the membrane or partially inserted into the membrane. The peptide-membrane interaction mechanism then shifted in the north-west direction (labeled *ii*), indicating that the membrane began to lose mass, while still experiencing lipid disorder. The traces subsequently changed direction (labeled *iii*-*iv*), suggesting that the lipid membrane became more rigid as it continued to lose lipid mass. The decrease in dissipation may have been due to the alamethicin molecules completely inserting into the membrane and reintroducing order to the system as it stabilized the edges of pores in the lipid bilayer. The results for 10 μM alamethicin revealed a similar trend indicating that the dynamic mechanisms did not change with peptide concentration.

In Figure 5.5, at both 5 μM and 10 μM alamethicin, the range of Δf is the same for both the 3rd and 11th overtones while the range of ΔD is larger for the 3rd overtone compared to the 11th overtone. This clearly suggests that at the water-bilayer interface (qualitatively indicated by the 3rd overtone behavior) there was considerable lipid disruption during the dynamic process while very close to the quartz surface (indicated by the 11th overtone), the lipid organization was not significantly perturbed. Note that the static data in Figure 5.3 shows that the net change in dissipation was negligibly small for both overtones, indicating similar rigidity of the membrane

before and after interactions with alamethicin. Evidently, one could not analyze the process dynamics if only the static data were available.

5.4.3 Calculation of bilayer properties from QCM-D data

The area per lipid in the bilayer (denoted as a_L) and the thickness of the bilayer were calculated from the measured frequency change of ~25 Hz, accompanying the formation of the supported bilayer. Noting that the proportionality constant C in the Sauerbrey equation is 17.8 ng/cm^2 for a crystal oscillating at 5 MHz natural frequency, the bilayer areal mass corresponding to a frequency change of 25 Hz is equal to 445 ng/cm^2. It has been shown that this mass includes the mass of a layer of water between the quartz crystal and the supported lipid bilayer and the mass of this water layer has been determined to be ~ 102 ng/cm^2.[45] Correcting for this water mass, we estimate the areal mass of the lipid bilayer to be 343 ng/cm^2. The molecular mass M_L of the lipid is calculated to be 1.267x10^{-12} ng/molecule corresponding to an average molecular weight of 760 g/mol for the egg PC lipid. Dividing the areal mass of the lipid bilayer by the mass of a single lipid molecule M_L, we estimate there are 2.7 molecule/nm^2 on the bilayer or 1.35 molecules/nm^2, in each monolayer. This corresponds to a lipid area a_L of 0.739 nm^2 /molecule.

If the molecular volume v_L of the hydrophobic tail of the egg PC lipid is 0.96 nm^3/molecule (taken as the composition average based on the constituent C16 and C18 chains), then the thickness of the hydrophobic region of the bilayer $h_L = 2v_L/a_L = 2.6$ nm. Alternately, if we take the lipid density to be about 1 g/cm^3, then for a lipid average molecular weight of 760, the corresponding lipid molecular volume v_{lipid} is 1.267 nm^3. The lipid bilayer thickness will then be $h_{lipid} = 2v_{lipid}/a_L = 3.43$ nm. If we consider the lipid head groups on the two layers to take up 1 nm,[9] then the hydrophobic region of the bilayer will have a thickness of 2.43 nm. These estimates based on QCM-D data and molecular properties of lipids can be compared to the x-ray

measurements of Huang[9] who obtained a_L = 0.74 nm^2 and h_L = 2.66 nm for DOPC, and a_L = 0.68 nm^2 and h_L = 2.75 nm for POPC.

5.4.4 Differentiating pore formation vs. cluster formation based on the QCM-D data

We have used the QCM-D data along with model calculations to explore whether alamethicin inserts into the bilayer to create water-free clusters as suggested by Nagle et al.[32] in addition to their pore formation. Nagle et al. proposed the formation of hexagonally packed clusters of alamethicin with no water channels (Figure 5.6), with the small hydrophilic domains on the peptides facing each other and the larger hydrophobic domains facing other hydrophobic surfaces or the lipid. The cluster could be of any size generated from a trimeric motif as shown on the figure. They also surmised that because the number of peptides in a cluster would be larger than in a pore, the ratio of clusters to bundles would increase as the total peptide concentration increased.

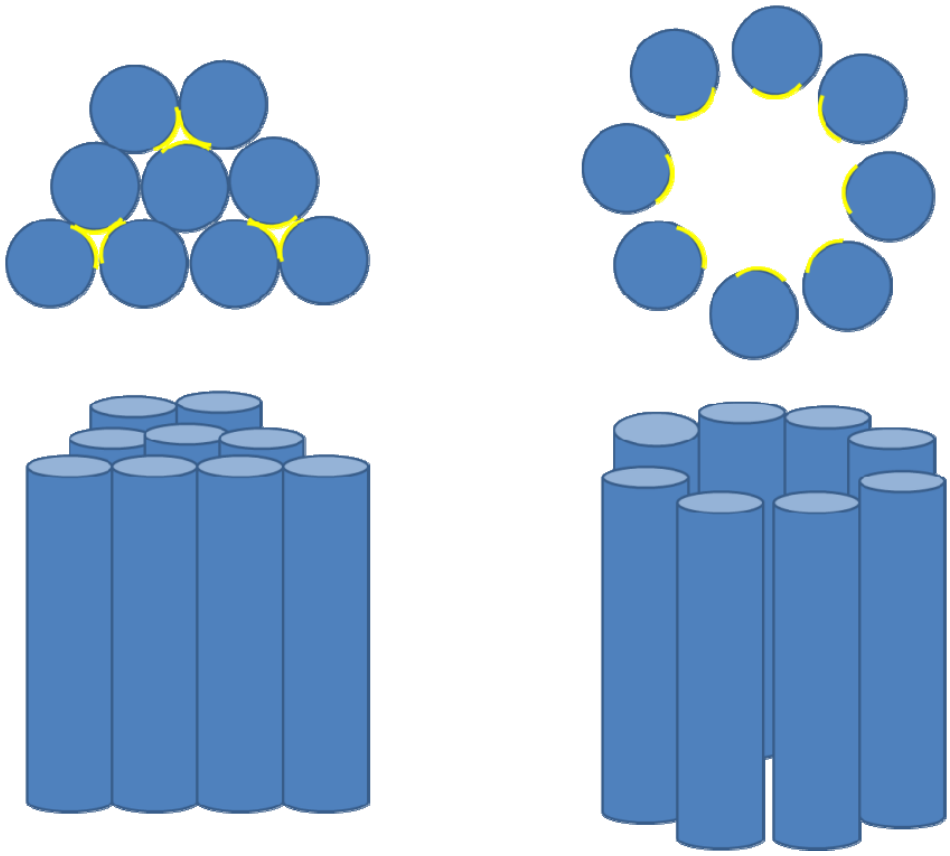

Figure 5.6. Schematic representation of alamethicin insertion into bilayer either as clusters or as pores. The lipids are not shown on the figure for clarity. On the left is an alamethicin cluster proposed in Ref.(32). It is shown as a cluster of 9 molecules made from 3 trimeric units. Ref.(32) suggests clusters of various sizes to be possible in trimeric units. On the right is a cylindrical pore, with 8 alamethicin molecules constituting the pore wall. The hydrophilic surface region of the peptide is small and is designated by the yellow color.

In the case of the peptide clusters, there are no associated lipids or water channels and the area per peptide a_P is calculated as $a_P = \pi d_P^2/4$ where d_P is the diameter of the peptide, visualized as a cylinder. The area per peptide a_P is estimated to be 0.945 nm^2/molecule, taking the diameter d_P of alamethicin to be 1.1 nm.[28] The molecular mass M_P of the peptide is calculated to be 3.275 x 10^{-12} ng/molecule, corresponding to a molecular weight 1965 g/mol of alamethicin.

In the case of a pore, the area per peptide is denoted as A_H/n, where A_H is the pore area and n is the number of peptide molecules constituting the pore. If we consider the approximate

pore size to be determined by the close packed arrangement of peptides at the pore boundary, then the outer diameter D_H of a pore with n peptides and the area of the pore per peptide A_H/n can both be calculated from

$$D_H = \frac{n\, d_P}{\pi} + d_P\,, \qquad \frac{A_H}{n} = \frac{1}{n}\frac{\pi D_H^2}{4} = \frac{1}{n}\frac{\pi d_P^2}{4}\left(\frac{n}{\pi}+1\right)^2 \tag{5.4}$$

For alamethicin, taking the peptide diameter d_P to be 1.1 nm, the pore diameter D_H estimated from eq.(7.4) will be about 3.9 nm for n = 8, and 4.6 nm for n = 10. Indeed, Huang[28] has estimated the number of peptides per pore to be 8 and the pore diameter of 3.9 nm (close to the estimate from eq.(7.4)). For the purpose of our model calculations, we will consider two values for the number of peptides in the pore, n = 8, 10 corresponding to which the pore area per peptide A_H/n will be 1.494 and 1.663 nm^2/peptide.

On the addition of peptide to the bilayer, lipid molecules are removed from a fraction λ of the bilayer area and replaced either by peptide clusters or pores. The number of lipid molecules removed will be $2\lambda A/a_L$, with the factor 2 again accounting for the two layers of the bilayer. We will denote by β, the fraction of the affected area where clusters form and by (1-β), the fraction of the affected area where pores form. Therefore, the $2\lambda A/a_L$ lipids removed will be replaced by $\lambda\beta A/a_P$ peptides in the clusters and by $\lambda(1-\beta)A/(A_H/n)$ peptides, in the pores. The resulting mass change per unit area can be equated to the areal mass change measured by QCM-D:

$$\Delta m = -C\,\Delta f = \lambda\left[\beta\frac{M_P}{a_P} + (1-\beta)\frac{M_P}{A_H/n} - 2\frac{M_L}{a_L}\right] \tag{5.5}$$

In this equation C is the proportionality constant between frequency change and mass change in the Sauerbrey equation, and M_P and M_L are molecular masses of the peptide and lipid molecule, respectively. The right hand side of eq.(7.5) accounts for the lipid leaving the bilayer and the

peptide entering the bilayer either as clusters or as pores. With the measured Δf, the fractional area λ affected by peptide-lipid interactions can be calculated using eq.(7.5) for assumed values of n and β. When $\beta = 0$, we have only pore formation and for any value of $\beta > 0$, we also have peptides inserted as close-packed clusters.

Having estimated all the molecular constants, and assuming values for β and n, we can calculate the fractional area λ affected by alamethicin–egg PC bilayer interactions using eq.(7.5) as a function of the alamethicin concentration in the aqueous phase. The calculated results are shown on Figure 5.7 for three assumed values of β and for $n = 8$ and 10. As mentioned already, $\beta = 0$ corresponds to the case when all inserted peptides are part of pores with water channels. The areal mass change is very small when alamethicin molecules are inserted as clusters since the area vacated by the egg-PC lipids is taken up by the peptides, and the net mass of lipids removed is not too different from the net mass of peptide added. (It should be noted that the areal mass change on cluster insertion could be larger for other choices of peptide-lipid molecules, depending on their molecular properties). The areal mass change is much larger when peptides are inserted as pores because in this case some of the area from which the lipid has been removed is replaced by the water channel that does not contribute to the film mass. Obviously, the change in areal mass increases with n since that increases the pore and water channel diameters. As a consequence the calculated results in Figure 5.7 show that in order to account for a given mass change, the affected area must be larger for $\beta > 0$ compared to when $\beta = 0$. For the same reasons, the affected area can be smaller when n is larger.

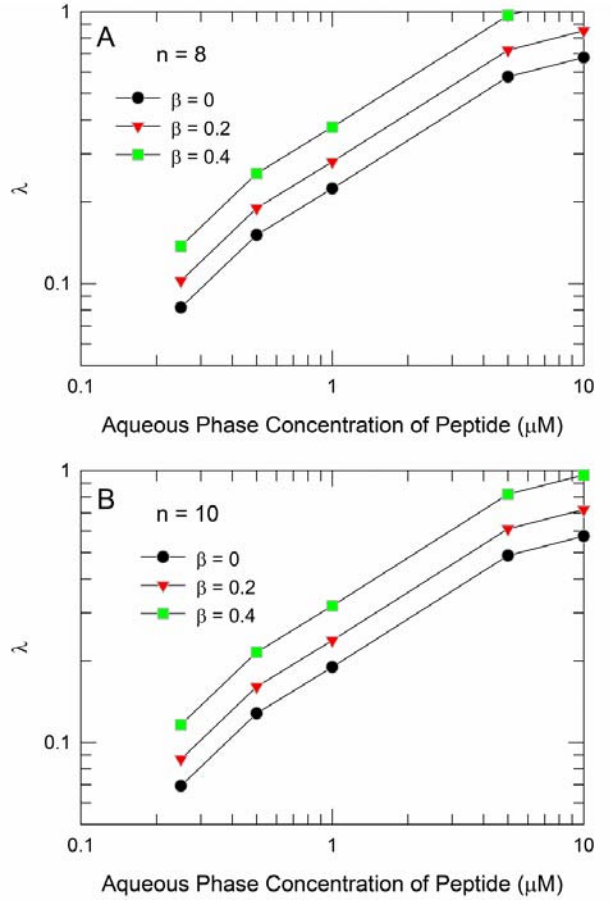

Figure 5.7. The calculated fractional area affected by alamethicin-egg PC bilayer interactions for different assumed values of the parameter β as a function of the aqueous phase alamethicin concentration. Two values of n are represented: (A) n = 8, (B) n = 10. The fractional area affected is larger for smaller n and larger β.

The ratio between the peptide in clusters and that in water-filled pores (P_C/P_P) can be calculated from eq. (7.6).

$$\frac{P_C}{P_P} = \left[\frac{\beta}{1-\beta}\frac{\frac{A_H}{n}}{a_P}\right] \tag{5.6}$$

For n = 8, the ratio P_C/P_P is 0, 0.39 and 1.06 for β = 0, 0.2 and 0.4, respectively. For n = 10, the ratio P_C/P_P is 0, 0.44, and 1.17 for β = 0, 0.2 and 0.4, respectively. As β increases, the peptides in

clusters become relatively more significant; and for a given β, the larger the n, the larger the P_C/P_P ratio. Nagle et al. have estimated P_C/P_P values of about 0.6 for DOPC multilayers when P/L values were about 0.05 to 0.10. From Figure 5.7 we note that cluster formation is possible but the QCM-D data cannot confirm or deny the coexistence of clusters. If an alternate technique is available to determine the fractional area affected at a given aqueous phase alamethicin concentration, then the QCM-D data coupled to these model calculations can be used to draw more definitive conclusions.

5.4.5 Estimation of P/L ratio in the inserted state

The peptide to lipid (P/L) ratio was a pre-determined experimental value in all of the multilayer membrane experiments. However, in the QCM-D experiments it is an outcome of the dynamic peptide-membrane interaction process. The P/L ratio in the bilayer was calculated from eq. (7.7).

$$\frac{P}{L} = \frac{\beta\left(\frac{\lambda A}{a_P}\right) + (1-\beta)\left(\frac{\lambda A}{\frac{A_H}{n}}\right)}{N_{LO} - \left(\frac{2\lambda A}{a_L}\right)} = \frac{\lambda}{(1-\lambda)}\frac{a_L}{2}\left[\frac{\beta}{a_P} + \frac{(1-\beta)}{\frac{A_H}{n}}\right] \tag{5.7}$$

Here, N_{LO} (= $2A/a_L$) is the total number of lipid molecules initially present in the bilayer. The numerator accounts for the number of peptide molecules present as clusters and as pores. The denominator represents the number of residual lipid molecules after some of the lipid has been displaced by the peptide. Having already calculated λ from eq.(5.5) as a function of the peptide concentration in the aqueous phase for assumed values of β and n, we can use eq.(5.7) to calculate the corresponding P/L ratio. In this manner, the peptide concentration in the aqueous phase can be related to the P/L ratio in the membrane inserted state. The calculated P/L ratios for

different aqueous phase concentrations of the peptide are plotted in Figure 5.8. The calculations show that in order to account for a given mass change, the *P/L* ratio would be larger for $\beta > 0$ compared to when $\beta = 0$; further, *P/L* would be larger for smaller *n* (e.g. *n*=8 compared to *n*=10). This is intuitively obvious because replacing lipids by peptides results in a smaller mass change compared to replacing lipids by pores. Also shown in Figure 5.8 are experimental estimates of *P/L* in DMPC vesicles at 21°C and DOPC vesicles at 34°C as a function of the aqueous phase alamethicin concentration, obtained more than two decades ago using circular dichroism (CD) spectroscopy and phenylalaninol fluorescence spectroscopy.[23] Although the lipids are different from egg PC and the membrane system is a vesicle rather than a supported bilayer, the qualitative comparison between the QCM-D estimate for *P/L* and these experimental results is interesting to note.

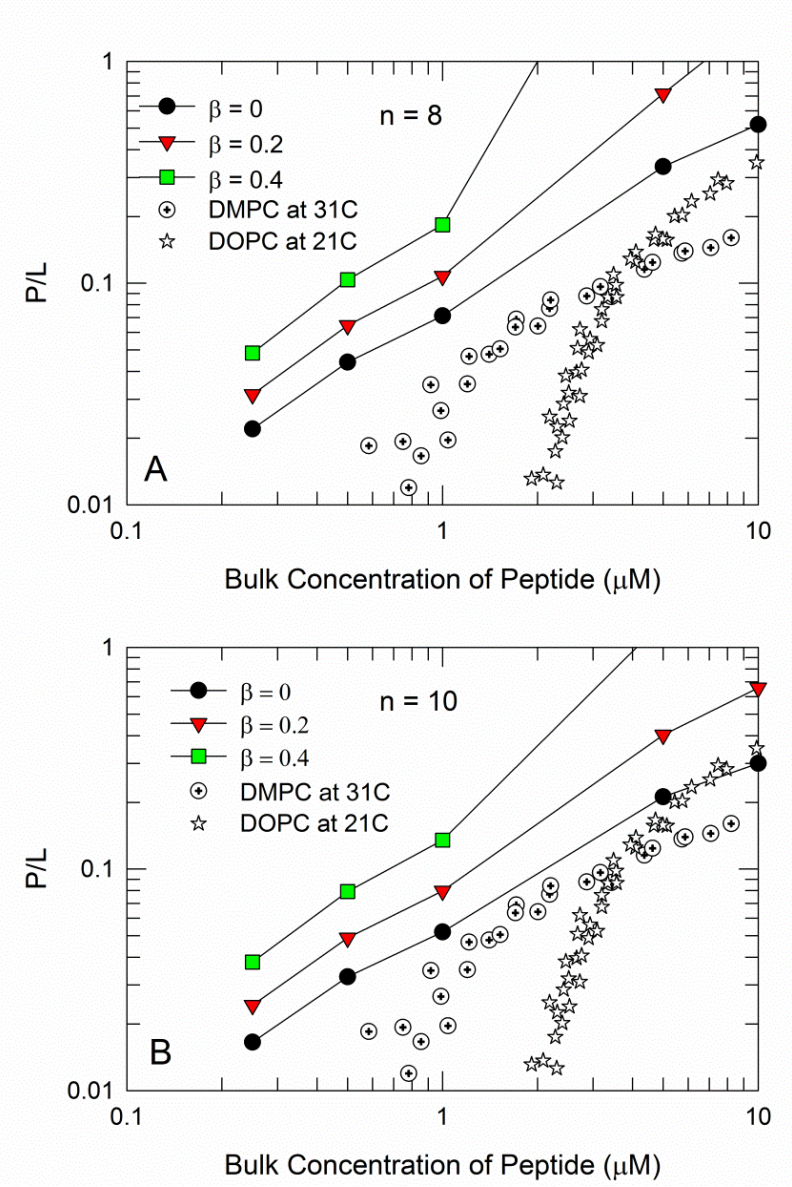

Figure 5.8. Calculated peptide-to-lipid ratio in the egg PC bilayer inserted state as a function of alamethicin concentration in the aqueous phase for different assumed values of the parameter β. Two values of n are represented: (A) $n = 8$, (B) $n = 10$. The P/L ratio is larger for smaller n and larger β. The experimental data for comparison [23] were obtained for DMPC and DOPC vesicles membranes using CD and fluorescence spectroscopy.

The discrepancies between the calculated and experimental P/L values may be explained by differences in experimental parameters and assumptions. For instance, the QCM-D results in this study were obtained for egg PC while the experimental data reported were for either DMPC

or DOPC. The experimental *P/L* values also corresponded to vesicles rather than flat bilayers. In the experiments, the average vesicle size changed and some vesicle fusion was observed during peptide interactions, which may affect the quantitative estimation of the *P/L* ratio. Also, the calculation of the *P/L* ratio at low peptide concentrations from CD and fluorescence measurements showed a larger intrinsic uncertainty. Finally, the consideration of a polydispersed pore model would modify the results calculated using the QCM-D data. The model assumes all pores to be the same size, which may not be the case in an experimental system. For these reasons, we have only mentioned the qualitative similarity between the QCM-D results and the vesicle experimental data on Figure 5.8. The QCM-D studies would have to be complemented with other experiments to obtain additional information needed for more rigorous quantitative comparisons.

5.5 Conclusions

We have explored the extent of useful information on alamethicin-membrane interactions that can be extracted from the application of quartz crystal microbalance with dissipation monitoring (QCM-D) technique. A supported phosphatidylcholine (PC) bilayer membrane in an aqueous environment was used as the membrane model. The QCM-D responses of changes in frequency (Δf) and dissipation (ΔD) at different overtones were used to estimate changes in mass and rigidity of the lipid bilayer as well as the orientation of the peptide in the bilayer. The frequency changes at various overtones were equal indicating a homogeneous membrane process suggesting a vertical insertion of the peptide. Such an orientation for the peptide coupled to a net mass loss in the system supports a cylindrical pore formation with enclosed water channel. The very small dissipation change confirming the retention of lipid organization supports the idea that the inserted peptides form the walls of the cylindrical pores retaining the lipid organization.

Further, an analysis of the time evolution of Δf vs. ΔD demonstrates that the peptide insertion kinetic process involved significant disordering of lipids, especially in the proximity of the membrane-water interface, even though this disordering was not present in the end state. By developing model calculations we concluded that the QCM-D data cannot confirm or rule out the coexistence of peptide clusters along with pores containing water channels. We also developed a way to calculate the peptide to lipid ratio in the membrane as a function of the aqueous phase peptide concentration and found that to be qualitatively similar to the experimental alamethicin partitioning data reported for vesicles.

5.6 Acknowledgements

The authors would like to thank Dr. Tanja Dominko for the use of her ultracentrifuge. This study was supported by an ORISE Fellowship funded by the Natick Soldier Research, Development & Engineering Center (NSRDEC) and the Koerner Family Graduate Fellowship.

5.7 References

(1) Skarnes, R. C. and Watson, D. W. (1957) Antimicrobial factors of normal tissues and fluids, *Bacteriol Rev 21*, 273-294.
(2) Gazit, E., Miller, I. R., Biggin, P. C., Sansom, M. S. and Shai, Y. (1996) Structure and orientation of the mammalian antibacterial peptide cecropin P1 within phospholipid membranes, *J Mol Biol 258*, 860-870.
(3) Brogden, K. A. (2005) Antimicrobial peptides: pore formers or metabolic inhibitors in bacteria?, *Nat Rev Microbiol 3*, 238-250.
(4) Marr, A. K., Gooderham, W. J. and Hancock, R. E. (2006) Antibacterial peptides for therapeutic use: obstacles and realistic outlook, *Curr Opin Pharmacol 6*, 468-472.
(5) Powers, J. P. and Hancock, R. E. (2003) The relationship between peptide structure and antibacterial activity, *Peptides 24*, 1681-1691.
(6) Nizet, V. (2006) Antimicrobial peptide resistance mechanisms of human bacterial pathogens, *Curr Issues Mol Biol 8*, 11-26.
(7) Fulmer, P. A., Lundin, J. G. and Wynne, J. H. (2010) Development of antimicrobial peptides (AMPs) for use in self-decontaminating coatings, *ACS Appl Mater Interfaces 2*, 1266-1270.
(8) Eckert, R. (2011) Road to clinical efficacy: challenges and novel strategies for antimicrobial peptide development, *Future Microbiol 6*, 635-651.

(9) Huang, H. W. (2006) Molecular mechanism of antimicrobial peptides: the origin of cooperativity, *Biochim Biophys Acta 1758*, 1292-1302.
(10) Huang, H. W. (2000) Action of antimicrobial peptides: two-state model, *Biochemistry 39*, 8347-8352.
(11) Lee, M. T., Chen, F. Y. and Huang, H. W. (2004) Energetics of pore formation induced by membrane active peptides, *Biochemistry 43*, 3590-3599.
(12) Huang, H. W. (2009) Free energies of molecular bound states in lipid bilayers: lethal concentrations of antimicrobial peptides, *Biophys J 96*, 3263-3272.
(13) Yang, L., Harroun, T. A., Weiss, T. M., Ding, L. and Huang, H. W. (2001) Barrel-stave model or toroidal model? A case study on melittin pores, *Biophys J 81*, 1475-1485.
(14) Shai, Y. (2002) Mode of action of membrane active antimicrobial peptides, *Biopolymers 66*, 236-248.
(15) Boman, H. G., Agerberth, B. and Boman, A. (1993) Mechanisms of action on Escherichia coli of cecropin P1 and PR-39, two antibacterial peptides from pig intestine, *Infect Immun 61*, 2978-2984.
(16) Leitgeb, B., Szekeres, A., Manczinger, L., Vagvolgyi, C. and Kredics, L. (2007) The history of alamethicin: a review of the most extensively studied peptaibol, *Chem Biodivers 4*, 1027-1051.
(17) Beven, L., Duval, D., Rebuffat, S., Riddell, F. G., Bodo, B. and Wroblewski, H. (1998) Membrane permeabilisation and antimycoplasmic activity of the 18-residue peptaibols, trichorzins PA, *Biochim Biophys Acta 1372*, 78-90.
(18) Beven, L. and Wroblewski, H. (1997) Effect of natural amphipathic peptides on viability, membrane potential, cell shape and motility of mollicutes, *Res Microbiol 148*, 163-175.
(19) Nir-Paz, R., Prevost, M. C., Nicolas, P., Blanchard, A. and Wroblewski, H. (2002) Susceptibilities of Mycoplasma fermentans and Mycoplasma hyorhinis to membrane-active peptides and enrofloxacin in human tissue cell cultures, *Antimicrob Agents Chemother 46*, 1218-1225.
(20) Amiche, M., Seon, A. A., Wroblewski, H. and Nicolas, P. (2000) Isolation of dermatoxin from frog skin, an antibacterial peptide encoded by a novel member of the dermaseptin genes family, *Eur J Biochem 267*, 4583-4592.
(21) Fox, R. O., Jr. and Richards, F. M. (1982) A voltage-gated ion channel model inferred from the crystal structure of alamethicin at 1.5-A resolution, *Nature 300*, 325-330.
(22) He, K., Ludtke, S. J., Huang, H. W. and Worcester, D. L. (1995) Antimicrobial peptide pores in membranes detected by neutron in-plane scattering, *Biochemistry 34*, 15614-15618.
(23) Rizzo, V., Stankowski, S. and Schwarz, G. (1987) Alamethicin incorporation in lipid bilayers: a thermodynamic study, *Biochemistry 26*, 2751-2759.
(24) Huang, H. W. and Wu, Y. (1991) Lipid-alamethicin interactions influence alamethicin orientation, *Biophys J 60*, 1079-1087.
(25) Wu, Y., He, K., Ludtke, S. J. and Huang, H. W. (1995) X-ray diffraction study of lipid bilayer membranes interacting with amphiphilic helical peptides: diphytanoyl phosphatidylcholine with alamethicin at low concentrations, *Biophys J 68*, 2361-2369.
(26) He, K., Ludtke, S. J., Worcester, D. L. and Huang, H. W. (1996) Neutron scattering in the plane of membranes: structure of alamethicin pores, *Biophys J 70*, 2659-2666.
(27) Chen, F. Y., Lee, M. T. and Huang, H. W. (2002) Sigmoidal concentration dependence of antimicrobial peptide activities: a case study on alamethicin, *Biophys J 82*, 908-914.

(28) Qian, S., Wang, W., Yang, L. and Huang, H. W. (2008) Structure of the alamethicin pore reconstructed by x-ray diffraction analysis, *Biophys J 94*, 3512-3522.
(29) Oliynyk, V., Jager, M., Heimburg, T., Buckin, V. and Kaatze, U. (2008) Lipid membrane domain formation and alamethicin aggregation studied by calorimetry, sound velocity measurements, and atomic force microscopy, *Biophys Chem 134*, 168-177.
(30) Salnikov, E. S., De Zotti, M., Formaggio, F., Li, X., Toniolo, C., O'Neil, J. D., Raap, J., Dzuba, S. A. and Bechinger, B. (2009) Alamethicin topology in phospholipid membranes by oriented solid-state NMR and EPR spectroscopies: a comparison, *J Phys Chem B 113*, 3034-3042.
(31) Pan, J., Tieleman, D. P., Nagle, J. F., Kucerka, N. and Tristram-Nagle, S. (2009) Alamethicin in lipid bilayers: combined use of X-ray scattering and MD simulations, *Biochim Biophys Acta 1788*, 1387-1397.
(32) Pan, J., Tristram-Nagle, S. and Nagle, J. F. (2009) Alamethicin aggregation in lipid membranes, *J Membr Biol 231*, 11-27.
(33) Wessman, P., Morin, M., Reijmar, K. and Edwards, K. (2010) Effect of alpha-helical peptides on liposome structure: a comparative study of melittin and alamethicin, *J Colloid Interface Sci 346*, 127-135.
(34) Qian, S. and Heller, W. T. (2011) Peptide-induced asymmetric distribution of charged lipids in a vesicle bilayer revealed by small-angle neutron scattering, *J Phys Chem B 115*, 9831-9837.
(35) Ye, S., Nguyen, K. T. and Chen, Z. (2010) Interactions of alamethicin with model cell membranes investigated using sum frequency generation vibrational spectroscopy in real time in situ, *J Phys Chem B 114*, 3334-3340.
(36) Yang, P., Wu, F. G. and Chen, Z. (2013) Dependence of Alamethicin Membrane Orientation on the Solution Concentration, *J Phys Chem C Nanomater Interfaces 117*, 3358-3365.
(37) Pieta, P., Mirza, J. and Lipkowski, J. (2012) Direct visualization of the alamethicin pore formed in a planar phospholipid matrix, *Proc Natl Acad Sci U S A 109*, 21223-21227.
(38) Barenholz, Y., Gibbes, D., Litman, B. J., Goll, J., Thompson, T. E. and Carlson, R. D. (1977) A simple method for the preparation of homogeneous phospholipid vesicles, *Biochemistry 16*, 2806-2810.
(39) Keller, C. A., Glasmastar, K., Zhdanov, V. P. and Kasemo, B. (2000) Formation of supported membranes from vesicles, *Phys Rev Lett 84*, 5443-5446.
(40) Keller, C. A. and Kasemo, B. (1998) Surface specific kinetics of lipid vesicle adsorption measured with a quartz crystal microbalance, *Biophys J 75*, 1397-1402.
(41) Wang, K. F., Nagarajan, R., Mello, C. M. and Camesano, T. A. (2011) Characterization of supported lipid bilayer disruption by chrysophsin-3 using QCM-D, *J Phys Chem B 115*, 15228-15235.
(42) Voinova, M. V., Jonson, M. and Kasemo, B. (2002) Missing mass effect in biosensor's QCM applications, *Biosens Bioelectron 17*, 835-841.
(43) Mechler, A., Praporski, S., Atmuri, K., Boland, M., Separovic, F. and Martin, L. L. (2007) Specific and selective peptide-membrane interactions revealed using quartz crystal microbalance, *Biophys J 93*, 3907-3916.
(44) McCubbin, G. A., Praporski, S., Piantavigna, S., Knappe, D., Hoffmann, R., Bowie, J. H., Separovic, F. and Martin, L. L. (2011) QCM-D fingerprinting of membrane-active peptides, *Eur Biophys J 40*, 437-446.

(45) Zwang, T. J., Fletcher, W. R., Lane, T. J. and Johal, M. S. (2010) Quantification of the layer of hydration of a supported lipid bilayer, *Langmuir 26*, 4598-4601.

Chapter 6

AFM Imaging of AMP-induced membrane defects

6.1 Abstract

The active mechanism that membrane-active antimicrobial peptides (AMPs) use to destabilize bacterial membranes and cause lysis is not well understood, largely due to the nanoscale nature of peptide-membrane interactions. Numerous techniques, such as quartz crystal microbalance with dissipation monitoring (QCM-D) and oriented circular dichroism (OCD) have been used to characterize these interactions by determining the orientation and structural organization of the molecules within cell membranes exposed to AMPs. However, the effect of these peptides on membrane structure and stability is often difficult to infer from these techniques. In this study, atomic force microscopy (AFM) was used to investigate the effect of various concentrations of two peptides, alamethicin and indolicidin, on a model cell membrane by imaging changes produced in the membrane. Alamethicin and indolicidin were chosen for study because they exhibit varied structures and demonstrated different membrane interaction mechanisms in previous QCM-D studies. Alamethicin, a 20-amino acid α-helical peptide, produced large, unstable defects in the membrane at 5 μM concentrations and completely removed the bilayer at 10 μM. The smaller non-α-helical peptide, indolicidin, produced smaller holes in the bilayer at 5 and 10 μM, which filled in again over time. Root-mean-square (RMS) roughness values for the images showed that surface roughness caused by visible defects peaked after peptide injection and gradually decreased over time. Understanding the dynamic interactions between different AMPs and cell membranes will facilitate the selection and design of more efficient AMPs for use in therapeutics and antimicrobial surfaces.

6.2 Introduction

Due to the escalating phenomenon of antibiotic resistance in bacteria in the past several decades, interest in the identification and development of antibiotic alternatives, such as

antimicrobial peptides (AMPs), has increased. Although many AMPs, which are part of the innate immune systems of most eukaryotic organisms, are thought to kill pathogens through cell membrane disruption, the active mechanism behind the membrane destabilization is not well understood. Membrane-active AMPs are believed to initially associate with cell membranes through electrostatic interactions between the peptides and lipid headgroups. Techniques such as oriented circular dichroism (OCD), nuclear magnetic resonance (NMR) spectroscopy and quartz crystal microbalance with dissipation monitoring (QCM-D) have determined that peptides can exhibit distinct states once they are associated with lipid the bilayers.[1-5] According to the carpet model, AMPs may adsorb parallel to the bilayer membrane and "carpet" the lipid surface.[6] As the peptide concentration reaches a critical level, the peptides and lipids reorganize to leave the membrane as aggregates or micelles. The barrel-stave model supposes that AMPs may insert perpendicularly into the lipid bilayer and form cylindrical or toroidal pores, through which large molecules can travel, disrupting ion gradients and causing the cell to die.

The membrane-active antimicrobial peptides alamethicin and indolicidin were chosen for examination in this study due to their different structures and mechanisms of action. Alamethicin, an α-helical peptide of neutral charge, has been shown to form voltage-gated ion channels in membranes.[7-9] The peptide is thought to attach to the lipid headgroups and insert into membranes, forming pores that can contain 3-11 peptide molecules.[10-14] Neutron in-plane scattering experiments have shown that in 1,2-dilauroyl-*sn*-glycero-3-phosphatidylcholine (DLPC) membranes, these pores exhibit inner and outer diameters of ~1.8 nm and ~4.0 nm, respectively.[15] Indolicidin is a shorter, cationic peptide that exhibits a folded, boat-shaped conformation due to intramolecular cation-π interactions.[16] QCM-D studies suggest that indolicidin will adsorb to a supported phosphatidylcholine (PC) membrane and partially insert

into the bilayer.[4] While alamethicin's α-helicity and amphiphilicity promotes membrane insertion, indolicidin favors a surface adsorption mechanism over insertion, largely due to its folded structure. Indolicidin contains hydrophobic amino acid residues, however, that allowed it to also partially insert into the membrane.

To analyze the effect of AMPs on membrane structure and stability, we chose to use atomic force microscopy (AFM) imaging to examine AMP-induced changes to supported lipid bilayers (SLBs) that mimic cell membranes. AFM is a sensitive technique that uses a sharp-tipped cantilever to scan the surface of samples and produce images with nanoscale resolution. Forces between the tip and sample cause cantilever deflections that are measured by a laser spot reflected into a photodiode array, producing an image reflecting the height variations on the surface. AFM has been used to examine changes in supported lipid membrane structure and thickness due to exposure to peptides,[17-28] surfactants[29, 30] and dendrimers.[31] For instance, Lam et al. recently used AFM to image structural transformations in a zwitterionic 1,2-dimyristoyl-*sn*-glycero-3-phosphocholine (DMPC) supported lipid membrane exposed to the cationic AMP protegrin-1 and saw evidence of pore formation and wormlike micelles in the membrane.[18]

The goal of this study was to elucidate the underlying mechanism of action of alamethicin and indolicidin on a supported phosphatidylcholine (PC) lipid membrane using AFM. By deriving mechanistic information from AFM images, we aimed to validate mechanistic models of alamethicin- and indolicidin-membrane interactions that were developed in previous QCM-D studies.[4, 32] Various AMP concentrations were examined, as well as time progression of AMP-induced membrane destabilization. Understanding the interaction mechanisms between AMPs and cell membranes is a crucial step in developing AMPs as an alternative to antibiotics in therapeutics.

6.3 Materials and methods

6.3.1 Antimicrobial peptides

Alamethicin and indolicidin were obtained from Sigma Aldrich (St. Louis, MO) and New England Peptide (Gardner, MA), respectively. All peptides were suspended in Tris-NaCl buffer (100 mM sodium chloride and 10 mM tris(hydroxymethyl)aminomethane, pH 7.8) and stored at -20˚C. A range of AMP concentrations (1, 5, and 10 μM) were tested to examine the concentration dependency of AMP-membrane interactions.

6.3.2 Supported lipid bilayer preparation

Egg phosphatidylcholine (Avanti Polar Lipids, Alabaster, AL) vesicles were made and stored in Tris-Nacl buffer. Egg phosphatidylcholine (PC) lipids dissolved in ethanol were dried under a stream of nitrogen gas and placed in a vacuum desiccator overnight. The dried lipids were reconstituted in Tris-NaCl buffer to create a stock concentration of 2.5 mg/mL. The lipid mixture was then vortexed and homogenized through 5 freeze-thaw cycles.

The egg PC lipids were sonicated with an ultrasonic dismembrator (Model 150T, Fisher Scientific, Waltham, MA) in an ice bath for 30 min in pulsed mode with a 30% duty cycle (3 s on, followed by 7 s pause) at an amplitude of 60 to form small unilamellar vesicles (SUVs). Sonicator probe particles were removed from solution through centrifugation (5415D Microcentrifuge, Eppendorf, Hamburg, Germany) at 16,000g for 10 min. The stock solution was diluted using Tris-NaCl buffer to 0.1 mg/mL for each experiment.

Supported egg PC bilayers were formed on muscovite mica (Electron Microscopy Sciences, Hatfield, PA), which was cut into 0.7-cm-diameter circular sheets using a 3-hole

punch. The mica circles were fixed in a 1.5-cm-diameter well in a 1.2-mm-thick depression slide using epoxy. Before each experiment, the microscope slides were rinsed with 2% sodium dodecyl sulfate and DI water and dried with nitrogen gas. The mica was cleaved so that the surface was visually smooth and etched with a SPI Plasma Prep II Plasma Etcher (SPI Supplies, West Chester, PA).

6.3.3 Atomic force microscopy (AFM)

All samples were scanned in liquid using a Veeco Dimension Icon with ScanAsyst (Bruker, Santa Barbara, CA). A silicon nitride ScanAsyst Fluid+ cantilever with a spring constant of 0.7 N/m and nominal tip radius of 2 nm was used. Images were captured with 512 x 512 resolution at a scan rate of 1 Hz.

After the mica surface was scanned in Tris-NaCl buffer to validate the smoothness of the surface, excess buffer was pipetted from the mica surface and replaced with ~0.1 mL of 0.1 mg/mL egg PC vesicle solution. AFM image scanning began at least 5 minutes after the introduction of vesicles to allow sufficient time for stable supported lipid bilayer (SLB) formation. Once the presence of a smooth SLB on the mica surface was established, AMPs were introduced into the system. At least 0.25 mL of the experimental concentration of alamethicin or indolicidin was pipetted onto the periphery of the well in 10 μL increments every 5 s, while simultaneously removing lipid vesicle solution in 10 μL increments to simulate slow pump flow that was present in our QCM-D experiments. Before bringing the AFM tip to the mica surface in liquid, a drop of AMP solution was placed on the tip, instead of buffer, so that the AMP concentration would not be diluted. The surface was then scanned to image AMP-induced changes to the SLB at a minimum of 3 different locations on the sample.

All images were flattened using the first order polynomial flatten command in the NanoScope Analysis software to delete low frequency noise and remove tilt. Scan lines resulting from noise or skips were also removed from the final images. Roughness values were reported for each 5μm x 5μm image as the root mean square (RMS) average of height deviations in the image:

$$R_q = \sqrt{\frac{\sum {Z_i}^2}{N_P}} \tag{6.1}$$

where Z_i is a specific Z (height) value and N_p is the total number of points. Roughness measurements were used as a quantitative method of analyzing changes to the SLB over time.

6.4 Results and discussion

6.4.1 Alamethicin forms large defects and causes complete lipid removal

AFM imaging of the supported PC bilayer revealed a smooth membrane with small particles on the surface (Figure 6.1). These particles may have been small lipid aggregates that were present after lipid bilayer formation. Upon injection of 1 μM alamethicin, many of the particles were removed and no visible membrane destabilization took place over the course of 1 h.

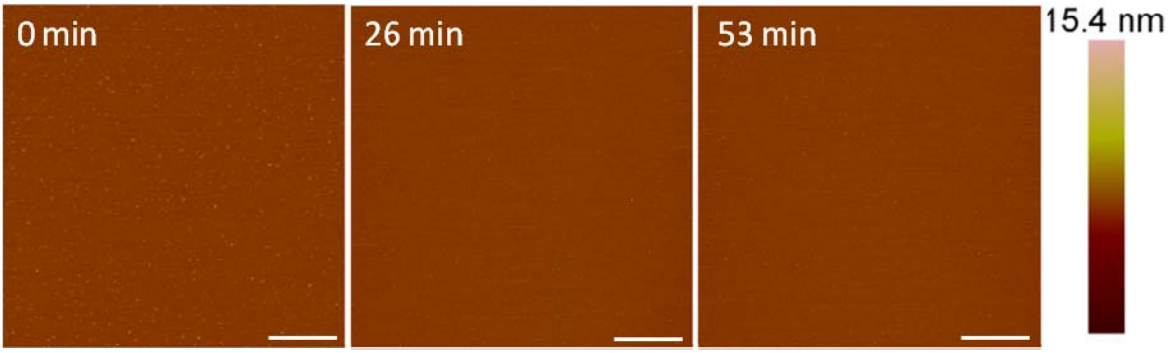

Figure 6.1. Representative AFM images of a supported PC membrane after exposure to 1 μM alamethicin. The stable lipid membrane before peptide injection is shown at t = 0 min. The scale bars represent a distance of 1 μm.

Large defects, or pores, formed in the lipid membrane upon exposure to 5 μM alamethicin, leaving small islands of lipids amidst larger, connected lipid bilayer patches (Figure 6.2). Due to the rapid nature of peptide-membrane interactions, we were unable to capture the initial stages of peptide binding and membrane removal. QCM-D studies have shown that the initial peptide binding interactions of alamethicin and indolicidin occur in less than 10 minutes.[33] Since each image required approximately 9 minutes of scanning, these initial interactions could not be captured with AFM. Over 3.5 h, lipids continuously shifted around the perimeter of the patches and were removed from the mica surface. Smaller patches of lipids also gradually left the mica surface or combined with neighboring planar lipid patches over time.

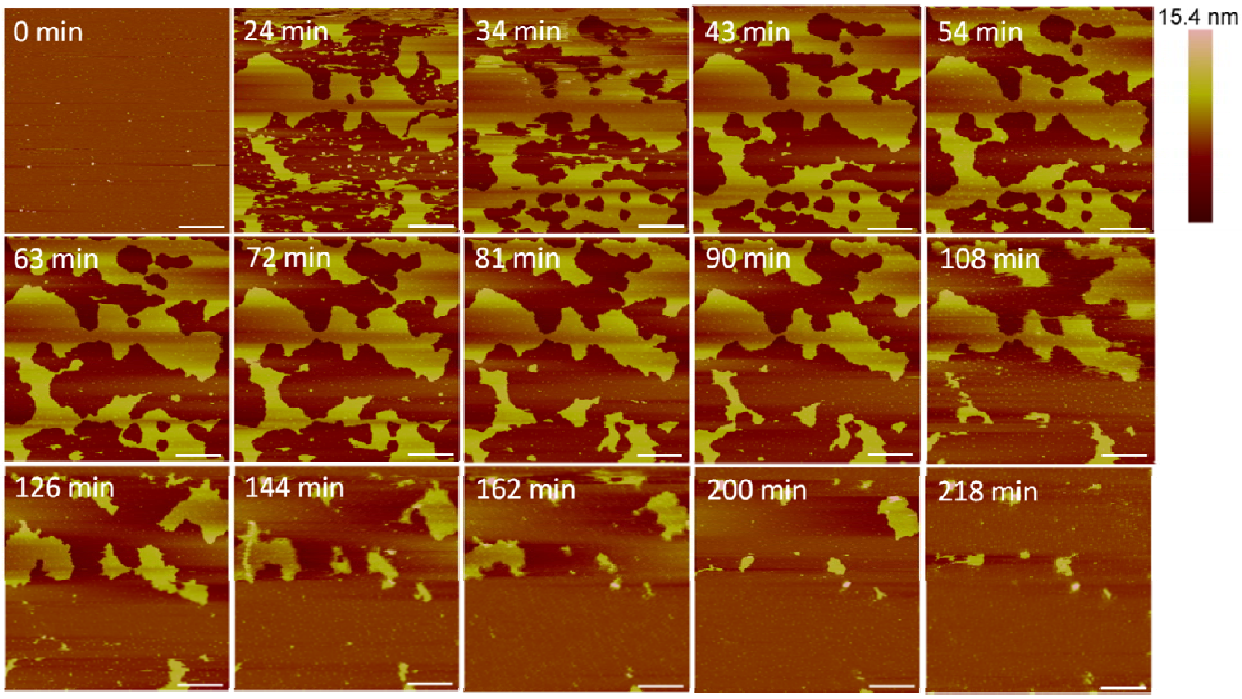

Figure 6.2. Defects formed in a supported PC bilayer after injection of 5 μM alamethicin over 218 minutes. Each AFM image was scanned in the same location on the substrate. The scale bars represent a distance of 1 μm.

Height profiles of the membrane at the same location on the substrate (Figure 6.3A) show some defects widening and others filling in as time progressed, indicating that the lipids at the perimeter of the planar membrane were fluid. Before alamethicin was introduced to the system (t=0 min), the lipid bilayer was a relatively smooth surface with 1-2 nm particles on the surface (Figure 6.3B). At 24 min, large membrane defects had formed that were approximately 5 nm deep, which is the expected height of a PC bilayer. In the height profile plots, the height of the bilayer surface at 0 min is different than that at 24 min (roughly 2 nm) because AFM does not allow for the direct comparison of heights between images. Therefore, the y-axis is meant to show the depth of the defects, rather than allow for the direct comparison of height value at a specific position on the substrate. After the membrane had been exposed to the peptide for 34

min, the lipids shifted to fill in some of the spaces observed in the height profile. The membrane defects expanded and lipid material left gaps in the membrane at 108 min. At 162 min, most of the lipids had been removed and the profile shown at a height of 0 nm represents the mica substrate.

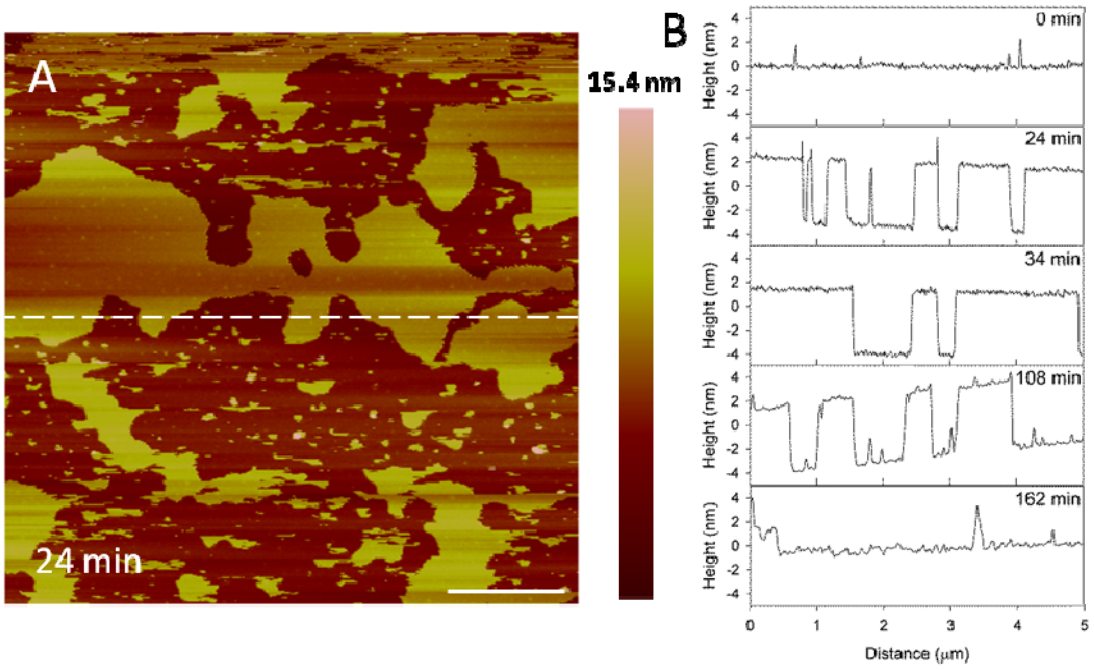

Figure 6.3. Evolution of membrane defects over time during incubation with 5 μM alamethicin. The dashed line (A) shows the location of the height profiles (B). The scale bar represents 1 μm.

At a concentration of 10 μM, alamethicin appeared to remove the bilayer entirely before the first image was taken at 18 min (Figure 6.4). Unfortunately, due to the length of time required to position the AFM tip on the sample surface and scan an image, the first image could not be taken sooner than ~18 min. Therefore, any action between the peptides and lipid membrane that occurred in the first several minutes could not be captured using AFM.

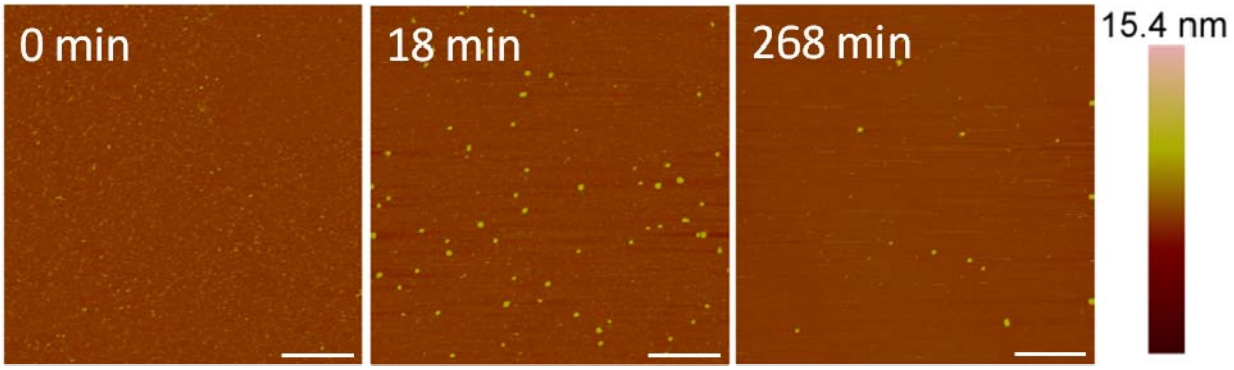

Figure 6.4. AFM images of the supported PC membrane after exposure to 10 μM alamethicin. The scale bars represent a distance of 1 μm.

Although differentiating between an SLB and the mica substrate is difficult in these images, the particles (<10 nm in height) visible on the substrate surface after 18 minutes of AMP exposure (Figure 6.4) offer clues about the nature of the surface. Since large membrane defect formation was observed with an alamethicin concentration of 5 μM, we expected to see defects or bilayer patches remaining on the mica surface if the lipid bilayer were still supported on the mica. These particles, which are likely lipid or peptide-lipid aggregates, appear to be all that remained of the lipid bilayer on the mica surface, however. Over the course of 4 h, some aggregates attached to the surface and most of the original particles present at 18 min gradually left the mica surface. The scanning motion of the AFM tip may have also contributed to the removal of these particles.

Root mean square (RMS) roughness values were calculated to provide a quantitative method of analyzing changes in the membrane over time (Figure 6.5). As observed in the AFM images, 1 μM alamethicin did not change the surface of the membrane over ~1 hr and, therefore, the roughness did not change. At 5 μM, alamethicin substantially increased the roughness of the membrane surface within 24 min. The roughness peaked at 54 min and gradually decreased over

the next 2.5 h. This decrease in roughness corresponds with the loss of small islands of lipid on the mica surface and around the bilayer patches, revealing more of the smooth mica surface. The complete removal of lipids at 10 μM alamethicin produced lower roughness values that remained constant over 4 h. The RMS values for 10 μM alamethicin were higher than those for 1 uM concentrations, however, presumably due to the presence of aggregates left on the surface of the mica.

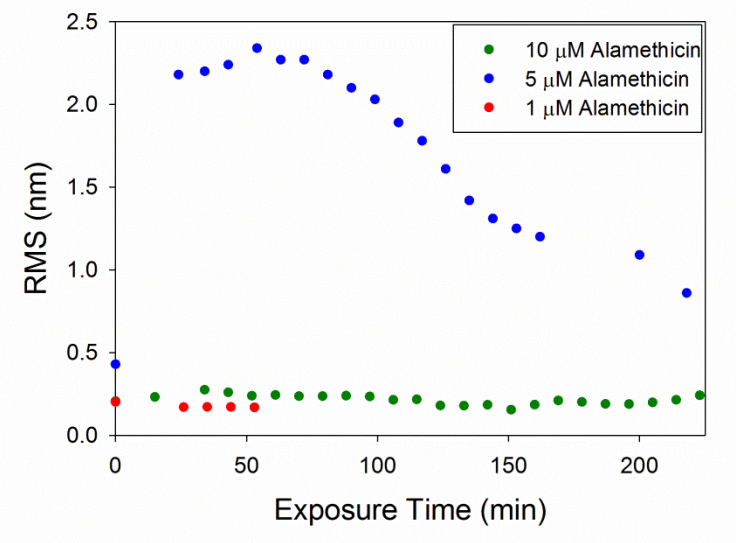

Figure 6.5. Root mean square (RMS) roughness values calculated for each 5μm x 5μm image of the supported PC bilayer after exposure to various alamethicin concentrations.

The concentration-dependent membrane disruption that was observed as a result of alamethicin exposure is consistent with a previous QCM-D study on PC membranes.[4] Monitoring the changes in mass and rigidity of a supported PC membrane formed on silica did not show substantial changes to the lipid bilayer when exposed to 1 μM alamethicin in QCM-D experiments. AFM imaging of the membrane after injection of 1 μM alamethicin also did not show visible membrane disruption (Figure 6.1).

The large defect formations observed in the membrane after exposure to 5 μM alamethicin (Figure 6.2) agreed with QCM-D results showing decreases in mass at all depths of the SLB after 1 h of incubation with the same peptide concentration.[4] In QCM-D experiments, the lipid membrane lost roughly 15-20% of its original mass. From visual analysis, more than 15-20% of the lipid bilayer appeared to be removed in the AFM images after 1 h, but this lipid removal could have been due to forces resulting from the motion of the cantilever. Previous studies have shown that the scanning AFM tip can affect the position of particles on a surface, resulting in movement of weakly adsorbed peptide aggregates on a bilayer or even the rupture of surface-adsorbed lipid vesicles.[19, 34] Although the QCM-D results indicated that alamethicin likely lined the pores in the membrane, the individual peptide molecules were not visible in these images. Since alamethicin monomers can be approximated as cylinders 3.2 nm long and 1.1 nm wide,[14, 35] they may not be distinguishable from the adjacent 5 nm tall lipid bilayer when scanning with a 2 nm-radius tip.

The membrane changes induced by 10 μM alamethicin observed using AFM (Figure 6.4) differed somewhat from the membrane disruption inferred from QCM-D experiments.[4] Although near-complete bilayer removal was observed in the AFM images, only about 20% of the original bilayer mass was removed from a silica surface in a similar QCM-D experiment. These variations were likely due to differences in the experimental setup of the two techniques. First, the QCM-D measurements were performed in a flow system, whereas the AFM images were scanned in a static system. The scanning motion of the AFM tip also may have caused more lipid removal than in an undisturbed lipid membrane. Furthermore, variations in the amount of lipid removal observed may have been due to differences in the substrates used as lipid bilayer supports. In the QCM-D experiments, a silica-coated quartz sensor was used as the substrate,

while the AFM images were scanned on a mica substrate. Mica was chosen as the substrate for the AFM experiments because its cleaved surface is smoother than that of the silica QCM-D sensor. The QCM-D sensor surface exhibits height variations ranging across several nanometers, making the identification of lipid membrane defects difficult on these substrates. Although mica is mainly composed of silicate minerals, which are related to silica, differences in the surface roughness and composition may have impacted the retention of lipid molecules on the surface. A previous study by Benes et al. found that supported 1,2-dioleoyl-*sn*-glycero-3-phosphocholine (DOPC) and DOPC/1,2-dioleoyl-*sn*-glycero-3-phospho-L-serine (DOPS) membranes formed and behaved differently on mica and silica surfaces.[36] Membranes were less stable in Tris-HCl buffer than in HEPES buffer when formed on mica, but the buffer did not influence membrane stability when supported on silica. These differences in membrane behavior suggest that the two surfaces exhibit different properties that can affect their interactions with lipids.

The loss of lipid mass from the membrane due to alamethicin action was also observed in a study by Oliynyk et al. on 1,2-dipalmitoyl-*sn*-glycero-3-phosphatidylcholine (DPPC) supported membranes.[23] Circular and elongated membrane defects were revealed using AFM imaging of DPPC membranes with 1 mol% and 4 mol% alamethicin that were formed by direct fusion of lipid-peptide SUVs on mica. Less mass loss and smaller membrane defects were observed than in our study. The results of the two studies could not be directly compared, however, since the peptide concentrations in our experiments were bulk concentrations and the ratio of peptide to lipid in our membranes was not known. Also, although DPPC is a major component of the lipid mixture that is included in egg PC, egg PC also contains 1,2-distearoyl-*sn*-glycero-3-phosphocholine (DSPC) and other phospholipids that may exhibit different behavior with the peptides.

6.4.2 Indolicidin forms smaller, unstable holes in the membrane

After exposure to 1 μM indolicidin, visible changes to the membrane were not observed (Figure 6.6). Before peptide was added, the PC membrane surface contained occasional small particles (~40-50 nm in height) that may have been vesicles. These particles remained after scanning for 2.5 h, although other particles, possibly peptides or peptide-lipid aggregates, were observed to attach to the membrane. Peptide-lipid aggregates may have formed in the solution if indolicidin attached to the membrane and displaced a small amount of lipids, resulting in defects that were too small to be resolved by the 2-nm AFM tip radius. Membrane-bound vesicles were also observed in an AFM study by Oreopoulos et al. examining indolicidin action on a DOPC:DSPC:cholesterol membrane.[24] These vesicles were hypothesized to be lipids displaced from the membrane by indolicidin action.

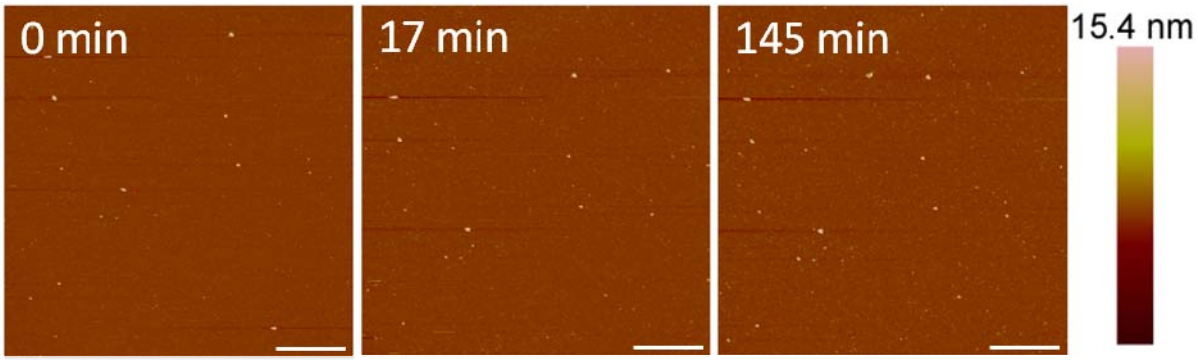

Figure 6.6. AFM image of a supported PC membrane exposed to 1 μM indolicidin. The scale bars represent a distance of 1 μm.

At 5 μM, indolicidin formed defects in the membrane that were smaller than those created by alamethicin at the same concentration (Figures 6.2, 6.7). Within 26 min, many of the

defects appeared to reorganize and consolidate to make the surface less rough. Over ~3 h, these defects filled in to form a smooth membrane.

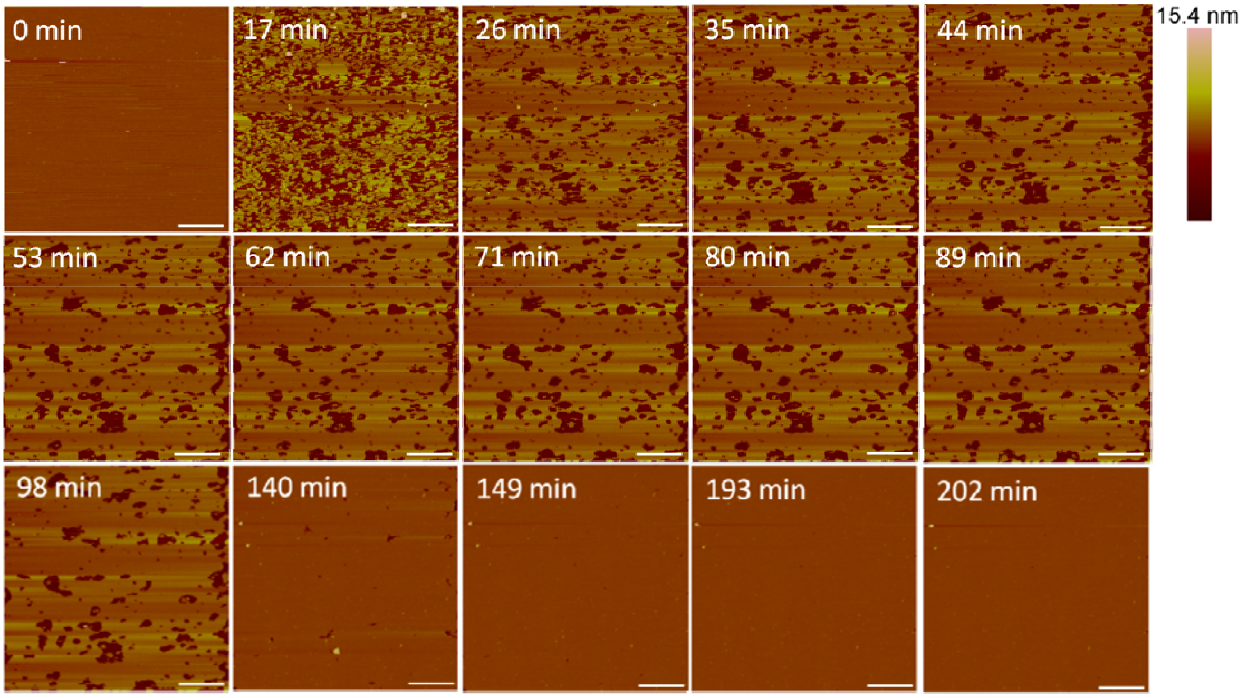

Figure 6.8. Defects formed in a supported PC membrane after injection of 5 μM indolicidin. The scale bars represent a distance of 1 μm.

Filling of the defects can also be observed in height profiles in Figure 6.8. The membrane defects may have been replaced with lipids, peptides, or both. The end result was a smooth bilayer that appeared to be the same height as the original bilayer, suggesting that the material used to seal the defects is a lipid bilayer, rather than peptide-lipid aggregates, which may not have resulted in the same height. The shrinking "pores" shown at 98 min maintained a relative height of 5 nm (the height of a PC bilayer), suggesting that the resulting membrane at 149 min was a lipid bilayer.

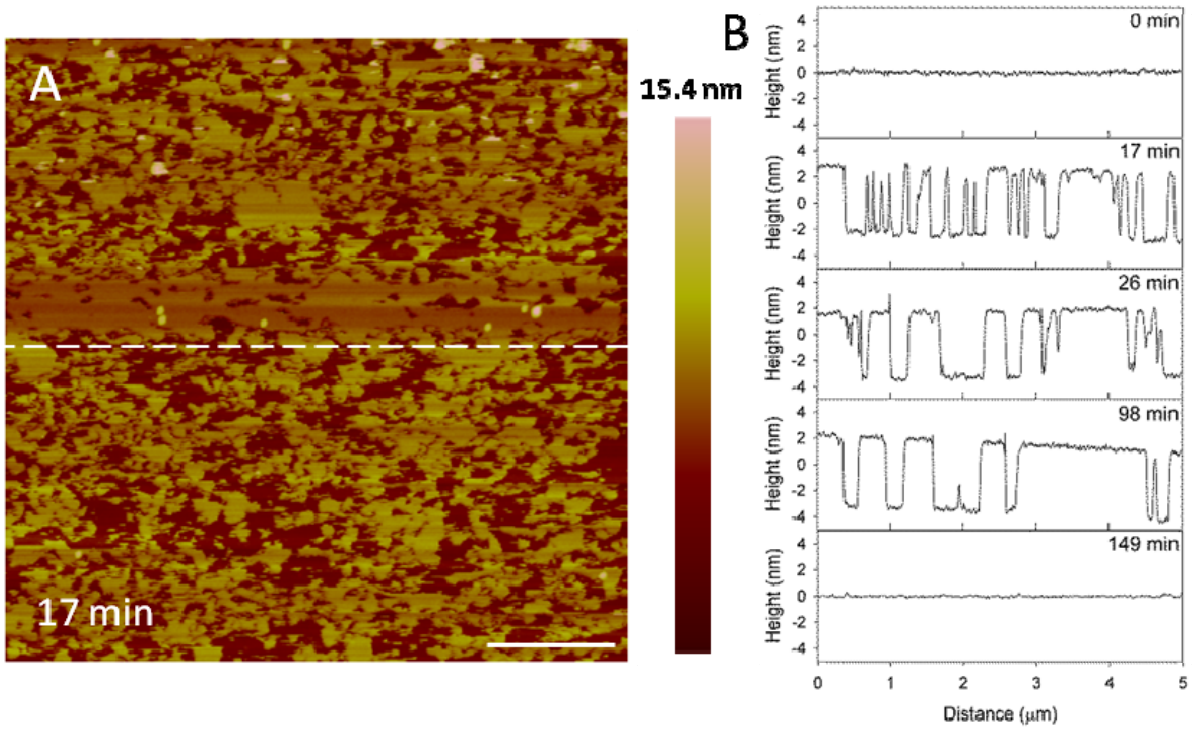

Figure 6.8. Evolution of PC membrane defects over time after exposure to 5 μM indolicidin. The dashed line (A) shows the location of the height profiles (B) on the substrate. The scale bar represents 1 μm.

Small holes and channels were formed in the membrane at 10 μM concentrations (Figure 6.9). These defects left smaller patches of interspersed lipid bilayer membranes than 5 μM indolicidin. These defects also appeared to fill in over ~3.5 h, although the pores did not remain as well-defined as they were with 5 μM indolicidin during this process. While the membrane pores were clearly differentiated from the lipid bilayer at 98 min in Figure 6.8, the AFM tip could not resolve the boundary between the lipid membrane and mica at 54 min in Figure 6.9. One possible reason for these "blurry" edges may have been that the lipids were not well attached to the mica and were moved by the force AFM tip as it scanned across the substrate surface.

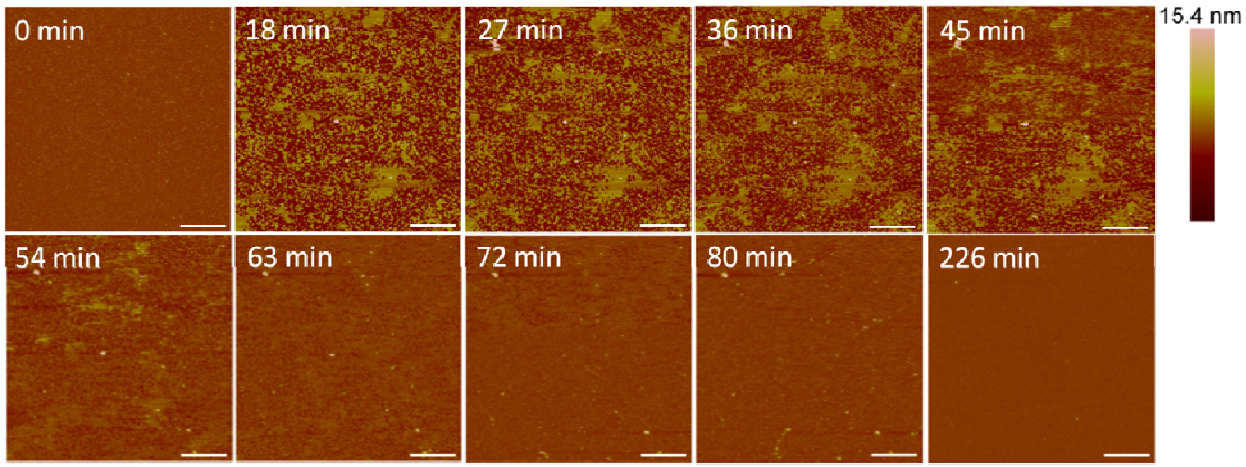

Figure 6.9. Defects formed in a mica-supported PC bilayer after exposure to 10 μM indolicidin. The scale bars represent a distance of 1 μm.

The height profiles in Figure 6.10 show that the membrane defects that had formed in the bilayer 18 min after peptide exposure were 5 nm deep, which was expected in a 5 nm-tall lipid bilayer. After 27 min, however, the depth of these defects decreased to 4 nm. Within 54 min, the defect heights decreased to 3 nm, leading to a smooth surface at 153 min. The initial 5-nm defects that were captured at 18 min may correspond with temporary complete insertion of the peptide into the membrane, but we cannot confirm or deny this hypothesis using these AFM images alone.

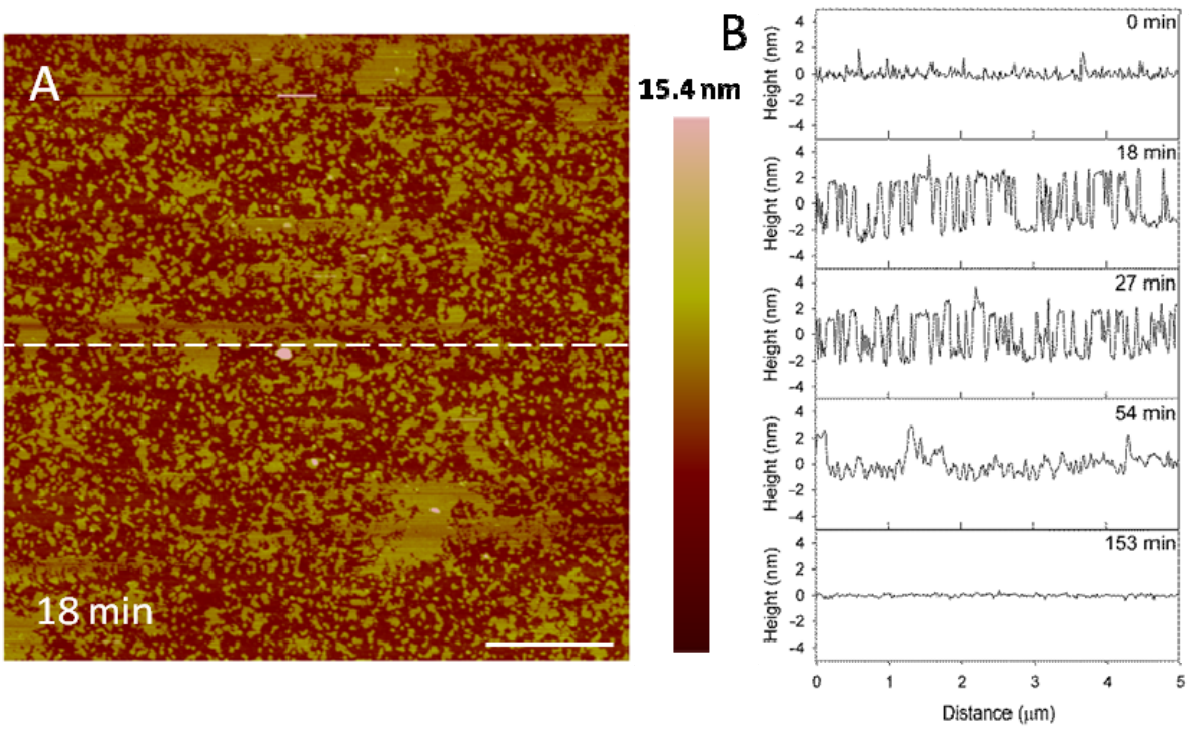

Figure 6.10. Filling of PC membrane defects over time with 10 μM indolicidin. The dashed line (A) shows the location of the height profiles (B). The scale bar is 1 μm.

The RMS roughness plots in Figure 6.11 show that not much change occurred in the membrane with 1 μM indolicidin. The roughness of the membrane exposed to 5 μM indolicidin peaked at or before 17 min. Then, as the defects reorganized and filled in, the roughness decreased to around 1.6 nm until 3 h after peptide exposure, when the majority of the membrane became smooth. The roughness of the membrane when exposed to 10 μM indolicidin peaked at 27 minutes and quickly decreased as the membrane filled in. A similar trend was seen in an AFM study by Askou et al. showing the effect of 25 μM indolicidin on a supported PC membrane.[20] A plot of the average height roughness of the images over time revealed a peak in roughness between 15 and 30 min, which was followed by a gradual decrease in roughness before stabilizing. This common trend indicates that at these concentrations, indolicidin-induced

membrane damage peaks at most 30 minutes after exposure to the peptide. Therefore, the maximum amount of damage to a cell membrane may be observed within this time period when incubated with indolicidin.

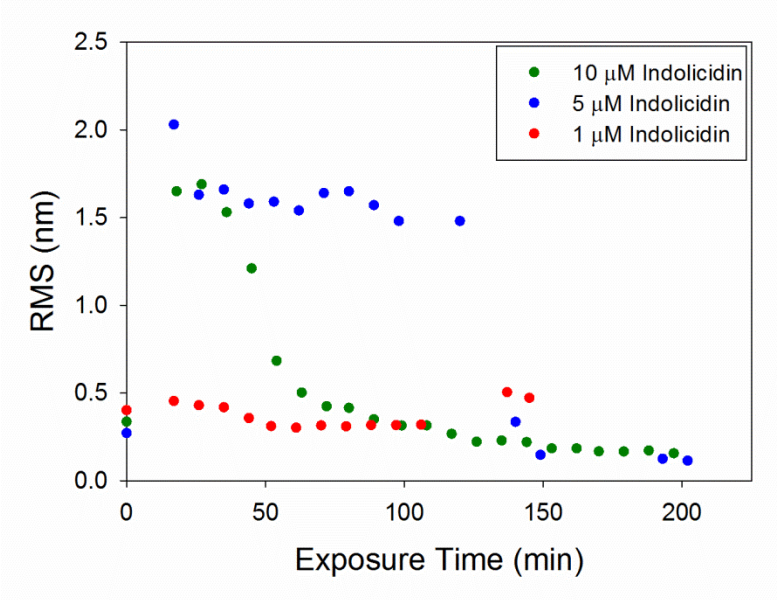

Figure 6.11. Root mean square (RMS) roughness values calculated for each 5μm x 5μm image of the supported PC bilayer after exposure to various indolicidin concentrations.

The RMS values for 1 μM indolicidin are about 2x larger than those for 1 μM alamethicin (Figure 6.5) due to the presence of particles originally on the surface of the membrane before indolicidin was injected. More particles (possibly peptide aggregates) also attached to the membrane surface after 2 hrs of incubation with 1 μM indolicidin, resulting in the increased RMS values at ~140 min. The roughness values calculated for alamethicin-induced defects at 5 μM and indolicidin-induced defects at 5 μM and 10 μM also showed that both peptides substantially changed the lipid membrane surface within the first 50 minutes of exposure and gradually stabilized within ~150 min.

The indolicidin-induced membrane disruption captured by AFM imaging in this study complements and elucidates the peptide-membrane interactions observed in a previous QCM-D study.[33] The lack visible defects in the PC membrane after exposure to 1 μM indolicidin (Figure 6.6) was consistent with QCM-D results, which showed little change to the mass and lipid organization of the membrane after a 1-h incubation.

The loss of lipid mass from within the membrane at 5 μM indolicidin (Figure 6.7) was also observed in QCM-D experiments using the same peptide-lipid system.[33] QCM-D measurements showed that approximately 10% of the lipid bilayer mass was removed from the substrate surface, which is similar to the amount of lipid removal observed in the AFM images at 62 min. However, the QCM-D results also showed a small amount of mass gain in peptide mass on the membrane surface, which the AFM tip may not have be able to capture due to the nanometer-scale size of individual peptide molecules.

At 10 μM indolicidin, the incomplete filling of the membrane defects at 54 min (Figure 6.9) may be explained by partial insertion of the peptide that occurred in previous QCM-D experiments.[33] The QCM-D results indicated that indolicidin adsorbed to the surface of the PC membrane and partially inserted into membrane space where lipids had been removed. The mechanistic model that was derived from QCM-D measurements showed indolicidin partially inserting into a space where the top layer of lipids had been removed and the peptide associating with the remaining monolayer of lipids. If accurate, this mechanistic model would be consistent with the 3 nm defects (roughly half the height of the membrane) observed using AFM. The QCM-D results also indicated that the lipids within the membrane had become very disordered

when exposed to 10 μM indolicidin, which may explain the "blurry" lipid patch edges that were captured in Figure 6.9.

Smoothing of peptide-induced defects in the lipid bilayer that was observed with 5 uM and 10 μM indolicidin has also appeared in several other AFM studies on indolicidin. Ha et al. found that ~15.7 μM indolicidin produced holes in mica-supported membranes (30-100 nm in diameter) composed of the synthetic lipid L-α-dipalmitoylphosphatidic acid (DPPA) that became smooth over time.[37] The membrane smoothing was thought to be due to the incorporation of peptides into the bilayer. Shaw et al. also imaged large, transient defects in the fluid domains of DOPC/DSPC membranes that disappeared slowly over time, which was hypothesized to be due to fluidity of the membranes.[26]

The concentration-dependence of peptide-membrane interactions shown in this study is similar to results obtained by Végh et al. on the effect of indolicidin on DPPC membranes formed on polyelectrolyte films on mica.[27] The polyelectrolyte film was present to create space for membrane-penetrating peptides between the bilayer and mica surface. As in our study, no membrane alterations were detected at low indolicidin concentrations (0.52 μM); though at higher concentrations (2.6 μM and 5.2 μM), the membrane remained intact, but particles appeared on the membrane surface. These particles were believed to be aggregates from excess amounts of indolicidin. This phenomenon also appeared in our AFM images with 1 μM indolicidin. In the study by Végh et al., the DPPC bilayer structure did not form detectable membrane defects before 50 min of exposure to 15.7 μM indolicidin. The membrane was completely destroyed after 140 min of incubation with 7.9 μM and 15.7 μM indolicidin, but smoothing of the membrane defects was not observed, as in our study. These differences were

likely due to the variations in lipid membrane composition, as well as the presence of a polyelectrolyte film between the lipid membrane and mica surface. The polyelectrolytes may have inhibited the filling of defects by lipid or peptide material.

6.5 Conclusions

AFM imaging of AMP-induced changes in the membrane is a valuable tool for visual analysis of lipid removal and the stability of defects. Using AFM to examine alamethicin- and indolicidin-induced defects in supported PC membranes revealed two distinct membrane-disruption mechanisms. The AFM images showed that 1 μM alamethicin did not substantially disturb the lipid bilayer, while 5 μM and 10 μM alamethicin concentrations resulted in substantial loss of lipids from the membrane. Membrane defects formed after exposure to 5 μM indolicidin continued to expand, causing complete destruction of the lipid bilayer. AFM also showed the formation of smaller defects in a supported membrane as a result of incubation with 5 μM and 10 μM indolicidin. The smoothing of membrane defects over time was also observed clearly in the images. The examples of AMP-induced membrane disruption observed in this study offer insight into how various concentrations of AMPs may interact with and disrupt cell membranes. Fundamental understanding of the molecular mechanisms and dynamics associated with AMP-membrane interactions is instrumental for the selection and design of AMPs for applications in therapeutics.

6.6 Acknowledgements

We would like to thank Mary Schwartz (WPI) and Dr. Paola D'Angelo at the U.S. Army Natick Soldier Research, Development & Engineering Center (NSRDEC) for their help with AFM and many helpful discussions. This study was supported by funding from NSRDEC, the

Koerner Family Graduate Fellowship, and the Oak Ridge Institute for Science and Education (ORISE) Graduate Fellowship.

6.7 References

(1) Huang, H. W. (2000) Action of antimicrobial peptides: two-state model, *Biochemistry 39*, 8347-8352.
(2) Yang, L., Harroun, T. A., Weiss, T. M., Ding, L. and Huang, H. W. (2001) Barrel-stave model or toroidal model? A case study on melittin pores, *Biophys J 81*, 1475-1485.
(3) Wang, K. F., Nagarajan, R., Mello, C. M. and Camesano, T. A. (2011) Characterization of supported lipid bilayer disruption by chrysophsin-3 using QCM-D, *J Phys Chem B 115*, 15228-15235.
(4) Wang, K. F., Nagarajan, R. and Camesano, T. A. (2014) Antimicrobial peptide alamethicin insertion into lipid bilayer: A QCM-D exploration, *Colloids Surf B Biointerfaces 116*, 472-481.
(5) Salnikov, E. S., De Zotti, M., Formaggio, F., Li, X., Toniolo, C., O'Neil, J. D., Raap, J., Dzuba, S. A. and Bechinger, B. (2009) Alamethicin topology in phospholipid membranes by oriented solid-state NMR and EPR spectroscopies: a comparison, *J Phys Chem B 113*, 3034-3042.
(6) Shai, Y. (2002) Mode of action of membrane active antimicrobial peptides, *Biopolymers 66*, 236-248.
(7) Hall, J. E., Vodyanoy, I., Balasubramanian, T. M. and Marshall, G. R. (1984) Alamethicin. A rich model for channel behavior, *Biophys J 45*, 233-247.
(8) Nagaraj, R., Balaram, P. (1981) Alamethicin, a transmembrane channel, *Acc. Chem. Res 14*, 356-362.
(9) Duclohier, H. and Wroblewski, H. (2001) Voltage-dependent pore formation and antimicrobial activity by alamethicin and analogues, *J Membr Biol 184*, 1-12.
(10) He, K., Ludtke, S. J., Heller, W. T. and Huang, H. W. (1996) Mechanism of alamethicin insertion into lipid bilayers, *Biophys J 71*, 2669-2679.
(11) Huang, H. W. and Wu, Y. (1991) Lipid-alamethicin interactions influence alamethicin orientation, *Biophys J 60*, 1079-1087.
(12) Meyer, C. E. and Reusser, F. (1967) A polypeptide antibacterial agent isolated from Trichoderma viride, *Experientia 23*, 85-86.
(13) He, K., Ludtke, S. J., Huang, H. W. and Worcester, D. L. (1995) Antimicrobial peptide pores in membranes detected by neutron in-plane scattering, *Biochemistry 34*, 15614-15618.
(14) Qian, S., Wang, W., Yang, L. and Huang, H. W. (2008) Structure of the alamethicin pore reconstructed by x-ray diffraction analysis, *Biophys J 94*, 3512-3522.
(15) He, K., Ludtke, S. J., Worcester, D. L. and Huang, H. W. (1996) Neutron scattering in the plane of membranes: structure of alamethicin pores, *Biophys J 70*, 2659-2666.

(16) Khandelia, H. and Kaznessis, Y. N. (2007) Cation-pi interactions stabilize the structure of the antimicrobial peptide indolicidin near membranes: molecular dynamics simulations, *J Phys Chem B 111*, 242-250.
(17) Mecke, A., Lee, D. K., Ramamoorthy, A., Orr, B. G. and Banaszak Holl, M. M. (2005) Membrane thinning due to antimicrobial peptide binding: an atomic force microscopy study of MSI-78 in lipid bilayers, *Biophys J 89*, 4043-4050.
(18) Lam, K. L., Wang, H., Siaw, T. A., Chapman, M. R., Waring, A. J., Kindt, J. T. and Lee, K. Y. (2012) Mechanism of structural transformations induced by antimicrobial peptides in lipid membranes, *Biochim Biophys Acta 1818*, 194-204.
(19) Choucair, A., Chakrapani, M., Chakravarthy, B., Katsaras, J. and Johnston, L. J. (2007) Preferential accumulation of Abeta(1-42) on gel phase domains of lipid bilayers: an AFM and fluorescence study, *Biochim Biophys Acta 1768*, 146-154.
(20) Askou, H. J., Jakobsen, R. N. and Fojan, P. (2008) An atomic force microscopy study of the interactions between indolicidin and supported planar bilayers, *J Nanosci Nanotechnol 8*, 4360-4369.
(21) Lam, K. L., Ishitsuka, Y., Cheng, Y., Chien, K., Waring, A. J., Lehrer, R. I. and Lee, K. Y. (2006) Mechanism of supported membrane disruption by antimicrobial peptide protegrin-1, *J Phys Chem B 110*, 21282-21286.
(22) Mechler, A., Praporski, S., Atmuri, K., Boland, M., Separovic, F. and Martin, L. L. (2007) Specific and selective peptide-membrane interactions revealed using quartz crystal microbalance, *Biophys J 93*, 3907-3916.
(23) Oliynyk, V., Kaatze, U. and Heimburg, T. (2007) Defect formation of lytic peptides in lipid membranes and their influence on the thermodynamic properties of the pore environment, *Biochim Biophys Acta 1768*, 236-245.
(24) Oreopoulos, J. and Yip, C. M. (2009) Combinatorial microscopy for the study of protein-membrane interactions in supported lipid bilayers: Order parameter measurements by combined polarized TIRFM/AFM, *J Struct Biol 168*, 21-36.
(25) Rakowska, P. D., Jiang, H., Ray, S., Pyne, A., Lamarre, B., Carr, M., Judge, P. J., Ravi, J., Gerling, U. I., Koksch, B., Martyna, G. J., Hoogenboom, B. W., Watts, A., Crain, J., Grovenor, C. R. and Ryadnov, M. G. (2013) Nanoscale imaging reveals laterally expanding antimicrobial pores in lipid bilayers, *Proc Natl Acad Sci U S A 110*, 8918-8923.
(26) Shaw, J. E., Alattia, J. R., Verity, J. E., Prive, G. G. and Yip, C. M. (2006) Mechanisms of antimicrobial peptide action: studies of indolicidin assembly at model membrane interfaces by in situ atomic force microscopy, *J Struct Biol 154*, 42-58.
(27) Vegh, A. G., Nagy, K., Balint, Z., Kerenyi, A., Rakhely, G., Varo, G. and Szegletes, Z. (2011) Effect of antimicrobial peptide-amide: indolicidin on biological membranes, *J Biomed Biotechnol 2011*, 670589.
(28) Shaw, J. E., Epand, R. F., Hsu, J. C., Mo, G. C., Epand, R. M. and Yip, C. M. (2008) Cationic peptide-induced remodelling of model membranes: direct visualization by in situ atomic force microscopy, *J Struct Biol 162*, 121-138.
(29) Francius, G., Dufour, S., Deleu, M., Paquot, M., Mingeot-Leclercq, M. P. and Dufrene, Y. F. (2008) Nanoscale membrane activity of surfactins: influence of geometry, charge and hydrophobicity, *Biochim Biophys Acta 1778*, 2058-2068.
(30) Green, J. D., Kreplak, L., Goldsbury, C., Li Blatter, X., Stolz, M., Cooper, G. S., Seelig, A., Kistler, J. and Aebi, U. (2004) Atomic force microscopy reveals defects within mica

supported lipid bilayers induced by the amyloidogenic human amylin peptide, *J Mol Biol 342*, 877-887.
(31) Lind, T. K., Zielinska, P., Wacklin, H. P., Urbanczyk-Lipkowska, Z. and Cardenas, M. (2014) Continuous flow atomic force microscopy imaging reveals fluidity and time-dependent interactions of antimicrobial dendrimer with model lipid membranes, *ACS Nano 8*, 396-408.
(32) Wang, K. F., Nagarajan, R. and Camesano, T. A. (submitted) Comparison of peptide structure-lipid bilayer interactions for alamethicin, chrysophsin-3, indolicidin and SMAP-29: Differentiation through QCM-D signatures,
(33) Wang, K. F., Nagarajan, R. and Camesano, T. A. ((submitted)) Comparison of peptide structure-lipid bilayer interactions for alamethicin, chrysophsin-3, indolicidin and SMAP-29: Differentiation through QCM-D signatures,
(34) Richter, R., Mukhopadhyay, A. and Brisson, A. (2003) Pathways of lipid vesicle deposition on solid surfaces: a combined QCM-D and AFM study, *Biophys J 85*, 3035-3047.
(35) Fox, R. O., Jr. and Richards, F. M. (1982) A voltage-gated ion channel model inferred from the crystal structure of alamethicin at 1.5-A resolution, *Nature 300*, 325-330.
(36) Benes, M., Billy, D., Benda, A., Speijer, H., Hof, M. and Hermens, W. T. (2004) Surface-dependent transitions during self-assembly of phospholipid membranes on mica, silica, and glass, *Langmuir 20*, 10129-10137.
(37) Ha, T. H., Kim, C.H., Park, J.S., Kim, K. (2000) Interaction of indolicidin with model lipid bilayer: quartz crystal microbalance and atomic force microscopy study, *Langmuir 16*, 871-875.

Chapter 7

A novel technique for forming supported anionic lipid membranes through vesicle fusion and an investigation of its interactions with chrysophsin-3

7.1 Abstract

Although supported lipid bilayer (SLBs) composed of zwitterionic lipids and zwitterionic-anionic lipid mixtures have been used extensively to mimic eukaryotic and Gram-negative bacterial cell membranes, attempts to form supported bilayers composed entirely of anionic lipids have been less successful. SLBs fully composed of anionic lipids are valuable models for Gram-positive bacterial membranes that can be used to study the membrane interactions of particles such as antimicrobial peptides (AMPs) or nanoparticles. We developed a novel method of forming robust anionic lipid bilayers containing 3:2 and 4:1 L-α-phosphatidylglycerol (PG) and 1-palmitoyl-2-hydroxy-***sn***-glycero-3-phospho-(1'-***rac***-glycerol) (LPG) lipid mixtures, which were supported on (3-aminopropyl)trimethoxysilane (APTMS)-coated silica. Quartz crystal microbalance with dissipation monitoring (QCM-D) was used to monitor the formation of the supported bilayers by measuring nano-scale mass changes on a sensor surface as anionic lipids vesicles attached and ruptured into a bilayer. Supported PG vesicle layers were also formed to enable experiments that monitor the behavior of anionic vesicles. These supported lipid membranes were exposed to various concentrations of the AMP chrysophsin-3 to demonstrate the anionic membranes' capacity as bacterial membrane mimics and investigate the molecular effects of the peptide on anionic bilayers. Chrysophsin-3 exhibited transmembrane insertion behavior and did not predominantly adsorb to the membrane surface as it did on zwitterionic lipid phosphatidylcholine (PC) membranes. Supported anionic lipid bilayers can be valuable tools for studying the behavior of Gram-positive bacterial membranes for the development of antimicrobial agents or therapeutics.

7.2 Introduction

One of the primary differences between the plasma membranes of eukaryotic and bacterial cells is in the charges of the phospholipids contained within the bilayer. Eukaryotic cells, such as erythrocytes, primarily contain zwitterionic lipids, while Gram-positive bacteria, such as *Staphylococcus aureus* (*S. aureus*), are composed of anionic lipids.[1] The plasma membranes of Gram-negative bacteria like *Escherichia coli* can contain a mixture of zwitterionic and anionic phospholipids.

This difference in membrane charge is believed to be a primary method by which antimicrobial peptides (AMPs) are able to target bacterial cells over eukaryotic cells. AMPs, which are often cationic, are thought to first become attracted to bacterial membranes through electrostatic interactions.[2, 3] Once attached, some membrane-active AMPs kill bacteria by destabilizing their lipid membranes and causing them to lyse. Other AMPs may enter the cell through this membrane and destroy intracellular components, killing the cell. Although membrane-active AMPs are believed to kill cells through membrane destabilization, the exact mechanism behind the membrane disruption is not fully understood.

Several theories have been developed to explain the mechanisms that allow membrane-active AMPs to destabilize cell membranes. In the barrel-stave model, AMPs are believed to insert into the membrane, forming pores through which large molecules can enter or exit the cell.[4] Ion gradients can also be disturbed, killing the cell. Alamethicin and other α-helical peptides are thought to be able to insert into the membranes as single molecules or as clusters.[5, 6] The carpet model supposes that the peptides can "carpet" the lipid headgroup surface of the membrane and rearrange with the membrane lipids to form micelles or peptide-lipid aggregates.[7] These aggregates can then leave the bilayer, destroying the membrane. Variations of these two

primary mechanisms can occur, such as the formation of toroidal pores, and can depend on peptide-to-lipid ratio in the membrane.[5, 8]

Due to the low risk of AMP-induced resistance in bacteria, AMPs are being researched extensively for their potential as therapeutics. AMPs are believed to avoid the development of bacterial resistance because of their unique membrane-destabilization mechanisms of bacterial killing. However, before AMPs can be used effectively in therapeutics, their interactions with both bacterial cells and eukaryotic cells need to be fully understood. Therapeutic AMPs must be able to effectively target and kill pathogens without harming eukaryotic cells in the patient.

Quartz crystal microbalance with dissipation monitoring (QCM-D) is a sensitive method of studying AMP interactions on the molecular level in real-time. AMPs are injected into a chamber containing a mimetic cell membrane, which is modeled by a lipid bilayer supported on the surface of a QCM-D sensor, or crystal. Measuring frequency and energy dissipation changes of the oscillating crystal gives information about changes in the mass and rigidity of the membrane. One can also interpret the various measured overtones to infer the organization and orientation of peptide and lipid molecules in the membrane. Since this method assumes that the mass on the sensor surface is uniform, the supported lipid bilayers must smooth and defect-free.

Previous QCM-D studies have investigated the action of AMPs on models of eukaryotic and Gram-negative bacterial membranes, which consist of purely zwitterionic lipids or a combination of zwitterionic and anionic lipids.[9-12] These studies revealed valuable information about AMP-membrane interactions and showed that QCM-D can be used to differentiate between surface adsorption of a peptide onto a membrane and insertion into the membrane.

However, examination of the action of AMPs on Gram-positive bacterial membrane mimics requires the development of smooth supported lipid bilayers fully composed of anionic lipids.

Due to the charges associated with anionic lipids, a simple procedure for forming smooth and consistent supported lipid bilayers composed entirely of anionic lipids has not been developed. Lipid bilayers composed of zwitterionic/anionic lipid mixtures have been formed and studied extensively, particularly those containing up to 50 mol% anionic lipids.[13, 14] Sparsely tethered bilayer membrane systems have also been developed with zwitterionic/anionic lipid mixtures, in which a synthetic lipid anchor is used to tether lipids to a surface and a short hydrophilic "backfiller," such as β-mercaptoethanol (βME) is used to dilute the grafting points.[15] Attempts to create bilayers composed purely of anionic lipids resulted in incomplete or defect-rich membranes, however. Blume et al. were able to form an anionic 1-palmitoyl-2-oleoyl-*sn*-glycero-3-phosphoglycerol (POPG) supported lipid bilayer using the Langmuir-Blodgett/Langmuir-Schaefer method, but epifluorescence images of the membrane showed the presence of ordered domains or defects in the membrane.[16] Also, the vesicle fusion method of bilayer formation is preferred for QCM-D experiments, since the entire bilayer formation procedure can be performed inside a closed QCM-D flow chamber. The vesicle fusion method for forming PC bilayers is a robust method that has been shown to form smooth membranes. The technique consists of injecting a solution of small unilamellar lipid vesicles (SUVs) over a silica surface. The vesicles attach to the surface and at rupture to form a lipid bilayer when they reach a critical concentration.

We developed a simple protocol for forming supported anionic membranes using various compositions of PG and LPG vesicles and verified the results using QCM-D. Once this protocol was shown to be robust and consistent, we exposed these membranes to various concentrations

of the AMP chrysophsin-3, an amphiphilic and cationic peptide derived from the gills of the red sea bream, *Chrysophrys major*. Chrysophsin-3 contains 20 amino acids that exhibit an α-helical conformation when in contact with a biological membrane. This peptide was chosen because its action with a zwitterionic PC membrane had been investigated in a previous study from our lab, which enabled a comparison of AMP-membrane interactions on membranes of varying charge. The peptide also contains 4 positively charged amino acid residues near the C-terminus, which may result in strong electrostatic interactions with an anionic membrane.

In this study, we developed a novel technique for forming anionic supported lipid membranes on (3-aminopropyl)trimethoxysilane (APTMS)-coated silica. A screening study was performed to identify lipid compositions and surface treatments that showed potential for forming robust supported bilayers. Three lipid membranes were chosen from this screening study for further study and were exposed to various concentrations of chrysophsin-3 to investigate AMP-membrane interactions using QCM-D. The AMP experiments were performed to demonstrate the capabilities of these membranes as bacterial membrane mimics, which will be valuable for investigating the behavior of these membranes in future studies.

7.3 Materials and methods

7.3.1 Peptides and lipids

Chrysophsin-3 (GenWay Biotech Inc., San Diego, CA) was suspended and stored in Tris-NaCl buffer (100 mM sodium chloride and 10 mM tris(hydroxymethyl)aminomethane, pH 7.8). Experimental concentrations of 0.5, 1, 5, and 10 μM chrysophsin-3 were examined.

Egg L-α-phosphatidylcholine (PC), egg L-α-phosphatidylglycerol (PG) and 1-palmitoyl-2-hydroxy-***sn***-glycero-3-phospho-(1'-***rac***-glycerol) (LPG) were purchased from Avanti Polar

Lipids (Alabaster, AL). PC was stored in ethanol at -20˚C and PG and LPG were stored in chloroform at the same temperature. Lipid vesicle solutions were typically suspended in HEPES buffer (10 mM HEPES, 150 mM NaCl, 2 mM NaN_3, pH 7.4) with or without the addition of 2 mM $CaCl_2$ or 4 mM ethylenediaminetetraacetic acid (EDTA). Tris-NaCl buffer (100 mM sodium chloride and 10 mM tris(hydroxymethyl)aminomethane, pH 7.8) was also used in vesicle solutions.

7.3.2 Lipid vesicle formation

Three anionic lipid membrane compositions were examined in this study: (i) PG, (ii) 3:2 PG/LPG (molar ratio), and (iii) 4:1 PG/LPG (molar ratio). The 3:2 and 4:1 ratios were chosen because they are similar to the lipid composition of *S. aureus* membranes.[1] Zwitterionic PC was also used in an initial screening study. The lipids were dried in the appropriate proportions to remove the chloroform or ethanol solvents and placed in a vacuum desiccator overnight. The dried lipids were suspended in enough of the appropriate buffer (Tris-NaCl or HEPES buffer with or without $CaCl_2$ or EDTA) to bring the total lipid concentration to 2.5 mg/mL. The lipid solution was mixed well and placed through 5 freeze-thaw cycles. The lipids were then sonicated with an ultrasonic dismembrator (Model 150T, Fisher Scientific, Waltham, MA) in pulsed mode for 30 min in a 70˚C water bath. A 30% duty cycle (3-sec sonication followed by a 7-sec pause) with an amplitude of 60 was used. The vesicles were then centrifuged for 10 min at 16,000g to remove probe particles and large lipid aggregates. The supernatant was removed and stored under nitrogen at 7˚C and diluted to a concentration of 0.1 mg/mL before each experiment.

Dynamic light scattering (Zetasizer Nano ZS, Malvern, Worcestershire, UK) (DLS) was used to measure vesicle size in solution. DLS measures the Brownian motion of the particles in a sample, from which the particle size can be derived. Small particles are known to move quickly

in a liquid, while large particles move slowly. The intensity distributions of the suspended lipid vesicle samples were measured and used to generate size distributions of the vesicles by volume.

7.3.3 Quartz crystal microbalance with dissipation monitoring (QCM-D)

The Q-Sense E4 system (Biolin Scientific, Sweden) was used to monitor the attachment of lipid vesicles to a sensor surface and the subsequent peptide-lipid interactions. QCM-D is a sensitive method that can capture nano-scale mass changes on a sensor surface. A voltage is applied to the QCM-D quartz sensor, causing it to oscillate at its resonant frequency. As mass (Δm) is added to the sensor surface, the frequency associated with this oscillation decreases (Δf) according to the Sauerbrey equation:

$$\Delta m = -C\Delta f \tag{7.1}$$

where C is a proportionality constant (17.8 ng/cm^2/Hz for a crystal with a natural frequency of 5 MHz). It should be noted that the Δf values are automatically normalized to each overtone so that $\Delta f = f/n$, where f is the frequency and n is the harmonic number.

Energy dissipation is also measured, which is related to the time it takes for the oscillation of the mass on the surface to stabilize when the crystal oscillation is stopped. Dissipation (D) is related to the rigidity of the mass and can be described by:

$$D = \frac{G''}{2\pi G'} \tag{7.2}$$

where G' and G'' are the loss modulus and storage modulus, respectively. Higher dissipation values are related to softer or hydrated mass on the sensor surface.

Various overtones, or harmonics, of the frequency and dissipation are also measured, providing information about changes occurring throughout different depths of the attached film. Due to the different penetration depths of the acoustic waves associated with the measured overtones, each overtone can be related to processes at various thicknesses of an adsorbed film.[11, 17] Higher overtones (e.g. 11^{th}) are more closely related to processes occurring near the sensor surface and lower overtones (e.g. 3^{rd}) are related to processes occurring farther from the sensor, near the membrane-liquid interface.

Previous studies have used overtone data to infer the attachment and organization of molecules at various depths of supported lipid bilayers.[9-12] Frequency decreases in lower overtones indicate that mass addition occurred on the bilayer surface, suggesting a mechanism involving peptide adsorption to the membrane surface, which was observed for chrysophsin-3 action on PC bilayers.[11] As shown for alamethicin interactions with PC membranes, uniform frequency changes at all overtones indicate mass changes throughout the entire membrane thickness, which could be a result of peptide insertion in to the membrane.[9] Variations of these two models can point to more complex interactions, such as partial peptide insertion into the membrane that was suggested by QCM-D studies of indolicidin action on PC membranes.[10]

To form supported lipid bilayers, a baseline was first established in the frequency and dissipation measurements by flowing the buffer that was present in the lipid vesicle solution. The lipid vesicle solutions were then injected into the QCM-D chambers at 0.15 mL/min for 35 min and the shifts in f and D were measured. The sensor surface was rinsed with another injection of the original buffer to remove any weakly attached particles. All experiments were performed at 23˚C.

7.3.4 Surface treatment

Anionic lipid membranes were formed on silica QCM-D sensor crystal surfaces treated with (3-aminopropyl)trimethoxysilane (APTMS) and polyethylenimine (PEI). APTMS and PEI were used to make the sensor surface cationic to facilitate the attachment of anionic lipid vesicles. Before each experiment, the sensors were rinsed with 2% sodium dodecyl sulfate (SDS) and DI water, dried with nitrogen gas and etched with a SPI Plasma Prep II Plasma Etcher (SPI Supplies, West Chester, PA). The sensors were then immersed in ethanol for 5 min, methanol for 5 min, and a 30% (vol%) APTMS/methanol mixture for 20 min. After rinsing with methanol and drying with nitrogen gas, the crystals were ready for use in QCM-D experiments. At the end of each experiment, the crystals were rinsed with 2% SDS, DI water and methanol and dried with nitrogen gas.

7.3.5 Monitoring of chrysophsin-3 interactions with anionic lipid films

After the anionic lipid films had stabilized under the final buffer rinse, Tris-NaCl buffer was flowed over the sensor surface to establish a new baseline in preparation for the injection of chrysophsin-3, which was suspended in Tris-NaCl buffer. Chrysophsin-3 was injected into the chamber for 10 min at a flow rate of 0.15 mL/min to ensure that it had replaced the previous buffer solution and the flow was paused for 1 hr. After the 1-hr incubation, the flow was restarted with Tris-NaCl buffer to remove weakly attached particles from the sensor surface. The final buffer rinse continued until the frequency and dissipation measurements stabilized.

7.4 Results and discussion

7.4.1 Anionic lipid vesicle and membrane formation

Various lipid compositions, vesicle sizes, buffers, and surface treatments were examined in a preliminary screening study to identify the most promising systems to pursue in our membrane formation experiments. These parameters were chosen because they were important factors in PC and dioleoylphosphatidylcholine (DOPC)/dioleoylphosphatidylserine (DOPS) lipid vesicle adsorption and bilayer formation in previous studies.[13, 18, 19] The results are summarized in Table 7.1. Rapid vesicle adsorption (negative frequency peaks) to the surface and subsequent stabilization of frequency and dissipation measurements ($\Delta D < 0$) indicated possible formation of a supported lipid bilayer.

From the preliminary screening study, we found that lipid composition, the buffer, and the surface treatment were the most critical parameters for enabling bilayer formation. Many vesicle systems that contained 3:2 and 4:1 PG/LPG (~20-30 nm in diameter) formed supported lipid bilayers when suspended in HEPES buffers containing 2 mM $CaCl_2$ or 4 mM EDTA. Both APTMS and PEI facilitated vesicle adsorption and rupturing at 30% and 20 mg/mL concentrations, respectively. Creating smaller vesicle sizes by repeating the sonication procedure did not impact vesicle adsorption or bilayer formation, however. Also, not all the lipid compositions examined were capable of forming SLBs. PG vesicles, for instance, adsorbed to the APTMS- and PEI-treated surfaces, but did not form a supported membrane after 40 minutes of flowing the vesicle solution over the QCM-D sensor surface.

Table 7.1. Results of anionic lipid membrane screening study

Lipid Composition	Vesicle Diameter (nm)	Buffer	SiO_2 Surface Treatment	Peak Δf (Hz)	Final Δf (Hz)	Peak ΔD (1E-6)	Final ΔD (1E-6)	Results	Conclusions
Egg PC	~37	Tris-NaCl, pH 7.8	None	-70	-26	4.5	0.5	Control: PC SLB formed normally	2 hr. incubation does not result in PC vesicle adsorption after stable bilayer formation
Egg PG	~ 35	Tris-NaCl, pH 7.79	~5 mg/mL PEI (10 min incubation)	0	0	0	0	No vesicle adsorption	PG vesicles in Tris-NaCl buffer will not attach to PEI-treated surface
Egg PG	123.3 ±45.74	HEPES+2 mM $CaCl_2$, pH 7.43	30% APTMS (20 min incubation)	-75	-68	5.5	4.5	- Vesicles adsorbed, but rupture was not directly observed - Adsorption not stabilized after 40 min	- PG vesicles do not appear to form SLB, but may form a supported vesicle layer - final buffer rinse did not result in substantial mass loss
Egg PG	123.3 ±45.74	HEPES+2 mM $CaCl_2$, pH 7.43	20 mg/mL PEI (20 min incubation)	-67	-62	5	3.7	- Vesicles adsorbed, but rupture was not directly observed - Adsorption not stabilized after 40 min	Same as above
3:2 PG/LPG	unknown	HEPES + 4 mM EDTA, pH 7.37	10% APTMS (20 min incubation)	-24	-17	0.5	0.8	Vesicle attachment and rapid rupturing may have occurred	10% APTMS will allow for some anionic vesicle attachment and rupture
3:2 PG/LPG	~35	HEPES+4 mM EDTA, pH 7.37	30% APTMS (20 min incubation)	-27	-25	0.7	1	Vesicle attachment and rapid rupturing may have occurred	Increased APTMS concentration (~4x) increases lipid retention after buffer rinse but only increases vesicle adsorption slightly (-3 Hz)
3:2 PG/LPG	25.02 ±18.95	HEPES+2 mM $CaCl_2$, pH 7.4	10% APTMS (20 min incubation)	-27-> -21	-14 ->-22	0.8 -> 0.2	1	- less initial vesicle attachment and irreversible mass attachment than with 30% APTMS - Possible vesicle rupturing	SLB may still form with lower APTMS concentration, but less mass is retained on crystal surface
3:2 PG/LPG	19.34 ±13.22	HEPES+2 mM $CaCl_2$, pH 7.38	30% APTMS (20 min incubation)	-31	-22	1	0.6	Vesicles adsorbed and may have ruptured to form a bilayer after 39 minutes of vesicle flow	$CaCl_2$ may enable SLB formation on APTMS-coated SiO_2, although final Δf is less than we expect for PC SLB
3:2 PG/LPG	2950 ±1018	HEPES, pH 7.41	30% APTMS (20 min incubation)	-25-> -21	-33	0.4 -> 0.2	0.4	- Vesicles attached to surface and some may have ruptured - Final buffer rinse added mass	PG/LPG vesicles are not stable without $CaCl_2$ or EDTA (possible aggregation)
3:2 PG/LPG	25.02 ±18.95	HEPES+2 mM $CaCl_2$, pH 7.4	2.5 mg/mL PEI (20 min incubation)	-26	-18-> -25	0.6	1.2	- less initial vesicle attachment than with 20 mg/mL PEI - Vesicles may have ruptured	SLB may still form with lower PEI concentration
3:2 PG/LPG	19.34 ±13.22	HEPES+2 mM $CaCl_2$, pH 7.38	20 mg/mL PEI (20 min incubation)	-30	-21	0.5	0.5	- Vesicles adsorption and possible rupture - stabilized after 5 min	3:2 PG/LPG in HEPES+$CaCl_2$ buffer did not adsorb more than 4:1 PG/LPG in HEPES+4mM EDTA on PEI-Coated SiO_2

Lipid Composition	Vesicle Diameter (nm)	Buffer	SiO_2 Surface Treatment	Peak Δf (Hz)	Final Δf (Hz)	Peak ΔD (1E-6)	Final ΔD (1E-6)	Results	Conclusions
3:2 PG/LPG	2950 ±1018	HEPES, pH 7.41	20 mg/mL PEI (20 min incubation)	-34 ->-27	-40	0.5	-0.5	- More vesicles attachment to surface with PEI than with APTMS; may have ruptured - Final buffer rinse added mass	PEI resulted in more mass attachment than APTMS coating in absence of $CaCl_2$ or EDTA
4:1 PG/LPG	21.87 ±42.45	HEPES+4 mM EDTA, pH 7.38	None	-1.5	1.7	0.5	0.5	A small amount of vesicles adsorbed to the bare SiO_2 surface	The surface treatments are primarily responsible for vesicle adsorption observed in other experiments
4:1 PG/LPG	21.87 ±42.45	HEPES+4 mM EDTA, pH 7.38	30% APTMS (20 min incubation)	-31	-27	1.25	0.7	- Vesicle rupture may have occurred - Stabilized after 30 min.	- 2 h incubation with APTMS surface may have led to observable SLB formation - the final Δf value is consistent with PC SLB formation; SLB may be forming rapidly
4:1 PG/LPG	29.47 ±23.79	HEPES+2 mM $CaCl_2$, pH 7.42	30% APTMS (20 min incubation)	-47	-36	2	~1	- Vesicle rupture may have occurred - Stabilized after 5 min	Most vesicle adsorption seen on APTMS using 4:1 lipid composition, rather than 3:2 PG/LPG
4:1 PG/LPG	22.37 ±18.12	HEPES+2 mM $CaCl_2$, pH 7.4	30% APTMS (20 min incubation)	-48	-35 ->-40	2	~1	- Vesicle rupture may have occurred - Adsorption stabilized after 5 min	Creating smaller vesicles does not substantially improve adsorption or rupturing behavior
4:1 PG/LPG	28.27	HEPES+4 mM EDTA, pH 7.37	2.5 mg/mL PEI (20 min incubation)	-50	-32	2	1	More vesicle attachment occurred, but no clear rupture	HEPES buffer may be better for anionic vesicle adsorption than tris-NaCl buffer (or PG/LPG vesicle mixture is preferred)
4:1 PG/LPG	~28.27	HEPES+4 mM EDTA, pH 7.38	10 mg/mL PEI (20 min incubation)	-68	-47	4	1.25	More vesicle attachment occurred, but no clear rupture	Increased PEI concentration increases vesicle adsorption
4:1 PG/LPG	19.76 ±6.162	HEPES+4 mM EDTA, pH 7.39	20 mg/mL PEI (20 min incubation)	-90	-65	-2 -> 6	0	- More vesicle attachment occurred, but no clear rupture	Increased PEI concentration increases vesicle adsorption, but does not lead to rupture
4:1 PG/LPG	21.87 ±42.45	HEPES+4 mM EDTA, pH 7.38	20 mg/mL PEI (20 min incubation)	-74	-50	6	1.5	- Vesicle rupture not observed - Vesicle adsorption stabilized after 1 h.	2 h incubation with PEI surface did not lead to observable SLB formation
4:1 PG/LPG	29.47 ±23.79	HEPES+2 mM $CaCl_2$, pH 7.42	20 mg/mL PEI (20 min incubation)	-27	-22	0.5	0.5	- Vesicles adsorption and rupture possible observed - Adsorption stabilized after 5 min	On PEI, 4:1 adsorbed less than 3:2 PG/LPG
4:1 PG/LPG	22.37 ±18.12	HEPES+2m M $CaCl_2$, pH 7.4	20 mg/mL PEI (20 min incubation)	-27	~-22	0.5	0.5	- Vesicles adsorbed, but rupture was not observed - Adsorption stabilized after 5 min	Creating smaller vesicles does not improve adsorption or rupturing behavior

Lipid Composition	Vesicle Diameter (nm)	Buffer	SiO_2 Surface Treatment	Peak Δf (Hz)	Final Δf (Hz)	Peak ΔD (1E-6)	Final ΔD (1E-6)	Results	Conclusions
4:1 PG/LPG	22.37 ±18.12	HEPES+2 mM $CaCl_2$, pH 7.4	20 mg/mL PEI (20 min incubation)	-27	~-22	0.5	0.5	- Vesicles adsorbed, but rupture was not observed - Adsorption stabilized after 5 min	Creating smaller vesicles does not improve adsorption or rupturing behavior

From this screening study, three anionic vesicle systems were chosen for further examination: PG, 3:2 PG/LPG, and 4:1 PG/LPG vesicles in HEPES + 2 mM $CaCl_2$ buffer. The PG system represented a supported vesicle layer, on which we could analyze the vesicle rupturing capabilities of AMPs. The mixed lipid systems (used to describe 3:2 PG/LPG, and 4:1 PG/LPG) were used to form supported lipid bilayers to investigate the behavior of different lipid compositions. The 30% APTMS surface treatment was chosen for all following experiments to increase the amount and rate of vesicle adsorption to the surface and improve the likelihood of forming a bilayer. The same buffer and surface treatment was used in the 3 systems so that the lipid compositions would be the only variable. Henceforth, all experiments were performed with HEPES + 2 mM $CaCl_2$ buffer on 30% APTMS-treated silica sensor surfaces.

DLS measurements revealed that the PG, 3:2 PG/LPG and 4:1 PG/LPG vesicles were approximately 125 nm, 20 nm, and 25 nm in diameter immediately following the sonication and centrifugation steps of the vesicle formation procedure (t = day 0). Figure 7.1 shows the size distributions of each experimental vesicle composition based on intensity and volume percentages. It is important to note that since larger particles scatter more light than smaller particles, the area of the intensity peak for larger particles will be greater than the area for smaller particles if the numbers of small and large particles in the solution are the same (Figure 7.1A). The same is true for the volume measurements (Figure 7.1B), since the volume of larger particles is greater than the volume of smaller particles. Therefore, these graphs cannot be used to directly infer the number of particles of each size present in the solution.

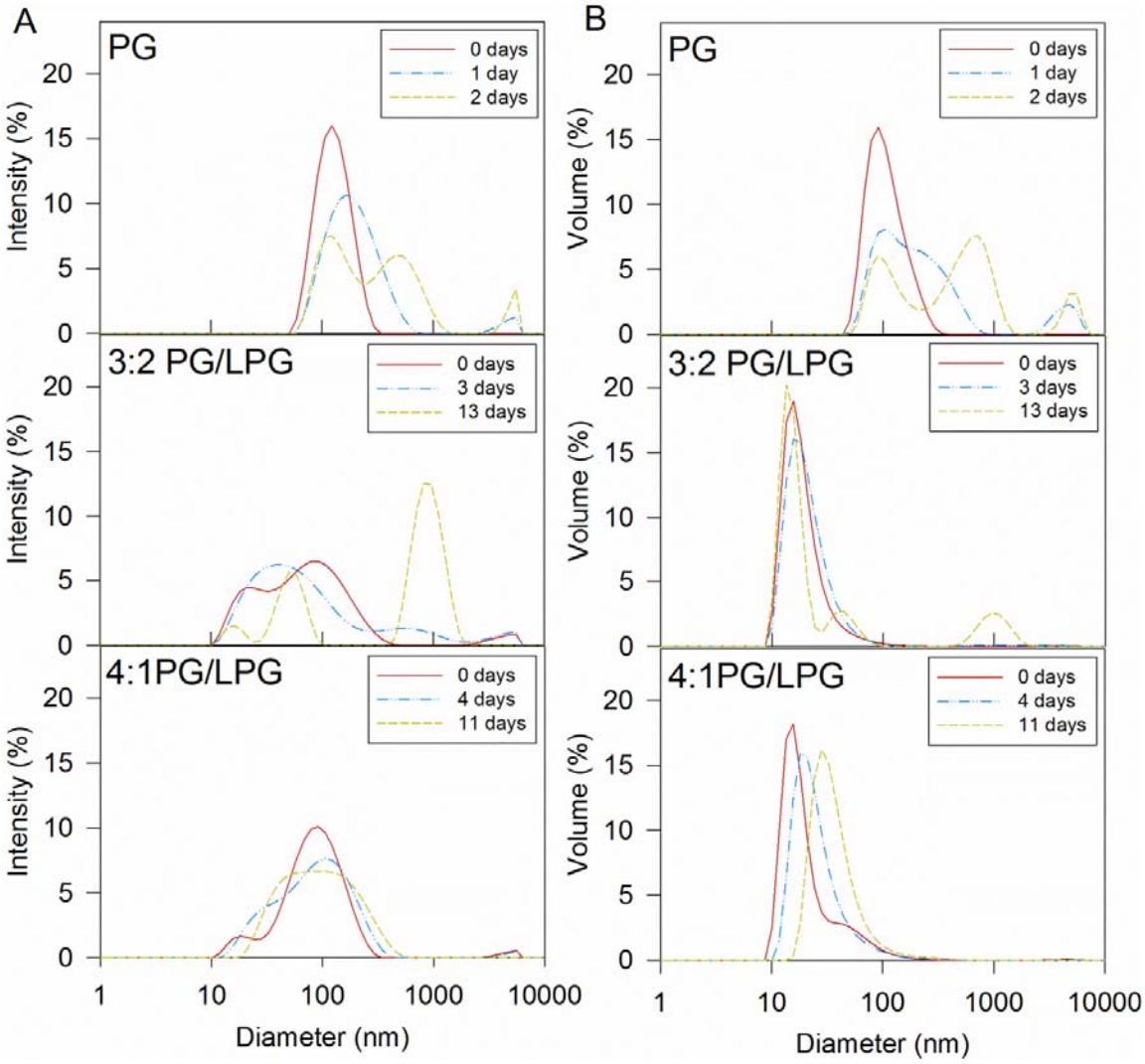

Figure 7.1. Size distribution of PG, 3:2 PG/LPG, and 4:1 PG/LPG vesicles by intensity (A) and volume (B) measured by DLS. Three time points have been shown for each vesicle type to show the stability of the vesicles over time

Stability of the anionic vesicles was also determined from DLS measurements. Vesicle size distributions were measured at various time points to monitor the aggregation and stability of the vesicles over time (Figure 7.1). Many of the particles in the PG vesicle solution increased in size within 1 day, suggesting that the vesicles had aggregated. The PG vesicle solutions were therefore sonicated before each QCM-D experiment to ensure that the vesicle sizes were consistent between QCM-D trials. The mixed lipid vesicles were more stable (for purposes of

clarity, all time points are not shown). These vesicles were used and stored under nitrogen at 7˚C for up to 4 days.

From previous studies on supported PC lipid bilayers, vesicle adsorption and rupturing have been identified as two primary mechanisms necessary in supported lipid membrane formation using the vesicle fusion method.[20, 21] As shown in Table 7.1 (row 1), an initial frequency decrease of -70 Hz (labeled peak Δf) was typically observed as PC vesicles adsorbed to the sensor surface. When the vesicles ruptured, releasing water mass, the frequency increased and stabilized around -26 Hz (final Δf) after a buffer rinse. The dissipation also peaked at a value of 4.5×10^{-6} as the hydrated and "soft" vesicles adsorbed and stabilized at 0.5×10^{-6} (peak and final ΔD) after the vesicles ruptured into a rigid bilayer. Since these frequency and dissipation responses were consistently characteristic of PC bilayer formation, we expected the f and D responses associated with anionic bilayer formation to be similar. Therefore, we used QCM-D to monitor the formation of anionic bilayers and compared the Δf and ΔD measurements to those for PC membranes for validation.

In QCM-D experiments, PG vesicles adsorbed to the surface during 40 minutes of vesicle flow and stabilized as a supported vesicle layer (SVL) during the final buffer rinse. Figure 7.2A shows the frequency and dissipation shifts resulting from anionic vesicle attachment to an APTMS-coated silica QCM-D sensor surface. The stabilized membrane in the representative graphs in Figure 7.2A showed a frequency shift of -48 Hz in the 3rd harmonic, which was almost twice as large as the frequency shift associated with stable PC bilayer formation (-26 Hz), but less than the Δf value observed for PC vesicle attachment in previous studies (-70 Hz). Based on the f and D responses, we believe that a bilayer was not formed, but a layer of anionic vesicles.

The stabilized Δf value was not consistent between experiments with PG vesicles and varied between -48 Hz and -75 Hz, however (all data not shown). This variation may have been a result of vesicle aggregation on the sensor surface. From DLS measurements (Figure 7.1), it is clear that PG vesicles are prone to aggregation, so it is possible that a layer of vesicle aggregates formed on the QCM-D sensor surface. Variation in stable Δf values could therefore have been a result of differences in aggregate sizes between experiments. The inconsistency in Δf values may also have been due to differences in the APTMS coating applied to the sensor surfaces. Each QCM-D sensor was used multiple times and treated with the same concentration of APTMS before each experiment. Although the crystals were cleaned before and after each experiment, residual APTMS from previous experiments may have remained on the surface in some cases and affected its interactions with the vesicles.

It should also be noted that the PG vesicle solution was only injected for 40 min and was not allowed to continue until vesicles had saturated the surface of the crystal. In preliminary experiments (data shown in Appendix 1.2), vesicle flow was maintained until the frequency change reached -70 Hz, but the frequency measurements did not stabilize. The continuing mass addition may have corresponded with the formation of multiple layers of vesicles or the adsorption of vesicle aggregates. Since the formation of a PG bilayer seemed unlikely, PG vesicle flow was stopped at 40 minutes in these experiments. The overtones also separated as more mass attached to the surface, as would be expected with hydrated films that are not uniform throughout their thickness (e.g. vesicles). The final dissipation value was large (3.4×10^{-6}), indicating that the film was more hydrated than a stable PC bilayer.

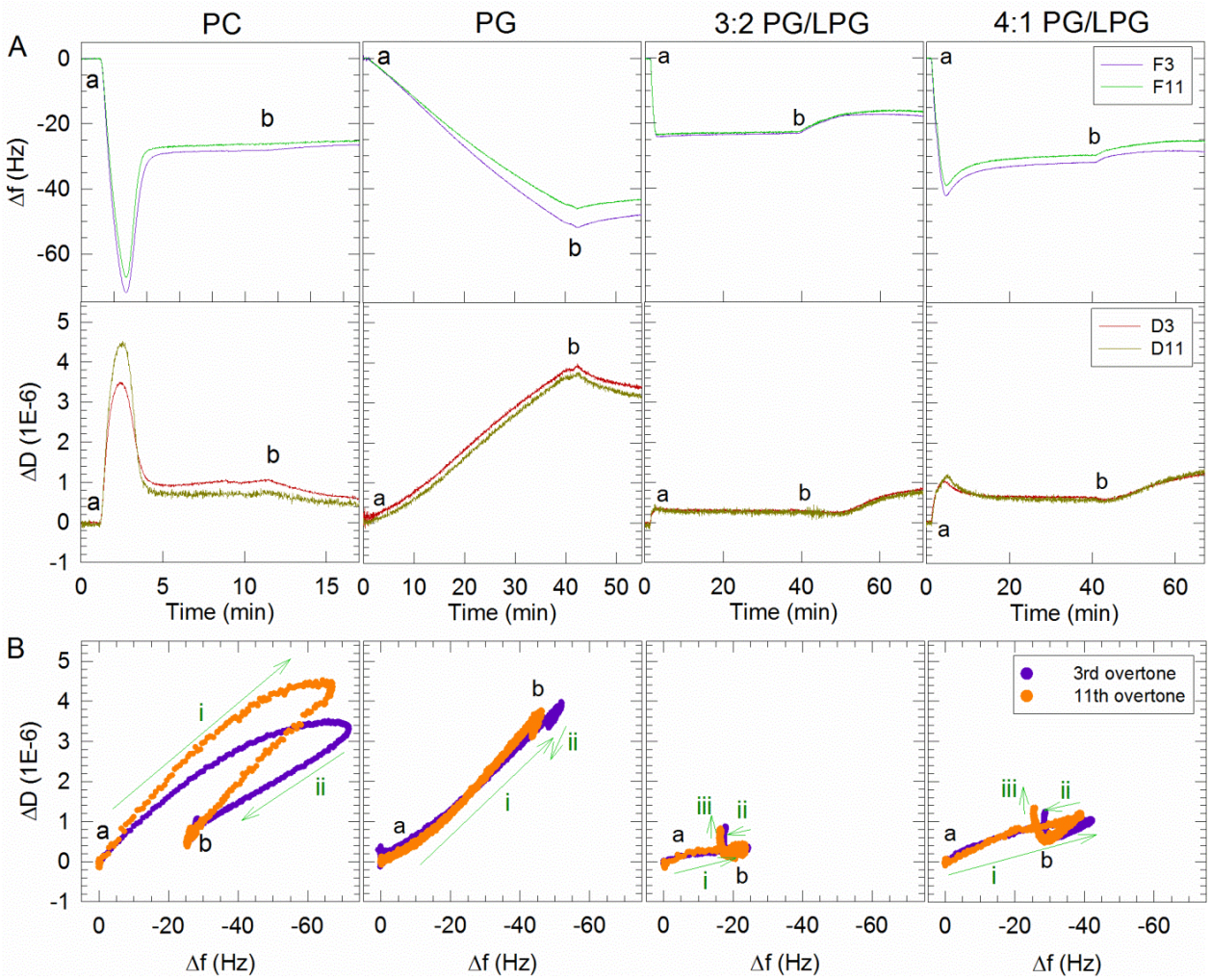

Figure 7.2. Attachment of PG, 3:2 PG/LPG, and 4:1 PG/LPG vesicles on APTMS-coated silica. Time points marking the start of vesicle flow (a) and HEPES+2 mM $CaCl_2$ buffer flow (b) are represented in (A) the frequency and dissipation shifts measured over time and (B) ΔD vs. Δf plots. Only the 3rd and 11th harmonics are shown for clarity. The frequency axes in (B) are reversed so that progression of points to the right represents mass increase. The green arrows (labeled *i*, *ii*, *iii*) show the progression of data points over time and the sequence of different processes occurring on the sensor surface. The data shown for PC bilayer formation was adapted from a previous publication from this lab.[9]

The 3:2 PG/LPG vesicles attached to the APTMS-treated surface and immediately ruptured into a rigid SLB, resulting in a Δf value of -18 Hz in the 3rd harmonic (Figure 7.2A). This process may have been too rapid for a minimum frequency "peak," the expected indicator of vesicle rupture, to be measured. The stable frequency value (-18 Hz) is lower than the expected value of PC SLBs, which could be due to differences in lipid masses (as LPG has a lower molecular mass than PC). The overtones remained close, indicating that the film was uniform at all depths, like a PC bilayer. The dissipation also remained low ($<1x10^{-6}$) after stabilization, as seen with supported PC membranes. The small final dissipation value suggests that the membrane formed on the surface is rigid, which was expected for a supported bilayer.

4:1 PG/LPG also ruptured into a membrane that was a supported lipid bilayer, but not as rapidly as with 3:2 PG/LPG (Figure 7.2A). The frequency decreased to -40 Hz as vesicles attached to the surface (starting from time point *a*), which indicated that more 4:1 PG/LPG vesicles adsorbed than 3:2 PG/LPG vesicles under the same conditions. Vesicle attachment was rapidly followed by mass and dissipation loss, which was likely caused by vesicle rupture. Before the final buffer rinse (time point *b*), the membrane stabilized at Δf = -32 Hz and ΔD = $0.5x10^{-6}$, which are similar to the *f* and *D* changes measured for PC membranes. After rinsing with HEPES + 2mM $CaCl_2$ buffer, the frequency and dissipation values stabilized at Δf = -28 Hz and ΔD = $1.2x10^{-6}$ in the 3rd harmonic. This final Δf value associated with the stable film showed more mass on the surface of the sensor than with PC bilayers, which may have been a result of the different lipids used. The stabilized dissipation value at time *b* (before the final buffer rinse) was similar to that of a PC bilayer, suggesting the formation of a 4:1 PG/LPG bilayer.

The difference in molecular weights between PC, PG and LPG and the greater repulsion between anionic lipids may explain difference in mass between the various bilayers. The final dissipation value of 1.2×10^{-6} associated with a stable 4:1 PG/LPG membrane indicates that the final buffer rinse created a film that was more hydrated or structurally disordered than a PC or 3:2 PG/LPG membrane. It is possible that the 4:1 PG/LPG composition is more conducive to greater hydration within the membrane. Since LPG is known to partition into water, the buffer rinse may have caused some LPG removal from the membrane, leaving spaces that were filled by water.

Plotting ΔD vs. Δf revealed changes in the dynamic processes that were occurring on the sensor surface and showed that anionic bilayer formation differed from that of PC SLB formation (Figure 7.2B). The points in these plots represent Δf and ΔD measurements taken at evenly spaced time intervals (0.7 s intervals) and therefore reveal the rate of each process. Processes occurring on the sensor surface, such as vesicle adsorption or rupture, are represented by the direction of the data points (labeled with arrows *i*, *ii*, and *iii*). Vesicle adsorption mechanisms are expected to result in the addition of mass on the surface, leading to a decline in frequency (or progression in the eastward direction in these plots). Vesicle rupture, however, is accompanied by mass loss from the adsorbed film in the form of water, resulting in increases in frequency and decreases in dissipation (or progression in the south-west direction). These processes can be followed in the ΔD vs. Δf plot for PC bilayer formation, in which the vesicle adsorption process (labeled *i*) is followed by vesicle rupture (*ii*).

PC bilayer formation consists of 2 clear stages (*i* and *ii*), which were also observed to some extent with 3:2 and 4:1 PG/LPG vesicles before the final buffer rinse (Figure 7.2B). The third process (*iii*) that occurred with the mixed lipid membranes was a result of the final buffer

rinse, which removed weakly attached particles from the membrane surface and allowed spaces in the membrane to be filled with water (resulting in greater hydration). PG adsorption to the surface occurred in a single-stage process (*i*), which was followed by mass and dissipation loss due to the final buffer rinse (*ii*). The addition of LPG in the vesicles seemed to allow this process to become a 2-stage series.

Comparison of the dynamic membrane formation processes of the 4 vesicle types reveals that PG adsorbed to the sensor surface at the slowest rate, but more lipid mass adsorbed without rupturing the adsorbed vesicles. The 3:2 and 4:1 PG/LPG lipid mixtures initially adsorbed more rapidly before stabilizing as bilayer. The lipid mixture containing more PG (4:1 PG/LPG) also resulted in more mass adsorption to the surface and was more structurally disordered or hydrated than the 3:2 PG/LPG bilayer.

Using the frequency changes that were observed in Figure 7.2A, we estimated the area per lipid (a_L) in each bilayer and the thickness of the bilayer's hydrophobic region. The frequency changes (Δf) measured for the stabilized 3:2 and 4:1 PG/LPG membranes were -18 Hz and -28 Hz, respectively. Using eqn. 7.1 ($\Delta m = -C\,\Delta f$), the areal mass of the 3:2 PG/LPG membrane was calculated to be 320.4 ng/cm^2. If we assume that the anionic membranes behave similarly to supported PC bilayers, this areal mass may include a layer of water between the bilayer and sensor surface, which has been shown to have a mass of 102 ng/cm^2 in PC bilayers supported on silica.[22] Correcting for the mass of this water layer, the mass of the lipid bilayer became 218.4 ng/cm^2. Calculating the average molecular weight of the 3:2 PG/LPG lipid mixture to be 671.99 g/mol (given that the molecular weights of PG and LPG are 782 g/mol and 506 g/mol, respectively), the average mass per lipid molecule (M_L) was determined to be 1.12×10^{-12} ng/lipid. Dividing the areal mass of the lipid bilayer by the mass of a single lipid

molecule M_L revealed that there were 1.96 lipids/nm^2 in the bilayer, which corresponds to a lipid area (a_L) of 1.03 nm^2/lipid (if a_L =2/M_L, accounting for the presence of two lipid layers). Assuming that the molecular volume v_L of the hydrophobic tail of the PG and LPG lipids are 0.96 nm^3/molecule and 0.46 nm^3/molecule, respectively, v_L for 3:2 PG/LPG was 0.76 nm^3/molecule (the average volume based on the constituent C16 and C18 chains), the thickness of the hydrophobic region of the 3:2 PG/LPG bilayer was calculated to be $h_L = 2v_L/a_L$ = 1.48 nm.

Using the same procedure for the 4:1 PG/LPG bilayer (average MW: 727 g/mol), in which M_L = 1.21x10^{-12} ng/lipid and v_L = 0.86nm3/lipid, the area per lipid was calculated to be a_L = 1.03 nm^2/lipid and the thickness of the hydrophobic region of the bilayer was determined to be h_L = 2.81 nm. In a previous study from our lab, a PC bilayer was calculated to allow a lipid area of a_L = 0.739 nm^2/lipid and have a hydrophobic region thickness of h_L = 2.6 nm.[10] The calculated lipid area in the 4:1 PG/LPG bilayer was smaller than that of the 3:2 PG/LPG and PC bilayers. This suggested that the 4:1 PG/LPG bilayer may have been more densely packed. Much of the additional mass in the membrane may have included water mass, however, which was evidenced by the high dissipation values associated with a stable membrane and may have allowed the 4:1 PG/LPG lipids more space than these calculations indicated.

The estimated thicknesses of the hydrophobic regions of the 3:2 and 4:1 PG/LPG bilayers were similar to that of a PC bilayer. The estimates for anionic membranes were reasonably similar to thickness values found for PC lipid bilayer and for the cytoplasmic membrane of bacteria, which are 5 nm and 7 nm thick, respectively. [23] The bacterial membrane thickness and stability may also be affected by the incorporation of protein molecules that are inherent in these membranes. Any discrepancies, however, could also have been due to erroneous estimates for the mass of hydration incorporated into the membranes.

We believe that anionic lipid bilayers were formed in these experiments with 3:2 and 4:1 PG/LPG lipid vesicles due to the similarity of frequency shifts associated with the stable membranes. Although the anionic membrane thicknesses varied, they were comparable to the thickness of a PC bilayer. Also, the dissipation shifts recorded for the anionic bilayers were similar to that of a rigid PC bilayer and did not resemble dissipation values recorded for surfaces covered with vesicles. QCM-D monitoring of the 4:1 PG/LPG membrane formation process also clearly showed vesicle adsorption and rupturing processes. To demonstrate the capabilities of these films as model Gram-positive bacterial membranes, we examined the interactions of the AMP chrysophsin-3 on PG supported vesicle layers, 3:2 PG/LPG supported bilayers, and 4:1 PG/LPG supported bilayers. These experiments also provided insight into the ability of chrysophsin-3 to rupture anionic vesicles and disrupt anionic SLBs of varying lipid compositions.

7.4.2 Chrysophsin-3 ruptures supported anionic vesicles

Once stable lipid films had been formed and verified with QCM-D measurements, the SVLs or SLBs were exposed to various chrysophsin-3 concentrations. The peptide solutions were allowed to flow into the QCM-D chamber for 10 min to ensure that the entire chamber was filled with the peptide solution. The flow was paused for 1 hr to allow the AMP solution to incubate with the lipid film and subsequently restarted with a buffer rinse to remove any poorly attached particles. To analyze AMP-induced changes in the membrane, shifts in frequency and dissipation resulting from chrysophsin-3 action were evaluated. These values were calculated at each overtone by taking the difference between measurements associated with 2 time points: (1) the stable bilayer before peptide injection and (2) the resulting mass after the final buffer rinse.

Measurements at these time points were used to capture the changes due to AMP action without the effects of other system variables.

When incubated with surface-adsorbed vesicles, all experimental concentrations of chrysophsin-3 caused vesicle rupture (Figure 7.3). The decline in dissipation at all overtones revealed decreases in membrane "softness," which implies that hydration had left the membrane system. This change was likely due to vesicle rupture, which released water within the vesicles, as was previously observed in the bilayer formation processes of 3:2 and 4:1 PG/LPG. Although the error bars on the frequency plots were large, making the frequency results inconclusive, the dissipation values reveal that hydration was lost from the membrane and suggest a vesicle rupturing process.

The large error bars associated with the frequency values may be explained by variations observed in PG vesicle layer formation, as previously discussed in Section 7.4.1. Variation in the amount of vesicle attachment to the surface, which may have been due to vesicle aggregation, resulted in variations in AMP-induced mass change in each QCM-D trial. A surface completely coated with vesicles would be expected to behave differently from a surface sparsely coated with vesicles. Studies on PC bilayer formation have shown that PC vesicles will only rupture to form a supported bilayer once the vesicle concentration on the surface reaches a critical level, demonstrating the significance of vesicle concentration in determining membrane behavior.[24] The amount of surface coverage and spaces between vesicles may also play a role in determining if lipids from a ruptured vesicle will adsorb to the sensor surface as a bilayer or leave the membrane altogether.

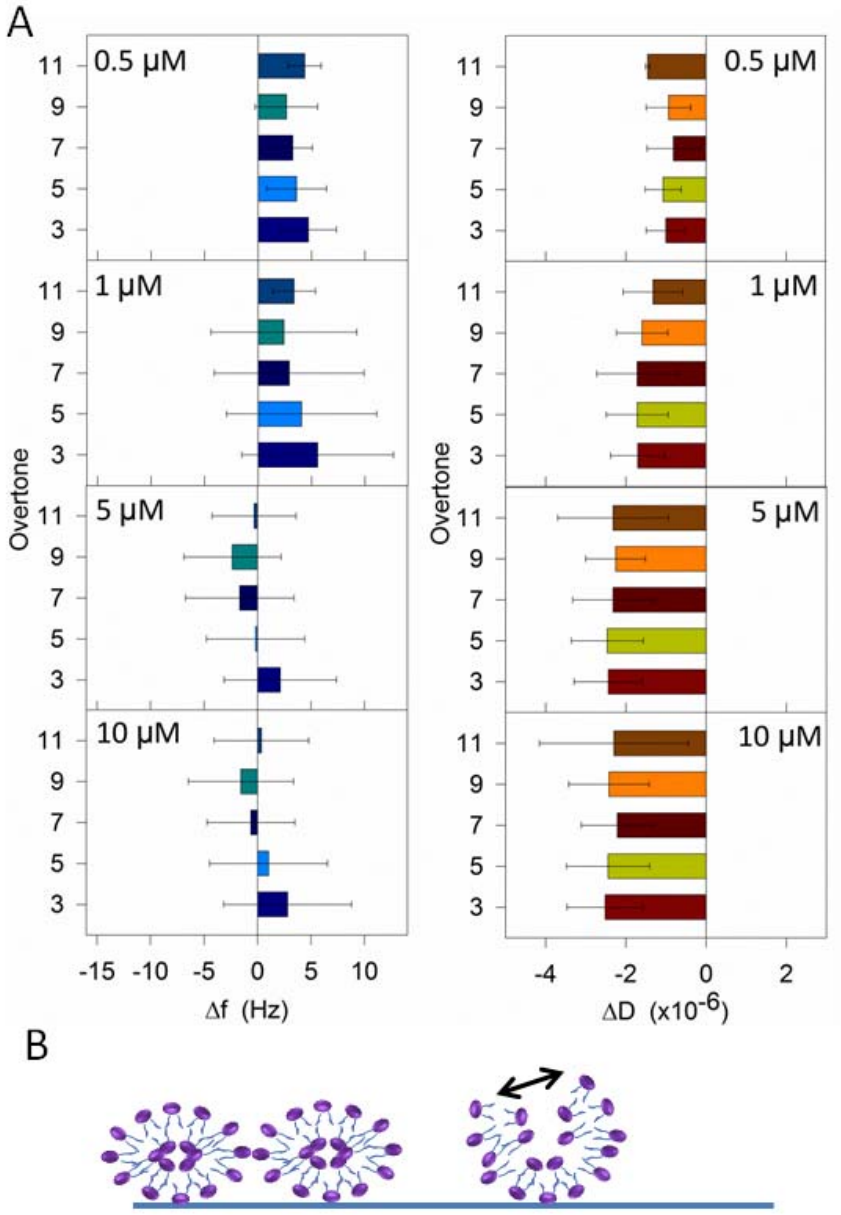

Figure 7.3. (A) Average frequency and dissipation shifts measured during the exposure of a supported PG vesicle layer to chrysophsin-3. Error bars represent the standard deviation based on at least 3 replicate experiments. (B) Proposed model of chrysophsin-3-induced rupture of supported PG vesicles.

ΔD vs. *Δf* plots showing QCM-D measurements taken during peptide exposure and the final buffer rinse provided information about the dynamics of chrysophsin-3 interactions with PG vesicles (Figure 7.4). Lower chrysophsin-3 concentrations (0.5 μM and 1 μM) primarily resulted

in single-stage mass and dissipation loss. In previous studies on chrysophsin-3 action on PC bilayers, membrane disruption was not observed at these concentrations.[10] In these bilayers, low peptide concentrations did not disrupt the membrane's mass or structure enough to be detected using QCM-D. When in contact with anionic SVLs, however, these peptide concentrations destabilized the vesicle membranes enough to break the vesicles, resulting in measureable frequency and dissipation changes. Therefore, SVL systems may be used as more sensitive methods of analyzing AMP-induced membrane disruption than SLB systems.

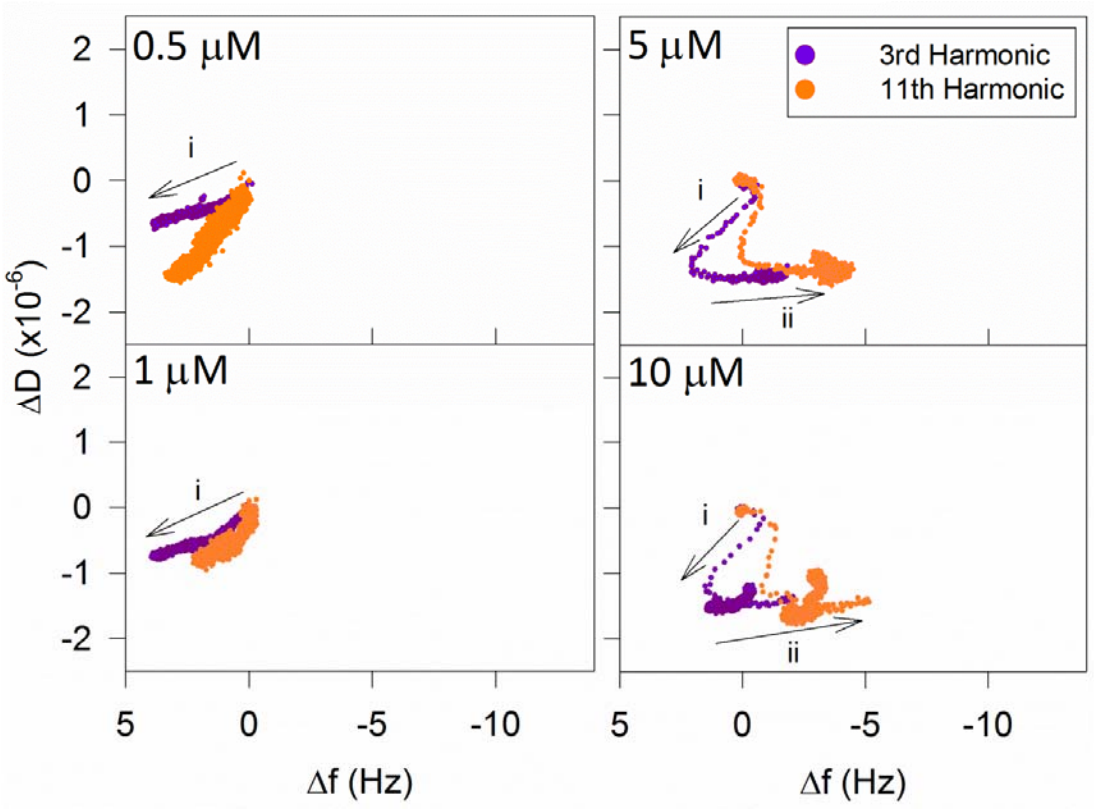

Figure 7.4. Representative *ΔD* vs. *Δf* plots showing dynamic processes occurring during chrysophsin-3 action on a PG vesicle layer. The frequency axis has been reversed so that mass gains are represented by progression to the right. The arrows labeled *i* and *ii* show the sequence of interactions that occurred during the vesicle destabilization.

Higher peptide concentrations (5 μM and 10 μM) resulted in two distinct interaction mechanisms. Following a small initial mass gain, likely from peptide adsorption, which was not observed at lower chrysophsin-3 concentrations, the PC vesicles rapidly lost mass and hydration (labeled *i*) as vesicles ruptured. As the resulting peptide-lipid film stabilized before and during the 1-h incubation, it gradually gained mass (*ii*). The dissipation did not change significantly during this second stage, suggesting that the hydration and lipid organization within the membrane did not change. The addition of mass was likely in the form of peptide or lipid particles filling in any holes on the APTMS-coated surface. The 3rd and 11th harmonics also showed separation throughout the experiment, indicating that different processes were occurring at different depths of the membrane. As demonstrated by the different overtone behavior that occurred during PC vesicle rupture into a bilayer (Figure 7.2A), overtone separation would be expected as PG vesicles ruptured to form a bilayer.

The vesicle rupture indicated by these experiments between 0.5 μM and 10 μM concentrations is consistent with the minimum inhibitory concentrations (MIC) of peptides like chrysophsin-3 that are active against Gram-positive and Gram-negative bacteria.[25] Dennison et al. have compiled a database of known peptides and their MIC values to identify features that determine AMP efficacy. Peptides with demonstrated activity against Gram-positive and Gram-negative bacteria exhibited an MIC range of 0.2-40 μM with a mean value of 7.9 μM.[26] This MIC range encompasses our experimental concentration range (0.5 μM - 10 μM) that exhibited membrane destabilization and vesicle rupturing activity, suggesting that the PG vesicle layer may be a plausible bacterial membrane mimic. Specific examples of effective AMPs include alamethicin, which has been shown to inhibit the growth of *Sinorhizobium meliloti*, a Gram-negative bacterium, at 25 μM.[27]

7.4.3 Chrysophsin-3 action on anionic lipid bilayers

At higher concentrations, chrysophsin-3 exhibited a peptide-insertion mechanism on supported 3:2 PG/LPG lipid bilayers (Figure 7.5). Substantial changes to the membrane did not occur at the lower chrysophsin-3 concentrations of 0.5 μM and 1 μM. Higher concentrations (0.5 μM and 1 μM), however, led to uniform mass gain in the membrane at all overtones, indicating that the same process was occurring throughout all depths of the membrane. The dissipation did not change substantially at any concentration, implying that the molecular structure of the membrane did not undergo substantial reorganization or hydration as a result of exposure to the peptide.

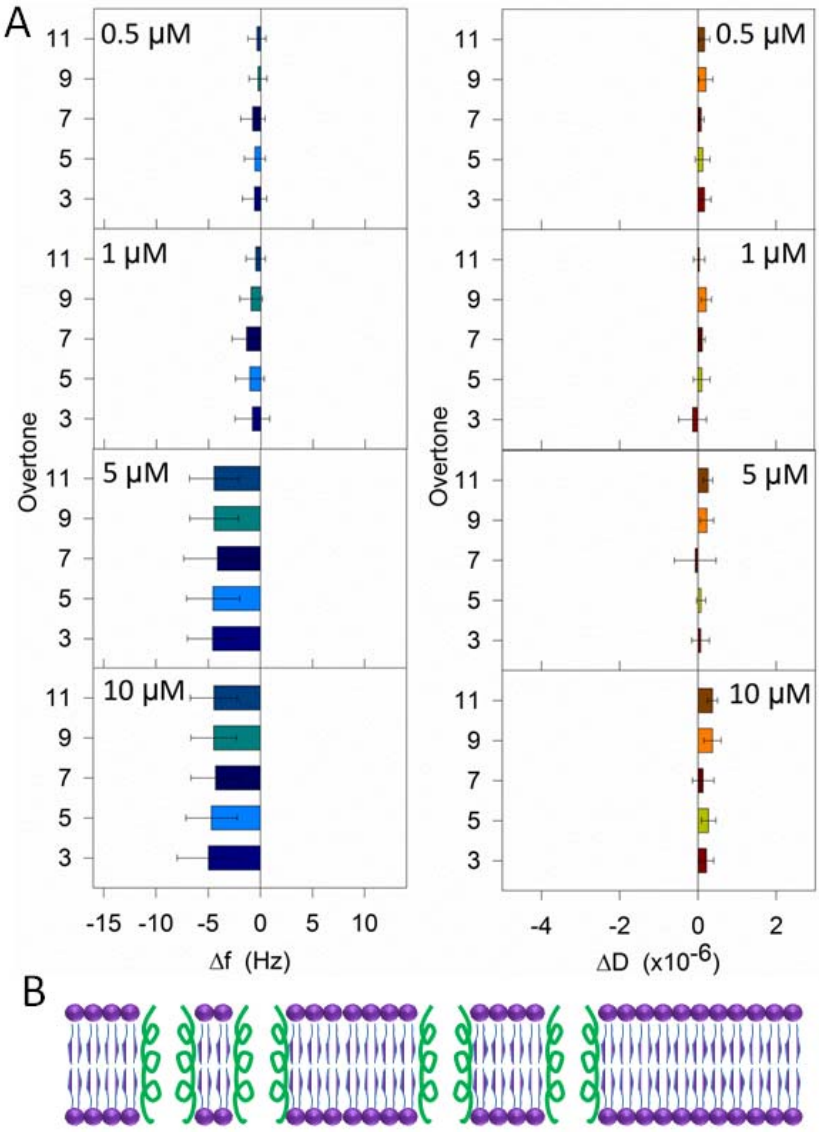

Figure 7.5. (A) Average *f* and *D* shifts resulting from the exposure of a supported 3:2 PG/LPG bilayer to chrysophsin-3. Error bars represent the standard deviation based on at least 3 replicate experiments. (B) Proposed model of chrysophsin-3 (green) insertion into 3:2 PG/LPG membranes (violet).

The dynamics of the peptide interactions with 3:2 PG/LPG bilayers were substantially different than those observed with the PG membrane (Figure 7.6). As revealed by the overall frequency and dissipation shifts in Figure 7.5, chrysophsin-3 did not have a measurable effect on the 3:2 PG/LPG bilayer at 0.5 μM and 1 μM concentrations. Upon exposure to 5 μM

chrysophsin-3, the SLB rapidly gained mass as peptides attached to the membrane (*i*). Mass was rapidly lost again (*ii*) before the membrane gradually regained mass during the 1-h incubation (*iii*). The membrane also became more disordered or hydrated during this time, as evidenced by the dissipation increase. During the final HEPES + 2 mM $CaCl_2$ buffer rinse, mass was again lost as dissipation increased (*iv*). This phenomenon may have been due to lipid and peptide mass leaving the membrane, causing the molecular structure to become disordered. Incubation with 10 μM chrysophsin-3 caused a faster increase in mass in the membrane (*i*), followed by rapid mass and dissipation decrease (*ii*) and ending with less mass than was present before the peptide injection. This net loss in mass, which suggests some lipid removal from the membrane, is promising because it shows that the cationic APTMS surface treatment likely does not prevent anionic lipids from leaving the crystal surface. During the final HEPES + 2 mM $CaCl_2$ buffer rinse, the membrane regained mass and dissipation before stabilizing (*iii* and *iv*).

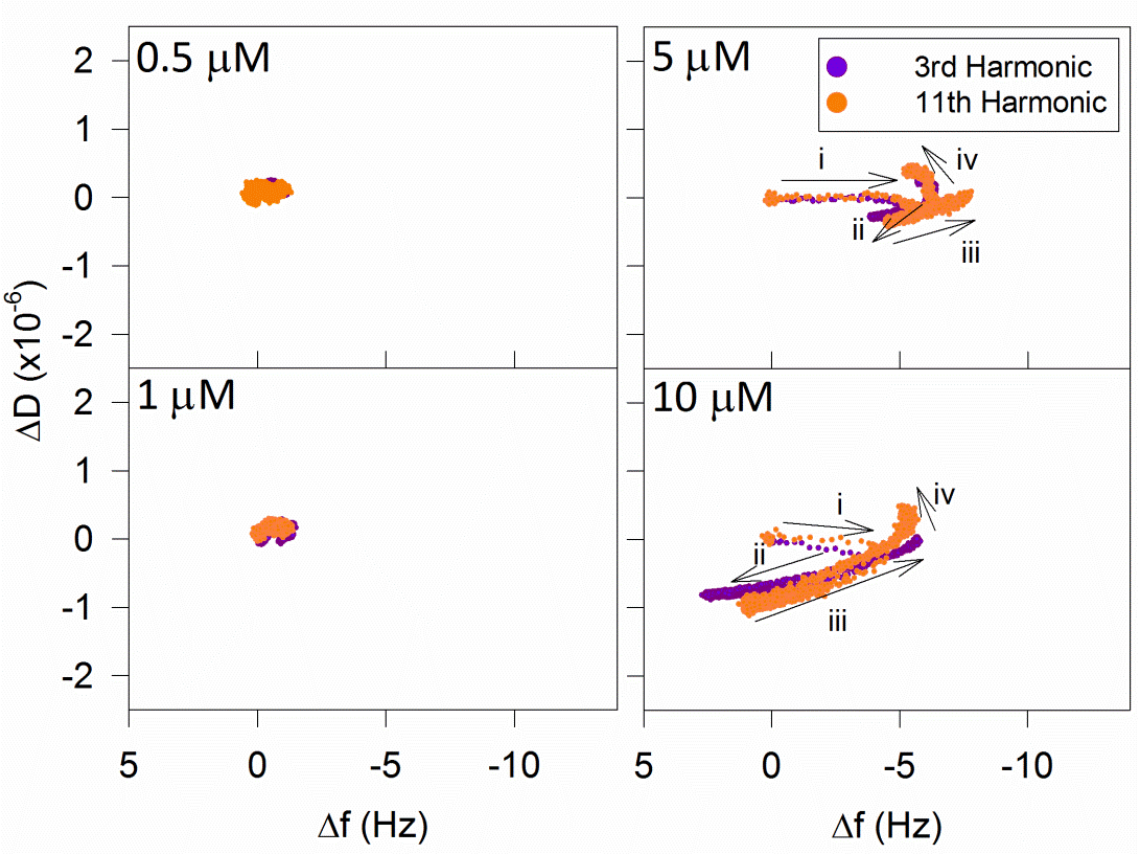

Figure 7.6. Representative *ΔD* vs. *Δf* plots showing dynamic processes occurring during chrysophsin-3 action on a 3:2 PG/LPG supported bilayer. The frequency axis has been reversed so that mass gains are represented by progression to the right. The arrows (*i*, *ii*, *iii* and *iv*) follow the progression of data points and show separate interaction mechanisms.

It is unclear why mass and dissipation increased during the final buffer rinse, since new particles should not have been introduced into the system to allow for such a change. If the mass increase had been a result of the incorporation of buffer into spaces left in the membrane by lipid removal, the dissipation should have also increased above $1x10^{-6}$, signifying a hydrated film. It is possible that some of the mass gain observed during the final buffer rinse was due to the incorporation of water molecules, but better understanding of the crystal surface and effects of the APTMS coating is required to fully interpret these results.

As seen with 3:2 PG/LPG membranes, chrysophsin-3 did not impact 4:1 PG/LPG membranes substantially at 0.5 μM and 1 μM concentrations (Figure 7.7). Exposure to 5 μM chrysophsin-3 resulted in mass gain to the membrane that was uniform at all overtones, suggesting a peptide-insertion mechanism. At 10 μM chrysophsin-3, nearly twice the mass gain was observed in 4:1 PG/LPG membranes than with 3:2 PG/LPG. Similar to 3:2 PG/LPG, substantial dissipation changes did not occur, indicating that the membrane did not undergo measureable structural disorder or hydration. The frequency changes (~-10 Hz) observed with 10 μM chrysophsin-3 action on the 4:1 PG/LPG membrane were greater than the maximum -3.36 Hz change estimated in a previous study[10] for insertion of the peptide as a monomer or a cluster into the membrane. A different interaction mechanism may therefore be responsible for this large mass addition, but again, better understanding about the effects of APTMS on the crystal surface and adsorbed lipids is necessary to fully interpret these results.

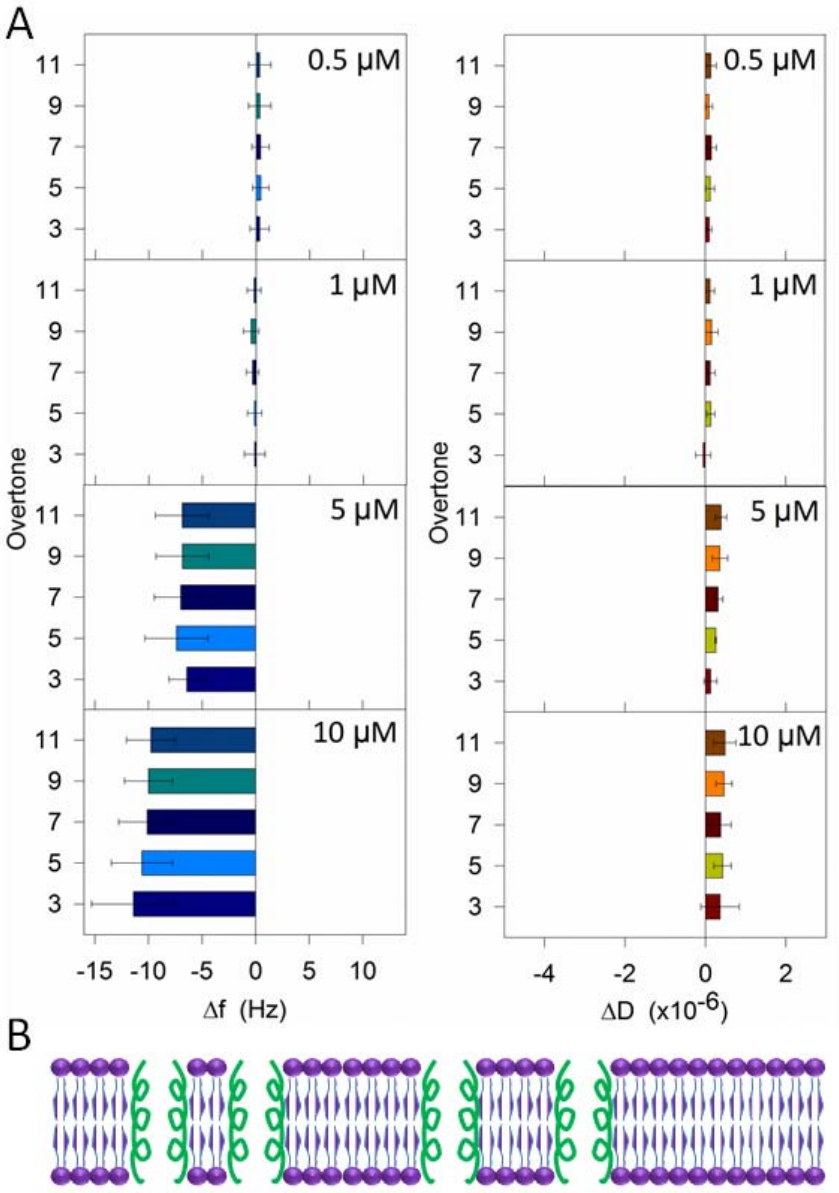

Figure 7.7. (A) Average *f* and *D* shifts resulting from the exposure of a supported 4:1 PG/LPG bilayer to chrysophsin-3. Error bars represent the standard deviation based on at least 3 replicate experiments. (B) Proposed model of chrysophsin-3 (green) insertion into 3:2 PG/LPG membranes (violet).

The dynamics of chrysophsin-3's interactions with 4:1 PG/LPG were similar to those for 3:2 PG/LPG. The lower chrysophsin-3 concentrations (0.5 μM and 1 μM) did not create measurable changes in the 4:1 PG/LPG membrane (Figure 7.8). Three distinct mechanisms were revealed for the action of 5 μM and 10 μM chrysophsin-3. As the peptides attached to the

membrane, mass rapidly increased without substantial dissipation change (*i*). Once a critical concentration of peptide on the membrane was reached, mass was removed from the membrane. At 5 μM chrysophsin-3, this mass removal was small and was not accompanied by a substantial change in dissipation, indicating that the membrane had not become more or less disordered. At 10 μM, however, the mass loss was accompanied by a decrease in dissipation (*ii*), suggesting that if spaces had formed in the membrane from mass loss, the peptides may have stabilized the lipids surrounding those spaces. This process was followed by an increase in mass and dissipation during the final buffer rinse (*iii*), which was more pronounced with 10 μM chrysophsin-3 than with 5 μM concentrations. This phenomenon (*iii*) likely corresponded with buffer filling in the spaces in the membrane that were left by the removal of lipid mass.

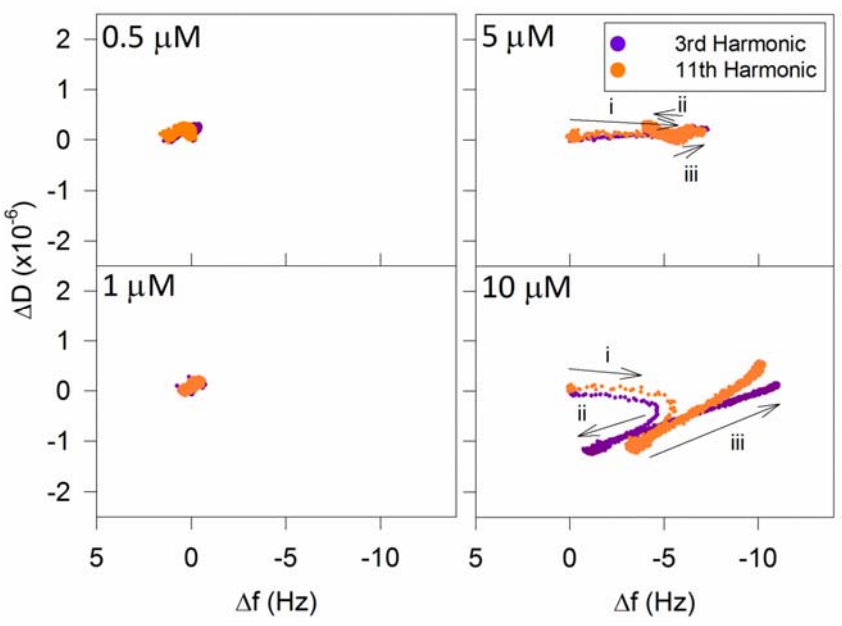

Figure 7.8. Representative *ΔD* vs. *Δf* plots showing dynamic processes occurring during chrysophsin-3 action on a 4:1 PG/LPG supported bilayer. The frequency axis has been reversed so that mass gains are represented by progression to the right. The arrows (*i*, *ii*, and *iii*) follow the progression of data points and show separate interaction mechanisms. The large gaps between the data points in *i* reveal the rapid rate of mass addition to the membrane.

The QCM-D results for chrysophsin-3 action on 3:2 and 4:1 PG/LPG membranes (Figures 7.5A and 7.7A) revealed that more mass addition resulted from peptide insertion into 4:1 PG/LPG bilayers. This result suggests that chrysophsin-3 displaced fewer lipids when inserting into bilayers containing lower concentrations of LPG. Perhaps the presence of LPG alters the stability of the lipid membrane structure, facilitating lipid removal. From QCM-D monitoring of anionic membrane formation, higher proportions of LPG (3:2 PG/LPG) allowed the anionic lipid vesicles to rupture more rapidly than systems with less LPG (4:1 PG/LPG), which may also have been a result of lower vesicle stability as a result of LPG (Figure 7.2A).

7.4.4 Interaction kinetics

The kinetics of these peptide-membrane interactions showed that all three anionic membranes initially interacted with chrysophsin-3 at similar rates (Figure 7.9). The total interaction time (Figure 7.9A) is a measure of the amount of time it takes for the peptide to reach peak initial adsorption to the lipid film or for it to reach peak initial mass removal from the film, depending on which is the predominant initial interaction. The various membranes had very similar interaction times at 10 μM concentrations and exhibited more variation at lower concentrations. Initial interactions also occurred more rapidly as peptide concentration increased.

The calculated interaction rates (Figure 7.9B) showed that the anionic membranes followed the same trends, although PG experienced initial mass loss, rather than the mass gain that occurred in the mixed lipid membranes. When compared to the initial interaction times and rates observed for chrysophsin-3 action on a PC membrane,[10] the time duration of the initial interaction was smaller in anionic membranes than for the zwitterionic PC membrane. This variation may be explained by the stronger attractive forces between cationic chrysophsin-3 and anionic membranes compared to zwitterionic lipids in initial electrostatic interactions. The initial

interaction rates between chrysophsin-3 and the two types of membranes were similar at all concentrations, however, indicating that although the peptide required more time to attach to the PC membrane, the overall rate of mass attachment was the same.

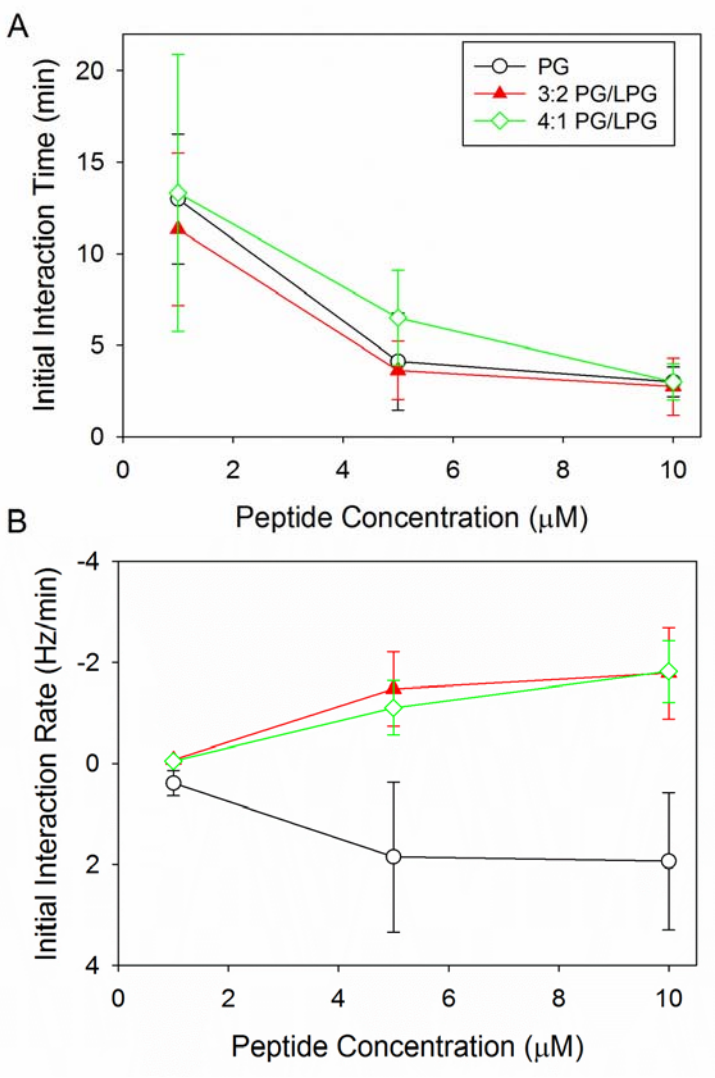

Figure 7.9. Initial interaction times and rates for chrysophsin-3 action on anionic lipid films. These values represent the rate of change during the initial stage of contact between the bilayer and the peptide.

7.4.5 Comparison of chrysophsin-3 action on zwitterionic and anionic membranes

The predominant mechanisms of action of chrysophsin-3 on zwitterionic and anionic lipid bilayers consisted of different interaction mechanisms and stages. When incubated with the anionic 3:2 and 4:1 PG/LPG bilayers in this study, chrysophsin-3 primarily demonstrated a peptide-insertion mechanism. In a previous study from this lab, chrysophsin-3 was found to adsorb to and insert into zwitterionic PC supported membranes at peptide concentrations between 1 μM and 10 μM.[11] At 10 μM, chrysophsin-3 caused the removal of at least 12% of the original lipid mass of the PC membrane. Substantial mass removal did not occur in the anionic membranes, although the reason for this is not clear. It is possible that lipids that were disrupted by the addition of peptide preferred to remain on the surface due to attractive forces between the lipids and the cationic APTMS coating on the QCM-D sensor surface.

The dynamics of these interactions also differed between the two membrane types. Compared to the anionic bilayers, when chrysophsin-3 was first introduced to PC bilayers, the initial mass addition to the membrane occurred for a longer time duration. This difference in adsorption rate was likely a result of the greater attraction of the cationic peptide to the anionic PG and LPG headgroups, since AMPs initially interact with cell membranes through electrostatic interactions. Also, the initial mass addition of chrysophsin-3 on anionic membranes (labeled *i* in Figures 7.6 and 7.8) was not accompanied by an increase in dissipation, which was observed in PC membranes. This indicated that the structure of the anionic membranes with attached peptides was more ordered (and less hydrated) than the PC membrane. Perhaps the attractive forces between cationic chrysophsin-3 and the anionic membrane caused the peptide molecules to immediately assume a more structured and stable orientation parallel to the membrane upon adsorption.

7.5 Conclusions

In this study, we successfully developed a simple method for forming anionic SLBs using various compositions of PG and LPG lipids. The creation of these stable bilayers was confirmed by monitoring their formation with QCM-D. The resulting frequency and dissipation measurements were compared with those obtained for PC bilayer formation, which is known to be a consistent and robust process. The lipid area and thickness of the hydrophobic regions of these bilayers were calculated from the frequency measurements. Various buffer types and surface treatments were also screened, revealing other supported lipid membrane systems that could be used in future studies. These anionic membranes are suitable for use as models of Gram-positive plasma membranes and may be valuable for examining membrane interactions of a wide variety of particles, such as AMPs or nanoparticles.

Anionic SVLs were formed using PG, on which vesicle breakage studies were performed. These experiments allowed us to monitor the effects of low AMP concentrations that would not have been detected in a supported lipid bilayer system. In effect, the membrane disruption effects are amplified, since vesicle rupture results in more measurable mass and dissipation changes on the QCM-D sensor surface. Chrysophsin-3 was found to rupture PG vesicles at concentrations as low as 0.5 μM and 1μM, which did not result in measureable changes to zwitterionic bilayers in previous studies.

The interactions between chrysophsin-3 on anionic SLBs were also examined, revealing faster initial interaction rates than those measured on zwitterionic membranes in previous studies. Chrysophsin-3 primarily demonstrated peptide insertion mechanisms, but not surface adsorption to the anionic membrane, which was a predominant mechanism observed on zwitterionic membranes. More understanding of the anionic membrane surface and structure is

needed to fully comprehend the effects of AMP exposure that were measured, however, and to fully understand the differences in AMP interactions with eukaryotic and bacterial cell membranes.

7.6 Acknowledgements

We would like to thank Dr. Hong Susan Zhou (WPI) for the use of the Zetasizer Nano ZS instrument for DLS measurements.

7.7 References

(1) Blondelle, S. E., Lohner, K. and Aguilar, M. (1999) Lipid-induced conformation and lipid-binding properties of cytolytic and antimicrobial peptides: determination and biological specificity, *Biochim Biophys Acta 1462*, 89-108.
(2) Brogden, K. A. (2005) Antimicrobial peptides: pore formers or metabolic inhibitors in bacteria?, *Nat Rev Microbiol 3*, 238-250.
(3) Skarnes, R. C. and Watson, D. W. (1957) Antimicrobial factors of normal tissues and fluids, *Bacteriol Rev 21*, 273-294.
(4) Shai, Y. (2002) Mode of action of membrane active antimicrobial peptides, *Biopolymers 66*, 236-248.
(5) Huang, H. W. (2000) Action of antimicrobial peptides: two-state model, *Biochemistry 39*, 8347-8352.
(6) Pan, J., Tristram-Nagle, S. and Nagle, J. F. (2009) Alamethicin aggregation in lipid membranes, *J Membr Biol 231*, 11-27.
(7) Shai, Y. and Oren, Z. (2001) From "carpet" mechanism to de-novo designed diastereomeric cell-selective antimicrobial peptides, *Peptides 22*, 1629-1641.
(8) Lee, M. T., Chen, F. Y. and Huang, H. W. (2004) Energetics of pore formation induced by membrane active peptides, *Biochemistry 43*, 3590-3599.
(9) Wang, K. F., Nagarajan, R. and Camesano, T. A. (2014) Antimicrobial peptide alamethicin insertion into lipid bilayer: A QCM-D exploration, *Colloids Surf B Biointerfaces 116*, 472-481.
(10) Wang, K. F., Nagarajan, R. and Camesano, T. A. (submitted) Comparison of peptide structure-lipid bilayer interactions for alamethicin, chrysophsin-3, indolicidin and SMAP-29: Differentiation through QCM-D signatures,
(11) Wang, K. F., Nagarajan, R., Mello, C. M. and Camesano, T. A. (2011) Characterization of supported lipid bilayer disruption by chrysophsin-3 using QCM-D, *J Phys Chem B 115*, 15228-15235.
(12) Mechler, A., Praporski, S., Atmuri, K., Boland, M., Separovic, F. and Martin, L. L. (2007) Specific and selective peptide-membrane interactions revealed using quartz crystal microbalance, *Biophys J 93*, 3907-3916.
(13) Richter, R., Mukhopadhyay, A. and Brisson, A. (2003) Pathways of lipid vesicle deposition on solid surfaces: a combined QCM-D and AFM study, *Biophys J 85*, 3035-3047.

(14) Evans, K. O. (2012) 1,2-Dielaidoylphosphocholine/1,2-dimyristoylphosphoglycerol supported phospholipid bilayer formation in calcium and calcium-free buffer, *Thin Solid Films 520*, 3026-3030.
(15) Heinrich, F., Ng, T., Vanderah, D. J., Shekhar, P., Mihailescu, M., Nanda, H. and Losche, M. (2009) A new lipid anchor for sparsely tethered bilayer lipid membranes, *Langmuir 25*, 4219-4229.
(16) Arouri, A., Kiessling, V., Tamm, L., Dathe, M. and Blume, A. (2011) Morphological changes induced by the action of antimicrobial peptides on supported lipid bilayers, *J Phys Chem B 115*, 158-167.
(17) Voinova, M. V., Rodahl, M., Jonson, M., Kasemo, B. (1999) Viscoelastic acoustic response of layered polymer films at fluid-solid interfaces: continuum mechanics approach, *Physica Scripta 59*, 391-396.
(18) Barenholz, Y., Gibbes, D., Litman, B. J., Goll, J., Thompson, T. E. and Carlson, R. D. (1977) A simple method for the preparation of homogeneous phospholipid vesicles, *Biochemistry 16*, 2806-2810.
(19) Reimhult, E., Hook, F. and Kasemo, B. (2002) Vesicle adsorption on SiO2 and TiO2: Dependence on vesicle size *Journal of Chemical Physics 117*, 7401-7404.
(20) Keller, C. A., Glasmastar, K., Zhdanov, V. P. and Kasemo, B. (2000) Formation of supported membranes from vesicles, *Phys Rev Lett 84*, 5443-5446.
(21) Keller, C. A. and Kasemo, B. (1998) Surface specific kinetics of lipid vesicle adsorption measured with a quartz crystal microbalance, *Biophys J 75*, 1397-1402.
(22) Zwang, T. J., Fletcher, W. R., Lane, T. J. and Johal, M. S. (2010) Quantification of the layer of hydration of a supported lipid bilayer, *Langmuir 26*, 4598-4601.
(23) Cohen, G., *Microbial Biochemistry*. Second Edition ed. 2011, New York: Springer.
(24) Richter, R. P., Berat, R. and Brisson, A. R. (2006) Formation of solid-supported lipid bilayers: an integrated view, *Langmuir 22*, 3497-3505.
(25) Iijima, N., Tanimoto, N., Emoto, Y., Morita, Y., Uematsu, K., Murakami, T. and Nakai, T. (2003) Purification and characterization of three isoforms of chrysophsin, a novel antimicrobial peptide in the gills of the red sea bream, Chrysophrys major, *Eur J Biochem 270*, 675-686.
(26) Dennison, S. R., Harris, F. and Phoenix, D. A. (2003) Factors determining the efficacy of alpha-helical antimicrobial peptides, *Protein Pept Lett 10*, 497-502.
(27) Amiche, M., Seon, A. A., Wroblewski, H. and Nicolas, P. (2000) Isolation of dermatoxin from frog skin, an antibacterial peptide encoded by a novel member of the dermaseptin genes family, *Eur J Biochem 267*, 4583-4592.

Chapter 8

Conclusions and Future Directions

Infections involving antibiotic-resistant microbes have increased dramatically in recent decades, posing a significant health threat to patients.[1] The short doubling time exhibited in bacteria enables them to evolve quickly, thereby increasing their likelihood of developing drug resistance. AMPs have shown promise as antibiotic alternatives due to their broad spectrum of activity and low occurrence of bacterial resistance.[2] Membrane-active AMPs are believed to be less prone to the development of pathogen resistance than antibiotics because of their unique mechanisms of bacterial killing.[3] However, these mechanisms must be fully understood before AMPs can be selected and designed to maximize effectiveness and ensure that the patient will not be harmed.

The studies presented in this thesis provided fundamental knowledge about how AMPs are able to destabilize and destroy cell membranes. These concentration-dependent interactions were related to specific characteristics known about AMP structural properties, such as charge, secondary structure, hydrophobicity and hydrophobic moment. QCM-D experiments showed that the α-helical peptides alamethicin, chrysophsin-3 and SMAP-29 demonstrated membrane insertion mechanisms when in contact with a zwitterionic PC membrane. The amphiphilic and α-helical properties of these peptides likely promoted insertion into the hydrophobic region of the bilayer. Chrysophsin-3 and SMAP-29, which contain many positive charges from amino acid residues, also adsorbed to the membrane surface in QCM-D experiments. This phenomenon was hypothesized to be due to attractive charge-dipole interactions with zwitterionic headgroups in the PC bilayer. Indolicidin, which exhibits a folded, boat-shaped conformation, showed evidence of surface adsorption and partial insertion into the bilayer. Indolicidin's lack of amphiphilicity and non-α-helical structure likely did not promote complete peptide insertion, but the presence

of hydrophobic amino acid residues within the peptide enabled it to partially insert into the bilayer.

In the context of therapeutic development, this understanding of AMP disruption of membranes is crucial for selecting and designing AMPs to kill pathogens. This study showed that α-helical structure and hydrophobic amino acid side chains promote peptide insertion into lipid membranes, indicating that peptides with these properties could be used to form holes in bacterial membranes and thereby cause cell death. These AMPs could also work in tandem with other therapeutics, including those that may experience difficulties passing through cell membranes, by forming holes through which these drugs can pass into the cell interior. AMPs can also be designed to carry large positive charges, which can target anionic lipid headgroups of bacterial membranes and facilitate adsorption to the surface of cell membranes (as shown in this study). Once on the membrane surface, other therapeutics combined with the peptides may be able to pass into the cell.

A novel process of interpreting QCM-D overtone data was developed to derive details about interactions occurring at different thicknesses of a supported membrane. Overall frequency and dissipation shifts in response to AMP exposure to supported lipid bilayers were used to infer changes to the membranes at equilibrium. ΔD vs. Δf plots revealed the dynamics of AMP-membrane interactions and showed that each AMP studied exhibited a unique QCM-D signature. These signatures indicated that each AMP interacted with the membranes differently. QCM-D data was also used to calculate the initial interaction rates of each AMP to estimate some kinetic information about peptide-membrane interactions. SMAP-29 exhibited the largest rate of initial mass change in the bilayer and alamethicin and chrysophsin-3 demonstrated the smallest rate. Bilayer characteristics and AMP-induced pore properties were also calculated from measured

frequency changes, revealing that the anionic membranes contained a larger hydrophobic region than the zwitterionic membranes.

AFM imaging was used to investigate morphological changes in lipid membranes that were produced during exposure to various concentrations of alamethicin and indolicidin. Visible membrane destabilization was observed at 5 μM and 10 μM concentrations of both peptides. Alamethicin formed large defects in the membrane that expanded over time until the membrane was completely destroyed. Indolicidin formed smaller membrane defects that filled in over time. At 10 μM indolicidin, partial filling of the bilayer was observed, which supported our interpretation of QCM-D results that showed membrane removal from parts of the bilayer and partial insertion of peptides.

A simple technique for forming supported lipid membranes composed purely of anionic lipids was developed to mimic Gram-positive bacterial membranes. A screening study was performed using QCM-D to identify combinations of lipid compositions, buffer types, and surface treatments that showed promise in bilayer formation. Three anionic lipid systems were chosen for further study: (1) a supported PG vesicle layer, (2) a supported 3:2 PG/LPG bilayer, and (3) a supported 4:1 PG/LPG bilayer. The QCM-D responses measured during membrane formation were compared to those recorded for PC bilayer formation to confirm the creation of stable anionic bilayers. Chrysophsin-3 ruptured PG vesicles at peptide concentrations as low as 0.5 μM, showing that supported vesicle layers are a sensitive platform for studying the membrane destabilization of AMPs at lower concentrations. The peptide also adsorbed to anionic bilayers more rapidly than with zwitterionic membranes and exhibited a membrane insertion mechanism.

The QCM-D overtone interpretation process developed in these studies may be valuable for the future examination of lipid bilayer behavior when exposed to other materials, such as nanoparticles. Unpublished work in our lab has shown that similar interpretation methods can be used to derive information about molecular-scale nanoparticle interactions with cell membranes. Frequency changes were measured at all overtones when zwitterionic lipid membranes were exposed to gold nanoparticles, suggesting that the nanoparticles interacted with all depths of the membrane rather than resting on the surface.[4] These experiments are valuable for understanding the potentially toxic effects of nanoparticles on organisms.

It is very likely that there is much more information buried in QCM-D overtone measurements that have not been discovered yet. The unique QCM-D signatures of each AMP in this study suggest that the frequency and dissipation measurements may be sensitive to nuances in interaction mechanisms that have not been identified. Some QCM-D responses recorded for chrysophsin-3 action on anionic membranes, such as a mass increase observed during the final buffer rinse when the bulk solution should not have contained more mass to be added to the membrane, are still unresolved. Therefore, further development of QCM-D data interpretation is necessary to advance our ability to examine AMP-membrane interactions.

From the information about peptide-membrane interactions gathered in these studies and the techniques that were developed, our ability to study AMP-membrane interactions and identify structural properties of peptides that promote specific behavior has expanded. We developed a novel process for analyzing QCM-D data that allowed us to derive detailed molecular-level mechanisms of AMP-membrane interactions that were validated by AFM imaging. QCM-D analysis revealed that peptide charge, amphiphilicity, and secondary structure play large roles in determining a peptide's preference for membrane insertion or surface

absorption. When designing multi-faceted therapeutics that target multiple cellular structures or processes, pore forming peptides could potentially be designed to create holes in the membrane through which other drugs could enter and target intracellular components.

More fundamental mechanistic research involving AMPs with varied structural properties is certainly necessary to fully understand AMP effects on bacterial and mammalian cells, however. Also, more studies investigating AMP interactions with the anionic lipid membranes developed in this study need to be conducted before AMP activity or specificity against bacterial or mammalian cells can be predicted based on peptide structural properties. Building on the techniques and information gained in this study will greatly facilitate the development of more effective peptides for use in therapeutics.[1]

References

(1) CDC. (2013) Antibiotic Resistance Threats in the United States, http://www.cdc.gov/drugresistance/threat-report-2013/pdf/ar-threats-2013-2508.pdf.
(2) Phoenix, D. A., Dennison, S. R. and Harris, F., *Antimicrobial Peptides*. 2013, Weinheim: Wiley-VCH.
(3) Peschel, A. and Sahl, H. G. (2006) The co-evolution of host cationic antimicrobial peptides and microbial resistance, *Nat Rev Microbiol 4*, 529-536.
(4) Bailey, C., *Characterizing gold nanoparticle interactions with biological cell membranes*. 2014.

Appendix 1: Relevant experimental data

This appendix includes data that was not included in the main thesis chapters. This includes Δf and ΔD results for low AMP concentrations and QCM-D results corresponding to supported PG vesicle layer formation.

A1.1 QCM-D results for all experimental AMP concentrations

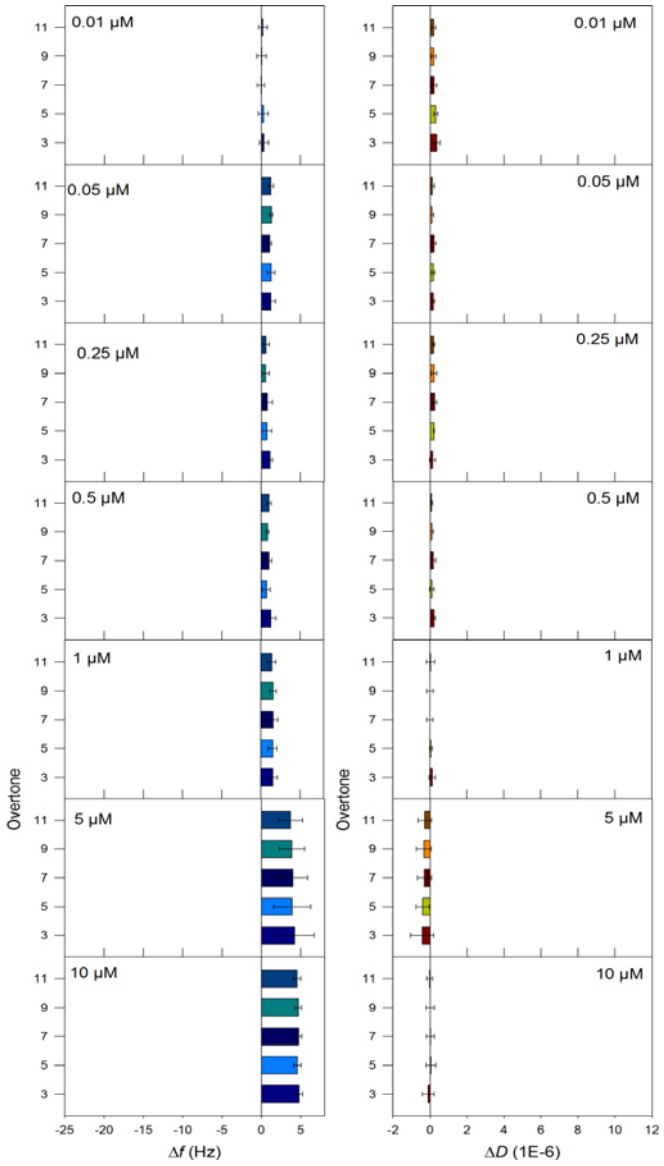

Figure A1.1. Changes in frequency and dissipation corresponding to various aqueous phase concentrations of alamethicin interacting with the PC membrane. Values for *Δf* and *ΔD* are shown for the 3rd through 11th overtones and represent the changes induced by alamethicin activity on a stable supported bilayer membrane. Initial measurements (t = 0 s) are taken after stable bilayer formation and final measurements are taken after the buffer rinse following 1 h of peptide incubation. Higher overtones are associated with changes closer to the sensor surface. Error bars represent the standard deviation based on at least 3 replicate experiments.

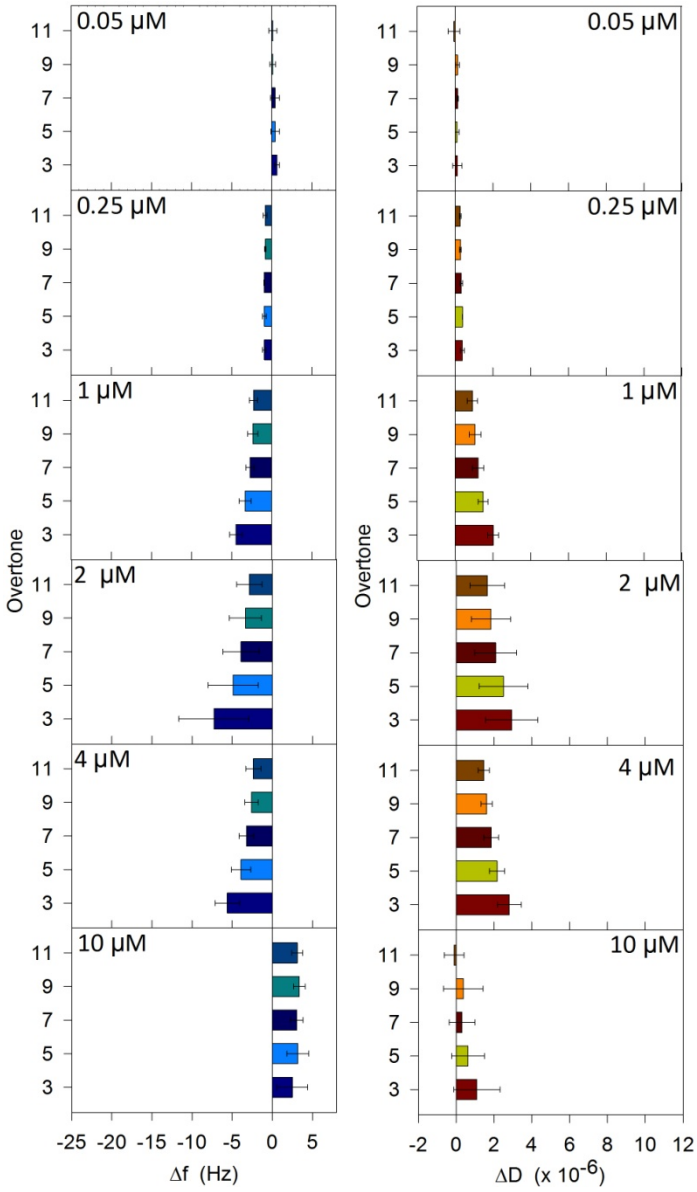

Figure A1.2. Changes in frequency and dissipation corresponding to various aqueous phase concentrations of chrysophsin-3 interacting with the PC membrane. Error bars represent the standard deviation based on at least 3 replicate experiments.

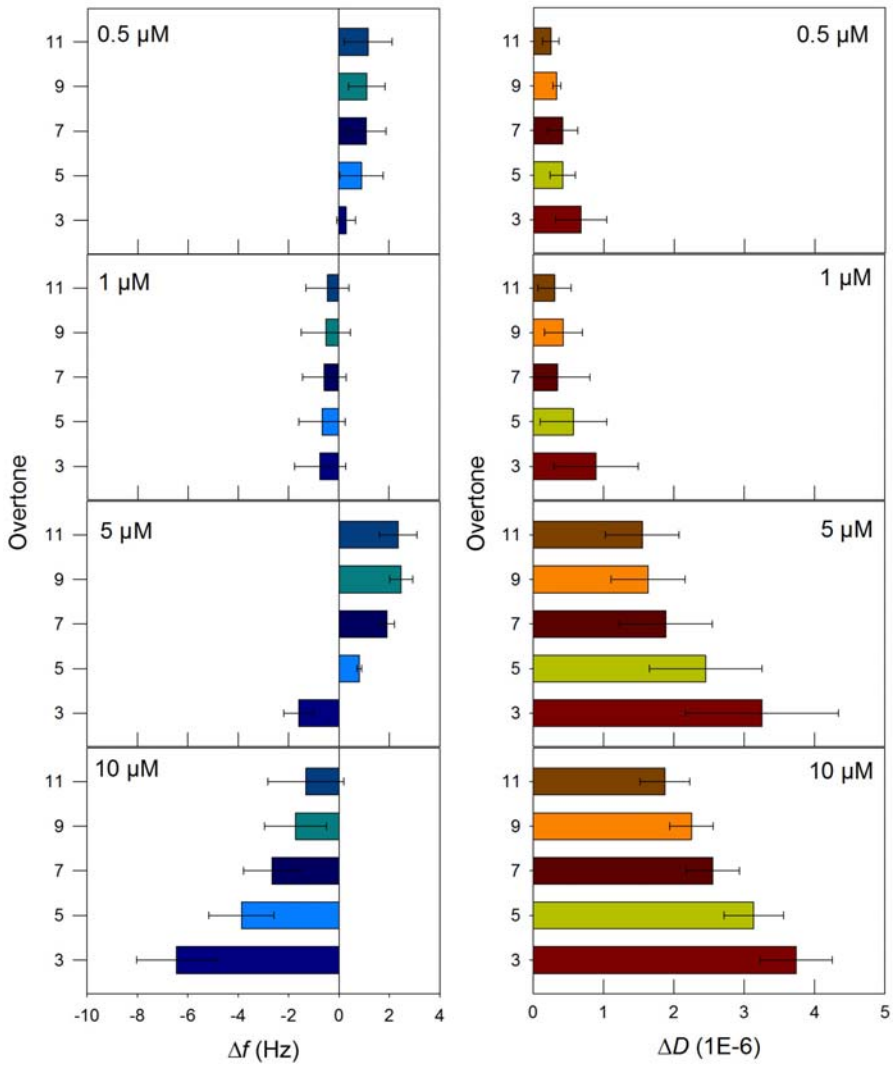

Figure A1.3. Changes in frequency and dissipation corresponding to various aqueous phase concentrations of indolicidin interacting with the PC membrane. Error bars represent the standard deviation based on at least 3 replicate experiments.

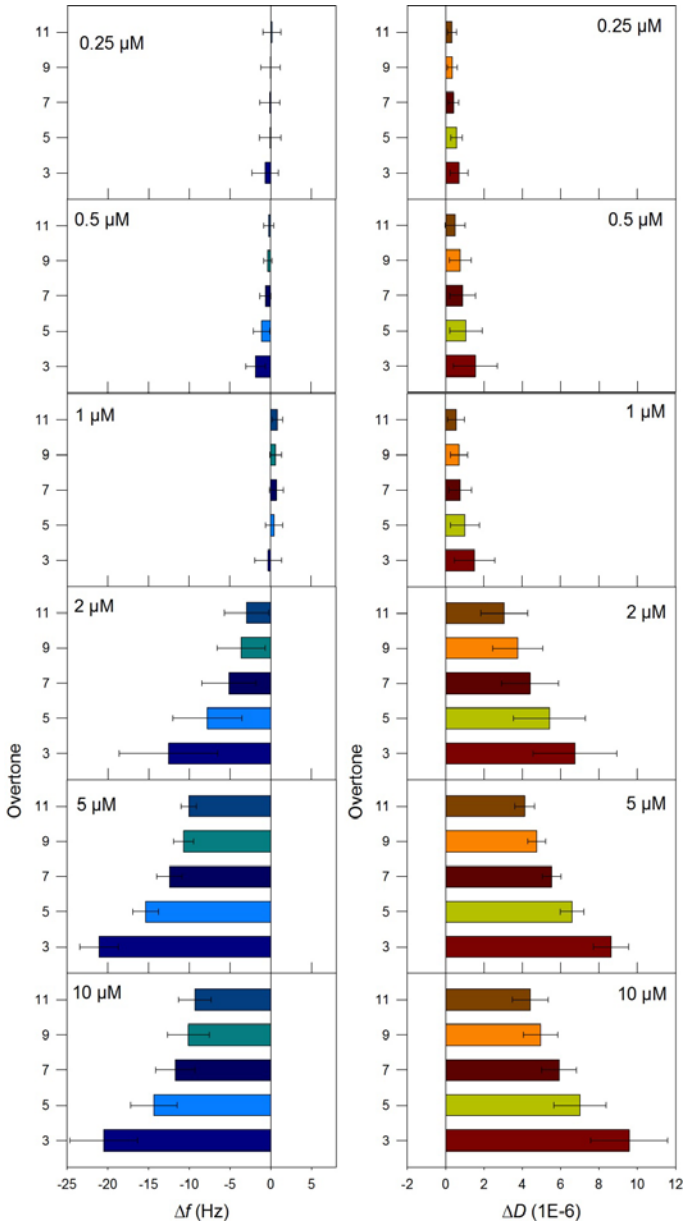

Figure A1.4. Changes in frequency and dissipation corresponding to various aqueous phase concentrations of SMAP-29 interacting with the PC membrane. Error bars represent the standard deviation based on at least 3 replicate experiments.

A1.2 PG Membrane Formation

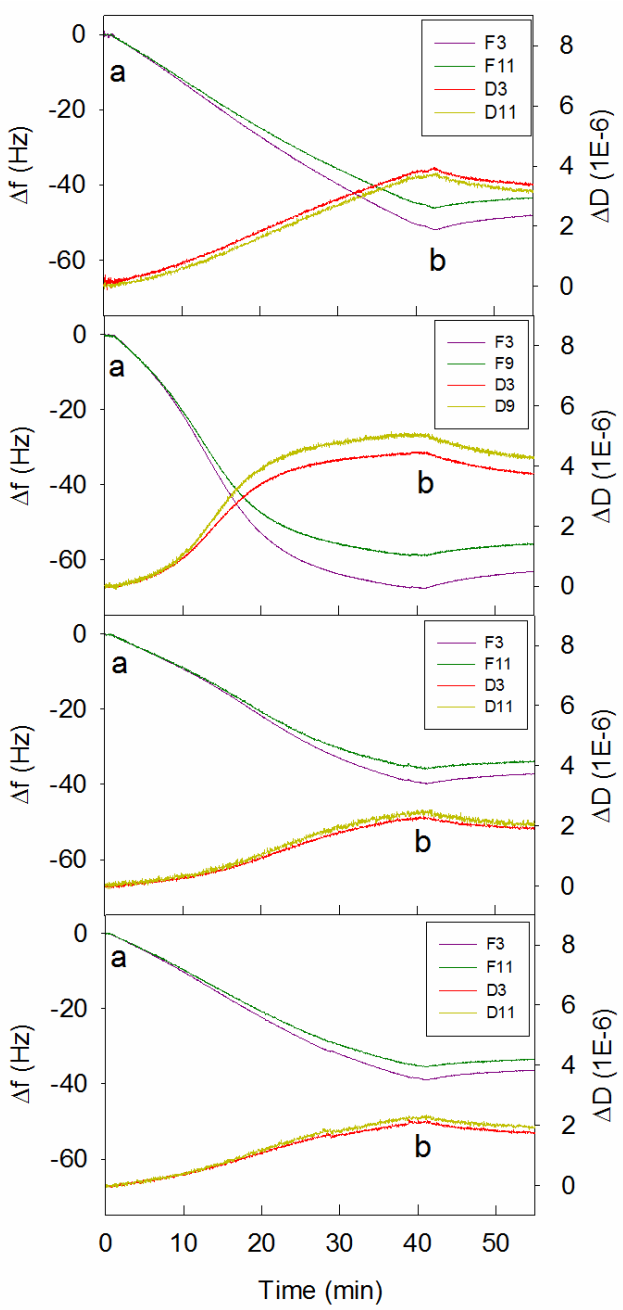

Figure A1.5. Examples of frequency and dissipation responses during PG membrane formation. Only two overtones are presented for simplicity. The 9th harmonic is shown in place of the 11th harmonic for the second figure because we were unable to measure the 11th harmonic during that experiment.

Appendix 2: Typical output from a QCM-D run

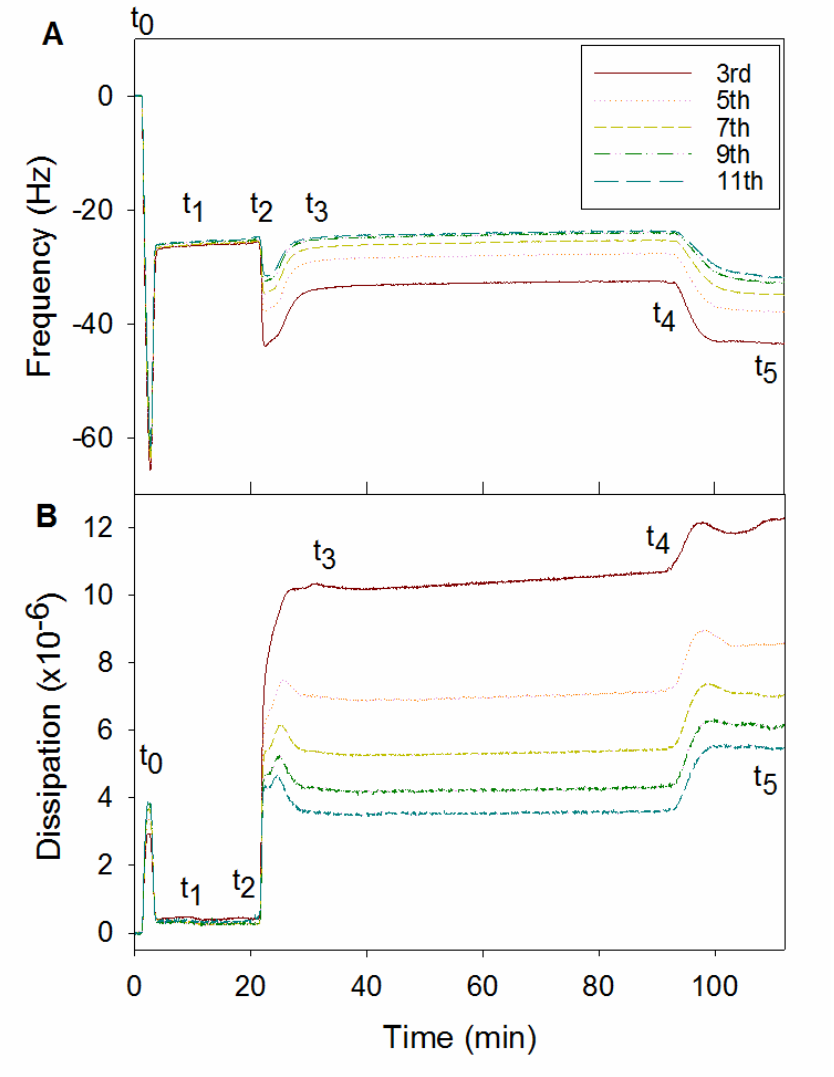

Figure A2.1. QCM-D run for 10 μM SMAP-29. At time t_0, a PC vesicle solution was allowed to flow over the QCM-D silica sensor surface. At time t_1, the buffer was injected into the QCM-D chamber to rinse away any unattached particles. At time t_2, a solution of the AMP in the buffer at the desired peptide concentration was allowed to flow. At time t_3, the flow was stopped and the system was left to equilibrate for 1 hr. At time t_4, a final buffer rinse was applied until the frequency and dissipation stabilized at time t_5.

Appendix 3: Calculation of maximum frequency changes for various peptide interaction modes

For different modes of interaction of the peptide with the bilayer, we can calculate what will be the anticipated maximum frequency change from the QCM-D experiment by considering the changes to the bilayer from the addition of peptide and possible removal of lipid. Since the peptide-induced changes occur on the supported bilayer, we first establish the characteristics of this bilayer. The area per lipid in the bilayer (denoted as a_L) and the thickness of the bilayer were calculated from the measured frequency change of ~25 Hz, accompanying the formation of the supported PC bilayer. Noting that the proportionality constant C relating the frequency change to mass change in the Sauerbrey equation ($C\,\Delta f = \Delta m$) is 17.8 ng/cm^2/Hz for a crystal oscillating at 5 MHz natural frequency, the bilayer areal mass corresponding to a frequency change of 25 Hz is equal to 445 ng/cm^2. It has been shown[1] that this mass includes the mass of a layer of water between the quartz crystal and the supported lipid bilayer and the mass of this water layer has been determined to be ~ 102 ng/cm^2[13313384]. Correcting for this water mass, we estimate the areal mass of the lipid bilayer to be 343 ng/cm^2. The molecular mass M_L of the lipid is 1.267x10^{-12} ng/molecule corresponding to an average molecular weight of 760 g/mol for the egg PC lipid. Dividing the areal mass of the lipid bilayer by the mass of a single lipid molecule M_L, we find there are 2.7 molecule/nm^2 on the bilayer. This corresponds to a lipid area a_L of 0.739 nm^2/molecule. If the molecular volume v_L of the hydrophobic tail of the egg PC lipid is 0.96 nm^3/molecule (taken as the composition average based on the constituent C16 and C18 chains), then the thickness of the hydrophobic region of the bilayer $h_L = 2v_L/a_L = 2.6$ nm. These estimates based on QCM-D data and molecular properties of lipids can be compared to the x-ray

measurements of Huang[2] who obtained a_L = 0.74 nm^2 and h_L = 2.66 nm for DOPC, and a_L = 0.68 nm^2 and h_L = 2.75 nm for POPC.

If a peptide enters the bilayer in the pore state or as inserted peptides or peptide clusters, some lipid molecules have to be removed from the bilayer area to create space. If a peptide or a peptide cluster (without a water pore) is inserted into the bilayer, the area cleared per peptide a_P is calculated as $a_P = \pi d_P^2/4$ where d_P is the diameter of the peptide, visualized as a cylinder. The area per peptide a_P is estimated to be 0.945 nm^2/molecule, taking the diameter d_P of alpha-helices to be 1.1 nm. If the peptide is part of a pore incorporating a water channel, then the area cleared per peptide is A_H/n, where A_H is the pore area and n is the number of peptide molecules constituting the pore. If we take the approximate pore size to be determined by the close packed arrangement of peptides at the pore boundary, then the outer diameter D_H of a pore with n peptides and the area of the pore per peptide A_H/n can both be calculated from

$$D_H = \frac{n\, d_P}{\pi} + d_P\,, \qquad \frac{A_H}{n} = \frac{1}{n}\frac{\pi D_H^2}{4} = \frac{1}{n}\frac{\pi d_P^2}{4}\left(\frac{n}{\pi}+1\right)^2 \tag{1}$$

For a peptide diameter d_p = 1.1 nm, the pore diameter D_H estimated from eq.(4) will be about 3.9 nm for n = 8. Indeed, for alamethicin, Huang[2] has estimated the number of peptides per pore to be 8 and the pore diameter of 3.9 nm. For the purpose of our interpretive needs, we will consider two values for the number of peptides in the pore, n = 8, 20 corresponding to which the pore diameters will be 3.9 nm and 4.6 nm and pore area per peptide A_H/n will be 1.494 and 1.663 nm^2/peptide.

On the addition of peptide to the bilayer, lipid molecules are removed from a fraction λ of the bilayer area and replaced either by pores or inserted peptides or peptide clusters. The number of lipid molecules removed will be $2\lambda A/a_L$, with the factor 2 accounting for the two layers of the

bilayer. The $2\lambda A/a_L$ lipids removed will be replaced by $\lambda A/a_P$ peptides if peptide or peptide clusters are inserted into the bilayer and by $\lambda A/(A_H/n)$ peptides, if the peptides are part of pores. However, if the peptide adsorbs on the bilayer surface without any lipid removal, then each adsorbed peptide occupies an area $A_p = \pi d_p L_p$ (L_p being the length of the peptide, calculated from its molecular volume and assuming the peptide is a cylinder of 1.1. nm diameter) and the number of peptides adsorbed will be $\lambda A/A_p$. The resulting frequency changes can be calculated as the areal mass change divided by C:

$$\Delta f = -\frac{\lambda}{C}\left[\frac{M_P}{a_P} - 2\frac{M_L}{a_L}\right] \quad \text{Insertion of peptide/peptide clusters}$$

$$\Delta f = -\frac{\lambda}{C}\left[\frac{M_P}{\frac{A_H}{n}} - 2\frac{M_L}{a_L}\right] \quad \text{Formation of pores} \qquad (2)$$

$$\Delta f = -\frac{\lambda}{C}\left[\frac{M_P}{\mathrm{Ap}}\right] \quad \text{Adsorption of peptides}$$

In this equation M_P and M_L are molecular masses of the peptide and lipid molecule, respectively, calculated from their molecular weights. Setting the fractional area λ to be unity, we can calculate the theoretical maximum in the frequency change.

References for Appendix 3

(1) T.J. Zwang, W.R. Fletcher, T.J. Lane and M.S. Johal, (2010) Quantification of the layer of hydration of a supported lipid bilayer, Langmuir, 26, 4598-4601.

(2) H.W. Huang, (2006) Molecular mechanism of antimicrobial peptides: The origin of cooperativity Biochim Biophys Acta, 1758, 1292–1302.

Appendix 4: Hydrophobicity scales

A number of hydrophobicity scales are available in the literature to represent the properties of amino acids. The first scale was proposed by Nozaki and Tanford[1] in 1971 based on free energies of transfer of amino-acid side chains from water to ethanol. Another is the scale of Wolfenden et al[2] for the transfer of the amino acids from water to vapor. The scales of Chothia[3] and Janin[4] are based on calculated free energy changes for the transfer of amino-acid side chains from the surface to the interior of a protein, based on the observed distribution (between surface and interior) of each residue type for globular proteins of known structure. von Heijne and Blomberg[5], developed a scale based on the free energy changes associated with the transfer from aqueous to non-aqueous media of the amino-acid side chains including the effects of buried non-polar atoms, removal of charges and decrease of hydrogen bonding during burial. These are among the earliest developments of hydrophobicity scales.

In the 90s, White and coworkers[6-8] proposed additional hydrophobicity scales, composed of experimentally determined transfer free energies for each amino acid. One corresponds to the transfer of unfolded chains from water to POPC bilayer interface and the other describes the transfer of folded chains into an *n*-octanol interior. These scales include the contributions of the peptide bonds and not just side chains and thus represent whole-residues. The experimental values have been obtained using host-guest pentapeptides.

A different type of hydrophobicity scale was developed by Urry[9,10] based on the hydrophobic association between peptides. The elastic model protein, (GVGVP)n in aqueous medium undergoes reversible phase transition on raising the temperature, with the hydrophobic residues going from water to a state of hydrophobic association. To determine the hydrophobicity of an amino acid X, the amino acid was included as a guest within the host

protein in the form (GXGVP) replacing the residue V, and from the temperature and enthalpy change at the transition, the contribution of X to the hydrophobic association free energy was determined.

A widely used hydrophobicity scale in the protein literature is that due to Eisenberg[11-14]. He developed a so-called "consensus scale" by averaging the normalized hydrophobicity for each residue over the five scales mentioned above[1-5].

All scales correspond to some sort of a free energy value and have units of kcal/mol, although the units are not needed and the numerical values are just used as measures of hydrophobicity for comparison purposes. Five different scales are listed on Table S1. As one can expect, the numerical values in the different scales differ from one another and therefore one should use a given scale consistently for calculating the hydrophobicity of an amino acid sequence.

One may expect the different hydrophobicity scales to have some correlation between one another. Figure S2 shows the relations between five different scales. Once can observe some correlation as well as deviations. The deviations clearly reflect the different basis on which the hydrophobicity values are derived and how the side chains and peptide bonds may contribute differently in each experimental method.

For the four peptides studied in this paper, the hydrophobicity was calculated and plotted in Figure S3 based on the Urry scale and Figure S4 based on the Eisenberg consensus scale. In calculating for alamethicin, for the unnatural amino acid aminoisobutyric acid, the values are taken to be the average of alanine and valine; for phenylalaninol, the values are taken to be those for phenylalanine.

Table A4.1: Examples of Hydrophobicity Scales from Literature

Amino Acid Designation		Hydrophobicity Scales				
		Urry–Phase Transition	Tanford–Ethanol	Eisenberg-Consensus	White-Interface	White-Octanol
W	Trp	-7.00	6.50	0.81	-1.85	-2.09
F	Phe	-6.15	5.00	1.20	-1.13	-1.71
Y	Tyr	-5.85	4.50	0.26	-0.94	-0.71
L	Leu	-4.05	3.50	1.10	-0.56	-1.25
I	Ile	-3.65	5.00	1.40	-0.31	-1.12
V	Val	-2.50	3.00	1.10	0.07	-0.46
M	Met	-1.50	2.50	0.64	-0.23	-0.67
H+	His+	-1.90	1.00	-0.40	0.96	2.33
C	Cys	-1.90	0.00	0.29	-0.24	-0.02
P	Pro	-1.10	1.50	0.12	0.45	0.14
A	Ala	-0.75	1.00	0.62	0.17	0.50
T	Thr	-0.60	0.50	-0.05	0.14	0.25
N	Asn	-0.05	-1.50	-0.78	0.42	0.85
G	Gly	0.00	0.00	0.48	0.01	1.15
S	Ser	0.55	-0.50	-0.18	0.13	0.46
R	Arg	0.80	nd*	-2.50	0.81	1.81
Q	Gln	0.75	-1.00	-0.85	0.58	0.77
D-	Asp	3.40	nd	-0.90	1.23	3.64
K+	Lys	2.94	nd	-1.50	0.99	2.80
E-	Glu	3.72	nd	-0.74	2.02	3.63

*nd indicates the value was not determined

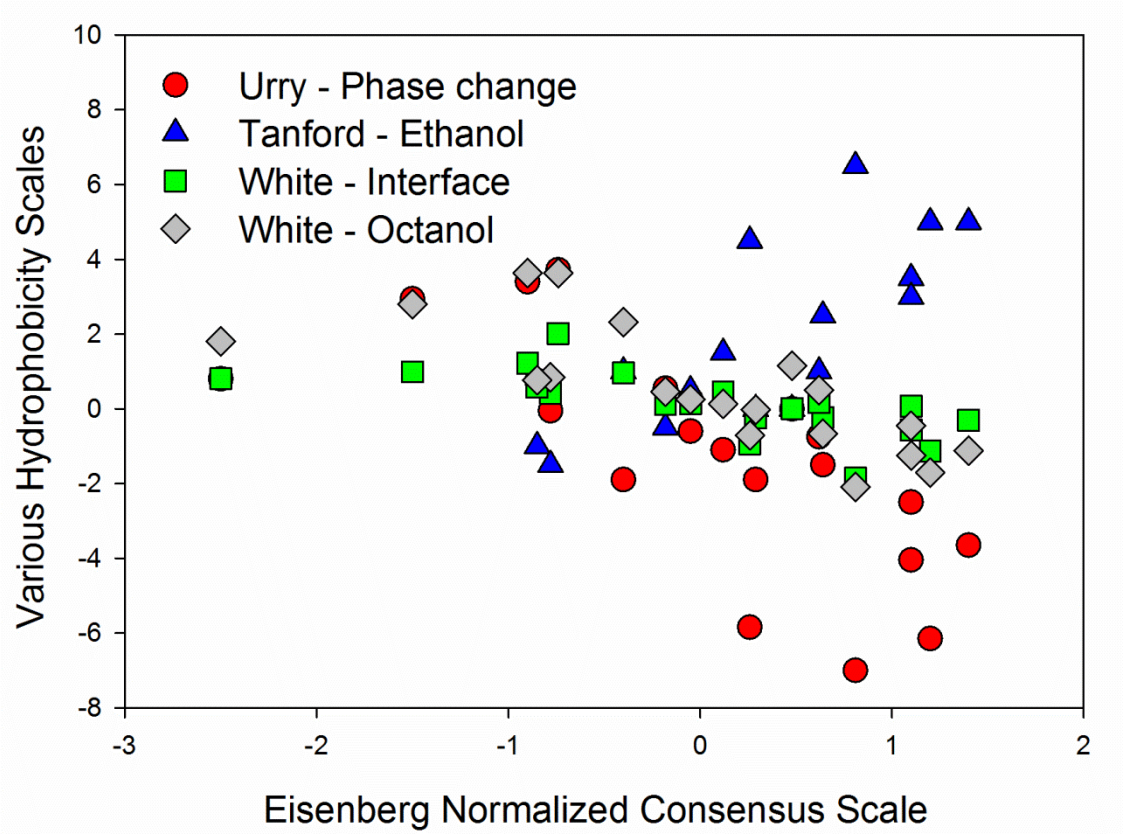

Figure A4.1. Correlation among different hydrophobicity scales

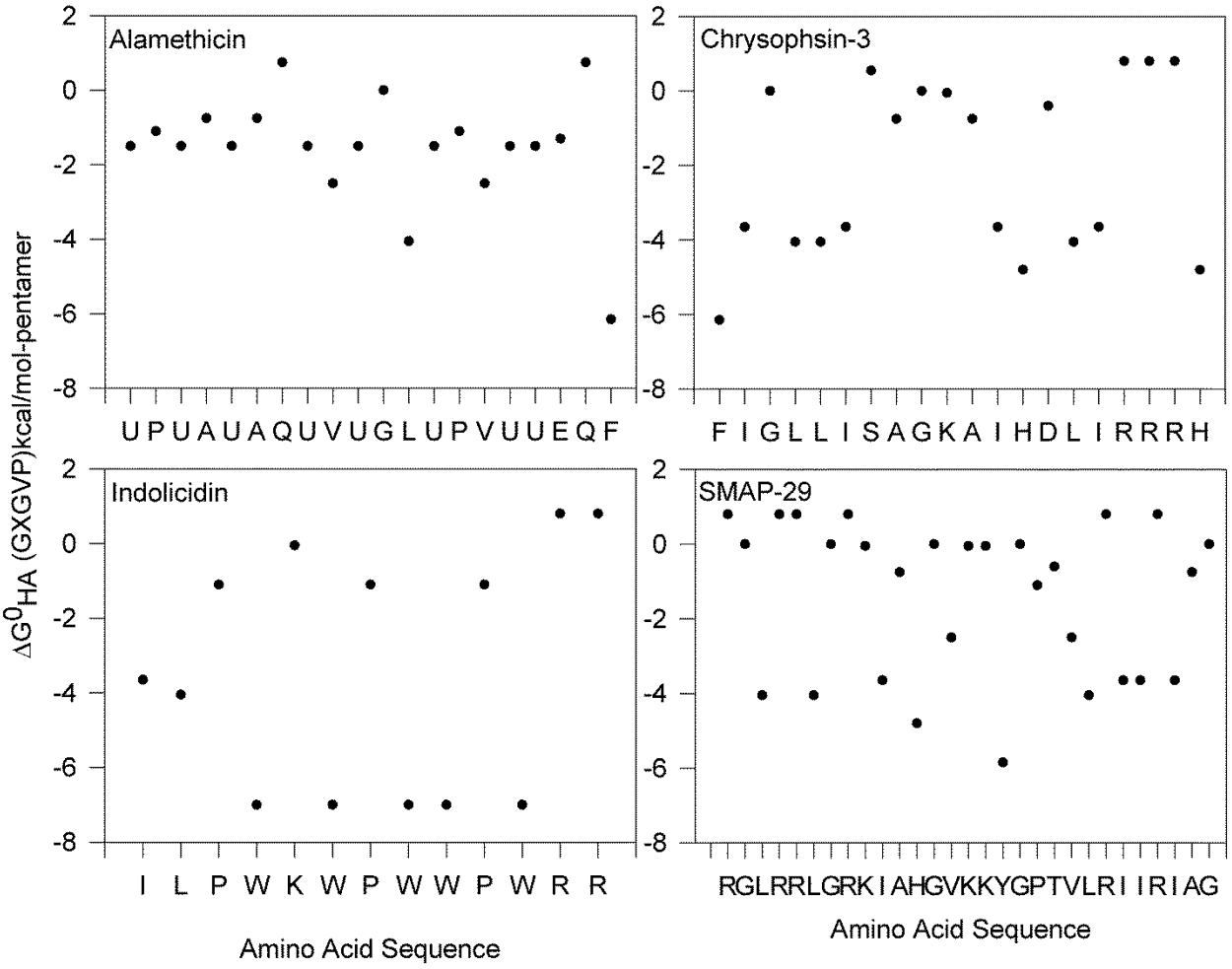

Figure A4.2. Hydrophobicity of peptides based on Urry hydrophobicity scale

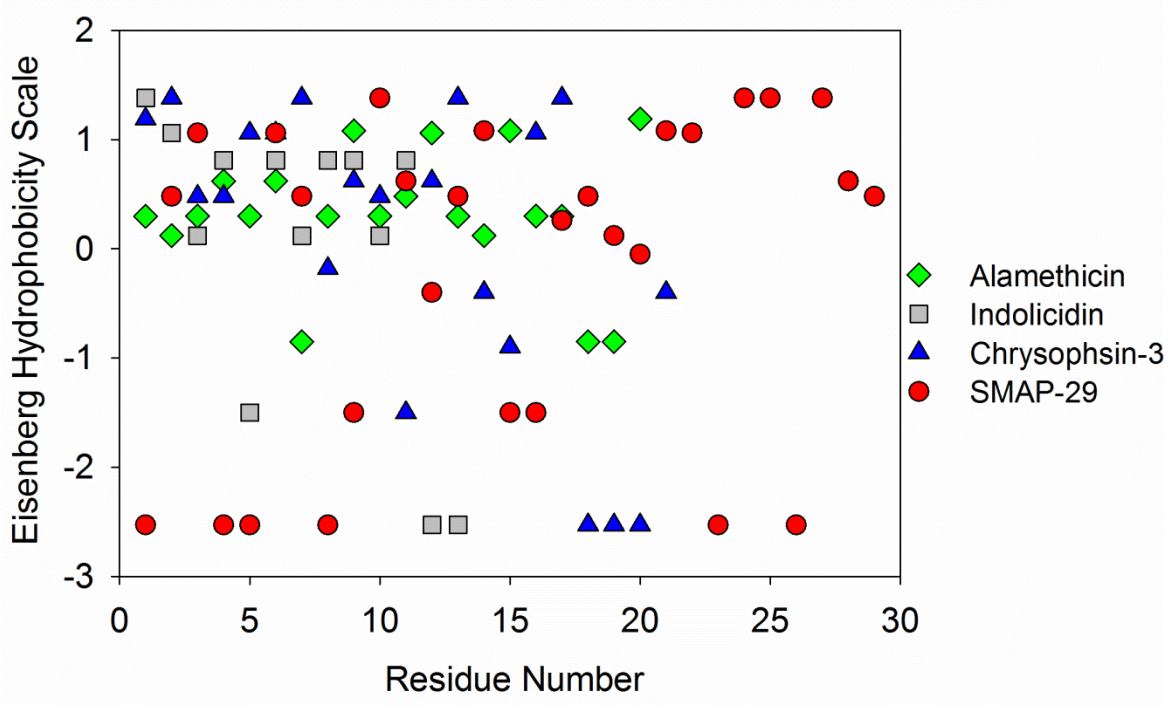

Figure A4.3. Hydrophobicity of peptides based on Eisenberg consensus scale

References for Appendix 4

(1) Nozaki Y, Tanford C., The solubility of amino acids and two glycine peptides in aqueous ethanol and dioxane solutions. Establishment of a hydrophobicity scale., *J Biol Chem.,* 1971, 246, 2211–2217

(2) Wolfenden R, Andersson L, Cullis PM, Southgate CC., Affinities of amino acid side chains for solvent water. *Biochemistry.*, 1981, 20, 849–855.

(3) Chothia C., The nature of the accessible and buried surfaces in proteins., *J Mol Biol.*, 1976, 105, 1–12.

(4) Janin J., Surface and inside volumes in globular proteins., *Nature,* 1979, 277, 491–492.

(5) von Heijne, G. and Blomberg, C., Trans-membrane translocation of proteins: The direct transfer model. *Eur.J. Biochem.,* 1979, **97,** 175–181.

(6) Wimley WC, White SH., Experimentally determined hydrophobicity scale for proteins at membrane interfaces., *Nat Struct Biol*, 1996, 3, 842–848.

(7) Wimley WC, Creamer TP, White SH., Solvation energies of amino acid side chains and backbone in a family of host-guest pentapeptides., *Biochemistry*, 1996, 35, 5109–5124.

(8) White SH, Wimley WC., Membrane protein folding and stability: physical principles., *Annu Rev Biophys Biomol Struct,* 1999, 28, 319–365.

(9) Urry, D. W. (2004) The change in Gibbs free energy for hydrophobic association: Derivation and evaluation by means of inverse temperature transitions, *Chemical Physics Letters 399*, 177-183.

(10) Urry, D. W. (1997) Physical chemistry of biological free energy transduction as demonstrated by elastic protein-based polymers, *J. Phys. Chem. B 101*, 11007-11028.

(11) Eisenberg. D., Weiss. R. M.. Terwilliger. T. (‘., and Wilcox. W. (1982). Hydrophobic moments and protein structure, Faraday Symp. Chem. Soc. 17, 109-120.

(12) Eisenberg, D., Weiss, R. M., and Terwilliger, T. C., *Nature,* 1982, The helical hydrophobic moment: a measure of the amphiphilicity of helix, 299, 371-374.

(13) Eisenberg, D., Schwarz, E. M., Komaromy, M., Wall, R., Analysis of membrane and surface protein sequences with the hydrophobic moment plot., *J. Mol. Biol*., 1984, 179, 125-142.

(14) Eisenberg, D. (1984) Three-dimensional structure of membrane and surface proteins, *Ann. Rev. Biochem. 53*, 595-623.